Technische Universität München
Fakultät für Medizin

Role of the Chromatin-Associated Proto-Oncogene DEK during Productive Infection with HAdV5 and Virus-Mediated Oncogenesis

Julia Luisa Mai

Vollständiger Abdruck der von der Fakultät für Medizin der Technischen Universität München zur Erlangung des akademischen Grades einer

Doktorin der Naturwissenschaften (Dr. rer. nat.)

genehmigten Dissertation.

Vorsitz: Prof. Dr. Markus Gerhard

Prüfer*innen der Dissertation:

1. Prof. Dr. Sabrina Schreiner
2. apl. Prof. Dr. Thomas Floss

Die Dissertation wurde am 01.07.2021 bei der Technischen Universität München eingereicht und durch die Fakultät für Medizin am 09.11.2021 angenommen.

Appendix I

Eidesstattliche Erklärung

Ich erkläre an Eides statt, dass ich die bei der Fakultät für Medizin der TUM zur Promotionsprüfung vorgelegte Arbeit mit dem Titel:

“Role of the chromatin-associated proto-oncogene DEK during productive infection with HAdV5 and virus-mediated oncogenesis”

in der Fakultät für Medizin am Institut für Virologie unter der Anleitung durch Prof. Dr. Sabrina Schreiner ohne sonstige Hilfe erstellt und bei der Abfassung nur die gemäß § 6 Ab. 6 und 7 Satz 2 angebotenen Hilfsmittel benutzt habe.

☒ Ich habe keine Organisation eingeschaltet, die gegen Entgelt Betreuerinnen und Betreuer für die Anfertigung von Dissertationen sucht, oder die mir obliegenden Pflichten hinsichtlich der Prüfungsleistungen für mich ganz oder teilweise erledigt.

☒ Ich habe die Dissertation in dieser oder ähnlicher Form in keinem anderen Prüfungsverfahren als Prüfungsleistung vorgelegt.

☐ Die vollständige Dissertation wurde in …….. veröffentlicht. Die Fakultät hat der Veröffentlichung zugestimmt.

☒ Ich habe den angestrebten Doktorgrad noch nicht erworben und bin nicht in einem früheren Promotionsverfahren für den angestrebten Doktorgrad endgültig gescheitert.

☐ Ich habe bereits am _____ bei der Fakultät für _____ der Hochschule _____ unter Vorlage einer Dissertation mit dem Thema _____ die Zulassung zur Promotion beantragt mit dem Ergebnis:_____

Die öffentlich zugängliche Promotionsordnung der TUM ist mir bekannt, insbesondere habe ich die Bedeutung von § 28 (Nichtigkeit der Promotion) und § 29 (Entzug des Doktorgrades) zur Kenntnis genommen. Ich bin mir der Konsequenzen einer falschen Eidesstattlichen Erklärung bewusst.

Mit der Aufnahme meiner personenbezogenen Daten in die Alumni-Datei der TUM bin ich

☒ einverstanden, ☐ nicht einverstanden.

_____

Ort, Datum, Unterschrift

Table of Content

Appendix I II

Eidesstattliche Erklärung II

Table of Content III

Index of Abbreviations VII

List of Tables XII

List of Figures XIV

Abstract 1

Zusammenfassung 3

1. Introduction 5

1.1. Adenoviruses 5

1.1.1. Virus Classification 5

1.1.2. Adenoviral Pathogenicity 7

1.1.3. Laboratory Diagnosis and Treatment 9

1.1.4. Structure and Genome Organization 10

1.1.5. Adenoviral Productive Infection Cycle 12

1.2. The SUMOylation Pathway and Promyelocytic Leukemia Nuclear Bodies . 15

1.2.1. SUMO Conjugation Pathway 15

1.2.2. Promyelocytic Leukemia Nuclear Bodies 17

1.2.3. SUMOylation and PML-NBs during HAdV Infection 18

1.3. Human Adenoviruses and Their Oncogenic Potential 20

1.4. The Chromatin-Associated Proto-Oncogene DEK 21

1.4.1. Structure of the Oncoprotein DEK 21

1.4.2. Localization and Molecular Function 22

1.4.3. DEK in Diseases, Cancer Development and Progression 23

1.5. Aim of Study 25

2. Material 27

2.1. Cells 27

2.1.1. Bacteria Strains 27
2.1.2. Mammalian Cell Lines 27
2.2. Viruses 28
2.3. Nucleic Acids 28
2.3.1. Oligonucleotides 28
2.3.2. Vectors 31
2.3.3. Recombinant Plasmids 31
2.4. Antibodies 32
2.4.1. Primary Antibodies 32
2.4.2. Secondary Antibodies 34
2.5. Standard and Markers 35
2.6. Enzymes and Buffers 35
2.7. Commercial Systems 37
2.8. Chemicals and Reagents 37
2.9. Laboratory Equipment 42
2.10. Disposable Laboratory Equipment 47
2.11. Software 49

3. Methods 51
3.1. Bacteria 51
3.1.1. Culture and Storage 51
3.1.2. Preparation of Chemically Competent Bacteria 52
3.1.3. Chemical Transformation of Bacteria 52
3.2. Tissue Culture Techniques 53
3.2.1. Cultivation of Mammalian Cell Lines 53
3.2.2. Cryopreservation of Mammalian Cells 54
3.2.3. Determination of Total Cell Number 54
3.2.4. Transfection of Mammalian Cells with Polyethylenimine 55
3.2.5. Harvest of Mammalian Cells 55
3.3. Generation of Stable Cell Lines by Lentiviral Transduction 55
3.3.1. Generation of Recombinant Lentiviral Particles 55
3.3.2. Infection of Mammalian Cell Lines with Lentiviral Particles 56
3.4. Adenovirus 56
3.4.1. Infection of Mammalian Cell Lines 56
3.4.2. Propagation and Storage of High-Titer Virus Stocks 56
3.4.3. Titration of Virus Stock 57
3.4.4. Determination of Virion Progeny Production 58
3.5. Quantitative Determination of Nucleic Acid Concentrations 58
3.6. DNA Techniques 59

3.6.1. Preparation of Plasmid-DNA from *Escherichia Coli* 59
3.6.2. Polymerase Chain Reaction (PCR) 60
3.6.3. Agarose Gel Electrophoresis 61
3.6.4. Cloning of DNA Fragments 61
3.6.5. Quantification of Viral DNA Synthesis 62
3.7. RNA Techniques 63
3.7.1. Preparation of Total Cellular RNA from Mammalian Cells 63
3.7.2. Reverse Transcription of RNA 64
3.7.3. Quantitative Real-Time PCR (RT-qPCR) 64
3.8. Protein Techniques 65
3.8.1. Preparation of Total-Cell Lysates 65
3.8.2. Determination of Protein Concentration 66
3.8.3. Co-Immunoprecipitation (IP) 67
3.8.4. Nickel-Nitrilotriacetic Acid (NiNTA) Precipitation 68
3.8.5. Sodium Dodecyl Sulfate Polyacrylamide Gel Electrophoresis (SDS-PAGE) 69
3.8.6. Western Blot Analysis 71
3.8.7. Indirect Immunofluorescence (IF) Assay 72
3.9. CUT&RUN assay 73
3.10. Reporter Gene Assay 73

4. Results 75
4.1. DEK is a Novel Host Factor Promoting HAdV Infection 75
4.1.1. HAdV Infection Modulates DEK Gene Expression 75
4.1.2. The Chromatin-Associated DEK Protein Modulates HAdV Infection 80
4.1.2.1. DEK N-Terminally Fused to FLAG-Tag Can Be Expressed in Human Cell Lines 80
4.1.2.2. HAdV Replication and Progeny Production Is Promoted by the DEK Protein 83
4.1.3. DEK Localizes with Early Viral Protein E1B-55K 90
4.1.4. DEK Interacts with Early E1B-55K in HAdV-Infected Cells 91
4.1.5. DEK Is a Novel Target for SUMO-2 Modification 92
4.1.5.1. DEK Protein Possesses Several Putative SUMOylation Consensus Motifs 92
4.1.5.2. Early Viral E1B-55K Facilitates SUMOylation of DEK 94
4.1.6. DEK Is Partially Recruited to PML Tracks and to the Sites of Viral Replication 96
4.1.6.1. DEK Associates with E4orf3-Containing PML Tracks during Infection 96
4.1.6.2. DEK Subcellular Localization Is Dependent on Viral Infection Stage 99
4.1.6.3. Viral Replication Center Marker E2A Binds to DEK Protein 106
4.1.7. DEK Binds to Viral Promoter Regions and Modifies Their Activity 107
4.1.7.1. Adenoviral Gene Expression Is Elevated by DEK Protein Expression 107
4.1.7.2. DEK Interacts with Adenoviral Early and Late Promoters Sequences 109
4.1.8. DEK Binding to Host Transcriptional Regulators Is Changed during HAdV Infection ... 110
4.1.9. Loss of DEK Protein Expression Negatively Influences Adenoviral Progeny Production 113
4.1.9.1. Establishment of a DEK-Negative Mammalian Cell Line 113

4.1.9.2. Depletion of DEK Expression Represses HAdV Infection 116
4.2. DEK Affects Virus-Mediated Oncogenic Transformation Processes 118
4.2.1. E1A Interaction with p300 Is Dependent on DEK Expression 118
4.2.2. DEK Depletion Interferes with Interaction of E1B-55K with Host Restrictive Factors ... 120
4.2.3. E1B-55K Is Not Able to Inhibit p53 Function in DEK-Negative Cells 121

5. Discussion 124
5.1. DEK Is a Novel Host Factor Promoting HAdV Infection 125
5.2. DEK Function Is Dependent on Its PTM 127
5.3. Dynamic Localization of DEK during Infection 129
5.4. DEK – a Novel Host Factor for Viral Epigenetic Regulation 131
5.5. DEK Might Represent a Potential Regulator of the HAdV Oncogenic Potential in Non-Permissive Cells 135
5.6. Clinical Relevance and Future Therapeutic Options 139

References 140

Appendix II 165
Publications in Peer-Reviewed Journals 165
Conferences 166
Trainings and Certification Courses 168
Grants 168

Acknowledgement 169

Index of Abbreviations

µ

µg *microgram*

µl *microliter*

µm *micrometer*

µM *micromolar*

A

A *adenine*

A.D. agent *adenoid degeneration agent*

A549 *human lung carcinoma cell line expressing wild-type p53*

aa *amino acid*

Ab *antibody*

AdV *Adenovirus*

AIDS *Acquired immunodeficiency syndrome*

AP-2α *activating enhancer binding protein 2α*

APC *adenoidal-pharyngeal-conjunctival*

APS *ammonium persulfate*

Arg *arginine*

Asp *aspartate*

AVP *adenovirus protease*

B

BLM *bloom helicase*

BMT *bone marrow transplant*

bp *base pair*

BSA *Bovine serum albumin*

C

$CaCl_2$ *Calcium chloride*

CAR *Coxsackie / Adenovirus receptor*

CBP *CREB-binding protein*

cDNA *complementary DNA*

ChIP *chromatin immunoprecipitation*

CK2 *casein kinase 2*

cm centimeter

CMV *Cytomegalovirus*

CNS *central nervous system*

CO_2 *Carbon dioxide*

CR3 conserved region 3

Ct *threshold cycle*

CTB *Cell titer blue*

CUL1 *Cullin-1*

D

D *aspartate*

DAPI *4',6-Diamidin-2-phenylindol*

Daxx *death-associated protein*, *Death-associated protein 6*

DBP *DNA-binding protein*

ddH_2O *double-distilled water*

DDR *DNA damage response*

DMEM *Dulbecco's modified eagle's medium*

DMSO *Dimethyl sulfoxide*

DNA *deoxyribonucleic acid*

dNTP *deoxyribose nucleoside triphosphate*

DP *dimerization partner*

ds *double-stranded*

DSG-2 *desmoglein 2*

E

E *Glutamic acid*

E. coli Escherichia coli

E1Ap *E1A promoter*

E1Bp *E1B promoter*

E2Ep *E2 early promoter*

E2Lp *E2 late promoter*

E4p *E4 promoter*

EBV *Epstein-Barr virus*

ECL *enhanced chemiluminescence*

ECM *extracellular matrix*

EDTA *Ethylenediaminetetraacetic acid*, *2,2',2'',2'''-(ethane-1,2-diyldinitrilo)tetraacetic acid*

EKC *epidemic keratoconjunctivitis*

F

FBS *Fetal Bovine Serum*

ffu *fluorescence forming units*

fwd *forward*

G

g *gram*

G *glycine*

GAPDH *glyceraldehyde 3-phosphate dehydrogenase*

Gly *glycine*

H

h *hour*

H1299 *Human non-small lung carcinoma cell line, p53 negative*

H_2O_2 *hydrogen peroxide*

H3 *histone 3*

HAdV *Human Adenovirus*

HAT *histone acetyltransferase*

HCl *hydrochloric acid*

HCMV *human cytomegalovirus*

HDAC II *histone deacetylase II*

HEK293 *Human embryonic kidney 293 cells*

HEK293T *HEK 293 cell line expressing large T antigen from SV40*

HepaRG *Human hepatic progenitor cell line expressing stem cell properties*

HG *hemagglutination group*

HIF-1α *hypoxia-inducible factor 1α*

His *histidin*

HIV-2 *human immunodeficiency virus 2*

HP1 *heterochromatin protein 1*

HPV *human papilloma virus*

HR *homologous recombination*

HRP *horseradish peroxidase*

HSPG *heparin sulfate-containing proteoglycans*

HSV *Herpes Simplex Virus*

HSV-TK herpes simplex virus thymidine kinase

I

IAA *iodacetamide*

ICTV *international Committee of the Taxonomy of Viruses*

IF *immunofluorescence*

IGC *interchromatin granule cluster*

IgG *immunoglobulin G*

ILI *influenza-like illness*

IP *immunoprecipitation*

ITR *inverted terminal repeats*

K

kbp *Kilobase pair*

KCl *potassium chloride*

kDa *kilodalton*

KH_2PO_4 *Potassium dihydrogen phosphate*

KOAc *Potassium acetate*

KSHV *Kaposi's sarcoma herpesvirus*

L

l *liter*

L2 *minor capsid protein L2*

LANA *latency-associated nuclear antigen*

LB medium *lysogeny broth medium*

M

M *molar*

mA *milliampere*

MDa *megadalton*

min *minute*

ml *milliliter*

MLP *major late promoter*, *major late promoter*

MLTU *major late transcription unit*

mm *millimeter*

mM *millimolar*

$MnCl_2$ *Magensium chloride*

MOI *multiplicity of infection*

MRN *Mre11-Rad50-Nbs1*

mRNA *messenger RNA*

N

Na_2HPO_4 *di-Sodium hydrogen phosphate*, *di-Sodium phosphate*

NaAc *Sodium acetate*

NaCl *Sodium chloride*

NaH_2PO_4 *Sodium phosphate monobasic monohydrate*

NaOH *Sodium hydroxide*

NEM *N-ethylmaleimide*

ng *nanogram*

NiNTA *Nickel-Nitrilotriacetic acid*

NLS *nuclear localization signal*

nm *nanometer*

NP-40 *Nonident P-40*

NPC *nuclear pore complex*

O

OD *optical density*

ori *origin of replication*

P

P *Proline*

p.i. *post-infection*

p.t. *post-transfection*

PAR *poly-ADP-ribose*

PARP1 *Poly [ADP-ribose] polymerase 1*

PBS *Phosphate buffered saline*

PBS-T *PBS-Tween-20*

PCAF *p300/CREB-binding protein-associated factor*

pcc *Pearson correlation coefficient*

PCR *polymerase chain reaction*

PEI *Polyethylenimine*, *polyethylenimine*

PFA *paraformaldehyde*

PK *Proteinase K*

PML *Promyelocytic leukemia protein*

PML-NB *PML nuclear body*

pmol *picomol*

PMSF *phenylmethylsolfonyl fluoride*

pp71 *71 kDa upper matrix phosphoprotein*

Pro *Proline*

Q

qPCR *quantitative PCR*

R

R *arginine*

Rb *Retinoblastoma*

$RbCl_2$ *Rubidium chloride*

RC *replication center*

rev *reverse*

RGD *arginine-glycine-aspartate*

RI *respiratory illness*

RIPA *radioimmunoprecipitation assay*

RNA *ribonucleic acid*

rpm *revolutions per minute*

RT *room temperature*

RT-qPCR *reverse transcription quantitative PCR*

S

SAF *nuclear scaffold attachment factor*

SAP *SAF, acinus, PIAS*

SARI *severe acute respiratory infection*

SDS *sodium dodecyl sulfate*

SDS-PAGE *SDS-polyacrylamide gel electrophoresis*

sec *second*

Ser *Serine*

shRNA *short-hairpin RNA*

SIM *SUMO interacting motif*

Sp100 *speckled protein 100 kDa*

SPT *Ser/Pro/Thr*

SR protein *serine/arginine-rich proteins*

ss *single-stranded*

STUbL *SUMO-targeted ubiquitin ligase*

SUMO *small ubiquitin-like modifier*

SV40 *simian virus 40*

SWI/SNF *SWItch/Sucrose Non-Fermentable*

T

T *thymine*

TBP *TATA-binding protein*

TCA *Trichloroacetic acid*

Thr *Threonine*

TK *thymidine kinase*

TP *terminal protein*

Tris *Tris(hydroxymethyl)aminomethane*

U

U *units*

UBL *ubiquitin-like protein*

Usp7 *ubiquitin specific protease 7*

UV *ultraviolet*

UXP *U exon protein*

V

V *volt*, *Valine*

v/v volume per volume

VA RNA *virus-associated RNA*

vDNA *viral DNA*

VEGF *vascular endothelial growth factor*

vRNA *viral RNA*

W

w/v *weight per volume*

WB *Western blot*

wt *wild-type*

X

x*g* *times gravity*

Y

Y *Tyrosine*

List of Tables

Table 1: Human mastadenoviruses grouped according to their hemagglutination group, types, associated disease, receptor binding and oncogenic potential (GenBank (http://www.ncbi.nlm.nih.gov/Taxonomy/)) 6

Table 2: Bacteria strain with genotype and reference. 27

Table 3: Mammalian cell lines with database number, genotype and reference. 27

Table 4: Human Adenovirus strains with data base number, genotype and reference. ... 28

Table 5: Oligonucleotides used in this study with data base number, sequence and purpose indicated. 29

Table 6: List of vectors used for subcloning and transfection experiments. 31

Table 7: Used recombinant plasmids with database number, application and reference. 31

Table 8: Primary antibodies used in this study. 32

Table 9: Secondary antibodies used for western blot analysis. 34

Table 10: Secondary antibodies used for immunofluorescence. 35

Table 11: Standards and molecular weight markers. 35

Table 12: Commercially available enzymes and buffers. 35

Table 13: Commercial systems. 37

Table 14: Chemicals and reagents. 37

Table 15: Laboratory equipment. 42

Table 16: Disposable laboratory equipment. 47

Table 17: Software and databases. 49

Table 18: Composition of LB medium. 51

Table 19: Antibiotic solution. 52

Table 20: TFB-I and TFB-II buffer. 52

Table 21: Composition of PBS. 53

Table 22: Composition of trypan blue solution. 54

Table 23: Composition of TBS-BG 57

Table 24: Composition of PBS-T. 57

Table 25: Composition of P1, P2 and P3 buffer for plasmid-DNA preparation. 59

Table 26: Standard PCR program. 60

Table 27: Buffer used for agarose gel electrophoresis. 61

Table 28: PCR program for viral DNA synthesis. 63

Table 29: Quantitative RT-PCR program. 64

Table 30: CUT&RUN qPCR program for DNA quantification. 65

Table 31: High stringent lysis buffer for whole-cell lysate preparation (RIPA). 66

Table 32: Nonident P-40 (NP-40) lysis buffer for total-cell lysate preparation. 66

Table 33: 5x laemmli buffer. 66

Table 34: 2x laemmli buffer. 67

Table 35: Buffers used for Nickel-nitrilotriacetic acid (NiNTA) precipitation 69

Table 36: Buffers and solutions used for SDS-PAGE. 70

Table 37: Buffers and solutions used for western blotting. 71

Table 38: Immunofluorescence assay buffers and solutions. 72

Table 39: Time-dependent DEK localization during HAdV-wt infection on the basis of pcc calculations. 106

Table 40: Regulation of mRNA production of p53-responsive genes in DEK-negative cells 123

List of Figures

Figure 1: Classification of the family *Adenoviridae*. 5

Figure 2: Human Adenovirus virion structure. 10

Figure 3: Genome organization of HAdV-C5. 11

Figure 4: HAdV productive infection cycle..... 14

Figure 5: SUMO conjugation pathway..... 15

Figure 6: Promyelocytic leukemia nuclear bodies. 17

Figure 7: Protein structure of DEK..... 21

Figure 8: HAdV-wt increases DEK mRNA production. 76

Figure 9: DEK protein levels are upregulated in A549 cells after HAdV-wt infection..... 77

Figure 10: HAdV-wt infection increased DEK protein levels H1299 cells..... 78

Figure 11: DEK levels increase during the course of adenoviral infection in HepaRG cells. 79

Figure 12: Cloning strategy for N-terminally FLAG-tagged DEK..... 81

Figure 13: Verification of elevated DEK expression after transfection of FLAG-DEK. 82

Figure 14: Expression profile of FLAG-DEK in H1299 and HepaRG cells. 83

Figure 15: Overexpression of DEK does not change the amount of viral DNA during productive infection..... 84

Figure 16: DEK increases viral E1A and hexon mRNA production in HepaRG and H1299 cells..... 85

Figure 17: DEK expression increases viral protein levels in HepaRG cells. 86

Figure 18: Viral protein levels are elevated by DEK in H1299 cells. 87

Figure 19: Relative quantification of viral protein levels upon DEK expression in HepaRG and H1299 cells. 88

Figure 20: DEK is a positive factor promoting viral progeny production. 89

Figure 21: DEK partially co-localizes with early viral E1B-55K and PML tracks..... 91

Figure 22: E1B-55K was co-immunoprecipitated with DEK in HAdV-wt infected HepaRG cells..... 92

Figure 23: Prediction of DEK SUMOylation sites. 93

Figure 24: DEK is SUMOylated by E1B-55K during HAdV infection. 95

Figure 25: DEK is interacting with the PML-NB-disrupting early viral protein E4orf43 in HAdV-wt infected cells. 96

Figure 26: DEK localizes in ring-like structures and is recruited to E4orf-3-containing tracks during HAdV-wt infection. 97

Figure 27: DEK is recruited to PML tracks during HAdV-wt infection. 98

Figure 28: DEK localization with E1B-55K is changed during the course of infection. .. 100

Figure 29: Calculation of DEK co-localization with E1B-55K during HAdV-wt infection. 101

Figure 30: DEK co-localizes with E4orf3 until 36 h p.i. 102

Figure 31: Calculation of DEK co-localization with E4orf3 during HAdV-wt infection. ... 103

Figure 32: DEK is recruited to replication center marker E2A during HAdV-wt infection. 104

Figure 33: Calculation of DEK co-localization with viral replication center marker E2A. 105

Figure 34: Replication center marker E2A is a novel interaction partner of DEK. 107

Figure 35: DEK activates gene transcription from viral promoters. 108

Figure 36: DEK is associated to viral promoters during HAdV-wt infection in A549 cells. 110

Figure 37: Interaction of DEK with p300 is abolished during HAdV-wt infection. 111

Figure 38: HAdV-wt infection decreases DEK association with Daxx. 112

Figure 39: DEK depletion does not affect cell viability of A549 cells. 113

Figure 40: The chromatin-associated DEK protein is efficiently depleted in A549 cells after transduction with shRNA. 114

Figure 41: Efficient DEK depletion increases number of PML-NBs in A549 cells. 116

Figure 42: Viral mRNA production is decreased in DEK negative cells. 117

Figure 43: HAdV progeny production is diminished in DEK-negative A549 cells. 118

Figure 44: DEK mediates interaction of early viral E1A with p300. 119

Figure 45: DEK is essential for early viral E1B-55K interaction with tumor suppressor p53. 121

Figure 46: E1B-55K-mediated inhibition of p53 transactivating functions are diminished after DEK depletion. 122

Figure 47: DEK PTM is changed during infection promoting its DNA-binding capacity and viral progeny production. 129

Figure 48: Graphic representation of epigenetic regulation by DEK during HAdV infection. 132

Figure 49: Schematic representation of repressed DEK expression during HAdV infection. 137

Abstract

Human Adenoviruses (HAdV) are non-enveloped double-stranded (ds) DNA viruses with high prevalence. They can cause lytic as well as persistent infections associated with an array of clinical diseases such as gastroenteritis, conjunctivitis, hepatitis, meningoencephalitis, urinary tract infections, and pneumonia. PML-NBs (PML nuclear bodies) are nuclear matrix-associated multiprotein complexes consisting of a variety of proteins involved in several cellular key processes, such as transcription regulation, posttranslational modifications, and DNA damage repair. Studies postulate a key role of PML-NBs in antiviral immune responses. In this connection, the SWI/SNF (SWItch/Sucrose Non-Fermentable) complex consisting of the proteins Daxx and ATRX plays a crucial role during HAdV infection. Our lab reported a repressive function of the Daxx/ATRX complex during HAdV transcription and a significant increase in adenoviral progeny production after knockdown of these host factors.

DEK is a multifunctional protein capable of binding sequence unspecific to DNA and chromatin and thereby actively changes the topology of DNA and regulates active transcription of genes. The function and association of DEK with interaction partners and DNA is highly dependent on its posttranslational modification. This cellular protein was discovered as a novel interaction partner of Daxx, regulating the Daxx/ATRX-dependent distribution of H3.3 and recruiting histone deacetylases (HDACs). Besides its role in epigenetic regulations and gene transcription, DEK is considered to be an oncogenic mediator during human papilloma virus (HPV) and Epstein-Barr virus (EBV) infection. Additionally, DEK overexpression is highly correlated with tumor progression and invasiveness, whereas DEK serves as a prognostic marker for breast cancer and melanoma.

Here we show that after DEK overexpression during HAdV infection, viral mRNA production, protein synthesis and progeny production is increased. DEK was shown to be a regulator of HAdV gene expression by binding to viral DNA and inducing transcription from viral promoters. Early HAdV proteins interact with DEK and modulate DEK posttranslational modification, thereby changing the association of DEK with PML-NBs and the localization of DEK to adenoviral sites of transcription and replication. Additionally, association of DEK with chromatin remodelers and acetylases was shown to be altered upon HAdV infection.

Furthermore, we identified DEK as the missing factor mediating the interaction of early viral oncoproteins with host factors involved in transformation processes in the cell. Under DEK depletion we observed significantly reduced E1A binding to the transcription factor p300 as well as repressed interaction between E1B-55K and the tumor suppressor p53. This results in decreased E1B-55K mediated p53 SUMOylation and thus, insufficient repression of p53-responsive gene activation by HAdV.

Taken together, we provide evidence that DEK is a novel host factor promoting HAdV gene expression and progeny production, representing a potential new target for antiviral therapy approaches. Besides this role on viral gene expression, DEK might be a novel player in virus-mediated transformation of cells.

Zusammenfassung

Bei humanen Adenoviren (HAdV) handelt es sich um unbehüllte DNA-Doppelstrang Viren, die weltweit mit einer hohen Prävalenz verbreitet sind. HAdV verursachen sowohl lytische, als auch persistierende Infektionen und sind mit einer Vielzahl klinischer Syndrome assoziiert, wie Gastroenteritis, Konjunktivitis, Hepatitis, Meningoenzephalitis, Harnwegsinfektionen und Pneumonien. PML-NBs (*PML nuclear bodies*) sind nukleäre, matrixassoziierte Multiproteinkomplexe, die an einer Vielzahl verschiedener Kernprozesse, wie Transkription, posttranslationale Modifikationen und DNA Reparaturmechanismen der Wirtszelle beteiligt sind. In diesem Zusammenhang wurden bis heute zahlreiche virale Proteine identifiziert, die eine gezielte Modulation des PML Proteins oder assoziierter Proteine vermitteln. Hierbei spielen ATP-abhängige, chromatinmodifizierende Multiproteinkomplexe, wie der SWI/SNF (SWItch/Sucrose Non-Fermentable) Komplex aus Daxx und ATRX eine zentrale Rolle. Vorhergehende Studien konnten den Daxx/ATRX Komplex als reprimierenden Wirtszellfaktor identifizieren, was sich durch den signifikanten Anstieg von Virusnachkommenschaft nach gezielter Inaktivierung des Komplexes verifizieren lässt.

DEK ist ein multifunktionales Protein, welches Gentranskription reguliert und sequenzunspezifisch an Chromatin binden kann, was dort aktiv zur Änderung der DNA Topologie führt. Die Funktion, sowie das Interaktom von DEK ist vorrangig abhängig von den posttranslationalen Modifikationen des zellulären Kontrollproteins. Molekularbiologische Analysen haben DEK als einen regulatorischen Interaktionspartner von Daxx identifiziert, wodurch die Verteilung von H3.3 an DNA und die Rekrutierung von Histondeacetylasen (HDACs) moduliert wird. Des Weiteren spielt DEK nicht nur in der Regulierung epigenetischer Vorgänge eine Rolle, sondern fungiert auch als onkogener Mediator während der Infektion mit humanen Papillomaviren (HPV), oder dem Epstein-Barr Virus (EBV). Zusätzlich wird DEK-Überexpression mit Progression und Invasivität verschiedener Tumore in Verbindung gebracht, weshalb die Expression von DEK als Prognosefaktor für Brustkrebs und Melanome dient.

In dieser Arbeit konnte gezeigt werden, dass die DEK Überexpression zu einem Anstieg der viralen mRNA Synthese, Proteinsynthese und der Produktion von Virusnachkommenschaft führt. DEK konnte als ein regulierender Faktor für virale Genexpression identifiziert werden, der aktiv an virale Promotoren bindet und somit die

Gentranskription startet. Frühe virale Proteine interagieren mit DEK und modulieren dessen posttranslationale Modifikationen. Dadurch ändert sich die Assoziierung von DEK mit PML-NBs und dessen Lokalisierung in die Bereiche, in denen virale Transkription und Replikation stattfindet. Zusätzlich ändert sich die Interaktion DEKs mit Chromatinmodulatoren und Acetylasen während der Infektion mit HAdV.

Zusammengefasst konnten wir mit der vorliegenden Arbeit zeigen, dass es sich bei DEK um einen neuen Wirtsfaktor handelt, der die HAdV Genexpression und die Produktion viraler Nachkommenschaft steigert. Auf dieser Grundlage können neue Therapiestrategien gegen HAdV entwickelt werden, die sich gegen DEK als Zielmolekül richten.

Zudem konnten wir im Laufe unserer Studien DEK als das fehlende Bindeglied identifizieren, welches die Interaktion früher viraler Proteine mit Wirtszellfaktoren vermittelt, die nicht nur in der Transkriptionsaktivierung, sondern auch in der virusinduzierten Transformation durch adenovirale Onkoproteine eine Rolle spielen. Durch klassische Interaktionsstudien in DEK-negativen Zellen konnte gezeigt werden, dass die Interaktion von E1A mit p300 wie auch die Interaktion von E1B-55K mit p53 von DEK abhängig ist. Dies resultierte in verminderter posttranslationaler Modifizierung des Tumorsuppressors p53, wodurch die Repression der p53-vermittelten Transkription durch E1B-55K beeinträchtigt wird. Auf Grundlage dieser Ergebnisse kann angenommen werden, dass DEK nicht nur eine Rolle bei der Transkription viraler Gene und Produktion der Virusnachkommenschaft spielt, sondern auch ein Verbindungsglied in der virusvermittelten Onkogenese darstellt.

1. Introduction

1.1. Adenoviruses

1.1.1. Virus Classification

Adenoviruses (AdV) were first described by Rowe and colleagues in 1953, while searching a new cytopathogenic and causative agent of an epidemic acute respiratory disease [1, 2]. Initially, they were named '*adenoid degeneration agent'* (A.D. agent) after the tissue they were isolated from, the human lymphadenoid tissue, which undergoes spontaneous degeneration upon infection [1]. Further notations were proposed according to their clinical appearance, such as *respiratory illness* (RI) and *adenoidal-pharyngeal-conjunctival* (APC), until they were summarized due to their shared properties and named a*denoviruses* in 1956 [3]. The family of *Adenoviridae* infects a broad range of vertebrates and consists of six genera categorized depending on their host specificity. *Atadenovirus*, isolated from avian, reptilian and ruminant hosts, comprise a rarely high amount of A + T bases [4]. *Mastadenoviruses* infect mammals [4], while *Siadenoviruses* [5, 6] infect amphibians and *Aviadenoviruses* were isolated from birds [4]. The genus of *Ichtadenovirus* infects fish hosts with a single known AdV type [7]. Furthermore, a new sixth genus of *Testadenovirus* isolated from tortoise was proposed; however, the full genome has not been amplified completely and with the missing characteristic of the genera, the novel *Testadenovirus* has not been approved until now [4-10]. The group of human-pathogenic Adenoviruses (HAdV) belong to the genus *Mastadenovirus*, which has been clustered into seven distinct species from A–G (Figure 1, p. 5) [11, 12].

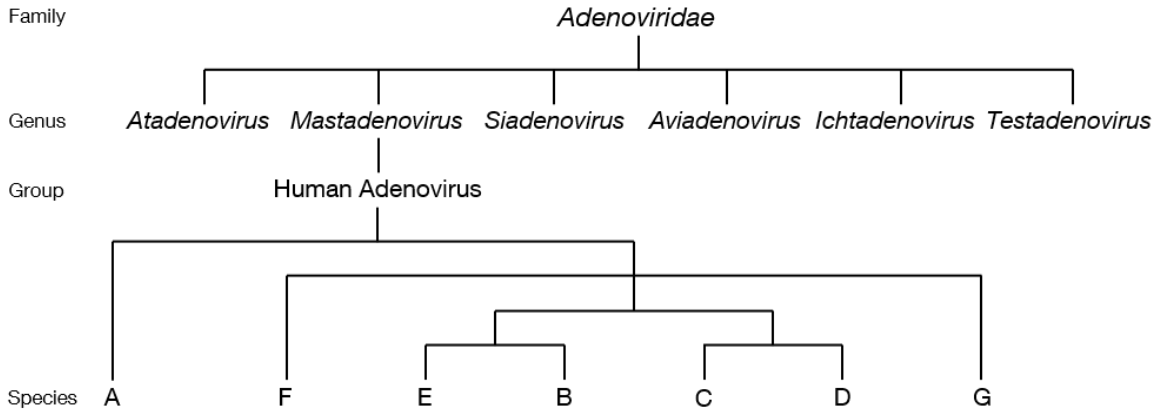

Figure 1: Classification of the family *Adenoviridae*. Illustration of the phylogenic tree showing the taxonomy of *Adenoviridae* classified according to Davison et. al. [8, 9, 11] and the International Committee of the Taxonomy of Viruses (ICTV).

Table 1: Human mastadenoviruses grouped according to their hemagglutination group, types, associated disease, receptor binding and oncogenic potential (GenBank (http://www.ncbi.nlm.nih.gov/Taxonomy/)) [5, 10, 13-16].

Species	HG*	Types	Associated disease	Receptor	Oncogenic potential
A	IV	12, 18, 31, 61	Cryptic enteric infection	CAR	++
B	I	B1: 3, 7, 16, 21, 50, 66, 68 B2: 11, 14, 34, 35, 55, 79	Conjunctivitis, acute respiratory disease, hemorrhagic cystis, central nervous system, myocarditis	CD46, DSG-2	+
C	III	1, 2, 5, 6, 57, 89	Endemic infection, respiratory symptoms, myocarditis	CAR	-
D	II	8-10, 13, 15, 17, 19, 20, 22-30, 32, 33, 36-39, 42-49, 51, 53-56, 58-60, 62-65, 67, 69, 70, 73-75, 85	Keratoconjunctivitis in immunocompromised patients	CAR, Salicylic acid, GD1a (37)	- types 9/10 ++
E	III	4	Conjunctivitis, acute respiratory disease	CAR	-
F	III	40, 41	Infantile diarrhea	CAR	-
G	Unknown	52	Gastroenteritis	Unknown	-
Unclassified	Unknown	72, 76, 77, 78, 81, 86	Unknown	Unknown	Unknown

*HG = Hemagglutination group; ++ highly oncogenic, + oncogenic, - not oncogenic

HAdV serotypes 1–51 were classified by serotyping based on their agglutination and serum neutralization properties with human serums until 2007 [11, 12, 17]. Further classification methods were developed and until now over 80 human-pathogenic AdV types have been approved and according to the *Human Adenovirus Working Group* already 103 genotypes have been assigned (http://hadvwg.gmu.edu/) [16, 18]. The assignment of those types was based on electrophoretic mobility of virion proteins, phylogenetic distance of the adenoviruses, nucleotide composition (GC-content), number of VA RNAs (virus-associated RNAs), their oncogenic potential in rodents and mainly through bioinformatic analyses of

genome organization, whereas the term ‘serotype’ was replaced by ‘type’. Homologous recombination (HR) and mutations are the major cause of the genetic variations within HAdV genomes. In immunocompetent as well as in immunocompromised patients sequential and concomitant HAdV infection from the same and different species were detected. Furthermore, sequencing of HAdV-A, -B and –D and bioinformatic analyses proposed the possibility of recombination of distinct HAdV types [19-23]. Comparison of the DNA sequence data for the inverted terminal repeats (ITR), E1A, E2A, E3B, major late promoter (MLP), hexon, protease and fiber were applied to construct a phylogenetic tree, unravelling a varying evolutionary process for HAdVs infecting the gastrointestinal tract from types, which cause respiratory diseases. The sequence analyses revealed a more striking change in hexon, fiber and especially in E3A genes, certainly associated with pathogenicity of the various HAdV types (Table 1, p. 6) [6, 15, 19, 20, 22, 24, 25].

1.1.2. Adenoviral Pathogenicity

HAdV are found as the causative agent of diseases worldwide, which infect a wide range of vertebrates with a high prevalence and lead to a great variety of sporadically and epidemically occurring clinical syndromes [26-28]. Infection with HAdV takes place in different age groups and the distinct types display different organ tropism, which influences, besides the geographic area, the disease severity. They mainly infect epithelial cells and lymphatic tissue of the respiratory or gastrointestinal tract, the urinary bladder and the eye, causing acute lytic as well as persistent infections [17]. HAdV types 1, 2, 5 and 6 of the species C were shown to be the most common with a level of endemic infection with around 80% of the human population. During an asymptomatic persistent infection, virions are shed in feces, while reactivation of latent viruses in mucosa-associated lymphoid tissue goes alongside with viral RNA transcription, DNA replication and the production of infectious progeny virions [29, 30]. Acute human AdV infection establishes various clinical syndromes, such as acute respiratory diseases with influenza-like illness (ILI) or severe acute respiratory infection (SARI), primarily caused by types of the species HAdV-B, -C and –E [31-36]. During a two decade survey from 1981 to 2001, AdV types 3, 4 and 7 were the most common types inducing respiratory diseases with a striking majority of 79% of patients under the age of 7 years and nearly half of the cases developing severe infections, such as pneumonia and acute bronchitis [31]. HAdV were shown to be the second most common cause of acute respiratory tract infections in hospitalized children resulting in necrotizing bronchitis and bronchiolitis with abundant typical adenoviral inclusion nuclear cells and diffuse alveolar damage [37]. Furthermore,

HAdVs, especially of species –B and –C, cause acute myocarditis outbreaks with an association of type 5 and type 3 with fatal cases and sudden death in childhood due to uncontrolled inflammatory responses [38-40]. Additionally, adenoviral infections of the central nervous system (CNS) by species HAdV-B include syndromes like cerebellitis and meningitis [41], while HAdV-D are the causative agent of a severe form of the highly contagious epidemic keratoconjunctivitis (EKC) with a significant high morbidity [18, 42]. Enteric HAdVs, like HAdV-F40, -F41, the HAdV-E52 and types of HAdV-A, are associated with acute gastroenteritis, where in one out of five [43] pediatric patients it is associated with life-threatening diseases and clinical syndromes, such as watery diarrhea, vomiting, low grade fever and mild dehydration, infrequently accompanied with respiratory infections and keratoconjunctivits [25, 34, 44-46]. However, recent publication suggest a crucial role of non-enteric viruses HAdV-B3, -C1 and –C2 in acute gastroenteritis as shown in infected children with diarrhea in Chiang Mai, Thailand (Table 1, p. 6) [47]. Intriguingly, recent studies propose a connection of HAdV type D36 with non-inflammatory conditions. Serological meta-analysis of 5739 subjects demonstrate the potential of HAdVs in diabetes and obesity [48, 49].

In immunocompetent patients, HAdVs can cause a mild non-febrile self-limiting local infection, however, there were also reports of severe and lethal cases of infection [38, 46, 50]. Globally, most human diseases caused by HAdV are connected to types –C1, -C2, -C5, -B3, -B7, -B21, -E4 and –F41 [19]. In immunosuppressed patients, such as acquired immunodeficiency syndrome (AIDS) patients, bone marrow transplant (BMT) recipients, allogeneic hematopoietic stem cell or solid organ transplant recipients and patients receiving radio- and chemotherapy, HAdVs cause severe life-threatening infections with clinical syndromes like encephalitis, hepatitis, pneumonia, hemorrhagic cystitis and gastroenteritis alongside a strikingly high morbidity and mortality rate of up to 82% (Table 1) [19, 51-57]. The most commonly reported HAdV types in immunocompromised patients are HAdV-A12, -A31, -B3, -B11, -B16, -B34, -B35, -C1, -C2 and –C5 and in most cases HAdV-C types cause severe complications [13, 58]. Those infections seem not to circulate seasonally with epidemics in winter and early spring, as it is for immunocompetent patients, but are revealed throughout the year. This indicates a reactivation of a persistent adenoviral infection in immunosuppressed patients due to their comprised immune system, rather than newly acquired infection. However the mechanism underlying is still unknown [29, 30, 59].

Moreover, in 1962, HAdV-A12 was the first human adenovirus assumed to be oncogenic, since it was the first HAdV shown to induce malignant tumors in rodents [60]. Over the years, further adenovirus types were identified inducing tumors in animals. While types of the species C, E, F and G were shown to be not oncogenic, species A is highly oncogenic inducing undifferentiated fibroadenomas and species B was shown to be oncogenic leading to undifferentiated retinoblastomas. Although, most types of species do not display an oncogenic potential, types –D9 and –D10 are highly oncogenic inducing mammary tumors in female rats (Table 1, p. 6) [15]. HAdV DNA from species B and D can be detected in different pediatric brain tumors, while DNA of species C is predominantly detected in infiltrating T-lymphocytes of distinct human sarcomas [61, 62]. However, it remains still unclear, whether HAdV can induce tumor development in human individuals. Nevertheless, to answer this question is of high importance, since HAdV types are used in clinical vector development for gene delivery and to design oncolytic viruses [15, 63].

1.1.3. Laboratory Diagnosis and Treatment

Identification and typing of HAdV is done by molecular methods. Virus isolation in cell culture, antigen detection and serology are performed in daily use to detect HAdV species. Further methods used in diagnostic laboratories are enzyme immunoassays (EIA), one-day rapid culture assay, in-situ hybridization, quantitative real-time PCR, tissue histopathology, PCR and multiplex PCR-microsphere flow cytometry [17, 64-72]. However, detection methods of HAdV are in certain cases not sensitive enough, whereby patients receiving immunosuppressive drugs, e.g. as part of allogeneic hematopoietic stem cell or solid organ transplantation, can experience reactivation of a HAdV infection [30, 59]. Currently, there is no adenovirus vaccine for the general public nor specific treatment available. HAdV infections are treated symptomatically and with an administration of anti-viral drugs, such as cidofovir and ribavirin. However, this treatment was shown to only have modest efficacy and to be very toxic [73, 74]. Cidofovir is used to treat HAdV in immunocompromised patients and was identified as the most promising drug [75-77]. Nevertheless, cidofovir accumulates intracellularly leading to nephritis and has a low bioavailability, where >90% of the drug is not metabolized and excreted via the urine [78, 79]. This underlines the emerging need to develop new detection methods, specific anti-adenoviral drugs and novel treatment options.

1.1.4. Structure and Genome Organization

Human adenoviruses are large non-enveloped viruses with a icosahedral capsid of 80–110 nm and a mass of ~150 MDa [80, 81]. The viral capsid is constructed of 252 capsomers: 240 hexon (II) trimers and 12 fiber (IV) trimers projecting from the penton base (II) at the vertices of the virus (Figure 2, p. 10) [24, 82-84]. The non-covalently linked fibers are responsible for the virus characteristic structure (spikes) and mediate via the C-terminal fiber knob the absorption and internalization of the virus via the primary host cell Coxsackie / Adenovirus receptor (CAR) [85, 86]. Furthermore, desmoglein 2 (DSG-2) [87] and CD46 were identified as the primary high-affinity receptors used by HAdV of species B [88, 89]. As low-affinity attachment sites serve negatively charged sialic acids on the cell surface and the heparin sulfate-containing proteoglycans (HSPG) of the extracellular matrix (ECM) (Table 1, p. 6) [90]. However, binding receptors of HAdV-F40, -F41 are not identified until now. Additionally, for efficient uptake of the virus via clathrin-mediated endocytosis, the penton base containing a conserved Arg-Gly-Asp (RGD) sequence on each of the five loops protruding from the top of the pentameric penton base complex interacts with specific cell surface αv integrins. Intriguingly, the RGD motif is highly conserved, but not among all adenovirus types (HAdV40, -41) [91-97].

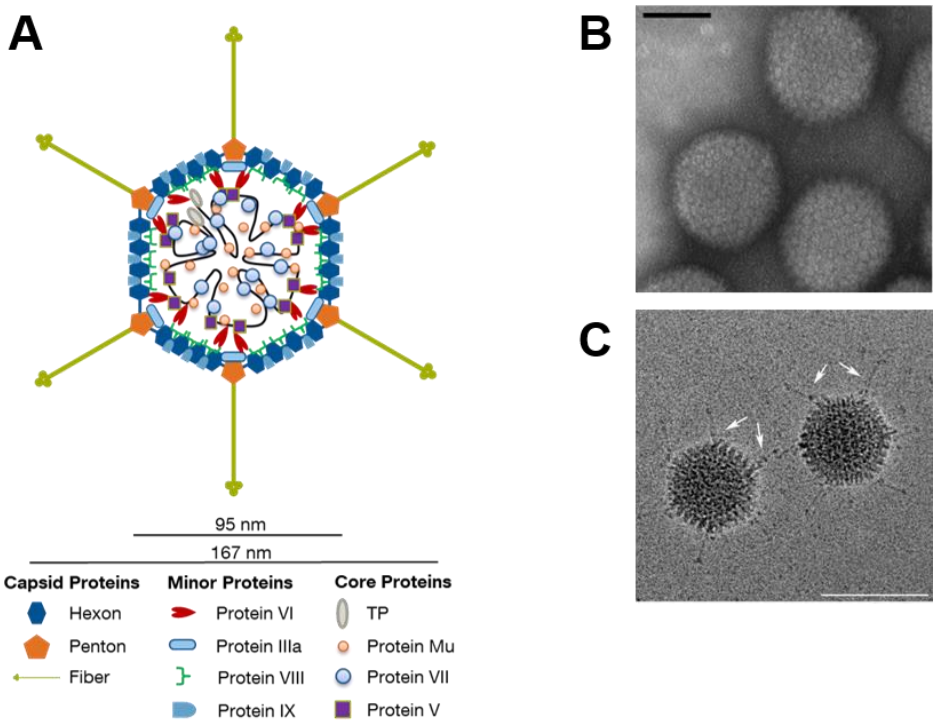

Figure 2: Human Adenovirus virion structure. (A) Schematic cross section of a HAdV virion particle with indication of the proximate localization of the structural proteins. The proteins are represented in different colors and shapes with the corresponding names listed below. The depicted protein distribution is based on X-ray studies (adapted from [83, 98, 99]). **(B)** Electron microscopy image of icosahedral adenoviral particles (scale bar 50 nm) [100]. **(C)** Cryo-electron micrograph of a HAdV-C5. Fibers indicated with white arrows (scale bar 100 nm) [101].

Inside of the icosahedral capsid, HAdV comprise a linear double-stranded (ds) DNA genome, tightly associated with the core proteins V, VII and Mu due to their basic character promoting the nucleoprotein formation [15, 102]. The adenoviral genome is around 26–45 kbp and flanked by inverted terminal repeats (ITR). At each 5' end of the genome, the 55 kDa terminal protein (TP) is covalently linked to the genome, which is essential for DNA replication and serves as a primer for the initiation [11]. Protein pV functions as a bridge between the inner viral core, of which it is part of, with the adenoviral capsid due to its interaction with the 'cement protein' pVI, thereby ensuring spatial organization of the condensed viral genome inside of the icosahedral capsid [99, 102]. Together with the other minor capsid proteins (IIIa, VIII, IX), pVI is incorporated in the adenoviral capsid, which stabilizes the interaction of hexon trimers, pentons and the assembly of virions (Figure 1, p. 5) [99, 103]. Moreover, virions contain a low copy of the protein pIVa2, which is essential for the packaging of the viral genome during assembly of the virion [104], and the viral protease, which is crucial for the maturation of proteins and the escape from endosomes during infection [105].

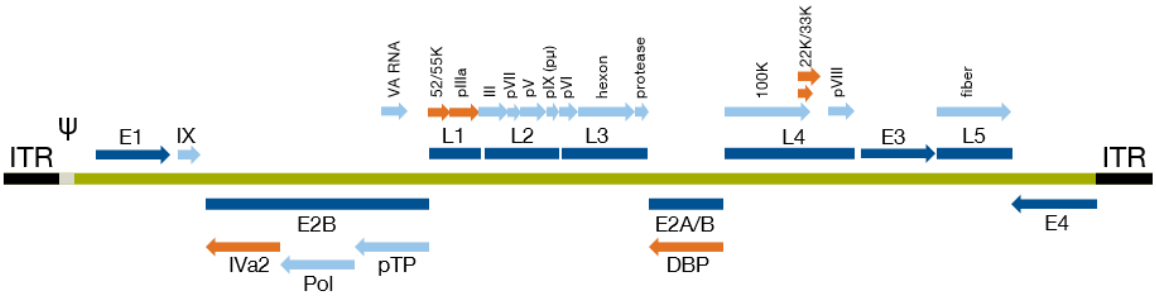

Figure 3: Genome organization of HAdV-C5. Schematic overview of the early (E1, E2A (DBP), E2B (Pol, pTP)), delayed (pIX, IVa2) and late (L1 – L5) transcription units of the viral genome. The viral DNA is shown in green, inverted terminal repeats (ITR) in black, viral packaging sequence (ψ) in grey, early (E1, E2, E3 and E4) and late regions (L1 – L5) are shown in dark blue and proteins involved in packaging are indicated in orange. The arrows represent the expressed proteins with indicated orientation [106].

The minor core protein pVII is the most abundant and tightly associated with the viral DNA. Its N-terminal part shares a high sequence homology with the human histone 3 (H3) [81, 107] and it is proposed that pVII organizes the viral DNA in nucleosome-like structures with 180–200 subunits, the so-called "adenosomes" [108-111]. Thus, pVII induces superhelical condensation of the viral DNA, suggesting a viral histone-like function [112, 113]. The core does not follow a distinct symmetric order, however, pV is proposed to localize in the inter-adenosome spacing and together with pVII and Mu contributes to the condensation of the viral genome. The mature pVII protects the incoming viral DNA from antiviral mechanisms, such as cellular DNA damage response (DDR), and stays tightly bound with the viral genome. It serves as molecule for viral DNA import and as a transcriptional repressor, since

the viral DNA needs to be remodeled and unwrapped from pVII to ensure viral gene expression and efficient DNA replication [114-117].

The HAdV genome is flanked by the ITRs at each 5' end, which ranges from 36–200 bp in size. The terminal 18 bp of the ITR serve as a origin of replication (ori) [118, 119]. Next to the left ITR, there is a cis-acting packaging sequence (ψ) located, coordinating the proper packaging of the genome into the newly synthesized virions [120]. The genome is organized in ten transcriptional units encoding for 40 structural and regulatory proteins, as well as two non-coding virus-associated RNAs (VA RNAs) [11]; the five early: E1A, E1B, E2 and E3; the intermediate early: IX, IVa2, E2 late; and the major late transcription unit (MLTU) regulated by the major late promoter (MLP), which encodes for structural proteins (Figure 3, p. 11) [106]. There is no onset of late gene transcription until the initiation of viral DNA replication. The primary transcript results in five late mRNAs (L1 – L5) after processing. Except for IVa2, which is synthesized by the RNA polymerase III, all units of the HAdV genome are transcribed by the viral DNA-dependent RNA polymerase II (Pol II) [80, 121]. Additionally, a late l-strand transcription unit encoding the U exon protein (UXP) has been identified recently [122, 123]. All transcripts generated by Pol II produce multiple mRNAs, either due to alternative splicing or by use of different polyadenylation sites [124].

1.1.5. Adenoviral Productive Infection Cycle

The HAdV productive infection cycle can be divided into two phases, the early and late phase (Figure 4, p. 14). During early phase of infection, the entry of the virus particle is initiated by receptor-mediated internalization via clathrin-mediated endocytosis. Afterwards, the clathrin vesicles maturate to endosomes with the virus capsid located inside [125, 126]. Virus escape from the endosome sets in through the loss of the peripentonal hexons, IIIa, VIII, IX, whereby the capsid disassembly causes an acidic pH and the release of protein VI, which functions as a membrane lytic factor permeabilizing the endosomal membrane [125, 127, 128]. The partially released viral genome is then transported to the nucleus using microtubule-dependent motor complex dynein / dynactin and attaches to the nuclear pore complex (NPC) leading to the import of the viral DNA into the nucleus [127].

Following the viral entry and the translocation of the viral genome, the viral capsid protein pVI counteracts the restrictive function of Daxx, thereby mediating the transcription of the "immediate early" genes with E1A as first transcription unit to be expressed [129, 130]. The viral transactivating E1A protein induces the expression of early transcription units E1–E4,

whose gene products are alternatively spliced to generate a wide array of early viral proteins that are capable of building a proviral microenvironment to promote efficient viral replication and growth. E1A gene products -12S and -13S regulate the cell cycle control to induce transition to the S phase of the host cell by inhibiting the cellular protein Retinoblastoma (Rb), whereas the E2F transcription factor is activated [130-133]. E1A is associated with distinct chromatin remodeling factors and transcriptional modulators, including histone acetyltransferases and histone deacetylases [134-136]. Additionally, E1A is not merely able to activate viral transcription, but to modulate host cell transcription as well. Therefore, p53 is stabilized and accumulated in the host cell nucleus due to E1A gene products, which, as a consequence, would induce apoptosis of the host cell [137]. However, to inhibit E1A-induced apoptosis and to stimulate cell proliferation, early viral oncoproteins E1B-19K and -55K inactivate the tumor suppressor p53 [138-144]. In cooperation with E4orf6, E1B-55K assembles a Cullin-based E3 ubiquitin ligase complex and targets various host restriction factors, such as p53, for proteasomal degradation [145, 146].

Subsequently, the early viral transcription units E2A and E2B, which encode for the DNA-binding protein, viral DNA polymerase and the terminal protein (TP), respectively, are transcribed. Those proteins are essential for DNA replication, since E2A possesses unwinding activity of DNA and binds both to ssDNA and dsDNA to promote strand displacement during elongation inhibiting degradation of the viral DNA. Therefore, E2A is considered to be a marker for viral replication centers (RCs) [147].

The early viral regulatory protein E3 counteracts various antiviral defenses of the host organism, such as apoptosis, growth arrest or immune response to ensure viral replication [80]. Additionally, E3 products abolish expression of MHC class I molecules to modulate and repress the host immune response [148].

The E4 region encodes for at least six different products transcribed from several open reading frames, namely E4orf1, E4orf2, E4orf3, E4orf4, E4orf6 and E4orf6/7, which mediate essential functions during efficient virus replication, such as inhibition of apoptosis and DNA damage response (DDR) [149-152].

Late phase of the lytic infectious cycle starts with transcription of the major late transcription unit (MLTU) from the major late promotor (MLP). Transcription is activated by the delayed proteins IX and IVa2 after the onset of the viral replication. The synthesized 29

kb pre-mRNA results in five families of mRNA (L1 – L5) by alternative splicing, that encode mainly for structural proteins of the icosahedral capsid like fiber and hexon [153-155]. All five groups of the processed mRNAs share the same 5'-non-coding end, the so-called tripartite leader (TPL), which is crucial during late phase of infection. Cellular protein biosynthesis is shut-off during late stages of infection through inhibiting the transport of the host mRNA into the cytoplasm, while selective export of viral mRNA and enhanced viral protein synthesis is promoted [156, 157]. Following protein synthesis, structural proteins are imported back into the nucleus, where the assembly of progeny virions and packaging of viral DNA takes place, conducted by late (L4-100K, L4-33K, L4-22K) and early regulatory (E1B-55K, E4orf6, E2A) proteins. Maturation of the structural proteins is triggered through the cleavage of the C-terminal part by the adenoviral protease. Viral life cycle is completed after 24–36 h p.i. and up to 10^4 progeny virions are released by cell lysis [158].

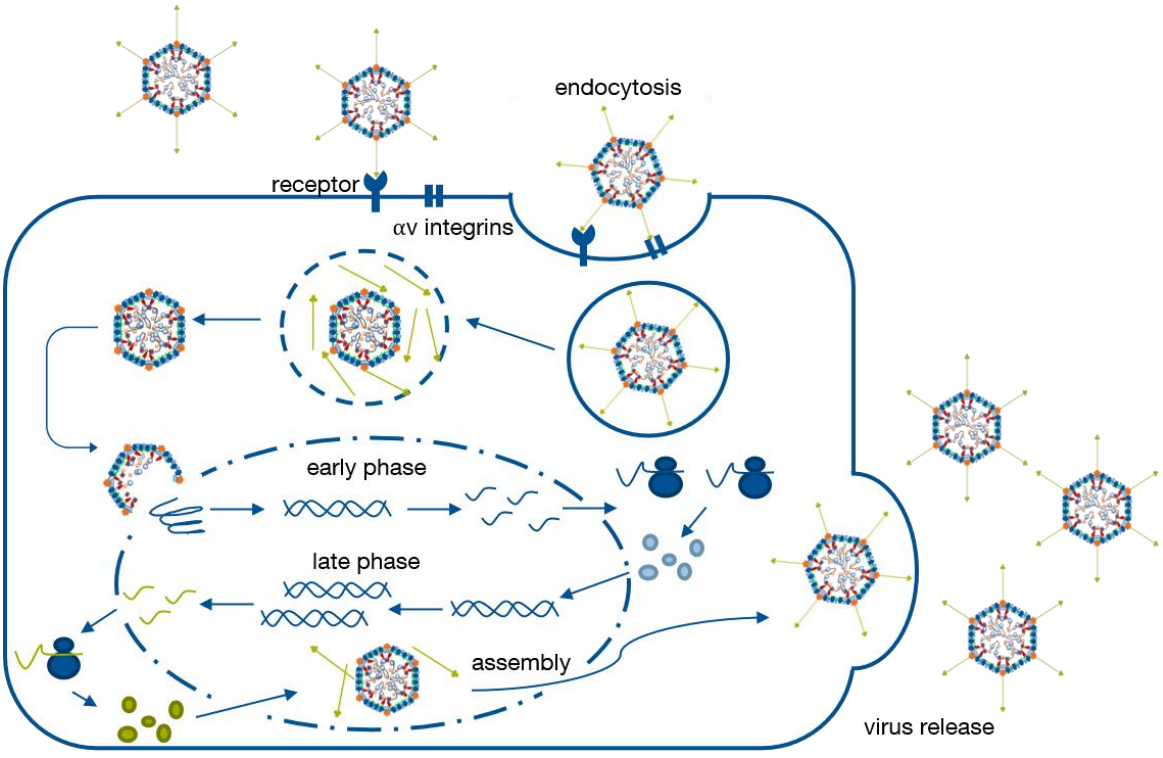

Figure 4: HAdV productive infection cycle. Schematic representation of the early and late phase of adenoviral life cycle. Adapted from [159].

1.2. The SUMOylation Pathway and Promyelocytic Leukemia Nuclear Bodies

1.2.1. SUMO Conjugation Pathway

Small ubiquitin like modifiers (SUMO) are 11 kDa polypeptides that are covalently linked to proteins analogous to ubiquitinylation [160]. Although SUMO proteins share only approximately 18% sequence identity with ubiquitin, their tertiary structure and the molecular pathway of covalent attachment is highly similar, thus SUMO proteins belong to the family of ubiquitin-like proteins (UBLs). In mammals, five different paralogues of the SUMO protein are known to be expressed, namely SUMO-1 to SUMO-5 [161, 162]. SUMO-2 and SUMO-3 share an identity of nearly 95% and are capable of building protein chains through an internal SUMO conjugation motif, SUMO-1 is functionally distinct and shares only 50% sequence identity with SUMO-2/3 [163]. In contrast, SUMO-4 shares a sequence similarity of 87% to the SUMO-2 protein. Additionally, the *sumo-4* gene contains no introns indicating that SUMO-4 might be a pseudogene of SUMO-2 [164]. SUMO-5 was recently identified as a species- and tissue-specific novel isoform regulating the formation and disruption of PML-NBs as well as the recruitment of PML-NBs components [161].

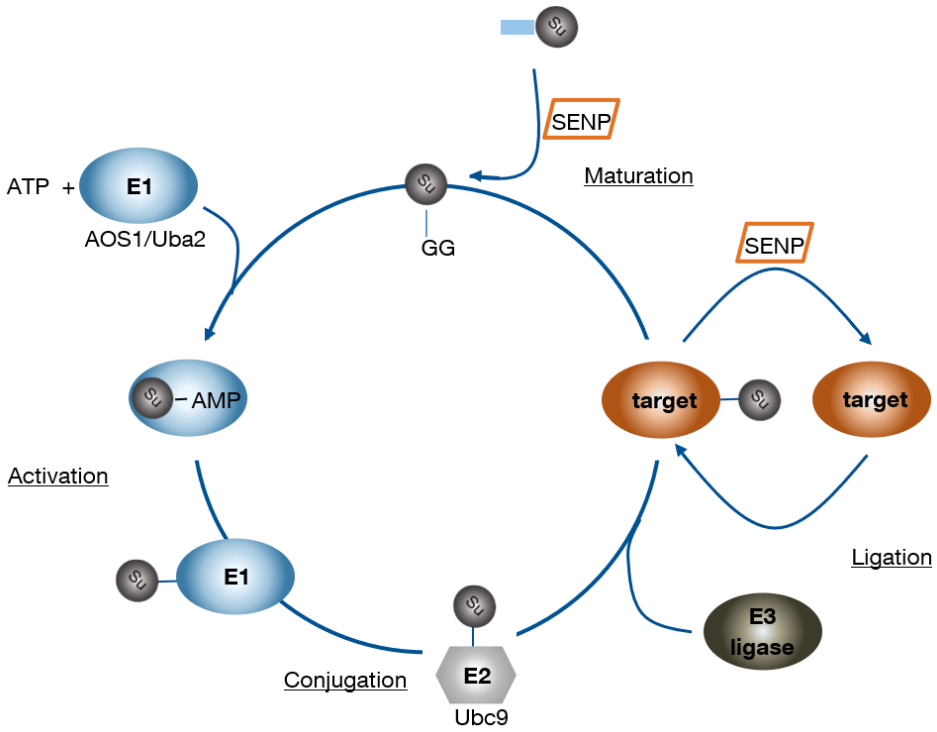

Figure 5: SUMO conjugation pathway. Schematic representation of the three-step enzymatic SUMO conjugation pathway. The SUMO precursor proteins are maturated by SENPs, followed by activation by AOS1 and Uba2 in an ATP-dependent manner. SUMO is conjugated to the E2 enzyme Ubc9. The SUMO E3 ligase recruits the cognate target protein and mediates the ligation of the SUMO protein. DeSUMOylation occurs due to cleavage by SENPs. Adapted from [165].

Covalent attachment of the SUMO proteins is mediated by a three-step enzymatic pathway similar to ubiquitinylation (Figure 5, p. 15). First the inactive precursor SUMO protein is processed by so called SUMO specific proteases (SENPs) exposing a di-glycine motif, which is essential for the attachment to the lysine residue of the target protein [166, 167]. The maturated SUMO protein is then activated in an ATP-dependent manner via the E1 enzyme, a heterodimer of the SUMO-activating enzymes AOS1/Uba2, including the formation of a thioester bond between the active-site cysteine residue of SUMO activating enzyme 2 and the C-terminal glycine residue of SUMO. Subsequently, SUMO is conjugated to the active site cysteine of the conjugating enzyme Ubc9 (ubiquitin-conjugating 9), which mediates the recruitment of the target proteins [165, 168-171]. Finally, SUMO is covalently attached to the cognate target protein through an isopeptide bond between the terminal glycine group and the ε-amino group of the targets lysine residue by the E3 ligase at the consensus motif ψKxD/E (where ψ is a large hydrophobic residue and x represents any amino acid). The SUMO conjugation pathway can be reversed by SUMO specific endopeptidases, therefore SENPs are necessary for initiation of the SUMO pathway and deconjugation of the SUMO [165, 172].

Various key processes are mediated by protein SUMOylation, such as subcellular localization, protein partnering, DDR and DNA-binding and transactivation functions of transcription factors, which is crucial to regulate gene expression [173-175]. Additionally, SUMOylation of proteins alters their function, activity and stability and SUMO substrates include many proteins with important roles in regulating cell proliferation and differentiation, as well as nuclear targets of many signaling pathways including TGFβ, Wnt, and cytokines [173-180]. Recent publications suggest that dysregulation of the SUMO pathway promotes tumor proliferation in cells, since knockdown of the E1 activating enzyme induces apoptosis, endoreduplication and senescence with elevated levels of p53 and p21, alongside with disruption of PML-NBs and compromising tumor growth [178, 181, 182].

PML nuclear bodies (PML-NBs) are known to be hotspots for SUMOylation with most of the required pathway enzymes localizing at PML-NBs and 56% of PML-NB-associated proteins being modified by SUMO [165]. Moreover, SUMOylation plays a key role in formation, integrity and composition of PML-NBs [165, 176]. Both, the covalent attachment of SUMO to the SCM as well as non-covalent interaction with the SUMO interacting motif (SIM) of PML and associated proteins is integral for the formation and function of PML-

NBs, since e.g. PML proteins unable to be SUMO-1 modified fail nuclear localization, proper NB formation and recruitment of Daxx [183-186].

1.2.2. Promyelocytic Leukemia Nuclear Bodies

PML-NBs are spherical multiprotein complexes with an average size of 0.2 – 1.0 µm. They are matrix-associated dynamic structures with over 160 proteins located to these domains, either constitutively or transiently depending on different conditions, e.g. transformation, stress, interferon expression or viral infections [165, 187]. PML-NBs, also referred to as PML oncogenic domains (POD) or nuclear domain-10 (ND10), appear as ring-like structures although abundance, composition, structure and function greatly depend on cell type, cell cycle stage and stress response [188-191].

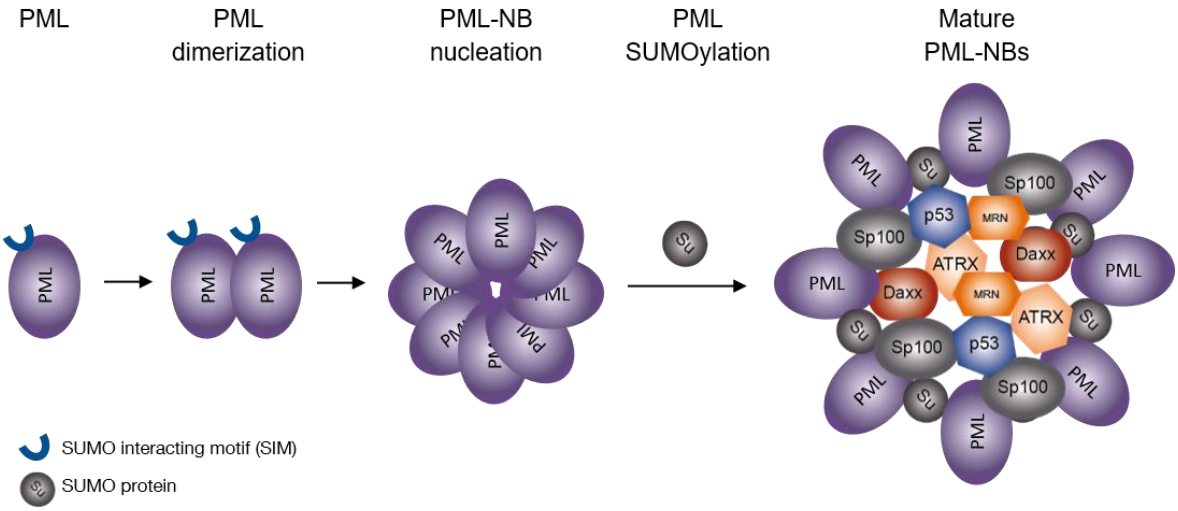

Figure 6: Promyelocytic leukemia nuclear bodies. Formation of PML-NBs starts with dimerization of the PML protein via SUMOylation of its RBCC motif, followed by nucleation and maturation by SUMOylation of PML and the recruitment of nuclear body components via SUMOylation or their SIM (modified from [190]).

The PML protein was first described in acute promyelocytic leukemia (APL) patients, distinguished with the PML gene to be fused to the retinoic acid receptor α (RARα) gene due to a consistent chromosomal translocation of APL, t(15:17) [191]. The consequential oncogenic PML-RARα fusion protein mediates disruption of the nuclear bodies [192, 193] and PML proteins are relocalized from the NBs leading to dysfunction of PML-NBs, their associated proteins and RARα activity. The translocation of the PML gene is considered to be the molecular mechanism underlying in 98% of APL cases [191].

Formation of PML-NBs is initiated by dimerization of PML via its N-terminal RBCC motif prior to multimerization by nucleation (Figure 6, p. 17). The maturation of the nuclear bodies occurs through SUMOylation of PML and the recruitment of associated proteins.

Components of PML-NBs are recruited via the SUMO or SIM of the PML protein into the inner core of the spherical bodies, while the outer rim of the bodies is composed of the eponymous PML protein and the transcriptional modulator Sp100 (speckled protein 100 kDa) [183, 190, 193]. Except for the constitutive protein residents PML, Sp100, chromatin remodeling factor Daxx (death-associated protein), BLM (bloom helicase) and SUMO, PML-NBs are composed of several hundred transient components, such as ubiquitin specific protease Usp7, the transcriptional regulator ATRX, the double-strand break repair protein Mre11, the tumor suppressor p53 and Rb, the heterochromatin protein HP1 and the acetyltransferase CBP (CREB-binding protein) [186, 190, 193-196].

PML-NBs function in various cellular processes by regulating key processes, such as transcription, apoptosis, senescence, response to DNA-damage or resistance to micro-organisms [193, 197-199]. In response to DNA-damage, PMLs are phosphorylated by DNA-damage activated kinases ATM, ATR, HIPK2 or CHK2. Additionally, PML-NBs recruit DDR proteins, such as BLM, WRN, TOPBP1, or MRN complex [198, 200, 201]. Besides DDR, PML-NBs also function in stress response, growth control, and posttranscriptional regulation of gene expression. In cooperation with Daxx and Sp100, PML has a protective role against many viral infections [201-208]. Furthermore, PML plays a crucial role in normal and cancer stem cell fate by modulating the AKT pathway . The current suggestion how PML-NBs function in these key processes, is that they recruit and concentrate essential proteins in nuclear bodies together with many protein-modifying enzymes, whereby they alter their activity, sequestration, or degradation by posttranslational modification, such as phosphorylation, acetylation, ubiquitinylation, and SUMOylation [193, 195, 209].

1.2.3. SUMOylation and PML-NBs during HAdV Infection

HAdV proteins are known to be targeted by PTMs, however adenoviral proteins themselves are also able to exploit the host cell SUMO machinery for their own benefit [210-214]. Modulating PTM of certain host factors by HAdV ensures efficient viral replication and was revealed to be critical for adenoviral infection [215-223]. Besides cellular proteins, also viruses are known to be exposed to PTMs during infection [211, 213, 214, 222, 224, 225]. The early viral transactivating E1A modulates polySUMOylation of Ubc9, thereby affecting PML localization [221, 226-230]. Furthermore, it is suggested that interference with polySUMOylation of proteins could affect SUMO-dependent proteasomal degradation by ubiquitin ligases [192, 220, 231, 232]. Additionally, E1A induces cell cycle arrest in the S phase of the cell and enhances E2F-dependent transcriptional activation by inhibiting Rb SUMOylation [233-236]. Hence, E2F-responsive S phase genes and genes of the

adenoviral E2 transcription unit are starting to be expressed [130, 237-239]. Furthermore, transcriptional activation by E1A is mediated through its interaction with PML-II [240], which is suggested to be crucial for the activation of the transcriptional coactivator p300 by E1A-13S [234, 241, 242].

An adenoviral factor, which is not only known to be SUMOylated, but also to modulate SUMOylation and organization of PML-NBs is the early viral E1B-55K [215, 216, 222]. This multifunctional protein is covalently modified by SUMO-1, -2 and -3 at its lysine residue 104 regulating its functional repertoire [213, 222, 224, 225]. First, this multifunctional protein decreases KAP1 repressing function by attaching SUMO moieties to KAP1 accompanied by dephosphorylation [222]. Moreover, E1B-55K counteracts the restrictive chromatin remodeling Daxx/ATRX complex. Therefore, Daxx is targeted by a E1B-55K-containing E3 ubiquitin ligase for proteasomal degradation [243-245]. A second pathway whereby E1B-55K represses Daxx antiviral function, is the relocalization of Daxx to the insoluble nuclear matrix mediating SUMOylation of Daxx and the subsequent targeting by the SUMO-targeted ubiquitin ligase (STUbL) RNF4 for proteasomal degradation [220]. Additionally, E1B-55K interferes with p53 transactivating properties by SUMOylation of p53 [215, 216, 246] and interaction of E1B-55K with PML-IV and -V [139] as well as repressing Sp100A-mediated activation of p53-responsive activation [247].

Another early viral protein known to modulate components of PML-NBs is E4orf3. Through its interaction with PML-II it disrupts the dot-like localization of nuclear bodies and induces reorganization into track-like structures [248]. Furthermore, E4orf3 SUMOylates host factors, such as Mre11 and Nbs1 of the Mre11-Rad50-Nbs1 (MRN) complex, which initiates relocalization to counteract the repressive cellular DDR [249-251]. Additionally, E4orf3 possesses E4 SUMO elongase activity, whereby it can induce polySUMOylation of host factors, such as TIF1 and TFII-I, with subsequent ubiquitinylation by STUbLs and proteasomal degradation without the involvement of E1B-55K [252].

Just recently, the viral replication center marker E2A was identified as a novel target for SUMO modification facilitating its function and interaction partners. SUMOylation of E2A was shown to be crucial for its interaction with Sp100A suggesting this as the cause for E2A association with PML and localization of viral RCs in close proximity to PML tracks [214].

1.3. Human Adenoviruses and Their Oncogenic Potential

HAdV were suggested to have oncogenic properties, mainly facilitated by the early viral proteins E1A, E1B-55K, E4orf6 and E4orf3. Except for its role in transcriptional transactivation, E1A induces cellular transformation mainly by inactivation of the Rb protein [234, 236, 253-255]. Subsequently, the transcription factor E2F is released activating transcription of S phase genes [130, 237-239]. The uncontrolled cell proliferation is additionally supported by inhibition of the E3 ubiquitin ligase RBX1 and Cullin-1 (CUL1) [256], whereby proteins involved in the cell cycle progression are not targeted for proteasomal degradation anymore. E1A interacts with CBP/p300, whereas it regulates the histone acetyltransferase (HAT) activity of CBP/p300. As a consequence, E1A exploits CBP/p300 to ensure viral transcription, but simultaneously suppresses host gene transcription and p53-mediated activation of p21 to inhibit cell cycle arrest and apoptosis [234, 241, 242, 253, 257-262]. Moreover, E1A interaction with CBP/p300 induces extensive hypoacetylation of histone H3 at lysine residue K18, which is suggested to promote the transforming potential of E1A [235, 241, 263].

One of the functions of E1B-55K mediating cellular transformation is its ability to inhibit the tumor suppressor p53 by transcriptional repression and nucleoplasmic relocalization [139, 141-143, 213, 215, 216, 246, 264-266]. Later during infection, E1B-55K hijacks together with E4orf6 a Culin-5 based E3 ubiquitin ligase to efficiently target p53 for proteasomal degradation [145, 267-271]. A further target of this viral E3 ubiquitin ligase is the chromatin regulator Daxx, however in an E4orf6-independent manner [244, 245]. Additionally, E1B-55K mediates SUMOylation and translocation of Daxx to the nuclear membrane, where the STUbL RNF4 facilitates ubiquitinylation and subsequent proteasomal degradation of Daxx [220]. Previous studies reported, that E1B-55K mutant versions uncapable to silence or degrade such factors like Daxx are lacking their transforming potential [243, 272].

Proteins of the early viral E4 region, E4orf6 and E4orf3, were shown to cooperate together with E1A and E1B-55K to improve their oncogenic potential via acting on protein interactions, PTMs, transcription, DNA damage response, cell cycle control and apoptosis. E4orf3 reorganizes PML-NBs via its interaction with PML-II, mediating the track-like formation during HAdV infection. Moreover, E4orf3 modulates certain PML associated proteins or components of the DNA damage response, such as p53 and Mre11, indicating

its role in oncogenic transformation of cells by HAdVs [135, 145, 149, 208, 218, 223, 244, 249, 250, 252, 267, 273-280].

The mechanism inducing oncogenic transformation by HAdV is suggested to occur via 'hit-and-run'. During this process, there is no integration of the viral genome into the host cell DNA, however transformation is based on the mutagenic potential of the viral oncoproteins E1A, E1B-55K and of the E4 regions. By this means, the viral oncoproteins initiate the transformation without being detectable at later stages of the tumor development [150].

1.4. The Chromatin-Associated Proto-Oncogene DEK

1.4.1. Structure of the Oncoprotein DEK

DEK is a highly conserved protein abundantly expressed in most higher eukaryotes, but not in yeast. The human DEK protein exists in two splice variants, the canonical 43 kDa isoform 1 with 375 aa and the truncated 38 kDa isoform 2 with 341 aa (missing aa positions 49 to 82) [281-283]. Since DEK shares no sequence homologues, it is considered to be the sole protein of its kind. The comprehensive structure of DEK remains elusive, however NMR structures solved the 78-208 aa part of the N-terminus and a C-terminal (309-375 aa) part of DEK [284]. The N-terminal domain of the full-length human DEK protein consists of a helix-turn-helix structure with a pseudo-two fold plane symmetry [284]. It contains a SAF (nuclear scaffold attachment factor)/SAP (SAF, Acinus, PIAS)-domain (amino acids 87–187) with DNA-binding properties for unusual DNA structures like four-way junctions, supercoils and distorted DNA with sequence-unspecificity [284-288]. The pseudo-SAP and SAP domains build the major DNA-binding region of the human DEK protein mediating the structure-specific binding of DEK [284]. Furthermore, a nuclear localization signal (NLS) is located at aa positions 205-221. An additional DNA-binding domain and multimerization site is located at the C-terminal (aa 270-350) part of DEK. It contains a three-helix-bundle with high structure similarity to the E2F transcription factor (Figure 7, p. 21) [289].

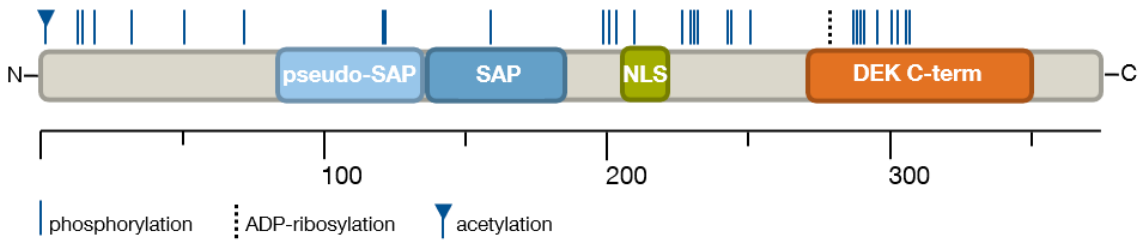

Figure 7: Protein structure of DEK. Schematic representation of the proto-oncogene DEK. Shown is the linear sequence and the functional domains with their location (pseudo-SAP; SAP: SAF-A/B, Acinus and PIAS; NLS: nuclear localization site; DEK C-term:

DEK C-terminal multimerization domain). PTMs of DEK are indicated as follows: blue line: phosphorylation, blue dotted line: ADP-ribosylation, blue triangle: acetylation.

DEK was shown to be highly diverse posttranslationally modified. The most abundant modification of DEK is phosphorylation at serine and threonine residues, which is mostly facilitated by the phosphorylation kinase casein kinase 2 (CK2) with a peak in the G_1 phase of the cell cycle [285, 290-294]. Additional covalent modifications are acetylation, induced by the HAT p300-associated factor PCAF (p300/CREB-binding protein-associated factor) [295-297], and PAR- (poly-ADP-ribose), mediated by poly-[ADP-ribose]-polymerase 1 (PARP1) [285, 290, 298]. Due to the multiple possibilities of PTMs, regulation of DEK is highly diverse and modulates its localization, interaction partners and functions. DEK multimerization is dependent on phosphorylation and ADP-ribosylation of DEK, however phosphorylation of DEK shows low affinity to DNA [285, 290, 294, 299]. Acetylation of DEK by p300 was shown to induce relocalization of DEK from chromatin to nuclear speckles and interchromosomal speckles [296].

1.4.2. Localization and Molecular Function

The nuclear DEK protein was first isolated from AML patients fused to the nuclear pore complex protein NUP214 (previously termed CAN) [300, 301]. The fusion gene is a product of chromosomal translocation of t(6;9)(p23;q34) resulting in an in frame 165 kDa gene product [301-303]. DEK-NUP214 influences protein synthesis in myeloid cells and is used as a prognostic marker in leukemia [293, 304, 305]. Moreover, it was shown that leukemogenesis from hematopoietic stem cells is initiated by DEK-NUP214 fusion protein [306]. Due to the correlation between DEK expression and cell proliferation, it is assumed that DEK is a proto-oncogene [307].

DEK is a non-histone DNA-binding protein, found to be associated with chromatin during all stages of the cell cycle [284]. Therefore, and due to its folding properties, DEK is considered to be an architectural protein involved in the remodeling of chromatin structure [284, 285, 308]. Additionally, DEK mediates changes in DNA topology by inducing positive supercoils in naked DNA promoting the formation of heterochromatin [147, 285, 287, 289, 290, 308-312]. Repression of gene transcription by DEK is also facilitated via its interaction with further chromatin remodeling and transcription factors, such as HP1α and the H3K9-specific histone methyltransferase SUV39H1/2. Loss of DEK induces delocalization of HP1α from chromatin to a nucleosolic fraction, whereas global trimethylation of H3K9 and heterochromatin stability is highly decreased [313]. Moreover, DEK possesses histone chaperone activity and binds to core histones H2A and H2B as well as the histone variant

macroH2A1.1 [292]. Previous studies investigated the role of the association of DEK with a complex of Daxx, histone deacetylase II (HDAC II) and the core histones [309], the co-localization of DEK with acetylated histone 4 chromatin [308], the H3.3 deposition on chromatin dependent on phosphorylation by CK2 and HIRA- and Daxx/ATRX-dependent distribution of H3.3 on chromosomes controlled by DEK. The loading of non-nucleosomal H3.3 to chromatin is inhibited by DEK expression resulting in the relocalization to PML-NBs by Daxx. Depletion of DEK induces a relaxed DNA topology promoting the re-deposition of H3.3 to chromatin in a HIRA-dependent manner and the loading of H3.3 to heterochromatic foci next to PML-NBs mediated by Daxx/ATRX [314].

However, DEK was shown to not only take part in the epigenetic silencing of gene transcription, but also to preferentially interact with active histone marks and be a component of a high molecular weight chromatin remodeling complex, the so-called B-WHICH, that is merely assembled at active transcription sites [315]. Furthermore, DEK interacts with the transcriptional activators AP-2α (activating Enhancer Binding Protein 2α), C/EBPα and MLLT 3 and the association of DEK with histones negatively influence p300 and PCAF-mediated histone acetyltransferase activity and transcription which is leading to H3 and H4 hypoacetylation of chromatin [297, 315, 316]. Therefore, functions of DEK are considered to be controversial and remain not completely understood.

The majority of DEK is found to be bound to DNA, however around 10% is associated with RNA and RNA splicing complexes [317-319]. As already mentioned, PTM of DEK is highly efficient in regulating DEK localization and function. Acetylation of DEK by p300 reduces its affinity to DNA and recruits it to sites considered to be involved in RNA splicing [296]. DEK regulates intron removal by enforcement of 3’ splice discrimination controlled by U2AF. The association of the splicing factor U2AF at AG-rich consensus 3’ splicing sites, instead of non-consensus sites, is mediated by the proofreading activity of DEK [320, 321]. Once more, DEK activity and function is depending on its phosphorylation status, stretching the importance of PTMs on DEK functions.

1.4.3. DEK in Diseases, Cancer Development and Progression

DEK has various role during viral infection, since it is either utilized for viral infection or it can act as a restrictive factor on the replication. For example, recent publications identified a negative impact of DEK on HIV-2 (human immunodeficiency virus 2) by specifically binding to the so-called peri-*Ets* (pets) sites, which are TG-rich upstream promotor elements in the HIV-2 enhancer, silencing HIV-2 transcription [322, 323]. Reduced

replication efficiency was observed for SV40 (simian virus 40) mini-chromosomes as well. Here, DEK changes the DNA topology of the mini-chromosomes of SV40 [281, 312]. A different picture is observed during Kaposi's sarcoma herpesvirus (KSHV) infection. Here, DEK is a pro-viral factor interacting with the latency-associated nuclear antigen (LANA), which enables the link between chromosomes and viral genomes during latent infection [324, 325]. During Epstein-Barr virus (EBV) and human papilloma virus (HPV) infections, DEK is considered to be an oncogenic mediator [325-327]. However, DEK protein levels were shown to be differentially regulated during those viral infections, as it is upregulated during HPV infection. The E7 protein of HPV inhibits Rb, releasing the transcription factor E2F, which activates the expression of the target genes, like e.g. DEK [325, 327-331]. Similar upregulation of DEK is observed in latent EBV infections, since EBV also inhibits Rb activity by hyperphosphorylation. Overexpression of DEK, due to Rb inactivity, blocks senescence and apoptosis of the infected cells [325, 326].

DEK is associated with different roles in human diseases, especially in tumor development and auto-immune diseases, such as the formation of DEK-specific autoantibodies during juvenile idiopathic arthritis [332]. DEK expression is dependent on the cell status of the tissue, since enhanced DEK levels are observed in proliferating cells, while in differentiated and healthy tissue only slight DEK expression is detected [282, 307, 333]. However, in different tumor types including colon cancer [329], bladder cancer [329], melanoma [329, 333, 334], breast cancer [335, 336], ovarian cancer [337], lung cancer [338], retinoblastoma [330] and pancreatic adenocarcinoma [339] a striking increase in DEK mRNA as well as protein levels is reported. Oncogenic potential of DEK was verified by comparison of differentiated and undifferentiated cells in their resistance to DEK depletion [340]. Remarkably, the differentiation of human keratinocytes is correlated with decreased DEK expression, while overexpression of DEK is inducing hyperplasia independently of p53 [341]. Additionally, DEK can function as a restrictive factor for p53 during HPV infection. It inhibits apoptosis and senescence in HPV-positive cervical cancer cells by destabilization and inactivation of p53 with subsequent silencing of p53-responsive genes [327, 328]. In breast cancer DEK recruits the transcription factor HIF-1α (hypoxia-inducible factor 1α) and p300 to the VEGF (vascular endothelial growth factor) promoter, whereby it is considered to be a key mediator of VEGF expression and tumor angiogenesis [342]. Furthermore, motility, growth, stem cell character and invasion of breast cancer cells is induced by DEK expression [343]. Due to the correlation of DEK overexpression with tumor

progression and invasiveness, DEK serves as a prognostic marker for breast cancer and melanoma [333, 336].

1.5. Aim of Study

HAdVs are double-stranded DNA viruses with a high prevalence world-wide. They can induce a variety of diseases such as gastroenteritis, keratoconjunctivitis, pneumonia, meningoencephalitis, hepatitis and infections of the urinary tract as well as kidneys. Typically, infections with HAdV are mild and self-limiting, however immunosuppressed patients and hospitalized children develop fatal infections in up to 82% of cases. Additionally, recent studies indicate new evolving HAdV types causing severe courses of diseases also in immunocompetent patients. In the last years, PML-NBs became one of the main topics focused on during basic virological research, since they modulate the replication cycle of various tumor viruses. In this connection, plenty of early adenoviral proteins were identified to modulate PML-NBs and their associated proteins. Hereby, the multiprotein complex SWI/SNF plays a crucial role in regulating HAdV infection, since Daxx was identified as a restrictive factor of viral gene transcription. However, HAdVs have developed distinct mechanisms to counteract the repressive function of Daxx. Therefore, the early viral protein E1B-55K targets Daxx for proteasomal degradation. A similar strategy is used to inhibit the apoptotic and transactivating properties of the tumor suppressor p53. Thus, HAdVs not only ensure the efficient replication, but can also mediate oncogenic transformation of cells. In this context, the regulation of Rb and p300 by the viral protein E1A has a crucial impact on the oncogenic properties. However, the regulation of viral transcription and virus-mediated oncogenesis still remains elusive. Moreover, until now neither vaccination nor specific therapeutic treatment against HAdV is available.

Recently, the cellular DEK protein was discovered as a novel interaction partner and regulator of the Daxx/ATRX-dependent distribution of H3.3 and recruits HADCs. Additionally, DEK is a DNA-binding protein regulating gene transcription by DNA topology change, histone modifications and recruiting transcription factors. The various functions are highly dependent on its own PTM status, such as phosphorylation, ADP-ribosylation or acetylation, which is e.g. regulated by the acetylase p300. In virological studies, it was already shown that DEK specifically changes the topology of the SV40 minichromosome, supports latency of KHSV and represses HIV promoters. DEK is proposed to be a proto-

oncogene playing a crucial role during oncogenesis, since it destabilizes and inactivates p53 leading to cell death, as shown during HPV infection.

After confirmation of viral transcription regulation by DEK, we investigated the modulation of DEK during HAdV infection to determine the mechanism how DEK promotes HAdV replication. To address this question, we identified changes in DEK PTMs and association with viral DNA as well as with transcriptional regulators. Subsequently, we generated a DEK-negative cell line to monitor viral infection in the absence of DEK. Thereby, we investigated the impact of DEK on functional regulation of early viral proteins. We further aimed to identify DEK regulation of viral transformation processes. In conclusion, the overall aim of this thesis was to unravel the impact of DEK on the molecular mechanism of HAdV gene transcription and its role in virus-mediated oncogenic transformation, to develop novel therapeutic strategies and to improve adenoviral gene vector application.

2. Material

2.1. Cells

2.1.1. Bacteria Strains

The following bacterial strain was used during this study.

Table 2: Bacteria strain with genotype and reference.

Strain	Genotype	Reference
Escherichia coli DH5α	*sup*E44, Δ*lac*U169, (ϕ80d*lacZ*Δ*M15*), *hsd*R17, *rec*A1, *end*A1, *gyr*A96, *thi*-1, *rel*A1	[344]

2.1.2. Mammalian Cell Lines

During this work the following mammalian cell lines were used.

Table 3: Mammalian cell lines with database number, genotype and reference.

Cell line	No.	Genotype	Reference
A549 parental	5	Human lung carcinoma cell line expressing wild-type p53.	[345]
A549 shCTR	103	A549 cells with stable expression of control shRNA.	This work
A549 shDEK	104	A549 cells with stable shRNA mediated depletion of DEK (shRNA:	This work
H1299 parental	15	Human non-small lung carcinoma cell line, p53 negative.	[346]
HeLa-6xHis SUMO-2	7	HeLa cells overexpressing N-terminal 6xHis-tagged SUMO-2.	[347, 348]
HeLa pDEK-6xHis-FLAG	113	HeLa cells overexpressing N-terminal 6xHis-FLAG-tagged DEK.	[291, 349]
HeLa pMIEG	112	HeLa cells transduced with lentiviral vector pMIEG; control cell line	[291, 349]

Cell line	No.	Genotype	Reference
HepaRG	1	Human hepatic progenitor cell line expressing stem cell properties, able to undergo complete hepatocyte differentiation, derived from hepatoma.	[350]
HEK293	16	Human embryonic kidney cell line transformed by HAdV-C5 and stably expressing the HAdV-C5 E1 region.	[351]
HEK293T	8	HEK 293 cell line expressing large T antigen from SV40.	[352]

2.2. Viruses

Table 4: Human Adenovirus strains with data base number, genotype and reference.

Adenovirus	No.	Characteristics	Reference
HAdV ΔE1B-55K	3	H5*pm*4149, HAdV-C5 E1B-55K null mutant, containing four stop codons in the E1B-55K region (aa position 3, 8, 86 and 88).	[353]
HAdV-wt	4	H5*pg*4100, HAdV-C5 wild-type containing an 1863 bp deletion (nt 28602-30465) in the E3 region.	[353]

2.3. Nucleic Acids

2.3.1. Oligonucleotides

The following oligonucleotides were used to perform sequencing, PCR, RT-qPCR, and cloning. All primers were ordered from Metabion (Planegg) and are listed according to the internal *FileMaker Pro* database. Externally provided oligonucleotides are labeled according to the institution providing them.

Table 5: Oligonucleotides used in this study with data base number, sequence and purpose indicated.

Name	No.	Sequence 5' – 3'	Purpose
18S fwd	187	CGG CTA CCA CAT CCA AGG AA	qPCR mRNA
18S rev	188	GCT GGA ATT ACC GCG GCT	qPCR mRNA
366CMVfwd	71	CCC ACT GCT TAC TGG C	Sequencing
675pCMX3Brev	72	CCA ATT ATG TCA CAC CA	Sequencing
DEK fwd	631	TGT TAA GAA AGC AGA TAG CAG CAC C	Sequencing & qPCR [331]
DEK rev	632	ATT AAA GGT TCA TCA TCT GAA CTA TCC T	Sequencing & qPCR [331]
DEK_XhoI_rev	626	ATA CTC GAG TCA AGA AAT TAG CTC	Cloning
E1A fwd	181	GTG CCC CAT TAA CCA GTT G	qPCR mRNA
E1A rev	182	GGC GTT TAC AGC TCA AGT CC	qPCR mRNA
E1Ap fwd	918	TCC GCG TTC CGG GTC AAA GT	CUT&RUN
E1Ap rev	919	GTC GGA GCG GCT CGG AG	CUT&RUN
E1B-55K fwd	323	ATG AGC GAC GAA GAA ACC CAT CTG AGC	qPCR mRNA
E1B-55K rev	324	CGG TGT CTG GTC ATT AAG CT	qPCR mRNA
E1Bp fwd	920	GGT GAG ATA ATG TTT AAC TTG C	CUT&RUN
E1Bp rev	921	TAA CCA AGA TTA GCC CAC GG	CUT&RUN
E2A fwd	183	GAA ATT ACG GTG ATG AAC CCG	qPCR mRNA
E2A rev	184	CAG CCT CCA TGC CCT TCT CC	qPCR mRNA
E2Ep fwd	922	TAC TGC GCG CTG ACT CTT AAG G	CUT&RUN
E2Ep rev	923	ATG GCG CTG ACA ACA GGT GCT	CUT&RUN
E2Lp fwd	925	ACC ACG CCC ACG AGA TTA GG	CUT&RUN

Name	No.	Sequence 5’ – 3’	Purpose
E2Lp rev	926	CTG GGT AAT GAC GCA GGC GGT A	CUT&RUN
E4orf6 fwd	134	GGA GGA TCA TCC GCT GCT G	qPCR mRNA
E4orf6 rev	135	GCA CAA CAC AGG CAC ACG	qPCR mRNA
E4p fwd	927	GGC TTT CGT TTC TGG GCG TA	CUT&RUN [354]
E4p rev	928	TAA ACA CCT GAA AAA CCC TCC TGC C	CUT&RUN [354]
GAPDH fwd	197	CAT CCT GGG CTA CAC TGA	qPCR vDNA
GAPDH rev	198	TTG ACA AAG TGG TCG TTG	qPCR vDNA
HA-DEK_BamHI-fwd	420	ATA GGA TCC TCC GCC TCG GCC CCT GC	Cloning
Hexon fwd	189	CGC TGG ACA TGA CTT TTG AG	qPCR mRNA & vDNA
Hexon rev	190	GAA CGG TGT GCG CAG GTA	qPCR mRNA & vDNA
MDM2 fwd	929	GCC TGG CTC TGT GTG TAA TAA GG	qPCR mRNA [355]
MDM2 rev	930	TGA ATC CTG ATC CAA CCA ATC A	qPCR mRNA [355]
MLP fwd	931	TGA TTG GTT TGT AGG TGT AGG	CUT&RUN
MLP rev	932	ACA GCG ATG CGG AAG AGA	CUT&RUN
p21 fwd	933	TGG AGA CTC TCA GGG TCG AAA	qPCR mRNA [355]
p21 rev	934	AGG ACT GCA GGC TTC CTG TG	qPCR mRNA [355]
pcDNA3fwd	92	TAA TAC GAC TCA CTA TAG GG	Sequencing

Name	No.	Sequence 5' – 3'	Purpose
PCNA fwd	935	TCA CTC CGT CTT TTG CAC AG	qPCR mRNA [354]
PCNA rev	936	GAA GCA CCA AAC CAG GAG AA	qPCR mRNA [354]

2.3.2. Vectors

Vectors used for subcloning and transfection during this work are listed in the following table according to the internal *FileMaker Pro* database number.

Table 6: List of vectors used for subcloning and transfection experiments.

Name	No.	Application	Reference
pGLbasic3	P100	Promoterless reporter vector for dual *Renilla*-luciferase assay with a modified coding region for firefly (*Photinus pyralis*) luciferase.	Promega
pCMX3b-FLAG	V32	Empty expression vector control with a CMV promoter and a N-terminal FLAG-tag	Group database
pRenilla-TK	83	Mammalian co-reporter vector for the weak constitutive expression of wild-type *Renilla* luciferase with a HSV-thymidine kinase promoter (pRL-TK).	Promega

2.3.3. Recombinant Plasmids

The following recombinant plasmids were used or generated during this work. The plasmids are indicated with the number of the internal *FileMaker Pro* database, application and reference. Externally provided oligonucleotides are labeled according to the institution providing them.

Table 7: Used recombinant plasmids with database number, application and reference.

Name	No.	Application	Reference
DEK-FLAG	P738	pCMX3b-FLAG vector encoding human DEK (GeneID: 7913).	This work
pCMV-VSV-G	L1	Plasmid encoding VSV-G antigen, for generation of lentiviral particles.	[356]

Name	No.	Application	Reference
pLKO-shCTR	SH14	Plasmid encoding a scrambled control shRNA and a puromycin resistance.	Sigma-Aldrich
pLKO-shDEK	SH16	PLKO.1_DEK832; targeting DEK mRNA at nucleotide positions 832 (nucleotides 860-879, GenBank NM_003472.2; kindly provided by Prof. Susanne Wells)	Sigma-Aldrich [290]
pMDLg-pRRE	L2	Plasmid encoding HIV Gag, integrase, Pol and Rev responsive element, for generation of lentiviral particles.	[357]
pMIEG His-FLAG-DEK	P801	Retroviral pMIEG vector encoding human DEK (GeneID: 7913) with a 6xHis and FLAG-tag.	[291]
pRSV-rev	L3	Plasmid encoding HIV Rev, for generation of lentiviral particles.	[357]
pGLbasic3 E1Ap	P91	HAdV5 E1A promoter reporter gene construct in a pGLbasic3 vector.	Group database [244]
pGLbasic3 E4p	P97	HAdV5 E4 promoter reporter gene construct in a pGLbasic3 vector.	Group database [244]

2.4. Antibodies

2.4.1. Primary Antibodies

The following primary antibodies (Ab) were used for western blot analysis (WB), immunoprecipitation (IP), ChIP assay, and immunofluorescence (IF). Primary antibodies are listed with properties, reference, purpose, and *FileMaker Pro* database number.

Table 8: Primary antibodies used in this study.

Name	No.	Properties	Purpose	Reference
2A6	62	Monoclonal mouse antibody raised against the N-terminus of HAdV E1B-55K.	WB (1:10)	[358]

Name	No.	Properties	Purpose	Reference
4E8	94	Monoclonal rat ab against the central region (aa 94-110) of HadV-C5 E1B-55K.	WB (1:10), IF (1:10)	[353]
6A11	105	Monoclonal rat antibody raised against HAdV E4orf3 protein.	WB (1:10), IF (1:200)	[152]
6-His	41	Monoclonal mouse antibody raised against 6xHis epitope.	WB (1:5000)	Clontech 631213
AC-15	88	Monoclonal mouse antibody raised against β-actin.	WB (1:5000)	Sigma-Aldrich A5441
B6-8	49	Monoclonal mouse antibody raised against HAdV DBP E2A.	WB (1:10), IF (1:10)	[359]
Daxx (H-7)	178	Monoclonal mouse antibody raised against aa 627-739 of the C-terminus of human Daxx.	WB (1:1000)	Santa Cruz Biotechnology sc-8043
DEK	156	Monoclonal rabbit antibody raised against human DEK [EPR11034].	WB (1:2000), IP (0.5 µl / sample)	abcam ab166624
DEK (H-300)	98	Polyclonal rabbit antibody raised against human DEK.	WB (1:1000)	Santa Cruz Biotechnology sc-30213
DEK (2)	84	Monoclonal mouse antibody raised against aa 19-169 of human DEK.	WB (1:1000), IF (1:50)	Santa Cruz Biotechnology sc-136222
DO-1	1	Monoclonal mouse antibody against the N-terminal aa 11-25 of human p53.	WB (1:2000), IP (0.5 µl / sample)	Santa Cruz Biotechnology sc-126
E2A	52	Polyclonal rabbit antibody raised against HAdV DBP E2A.	IF (1:500)	Kindly provided by Dr. R.T. Hay
FL-393	18	Polyclonal rabbit antibody raised against human p53.	WB (1:1000)	Santa Cruz Biotechnology

Name	No.	Properties	Purpose	Reference
FLAG-M2	19	Monoclonal mouse antibody raised against the FLAG-epitope.	WB (1:2000), IF (1:1000)	Sigma-Aldrich
L133	43	Polyclonal rabbit serum against HAdV capsid.	WB (1:5000)	[353]
M73	179	Monoclonal mouse antibody raised against HAdV5 E1A-12S and -13S.	WB (1:1000)	Santa Cruz Biotechnology sc-25
p300 (F-4)	106	Monoclonal mouse antibody raised against human p300.	WB (1:1000)	Santa Cruz Biotechnology sc-48343
PML	140	Polyclonal rabbit antibody raised against human PML protein.	IF (1:200)	abcam ab72137
pVI	93	Polyclonal rabbit antibody raised against HAdV pVI.	WB (1:1000)	[360]
RSA3	34	Monoclonal rat antibody against HAdV E4orf6.	WB (1:10)	[361]

2.4.2. Secondary Antibodies

The following secondary antibodies were used during this work. Secondary antibodies used for western blot analysis are listed in Table 9 (p. 34) and for immunofluorescence in Table **10** (p. 35) with properties, company and dilution, if not stated differently.

Table 9: Secondary antibodies used for western blot analysis.

Name	Properties	Dilution	Company
HRP-Anti-Mouse IgG (H+L)	HRP (horseradish peroxidase)-coupled; raised in sheep. F(ab')2.	1:10000	Jackson/Dianova Immunoresearch
HRP-Anti-Rabbit IgG (H+L)	HRP (horseradish peroxidase)-coupled; raised in sheep. F(ab')2.	1:10000	Jackson/Dianova Immunoresearch
HRP-Anti-Rat IgG (H+L)	HRP (horseradish peroxidase)-coupled; raised in sheep. F(ab')2.	1:10000	Jackson/Dianova Immunoresearch

Table 10: Secondary antibodies used for immunofluorescence.

Name	Properties	Dilution	Company
Alexa 488 Anti-Mouse IgG	Alexa 488 antibody raised in goat (H+L; F(ab')2 Fragment).	1:200	Invitrogen
Alexa 647 Anti-Rat IgG	Alexa 647 antibody raised in goat (H+L; F(ab')2 Fragment).	1:200	Jackson/Dianova Immunoresearch
Alexa 568 Anti-Rabbit IgG	Alexa 568 antibody raised in goat (H+L; F(ab')2 Fragment).	1:200	Invitrogen

2.5. Standard and Markers

Molecular weight markers and standards used for SDS-PAGE and agarose gel electrophoresis are listed in the following table.

Table 11: Standards and molecular weight markers.

Name	Purpose	Company
1 kb / 100 bp DNA ladder	Agarose gel electrophoresis	New England BioLabs, Inc., Frankfurt a. M., Germany
PageRuler™ Prestained Protein Ladder Plus	SDS-PAGE	Fermentas, Thermo Scientific, Waltham, USA

2.6. Enzymes and Buffers

The following commercially available enzymes and buffers were used during this study.

Table 12: Commercially available enzymes and buffers.

Enzyme/Buffer	Company
10x Antarctic phosphatase reaction buffer	New England BioLabs, Frankfurt a. M., Germany
1X NEBuffer™ r3.1	New England BioLabs, Inc., Frankfurt a. M., Germany

Enzyme/Buffer	Company
1X rCutSmart™ Buffer	New England BioLabs, Inc., Frankfurt a. M., Germany
Antarctic phosphatase	New England BioLabs, Frankfurt a. M., Germany
BamHI	New England BioLabs, Inc., Frankfurt a. M., Germany
DNase I	Carl Roth, Karlsruhe, Germany
DpnI (20000 U/ml)	New England BioLabs, Inc., Frankfurt a. M., Germany
NcoI	New England BioLabs, Inc., Frankfurt a. M., Germany
PfuUltra II Fusion HS DNA Polymerase	Agilent Technologies, Santa Clara, US
PfuUltra II Fusion Reaction buffer (10 x)	Agilent Technologies, Santa Clara, US
Proteinase K	Sigma-Aldrich, Darmstadt, Germany
RNase A	Carl Roth, Karlsruhe, Germany
T4 DNA ligase (400000 U/ml)	New England BioLabs, Frankfurt a. M., Germany
T4 ligase buffer (10X)	Roche, Basel, Switzerland
T4 Polynucleotide Kinase (PNK; 10000 U/ml)	New England BioLabs, Frankfurt a. M., Germany
XhoI	New England BioLabs, Inc., Frankfurt a. M., Germany

2.7. Commercial Systems

Commercial systems used in this study are listed in Table 13 (p. 37).

Table 13: Commercial systems.

Product	Company
ANTI-FLAG M2 Affinity-Gel	Sigma-Aldrich, Darmstadt, Germany
CUT&RUN Assay Kit #86652	Cell Signaling Technology, Cambridge, UK
DNA Purification Buffers and Spin Columns (ChIP, CUT&RUN) #14209	Cell Signaling Technology, Cambridge, UK
Dual-Luciferase Reporter Assay System	Promega Corporation, Madison, WI, USA
HisPur™ Ni-NTA Resin	Thermo Scientific, Dreieich, Germany
LightCycler 480 SYBR Green I Master mix	Roche, Mannheim, Germany
Luna Universal qPCR Master Mix	New England BioLabs, Frankfurt a. M., Germany
Protein Assay	BioRad, Munich, Germany
Qiagen Plasmid Mini, Midi and Maxi Kit	Qiagen, Valencia, CA, USA
SuperScript III First-Strand Synthesis SuperMix for qRT-PCR	Invitrogen, Carlsbad, CA, USA
SureBeads™ Protein A Magnetic Beads	BioRad, Munich, Germany

2.8. Chemicals and Reagents

Chemicals and reagents used during this work are listed in the following table.

Table 14: Chemicals and reagents.

Substance	Company
2-Propanol	Carl Roth, Karlsruhe, Germany

Substance	Company
30% acrylamide/bisacrylamide mixture	Carl Roth, Karlsruhe, Germany
4',6-Diamidin-2-phenylindol (DAPI)	Sigma-Aldrich, Darmstadt, Germany
6x DNA loading dye	New England BioLabs, Frankfurt a. M., Germany
Acetic acid	Merck, Darmstadt, Germany
Agarose SeaKem LE	Biozym, Hessisch Oldendorf, Germany
Ammonium persulfate (APS)	Carl Roth, Karlsruhe, Germany
Ampicillin	Sigma-Aldrich, Darmstadt, Germany
Aprotinin	Sigma-Aldrich, Darmstadt, Germany
Boric acid, > 99,8%	Sigma-Aldrich, Darmstadt, Germany
Bovine serum albumin (BSA)	Thermo Scientific, Dreieich, Germany
Bovine serum albumin fraction V	Sigma-Aldrich, Darmstadt, Germany
Bradford reagent	BioRad, Munich, Germany
Bromphenol blue	Carl Roth, Karlsruhe, Germany
Calcium chloride	Sigma-Aldrich, Darmstadt, Germany
Cell titer blue (CTB)	Promega Corporation, Madison, WI, USA
Chloroform	Carl Roth, Karlsruhe, Germany
Cot-1 DNA for FISH	Thermo Scientific, Dreieich, Germany
DEPC	Carl Roth, Karlsruhe, Germany
Developer solution	Tetenal, Norderstedt, Germany
Dextran sulfate	Sigma-Aldrich, Darmstadt, Germany
di-Lactate	Thermo Fisher Scientific, Dreieich, Germany

Substance	Company
Dimethyl sulfoxide (DMSO) ≥ 99.5%	Carl Roth, Karlsruhe, Germany
di-Sodium hydrogen phosphate	Sigma-Aldrich, Darmstadt, Germany
dNTP mix (100mM)	New England BioLabs, Frankfurt a. M., Germany
Dulbecco's modified eagle's medium (DMEM)	Sigma-Aldrich, Darmstadt, Germany
Ethanol absolute	Carl Roth, Karlsruhe, Germany
Ethidium bromide	Sigma-Aldrich, Darmstadt, Germany
Ethylenediaminetetraacetic acid (EDTA)	Carl Roth, Karlsruhe, Germany
Fetal Bovine Serum (FBS)	Thermo Scientific, Dreieich, Germany
Fixation solution	Tetenal, Norderstedt, Germany
Glycerine, 87%	AppliChem, Darmstadt, Germany
Glycerol	AppliChem, Darmstadt, Germany
Glycine	AppliChem, Darmstadt, Germany
Guanidinium hydrochloride	AppliChem, Darmstadt, Germany
HEPES	Carl Roth, Karlsruhe, Germany
Hydrochloric acid fuming 37% (HCl)	Carl Roth, Karlsruhe, Germany
Hydrocortisone 21-hemisucciante	Sigma-Aldrich, Darmstadt, Germany
Hydrogen peroxide (H_2O_2), 30% solution	Sigma-Aldrich, Darmstadt, Germany
Imidazole	AppliChem, Darmstadt, Germany
Insulin from bovine pancreas	Sigma-Aldrich, Darmstadt, Germany
Iodacetamide	Sigma-Aldrich, Darmstadt, Germany
Kanamycin Sulphate	Thermo Scientific, Dreieich, Germany

Substance	Company
LB agar	Carl Roth, Karlsruhe, Germany
LB media	Carl Roth, Karlsruhe, Germany
Leupeptin	Sigma-Aldrich, Darmstadt, Germany
Lithium chloride	Sigma-Aldrich, Darmstadt, Germany
Luminol sodium salt	Sigma-Aldrich, Darmstadt, Germany
Magnesium chloride 6-hydrate	AppliChem, Darmstadt, Germany
Manganese(II)-chloride	Sigma-Aldrich, Darmstadt, Germany
Methanol	Merck, Darmstadt, Germany
Methanol	Carl Roth, Karlsruhe, Germany
MOPS	Sigma-Aldrich, Darmstadt, Germany
Mowiol 4-88	Carl Roth, Karlsruhe, Germany
N-ethylmaleimide	Sigma-Aldrich, Darmstadt, Germany
Nonident-P40 (NP-40)	Carl Roth, Karlsruhe, Germany
p - Coumaric acid	Sigma-Aldrich, Darmstadt, Germany
Pansorbin	Calbiochem, Bad Soden, Germany
Paraformaldehyde (PFA)	Carl Roth, Karlsruhe, Germany
Penicillin/streptomycin	Sigma-Aldrich, Darmstadt, Germany
Pepstatin A	Sigma-Aldrich, Darmstadt, Germany
Phenol/chloroform/isoamyl alcohol (25:24:1)	Sigma-Aldrich, Darmstadt, Germany
Phenylmethylsolfonyl fluoride (PMSF)	Sigma-Aldrich, Darmstadt, Germany
Phosphate buffered saline (PBS)	Biochrom, Berlin, Germany
Polyethylenimine (PEI)	Sigma-Aldrich, Darmstadt, Germany

Substance	Company
Poly-Lysine	Sigma-Aldrich, Darmstadt, Germany
Potassium acetate	AppliChem, Darmstadt, Germany
Potassium chloride	Carl Roth, Karlsruhe, Germany
Potassium di-hydrogen phosphate	Carl Roth, Karlsruhe, Germany
Puromycin 10 mg/ml	Thermo Scientific, Dreieich, Germany
Saponin	Carl Roth, Karlsruhe, Germany
Sepharose A beads	Sigma-Aldrich, Darmstadt, Germany
Skim milk powder	Sigma-Aldrich, Darmstadt, Germany
Sodium acetate	Carl Roth, Karlsruhe, Germany
Sodium azide	AppliChem, Darmstadt, Germany
Sodium chloride	Carl Roth, Karlsruhe, Germany
Sodium citrate tribasic dihydrate	Sigma-Aldrich, Darmstadt, Germany
Sodium deoxycholate	AppliChem, Darmstadt, Germany
Sodium di-hydrogen phosphate	Sigma-Aldrich, Darmstadt, Germany
Sodium dodecyl sulfate (SDS)	Carl Roth, Karlsruhe, Germany
Sodium hydrogen carbonate	Sigma-Aldrich, Darmstadt, Germany
Sodium hydroxide	Sigma-Aldrich, Darmstadt, Germany
Sucrose	Sigma-Aldrich, Darmstadt, Germany
TEMED	AppliChem, Darmstadt, Germany
Tetracycline hydrochloride	AppliChem, Darmstadt, Germany
Trichloroacetic acid (TCA)	AppliChem, Darmstadt, Germany
Trichloromethane	Carl Roth, Karlsruhe, Germany

Substance	Company
Tris(hydroxymethyl)aminomethane (Tris)	Carl Roth, Karlsruhe, Germany
Triton® X-100	AppliChem, Darmstadt, Germany
TRIzol	Thermo Scientific, Dreieich, Germany
Trypsin/EDTA	Sigma-Aldrich, Darmstadt, Germany
Tween-20	AppliChem, Darmstadt, Germany
Urea	AppliChem, Darmstadt, Germany
Vanadyl-Ribonucleoside	Sigma-Aldrich, Darmstadt, Germany
β-mercaptoethanol	AppliChem, Darmstadt, Germany

2.9. Laboratory Equipment

The following laboratory equipment was used in this study.

Table 15: Laboratory equipment.

Device	Company
16-Tube SureBeads™ Magnetic Rack #1614916	Bio-Rad, Munich, Germany
Agfa Curix 60	AGFA, Mortsel, Belgium
Avanti Je centrifuge	Beckman Coulter, Munich, Germany
Axiovert 200 M microscope	Zeiss, Oberkochen, Germany
Biometra Minigel Twin	Analytik Jena, Jena, Germany
Biometra Multigel	Analytik Jena, Jena, Germany
Biometra Standard Power Pack P25 T	Analytik Jena, Jena, Germany

Device	Company
Bio-Rad PowerPac 3000 electrophoresis power supply	Bio-Rad, Munich, Germany
Bio-Rad Universal Hood II Gel Doc	Bio-Rad, Munich, Germany
Bioruptor plus	Diagenode, Seraing, Belgium
BRAND® accu-jet® pro pipette controller	Sigma-Aldrich, Darmstadt, Germany
Branson Ultrasonics Sonifier™ S-450 Digital Ultrasonic Cell Disruptor/Homogenizer	Thermo Fisher Scientific, Dreieich, Germany
ELMI Shaker S4	ELMI, Riga, Latvia
Eppendorf® 5427 R centrifuge	Eppendorf, Hamburg, Germany
Eppendorf® 6702 centrifuge	Eppendorf, Hamburg, Germany
Eppendorf® Biophotometer 6131	Eppendorf, Hamburg, Germany
Eppendorf® Concentrator 5301	Eppendorf, Hamburg, Germany
Eppendorf® Mastercycler	Eppendorf, Hamburg, Germany
Eppendorf® Mastercycler Gradient	Eppendorf, Hamburg, Germany
Eppendorf® Multipipette Plus	Eppendorf, Hamburg, Germany
Eppendorf® Research® plus pipette, 0.1 – 2.5 µl	Eppendorf, Hamburg, Germany
Eppendorf® Research® plus pipette, 0.5 – 10 µl	Eppendorf, Hamburg, Germany
Eppendorf® Research® plus pipette, 10 – 100 µl	Eppendorf, Hamburg, Germany
Eppendorf® Research® plus pipette, 100 – 1000 µl	Eppendorf, Hamburg, Germany
Eppendorf® Research® plus pipette, 2 – 20 µl	Eppendorf, Hamburg, Germany

Device	**Company**
Eppendorf® Research® plus pipette, 20 – 200 µl	Eppendorf, Hamburg, Germany
Eppendorf® Thermomixer Comfort 5355	Eppendorf, Hamburg, Germany
Eppendorf® Thermomixer Compact	Eppendorf, Hamburg, Germany
FiveEasy Plus FEP20 pH-Meter	Mettler Toledo, Fürstenfeldbruck, Germany
Freezer, -20°C	Liebherr-International Deutschland GmbH, Biberach and der Riß, Germany
Gel Doc™ XR+ Gel Documentation System	Bio-Rad, Munich, Germany
GFL 3031, orbital shaker	GFL, Großburgwedel, Germany
Glass Micro Pipette	Hamilton Company, Reno, US
GlowMax Multi Jr	Promega, Madison, Wiscons, USA
Hamilton syringe	A. Hartenstein GmbH, Würzburg, Germany
Heracell™ 150i CO2 incubator	Thermo Fisher Scientific, Dreieich, Germany
Heraeus HB 2448	Heraus, Hanau, Germany
Heraeus® BB16 Function Line CO_2 incubator	Heraeus Instruments GmbH, Hanaua, Germany
Heraeus™ Biofuge Pico™	Thermo Fisher Scientific, Dreieich, Germany
Heraeus™ Fresco™ 17 Microcentrifuge	Thermo Fisher Scientific, Dreieich, Germany
Heraeus™ Fresco™ 21 Microcentrifuge	Thermo Fisher Scientific, Dreieich, Germany
Heraeus™ Herafreeze HFU 586 Basic, -80°C	Thermo Fisher Scientific, Dreieich, Germany

Device	Company
Heraeus™ Laminair HLB 2448 GS	Thermo Fisher Scientific, Dreieich, Germany
Heraeus™ Megafuge™ 40 centrifuge	Thermo Fisher Scientific, Dreieich, Germany
Light Cycler 480 II	Roche, Mannheim, Germany
Memmert incubator model 200, D 06058	Memmert, Büchenbach, Germany
Microwave 9029GD	Privileg, Stuttgart, Germany
ML-DNY-43 NewClassic	Mettler Toledo, Greifensee, Switzerland
MS 3 basic vortexer	IKA® -Werke GmbH & Co. KG, Staufen, Germany
Multigel electrophoresis chamber	Analytik Jena, Jena, Germany
Multitron incubation shaker	Infors HT, Bottmingen, Switzerland
Nalgene Mr. FrostyTM Cryo 1°C freeze container	Thermo Fisher Scientific, Dreieich, Germany
NanoDrop 2000c UV-Vis Spectrophotometer	Thermo Fisher Scientific, Dreieich, Germany
Neubauer counting chamber (improved)	LO Laboroptik, Lancing, UK
No frost refrigerator and freezer CUN3523	Liebherr, Biberach an der Riß, Germany
PerfectBlu Wide Format Gel System Maxi ExW	VWR International, Darmstadt, Germany
Pipetboy acu	Integra Biosciences GmbH, Biebertal, Germany
Pipetboy acu 2	Integra Biosciences GmbH, Biebertal, Germany
PowerPacTM Basic Power Supply	Bio-Rad, Munich, Germany
PowerPacTM Universal Power Supply	Bio-Rad, Munich, Germany

Device	Company
Primovert light microscope	Zeiss, Oberkochen, Germany
PTC-100 Peltier Thermal Cycler	MJ Research, Reno, Nevada, USA
qTOWER^3 Real-Time Thermocycler	Analytik Jena, Jena, Germany
Quick-Freeze	A. Hartenstein GmbH, Würzburg, Germany
Reciprocating Shaker 3016 GFL	Gesellschaft für Labortechnik GmbH, Burgwedel, Germany
Rotina 420R centrifuge	Hettich Zentrifugen, Tuttlingen, Germany
Rotixa 50 RS centrifuge	Hettich Zentrifugen, Tuttlingen, Germany
Sartorius portable	Sartorius AG, Göttingen, Germany
Sigma 2K 15 centrifuge	Sigma, Osterode am Harz, Germany
SmartSpecTM Plus Spectrophotometer	Bio-Rad, Munich, Germany
Sprout® Mini Centrifuge	Heathrow Scientific Test Tube Rotating Shaker 3025 GFL, Burgwedel, Germany
TE62 Transfer Tank	Serwa Electrophoresis, Heidelberg, Germany
Test Tube Rotating Shaker 3025	GFL, Burgwedel, Germany
Thermocycler peqSTAR 96x universal gradient	VWR International GmbH, Darmstadt, Germany
Thermomixer comfort	Eppendorf, Hamburg, Germany
Trans-Blot® Cell	Bio-Rad, Munich, Germany
Vacusafe vacuum pump Integra	Biosciences GmbH, Biebertal, Germany
Vortex-Genie 2T	Scientific Industries, Inc., Bohemia, US

2.10. Disposable Laboratory Equipment

In the following table disposable laboratory equipment used in this work is listed.

Table 16: Disposable laboratory equipment.

Equipment	Company
96 Well 0.2 ml 8-transformer plate, transparent	Biozym Scientific GmbH, Hessisch Oldendorf, Germany
Blotting paper 460x570 mm, 195 g/m^2	A. Hartenstein GmbH, Würzburg, Germany
Cell scraper	Sarstedt, Nürnbrecht, Germany
Cover slides 12 mm round	A. Hartenstein GmbH, Würzburg, Germany
CryoPure Tube 72.379, 1.8 ml white	Nunc/Thermo Scientific, Dreieich, Germany
Eppendorf® Combitips advanced® pipette tips	Eppendorf, Hamburg, Germany
Falcon® 2059 polypropylene round-bottom tube	Fisher Scientific Company LLC, Pittsburgh, US
Filter tips 10 µl 70.1116.210	Sarstedt, Nürnbrecht, Germany
Filter tips 1000 µl 70.762.211	Sarstedt, Nürnbrecht, Germany
Filter tips 20 µl 70.760.213	Sarstedt, Nürnbrecht, Germany
Filter tips 200 µl 70.760.211	Sarstedt, Nürnbrecht, Germany
Greiner CELLSTAR® serological pipette, 10 ml	Sigma-Aldrich, Darmstadt, Germany
Greiner CELLSTAR® serological pipette, 2 ml	Sigma-Aldrich, Darmstadt, Germany
Greiner CELLSTAR® serological pipette, 25 ml	Sigma-Aldrich, Darmstadt, Germany
Greiner CELLSTAR® serological pipette, 5 ml	Sigma-Aldrich, Darmstadt, Germany
Kimtech Science* Purple Nitrile*gloves	Kimberly-Clark Worldwide, Inc., Koblenz, Germany

Equipment	Company
Micro tube 1.5 ml	Sarstedt, Nürnbrecht, Germany
Micro tube 2.0 ml	Sarstedt, Nürnbrecht, Germany
Microscope slides	A. Hartenstein GmbH, Würzburg, Germany
Multiply®-Pro tube 0.2 ml	Sarstedt, Nürnbrecht, Germany
Nitril® NextGen® gloves	Meditrade GmbH, Kiefersfelden, Germany
Nitrocellulose membrane 0.2 µm NC, Amersham™ Protran™	GE Healthcare, Solingen, Germany
Nitrocellulose membrane 0.45 µm NC, Amersham™ Protran™	GE Healthcare, Solingen, Germany
Parafilm® M All-Purpose Laboratory Film	Bemis Company, Inc., Oshkosh, US
qPCR 96-well plates	4titude, Berlin, Germany
Semi-micro cuvette 10 mm 67.742	Sarstedt, Nürnbrecht, Germany
Sterile filters (0.2 µm, 0.45 µm)	Merck, Millipore, Billerica, USA
TC dish 100, standard 83.3902	Sarstedt, Nürnbrecht, Germany
TC dish 12 well, standard F 83.3921	Sarstedt, Nürnbrecht, Germany
TC dish 150, standard 83.3903	Sarstedt, Nürnbrecht, Germany
TC dish 6 well, standard F 83.3920	Sarstedt, Nürnbrecht, Germany
Transformer cap strip plate, optical, flat	Biozym Scientific GmbH, Hessisch Oldendorf, Germany
Tube 15 ml, 120x17, PP, 62.554.502	Sarstedt, Nürnbrecht, Germany
Tube 50 ml, 114x23, PP, 62.547.254	Sarstedt, Nürnbrecht, Germany
X-ray films	Consumer Electronics Association (CEA), Arlington, US

2.11. Software

The following software and databases were used for processing text, image, figure, or data, for sequence analyses, biostatistics and management of literature, database and references.

Table 17: Software and databases.

Software	Purpose	Publisher
Adobe Reader XI	PDF data processing	Adobe
BioEdit	Sequence Alignment Editor	Ibis
BioRender	Figure processing	© BioRender
BLAST	Local alignment tool	NCBI
CLC Sequence Viewer 6	Genome and Sequencing analyses	CLC bio
Endnote X9	Reference organization	Thomson Reuters
Excel 2019	Data and table processing	Microsoft
Fiji - ImageJ	Microscope image processing and signal intensity calculation. version 1.53c	Fiji – ImageJ [362]
FileMaker Pro 14	Database management	Filemaker, Inc.
GPS-SUMO 1.0	Prediction of potential SCM and SIM	The CUCKOO Workgroup [363, 364]
GraphPad Prism 9	Figure processing and statistical analyses	GraphPad Software
JACoP : Just Another Co-localization Plugin	Co-localization analysis of pixel intensities	[365]
LightCycler 480 Software	Analysis of qPCR data	Roche
PowerPoint 2019	Presentation processing	Microsoft

Software	Purpose	Publisher
PubMed	Literature database, open sequence analysis software	Open Software (provided by NCBI)
qPCRsoft	Analysis of qPCR data	Analytik Jena
Serial Cloner	DNA cloning, sequence analysis and visualization	Serial Basics
Volocity	Microscope image processing	PerkinElmer Inc.
Word 2019	Text processing	Microsoft
Zeiss Zen 3.2 blue	Acquisition and processing of fluorescence pictures	Zeiss

3. Methods

3.1. Bacteria

3.1.1. Culture and Storage

Solid Plate Culture

Bacteria from glycerol culture or transformed bacteria were plated on a 100 mm dish containing LB (lysogeny broth) medium (Table 18, p. 6) supplemented with 15 g/l agar and the appropriate amount of antibiotics depending on the resistance of the plasmid-DNA (100 µg/ml ampicillin or 50 µg/ml kanamycin (Table 19, p. 52) and incubated at 30°C or 37°C overnight (*Memmert*). After incubation, single colonies were picked to inoculate liquid culture for mini- or maxi preparation. The solid plates can be stored for several weeks at 4°C, when sealed with parafilm.

Liquid Cultivation

For inoculation, a single colony was picked and transferred to sterile LB medium containing ampicillin or kanamycin in a final concentration of 100 µg/ml or 50 µg/ml kanamycin, respectively. The cultures were incubated at 30°C or 37°C for 16–20 h (*Multitron*).

Storage

For long-term storage, glycerol stocks from single colony bacteria were prepared from 5 ml of the corresponding liquid culture. Bacteria suspension was centrifuged at 4°C and 4000 rpm for 5 min (*Rotina 420R*). After disposal of the supernatant, the bacteria were resuspended in 1 ml of a 1:1 (v/v) mixture of LB medium and 87% glycerol. Subsequently, the suspension was transferred into CryoTubes™ (*Nunc*) and glycerol stocks were stored at -80°C.

Table 18: Composition of LB medium.

LB medium	10 g/l	Trypton
	5 g/l	Yeast extract
	5 g/l	NaCl
		(autoclaved)

Table 19: Antibiotic solution.

Antibiotic solution	50 mg/ml	Ampicillin (500x)
	10 mg/ml	Kanamycin (200x)
		(sterile filtered; storage -20°C)

3.1.2. Preparation of Chemically Competent Bacteria

Escherichia coli DH5α were plated on a solid LB medium plate without antibiotics and incubated at 37°C overnight. (*Memmert*). The following day, a single colony was used to inoculate 10 ml LB medium without selective antibiotics and incubated at 37°C and 220 rpm (*Multitron*) overnight. The next day, 200 ml of LB medium were inoculated with 2 ml of the overnight liquid culture and shaked at 37°C and 220 rpm (*Multitron*) until a OD_{600} of 0.3 – 0.5 (optimum 0.43) was reached (*SmartSpec™ Plus Spectrophotometer*). Subsequently, bacteria suspension was cooled in ice water for 20 min, followed by centrifugation at 4°C and 3000 rpm in a 50 ml falcon (*Rotina 420R*). The bacteria pellet was washed with 15 ml TFB-I buffer, centrifuged and resuspended in 4 ml TFB-II buffer (Table 20, p. 52). Afterwards, 100 µl of chemically competent bacteria was aliquoted in pre-cooled *Eppendorf* tubes and flash-frozen in liquid nitrogen. Aliquots were stored at -80°C.

Table 20: TFB-I and TFB-II buffer.

TFB-I	15% (w/v)	Glycerine	**TFB-II**	15% (w/v)	Glycerine
	10 mM	$CaCl_2$		10 mM	MOPS pH 7.0
	30 mM	KOAc		75 mM	$CaCl_2$
	100 mM	$RbCl_2$		10 mM	$RbCl_2$
	50 mM	$MnCl_2$			
		pH 5.8			

3.1.3. Chemical Transformation of Bacteria

Chemically competent bacteria (as described in 3.1.2, p. 52) were thawed on ice. For transformation 100 µl of competent bacteria suspension were mixed with 50 - 200 ng of plasmid-DNA in a pre-cooled *Falcon® 2059 polypropylene round bottom tube.* Subsequently, the bacteria-DNA mixture was incubated for 30 min on ice, followed by a heat shock. For the heat shock the suspension was incubated at 42°C for 30 sec and afterwards chilled on ice. After 2 min, 1 ml of LB medium without antibiotics was added to the bacteria suspension and incubated at 37°C and 150 rpm for approximately 1 h.

Afterwards, 100 µl were plated on a solid LB media plate. The leftover of the 1 ml was centrifuged for 3min at 4000rpm. The supernatant was removed and the pellet resuspended in the appropriate amount of LB medium, followed by plating on a solid LB media plate (see 3.1.1, p. 51) containing appropriate antibiotics and incubated at 37°C overnight. Single colonies were picked the following day and transferred to 5 ml liquid LB medium.

3.2. Tissue Culture Techniques

All used human cell lines were cultured under standard cell culture conditions and cell culture experiments were carried out with mycoplasma-negative cells under sterile conditions.

3.2.1. Cultivation of Mammalian Cell Lines

Adherent cell lines were cultured as a monolayer on polystyrene cell culture dishes (12-well, 6-well, 100 mm and 150 mm cell culture dishes, *Sarstedt*) with *Dulbecco's Modified Eagle Medium* (DMEM, *Sigma-Aldrich*) at 37°C, 5% CO_2 and 95% humidity. DMEM containing 0.11 g/l sodium pyruvate was supplemented with 1% of penicillin/streptomycin (1000 U/ml penicillin and 10 mg/ml streptomycin in 0.9% NaCl) and 5% FBS for A549, H1299 and HeLa cells, or 10% FBS for HEK293, HEK293T and HepaRG cells. For cultivation of hepatoma cell lines, like HepaRG, the media was additionally supplemented with 5 µg/ml of insulin and 0.5 µM hydrocortisone. For cell passaging, media was aspirated and the cells were washed with 1x phosphatase buffered saline (PBS) buffer (Table 21, p. 53), followed by incubation in an appropriate amount of trypsin/EDTA (*Sigma-Aldrich*) at 37°C for 5 – 10 min. Trypsin activity was blocked by adding culture medium containing 5% of FBS and detached cells were transferred to a 50 ml falcon tube (*Sarstedt*) with subsequent centrifugation at 2000 rpm for 3 min (*Heraeus™ Megafuge™ 40*).

Table 21: Composition of PBS.

PBS	140 mM	NaCl
	3 mM	KCl
	4 mM	Na_2HPO_4
	1.5 mM	KH_2PO_4
		pH 7.3, autoclaved

The pelleted cells were resuspended in an appropriate amount of supplemented fresh media and depending on the experimental procedure, either subcultivated (1:2 – 1:10) or counted for cell seeding as described in 3.2.3.

3.2.2. Cryopreservation of Mammalian Cells

Confluent adherent mammalian cells were harvested by trypsination as described in 3.2.1 (p. 53). After inactivation of trypsin and centrifugation, the cell pellet was resuspended in FBS containing 10% DMSO. For long-term storage, the resuspended cells were transferred into CryoTubes™ (*Nunc*) and gradually frozen to -80°C in a freezing container (*Nalgene Mr.Frosty*). For re-cultivation, cells were thawed rapidly in a water bath at 37°C, transferred into supplemented fresh media and subsequently pelleted at 2000 rpm for 3 min. The supernatant was discarded and the cells were resuspended in supplemented fresh media with subsequent seeding in appropriate cell culture dishes for cultivation as described in 3.2.1.

3.2.3. Determination of Total Cell Number

To seed a defined number of cells for experimental procedures, the total number of viable cells were determined. Therefore, cells were harvested by trypsination as described in 3.2.1 (p. 53) and afterwards resuspended in an appropriate amount of culture medium. 50 µl of the cell suspension was mixed 1:1 (v/v) with trypan blue solution and 10 µl were placed in the *Neubauer counting chamber*. After two manual counts of 16 squares under a light microscope, the total cell number was calculated with the following formula:

$$\textit{Cell number / ml} = \textit{counted cells} \times 2 \times 10^4$$

Table 22: Composition of trypan blue solution.

Trypan blue solution	0.15% (w/v)	Trypan blue
	0.85% (w/v)	NaCl

Cells were seeded depending on the surface area of the used cell culture dishes to reach 80% confluence 24 h later (1.2 – 2.5 x 10^5 for 12-well, 4 – 8 x 10^5 for 6-well, 4 – 6 x 10^6 per 100 mm dish). Cells were incubated at 37°C and 5% CO_2, followed by transfection and/or infection (3.2.4 ,p. 55; 3.4.1, p. 56).

3.2.4. Transfection of Mammalian Cells with Polyethylenimine

Polyethylenimine (linear, 25 kDa; PEI) was used to transfect plasmid-DNA into mammalian cells. PEI was dissolved in ddH_2O at a concentration of 1 mg/ml, neutralized with 0.1 M HCl (pH 7.2), filter sterilized (0.2 µm), aliquoted and stored at -80°C. For transfection mammalian cells were seeded 24 h prior, according to 3.2.3, to reach around 80% confluence. Desired concentration of plasmid-DNA was added to 2 ml *Eppendorf* reaction tube and dissolved in 1.8 ml pre-warmed DMEM without supplements. PEI was added in a ratio of 1:10 relating to the amount of DNA (1 µg DNA = 10 µl PEI). The solution was gently vortexed (*Vortex-Genie 2T; Scientific Industries*) and collected by brief centrifugation (*Biofuge pico; Heraeus*). Subsequently, the transfection solution was incubated at RT for 15 – 20 min to create a complex of DNA and synthetic polymer. Meanwhile, culture media was removed from the culture dishes and substituted by fresh un-supplemented DMEM to ensure a neutral pH. Transfection solution containing the positively charged PEI-DNA particles are added to the cells, followed by incubation at 37°C. Transfection media was aspirated after 3 h for HepaRG and after 5 – 6 h for other cell lines and fresh supplemented culture media was added to the dishes. Cells were incubated at 37°C until harvest (3.2.5).

3.2.5. Harvest of Mammalian Cells

Transfected and/or infected adherent mammalian cells were harvested using a cell scraper (*Sarstedt*). The culture media containing the detached cells were transferred into a 15 ml or 50 ml falcon tube, respectively, and centrifuged at 2000 rpm for 3 min (*Heraeus™ Megafuge™ 40*). After supernatant removal, the cell pellet was washed once with 1x PBS, followed by centrifugation and discarding the PBS. The cell pellet was frozen at -20°C for following experiments.

3.3. Generation of Stable Cell Lines by Lentiviral Transduction

To investigate the influence of specific proteins on adenoviral infection, cells were transduced by lentiviruses to generate cell lines, which either stably express a protein, express a protein after induction with doxycycline or with a stable knockdown of a certain protein.

3.3.1. Generation of Recombinant Lentiviral Particles

For generation of recombinant lentiviral particles, 80% confluent HEK293T cells were transfected with a lentiviral plasmid encoding for either scrambled shRNA, shRNA specific for a protein of interest or expressing a specific protein, together with the envelope and

packaging plasmids pCMV-VSV-G, pMDLg/pRRE and pRSV-Rev (according to 3.2.4). Transfection was stopped after 8 h with DMEM media containing 10% FCS, 1% penicillin/streptomycin and 20 mM HEPES. Transfected cells were harvested 72 h post-transfection (p.t.), subsequently centrifuged for 10 min at 2000 rpm and the supernatant was sterile filtered (0.45 µm). Aliquoted lentiviral particles were frozen rapidly with liquid nitrogen and long-term stored at -80°C.

3.3.2. Infection of Mammalian Cell Lines with Lentiviral Particles

Cell lines were grown in supplemented media on 12-well cell culture dishes until 70% - 80% confluence was reached. Culture media was substituted by DMEM without supplements and varying amounts, ranching from 100 µl to 1 ml, of recombinant lentiviral particles were added to the cells. Lentivirus transduction was stopped after 8 h by removing the media and adding fresh culture media with supplements. Cells were selected due to the antibiotic selection marker expressed by the lentiviral particles (2 µg/ml puromycin; 1 mg/ml geneticin). The generation of the stable cell lines was confirmed by western blot and qPCR analysis.

3.4. Adenovirus

3.4.1. Infection of Mammalian Cell Lines

Mammalian cells were seeded 24 h prior to infection as described in 3.2.3 (p. 54). Cells were infected at a confluence of around 80% - 90%. For infection HAdV stocks were defrosted and diluted in DMEM without supplements with the required multiplicity of infection (MOI). Therefore, virus titer (fluorescence forming units (ffu) per µl) (3.4.3, p. 57) and the amount of seeded was taken into account and virus dilution was calculated according to the following formula:

$$\textit{volume virus stock solution [µl]} = \frac{\textit{multiplicity of infection (MOI) [ffu/cell]} \times \textit{cell number}}{\textit{virus titer [ffu/µl]}}$$

Cells were incubated at standard cell culture conditions for 1 h, followed by removal of the infection media and adding fresh supplemented culture media. Depending on the experimental setup, the cells were harvested at certain time point post-infection (p.i.).

3.4.2. Propagation and Storage of High-Titer Virus Stocks

For propagation of high-titer virus stocks, H1299 cells were infected at a MOI of 50 (as described in 3.4.1, p. 56), when they reached a confluence of around 70% - 80%. Cells

were harvested according to 3.2.5 (p. 55) three to five days p.i., when a cytopathic effect was visible. After centrifugation at 2000 rpm for 3 min (*Heraeus™ Megafuge™ 40*), the cell pellet was washed once with 1x PBS (Table 21, p. 53) and resuspended in an adequate amount of fresh media without supplements (1 ml per 150 mm dish). Virions were isolated by breaking the cells through three subsequent freeze (liquid nitrogen) and thaw (37°C, water bath) cycles. Afterwards, virus solution was centrifuged at 4500 rpm for 10 min to pellet the cell debris. The supernatant was transferred into a new tube and mixed with 10% glycerol (v/v) (97%; sterile), frozen rapidly in liquid nitrogen and long-term stored at -80°C.

3.4.3. Titration of Virus Stock

Titration of virus stocks was performed by quantitative immunostaining of the early viral DNA-binding protein (DBP) E2A in HEK293 cells. Therefore, 8 x 10^5 cells per well were seeded in a 6-well culture dish. The following day cells were infected with virus dilutions ranging from 10^{-1} to 10^{-5} as described in 3.4.1. (p. 56) Methanol was used to fix the cells 24 h post-infection (p.i.). Therefore, media was removed and the cells were washed with 1 ml of 1X PBS (Table 21, p. 53). Subsequently, ice-cold methanol was added to the wells and the cells incubated at -20°C for 15 min. Afterwards, the methanol was removed and the cells were air-dried and either stored at -20°C or subjected to immunofluorescence staining to determine the fluorescence forming units. For blocking and reducing unspecific binding, the cells were incubated at RT for 1 h in TBS-BG (Table 23, p. 57).

Table 23: Composition of TBS-BG

TBS-BG	20 mM	Tris/HCl pH 7.6
	137 mM	NaCl
	3 mM	KCl
	1.5 mM	$MgCl_2$
	0.05% (v/v)	Tween-20
	0.05% (w/v)	Sodium azide
	5% (w/v)	Glycine
	5% (w/v)	BSA

Table 24: Composition of PBS-T.

PBS-T	0.1% (v/v)	Tween-20
		in 1x PBS

TBS-BG was completely aspirated from the wells and ~ 500 µl – 1 ml of primary polyclonal mouse B6-8 antibody raised against early viral E2A/DBP protein was added to the cells (1:10 in PBS-Tween (Table 24, p. 57)). The wells were incubated at 4°C overnight and primary antibody was removed the next day. Afterwards, the cells were washed three times with PBS-T prior to incubation in secondary Alexa™-488 anti-mouse antibody (*Invitrogen*; 1:1000 in PBS-T) at 4°C for 2 h in a dark environment. Subsequently, secondary antibody was removed from the cells, followed by three washing steps with PBS-T. Fluorescence forming units were determined by counting at least four different visual fields with uniform number of cells, in two different dilutions and with two different objectives at a Zeiss *Axiovert 200 M* microscope. The number of infectious particles [ffu/µl] was calculated by taking the number of infected cells, the dilution factor and the magnification into account.

3.4.4. Determination of Virion Progeny Production

To determine virion progeny production, an adequate amount of stable cell lines or parental cell lines were seeded in a 6-well plate. The following day cells can be transfected to express a specific protein to investigate its role in adenoviral replication (described in 3.2.4, p. 55). Afterwards, the cells were infected with adenoviruses as described in 3.4.1 and harvested at certain time points (3.2.5, p. 55). After centrifugation, cells were resuspended in an appropriate volume of un-supplemented DMEM. Virus particle were isolated by breaking the cells and the titer was determined by reinfection of HEK293 cells with virus dilutions as described above in 3.4.4 (p. 58). The average amount of viral progeny production was calculated by considering the amount of DMEM and of initially seeded cells [ffu/cell] as follows:

$$moi\ [ffu/cell] = \frac{virus\ titer\ [ffu/\mu l] \times dilution\ factor}{cell\ number}$$

3.5. Quantitative Determination of Nucleic Acid Concentrations

Concentration of nucleic acids (DNA and RNA) was determined by measuring the optical density (OD) at a wavelength of 260 nm at the *NanoDrop 2000C* spectrometer. The optical density of nucleic acids at 260 nm stands in correlation to their concentration. Therefore, an OD of 1 corresponds to an absolute concentration of 50 µg/ml for dsDNA and 33 µg/ml for ssDNA. The purity of the nucleic acid was calculated by the ratio of 260 / 280 nm, whereas the ratio should be above 1.8 to ensure DNA purity and at 2.0 for high-purity RNA without protein contamination.

3.6. DNA Techniques

3.6.1. Preparation of Plasmid-DNA from *Escherichia Coli*

For high-scale preparation of plasmid DNA from *Escherichia coli* (*E. coli*), 5 ml of LB medium with appropriate antibiotics were inoculated with a single colony of transformed bacteria picked from a solid agar plate. The pre-culture was incubated at 30°C/37°C overnight and the following day 200 – 500 µl were inoculated into 500 ml LB medium supplemented with antibiotics. The culture was incubated at 30°C/37°C for 16 h – 20 h, followed by centrifugation at 4500 rpm for 20 min (*Rotixa 50 RS*). The plasmid-DNA was extracted using the *Qiagen Plasmid DNA Purification* kit according to the manufacturer's protocol. Therefore, the pelleted bacteria cells were resuspended in 10 ml resuspension buffer P1 and transferred into a falcon. Afterwards, 10 ml of lysis buffer P2 was added and the suspension was incubated for 5 min at RT. Subsequently, 10 ml of neutralization puffer P3 was added, followed by centrifugation at 4000 rpm for 30 min (*Rotina 420R*) (for midi preparation 600 µl of P1 - P3 (Table 25, p. 59) per 50 ml culture; at 14800 rpm for 10 min). Meanwhile, the column was equilibrated with 10 ml of QBT (5 ml midi preparation) buffer before loading the samples. The supernatant was loaded on the columns without the cell pellet. Once the samples passed the columns, flows were discarded and the columns were washed twice with QC buffer. Afterwards, the plasmid-DNA was eluted with 15 ml / 840 µl QF buffer (maxi / midi), and mixed with 12.5 ml / 700 µl isopropanol. For precipitation the eluted DNA was gently shaken with isopropanol and centrifuged at 4500 rpm for 45 min for maxi and at 14800 rpm for 10 min for midi preparation. Isopropanol was discarded and the DNA pellets washed with 75% (v/v) ethanol with subsequent centrifugation (maxi at 4500 rpm for 5min; midi at 14800 for 5 min). After removal of the ethanol the pellet was dried at RT or 42°C, followed by dissolving the DNA in 20 – 500 µl of 10 mM Tris pH 8.0. Concentration of the DNA was measured as described in 3.5. The concentration was adapted to 1 µg/µl and 1 µg of DNA was analyzed directly and after enzymatic digestion (3.6.4, p. 61) on an agarose gel (3.6.3, p. 61) and sent for sequencing (3.6.4, p. 61).

Table 25: Composition of P1, P2 and P3 buffer for plasmid-DNA preparation.

P1	50 mM	Tris/HCl pH 8.0	**P2**	200 mM	NaOH
	10 mM	EDTA		1%	SDS
	100 µg/ml	RNase			
		store at 4°C	**P3**	7.5 M	Ammonium Acetate

For analytical approaches, single colonies of transformed bacteria were inoculated in 2 ml or 5 ml of LB medium supplemented with the appropriate antibiotics and incubated for 6 h or at 30°C/37°C overnight, respectively. 1 ml of bacteria suspension was centrifuged at 14800 rpm for 10 min and after removal of the supernatant, 300 µl of each buffer P1 – P3 was added to the cell pellet. The samples were centrifuged at 14800 rpm for 10 min and the supernatant was transferred into a fresh *Eppendorf tube* with 1 vol isopropanol and 0.1 vol 3 M NaAc. The solution was mixed to precipitate the DNA and centrifuged at 14800 rpm for 10 min. The DNA pellet was washed with 75% (v/v) ethanol with subsequent centrifugation at 14800 rpm for 5 min. After removal of the ethanol, the DNA pellet was dried in a vacuum pump centrifuge (*Integra Vacusafe*) at 42°C. The DNA pellet was directly digested and analyzed on an agarose gel (3.6.4, p. 61).

3.6.2. Polymerase Chain Reaction (PCR)

DNA fragments were amplified by performing PCR. The desired fragments can be amplified exponentially due to the ability of the polymerase to synthesize a new strand complementary to the introduced DNA template. The PCR mix was prepared in a 0.2 ml PCR tube by adding 25 – 100 ng of the DNA template, 10x PCR reaction buffer, 1 µl dNTPs (1 mM each, *NEB*), 125 ng of the forward (fwd) and reverse (rev) primer each and 1 µl polymerase (PfuUltra II 5 U/µl *Agilent Technologies* for cloning or DreamTaq 5 U/µl *ThermoFisher* for quantitative analysis of DNA fragments). Sterile Milli-Q was added to a total volume of 50 µl and the PCR program was set in an *Eppendorf Mastercycler*. The PCR reaction was performed according to the standard protocol shown in Table 26 (p. 60), however annealing and elongation were adapted to the theoretical primer melting temperature and the length of the DNA template, respectively. Subsequently, the efficiency of the PCR reaction was analyzed by loading 5 – 10 µl on an analytical agarose gel (3.6.3, p. 61). PCR-derived DNA, which should be used for cloning of specific DNA, was purified by preparative agarose-gel electrophoresis (3.6.3, p. 61).

Table 26: Standard PCR program.

Initial denaturation	2 min	95°C	
DNA denaturation	30 sec – 1min	95°C	25 – 30x
Annealing	30 sec – 1min	55°C - 70°C	
Elongation	1 min / kb	72°C	
Final Elongation	10 min	68°C	
Storage	Indefinitely	4°C	

3.6.3. Agarose Gel Electrophoresis

0.6 – 1% (w/v) agarose (*Biozym*) was dissolved in 1x TBE buffer (Table 27, p. 61) by melting the solution in a microwave. For preparative agarose gels 1 mM guanosine was added to the solution to protect the DNA from UV-light [366]. After cooling, ethidium bromide was added to the solution to a final concentration of 0.5 µg/ml. Afterwards, the gel solution was poured into an appropriate gel tray with fitting combs and left for hardening. DNA samples were supplemented with 6x loading buffer (Table 27, p. 61) and loaded into the gel pockets. For verification of the DNA fragments, either a 100 bp or 1 kbp DNA ladder (*NEB*) was used. Gel electrophoresis was carried out with 5 – 10 V/cm gel length in 1x TBE. Analytical agarose gels were visualized at a *Gel Doc™ XR+* under UV light at 365 nm. Preparative isolation of the DNA band of interest was performed in long wave UV light (365 nm) with minimal required intensities.

Table 27: Buffer used for agarose gel electrophoresis.

TBE	450 mM	Tris/HCl pH 7.8	**6x loading buffer**	10 mM	EDTA
	450 mM	Boric acid		50% (v/v)	Glycerol
	10 mM	EDTA		0.25% (w/v)	Bromphenol blue
				0.25% (w/v)	Xylene Cyanol

3.6.4. Cloning of DNA Fragments

Enzymatic DNA Restriction

Restriction enzymes from *New England Biolabs* were used for enzymatic restriction of DNA. For analytical approaches 1 µg of DNA (or DNA pellet from mini preparation) were incubated with 3 – 10 U restriction enzyme in the corresponding reaction buffer at 37°C for 2 h. The enzymatic digest reaction was subjected to an analytical agarose gel electrophoresis (3.6.3, p. 61) and sent for sequencing (see below). For preparative restriction digest, 20 µg of DNA were mixed with 50 U of the restriction enzymes and the corresponding buffer. The digest was incubated at 37°C for 3 h and subsequently loaded on a preparative agarose gel with guanosine (3.6.3, p. 61). The DNA band of interest was cut out of the gel and DNA was isolated by gel extraction.

Gel Extraction

DNA fragments separated by preparative agarose gel electrophoresis were cut out in long wave UV light (365 nm) with minimal required intensities and transferred to 1.5 ml

Eppendorf reaction tube. Afterwards, the gel pieces were ultra-centrifuged (*Avanti JE*) at 20000 rpm for 1.5 h and the supernatant was transferred into a fresh reaction tube. Subsequently, the supernatant was mixed with 0.1 vol 3M NaAc and 1 vol of isopropanol, inverted and centrifuged at 14800 rpm for 10 min. The isopropanol was discarded and the precipitated DNA was washed once with 75% (v/v) ethanol. After centrifugation at 14800 rpm for 5 min, the DNA pellet was dried at 42°C and dissolved in 30 – 40 µl of 10 mM Tris pH 8.0. Concentration was measured either at the *NanoDrop 2000C* spectrometer (3.5, p. 58) or estimated through comparison with the DNA ladder after performing analytical agarose gel electrophoresis (3.6.3).

Ligation of DNA Fragments

The cloning vector and PCR fragments for ligation were enzymatically digested and either purified by agarose gel electrophoresis or isopropanol precipitation. For standard ligation, 20 – 100 ng vector DNA was mixed with insert DNA in a ratio of 1:3, 2 µl of 2x ligation buffer, 1 U T4 DNA ligase (*Roche*) and Milli-Q to a total volume of 20 µl. The reaction was incubated at 13°C overnight and at 22°C for 1 h the following day. Before transformation of the ligated DNA into chemically competent bacteria (3.1.3), DNA was precipitated with isopropanol (see above). The transformed bacteria were plated on an agar plate with antibiotics and incubated at 30°C/37°C overnight. The following day, single colonies were picked to inoculate mini preparation. DNA was isolated from the bacteria culture (3.6.1, p. 59) and analytical verified via enzymatic restriction, agarose gel electrophoresis and DNA sequencing.

DNA Sequencing

The sequence of clones was verified by mixing 1 µg of isolated plasmid-DNA with 30 pmol of an appropriate primer and 10 mM Tris pH 8.0 to a total volume of 17 µl. The reaction was sent for sequencing performed by *Eurofins Genomics.* The received results were verified by using *BioEdit*, *BLAST*, and *Serial Cloner*.

3.6.5. Quantification of Viral DNA Synthesis

Mammalian cells were seeded (3.2.3, p. 54), transfected (3.2.4, p. 55) and/or infected (3.4.1, p. 56) and harvested at certain time points (3.2.5, p. 55). The cell pellet was lysed in RIPA buffer and incubated for 30 min on ice. The samples were vortexed every 10 min before sonification for 30 sec at 4°C (0.8 output impulse/sec) using a *Branson Ultrasonics Sonifier™.* Afterwards, the supernatant was transferred into a fresh reaction tube and

concentration was measured using Bradford reagent (3.8.2, p. 66). 10 µg of lysate in 20 µl of volume were incubated with Proteinase K to digest the proteins. Therefore, the lysate was mixed with 50% (v/v) Tween-20, 10% (v/v) proteinase K and Milli-Q to a total volume of 100 µl. The reaction was incubated at 55°C for 1 h, followed by enzyme deactivation at 95°C for 5min. Afterwards, detection and quantification of viral DNA was carried out by either qPCR (Primer: qPCR Hexon fwd, qPCR Hexon rev) (3.7.3) with an internal standard of genome copies or by PCR (Primer: qPCR E1B-55K fwd, qPCR E1B-55K rev, GAPDH fwd and GAPDH rev) using the following program:

Table 28: PCR program for viral DNA synthesis.

Initial denaturation	2 min	95°C	
DNA denaturation	30 sec	95°C	25x
Annealing	1min	55°C	
Elongation	2 min	72°C	
Final Elongation	10 min	72°C	
Storage	Indefinitely	4°C	

For PCR reaction, 12.5 µl of the PK digest was mixed with 5 µl of 10x *DreamTaq* buffer, 1 µl of dNTPs, 5 U/µl *DreamTaq* Polymerase and 125 ng of a forward and reverse primer each.

3.7. RNA Techniques

3.7.1. Preparation of Total Cellular RNA from Mammalian Cells

Mammalian cells were seeded, transfected/infected depending to the experimental procedure (3.2.3, p. 54; 3.2.4, p. 55; 3.4.1, p. 56) and harvested at certain time points as already described above (3.2.5, p. 55). Isolation of total RNA was performed on ice and with filter tips. After Harvesting, the cells were resuspended in 600 µl Trizol and either frozen at -20°C until further use or directly further processed. Therefore, 200 µl of chloroform was added to the samples and vortexed for 15 sec. Before transferring the watery phase to a fresh reaction tube containing 600 µl of isopropanol, the samples were centrifuged at 12000 x*g* and 4°C for 15 min. The RNA was precipitated by inverting the samples and subsequent centrifugation at 12000 x*g* and 4°C for 15 min. After removal of the isopropanol, the RNA pellet was washed with 1 ml of 75% (v/v) ethanol and centrifuged 7500 x*g* and 4°C for 5 min. The ethanol was removed and the pellet air-dried before the

RNA was dissolved in 20 – 50 µl nuclease-free water. RNA concentration was measured according to 3.5. The RNA was stored at -20°C or directly reversely transcribed into cDNA (3.7.2, p. 64).

3.7.2. Reverse Transcription of RNA

RNA isolated (3.7.1, p. 63) from mammalian cells was reverse transcribed using the *Promega Reverse Transcription System* according to the manufacturer's protocol. Therefore, 1 µg of RNA was mixed with 4 µl $MgCl_2$, 2 µl RT buffer, 2 µl dNTPs, 1 µl oligo / random primer, 0.5 µl recombinant RNAsin® ribonuclease inhibitor and 0.7 µl of AMV reverse transcriptase. The reaction was filled up to a total volume of 20 µl with RNase-free water, followed by incubation at 42°C for 1 h and subsequent inactivation at 95°C for 5 min (*Eppendorf® Thermomixer Comfort 5355*). The generated cDNA can be stored at -20°C until further use or directly subjected to subsequent experiments.

3.7.3. Quantitative Real-Time PCR (RT-qPCR)

Quantitative RT-PCR was performed with a first-strand method in a *LightCycler® 480 Instrument II* to compare the production of cellular mRNA or viral DNA in different samples relative to each other. Therefore, 5 µl of diluted cDNA (1:10) was mixed with 5 µl of *LightCycler® 480 Sybr green I Master* and 10 pmol forward and reverse primer in *FrameStar® 480 / 96* 96-well plate covered with adhesive seals. In case of determination viral DNA synthesis, PK digest was prepared as in 3.6.5 (p. 62) and 5 µl of a 1:200 dilution was used. The samples were measured in technical triplicates using the following protocol:

Table 29: Quantitative RT-PCR program.

Initial denaturation	10 min	95°C	
DNA denaturation	30 sec	95°C	
Annealing	30 sec	62°C	40x
Elongation	30 sec	72°C	

The average threshold cycle (Ct) value was normalized to the Ct value of the housekeeping gene GAPDH and the identities of the products obtained were verified by melting curve analysis.

Quantification of DNA obtained from *CUT&RUN assays* (3.9, p. 73) was performed in a *qTOWER³* by mixing 4 µl of the eluted DNA (dilution 1:2) with 5 µl of *Luna® Universal qPCR Master Mix* and 10 pmol forward and reverse primer in a 96 Well 0.2 ml 8-transformer plate.

The samples were measured in technical duplicates using the PCR program listed in Table 30 (p. 65). The average Ct value was normalized to the appropriate input sample and negative IgG isotope control. The identities of the products obtained were verified by melting curve analysis.

Table 30: CUT&RUN qPCR program for DNA quantification.

Initial denaturation	3 min	95°C	
DNA denaturation	15 sec	95°C	
Annealing and Elongation	60 sec	60°C	40x

3.8. Protein Techniques

3.8.1. Preparation of Total-Cell Lysates

Protein preparation of mammalian cells were prepared with either highly stringent RIPA lysis buffer (Table 31, p. 66) or NP-40 buffer (Table 32, p. 66) and carried out at 4°C. Therefore, harvested cell pellets (3.2.5, p. 55), transfected (3.2.4, p. 55) and infected (3.4.1, p. 56) according to the experimental procedure, were resuspended in an appropriate amount of lysis buffer freshly supplemented with protease inhibitors 0.2 mM PMSF, 1 mg/ml pepstatin A, 5 mg/ml aprotinin, 20 mg/ml leupeptin. To look for proteins involved in the SUMO conjugation pathway, 25 mM iodacetamide (IAA) and 25 mM N-ethylmaleimide (NEM) was additionally added to the buffer. The cells were lysed for 30 min on ice while being vortexed every 10 min (*Vortex-Genie 2T*). Subsequently, the samples were sonicated with a Branson Sonifier 450 (40 pulses output 0.8; 0.8 impulse/sec) for 30 sec or with a Diagenode Bioruptor on high setting for 30 sec on and 30 sec off for three rounds at 4°C, followed by centrifugation to separate the cell debris from the soluble protein fraction. After centrifugation at 11000 rpm and 4°C for 3 min, the supernatant was transferred into a fresh pre-cooled reaction tube. Protein concentration was measured by spectrophotometry via Bradford assay as described in 3.8.2 (p. 66). Finally, the preferred volume was calculated and diluted to the desired concentration with ddH_2O. The proteins were denatured by adding 5x laemmli buffer (Table 33, p. 66) [367], followed by incubation at 95°C for 3 min. Total-cell lysates were stored at -20°C until subjection to SDS-PAGE (3.8.5, p. 69) and immunoblotting analysis (3.8.6, p. 71).

Table 31: High stringent lysis buffer for whole-cell lysate preparation (RIPA).

RIPA	50 mM	Tris/HCl pH 8.0
	150 mM	NaCl
	5 mM	EDTA
	1% (v/v)	Nonident P-40
	0.1% (w/v)	SDS
	0.5% (w/v)	Sodium Deoxycholate

Table 32: Nonident P-40 (NP-40) lysis buffer for total-cell lysate preparation.

NP-40	50 mM	Tris/HCl pH 8.0
	150 mM	NaCl
	5 mM	EDTA
	0.14% (v/v)	Nonident P-40

Table 33: 5x laemmli buffer.

5x laemmli buffer	250 mM	Tris/HCl pH 6.8
	50% (v/v)	Glycerol
	10% (w/v)	SDS
	0.5% (w/v)	Bromphenol blue
	3.75% (v/v)	β-Mercaptoethanol
	ad	ddH_2O

3.8.2. Determination of Protein Concentration

Protein concentrations were measured using spectrophotometry (*SmartSpec™ Plus*) against a blank sample. Therefore, protein-bound chromogenic substrate absorption was detected at 595 nm using Bradford-based *BioRad Protein-Assay* [368]. 1 µl of cell lysates, prepared as described in 3.8.1, are diluted in 800 µl of ddH_2O and 200 µl of Bradford reagent. Protein concentration was calculated on the basis of a concurrently determined standard curve of BSA dilutions (concentrations 1 – 16 µg/µl; *NEB*) according to the Beer-Lambert law [369].

3.8.3. Co-Immunoprecipitation (IP)

Immunoprecipitation was performed from total-cell lysates (3.8.1, p. 65; 3.8.2, p. 66) and 1000 µg – 2000 µg of total-protein were used per sample. To avoid unspecific protein binding to the sepharose A beads (*Sigma-Aldrich*), samples were pre-cleared using 30 µl of Pansorbin (*Calbiochem*) at 4°C for 1 h on a rotator.

Immunoprecipitation using sepharose A beads

Simultaneously to pre-clearing, sepharose A beads, beforehand shaken with lysis buffer (Table 31 and Table 32, p. 66) in a rotator at 4°C for swelling (3 mg/sample), were coupled with purified antibodies or hybridoma supernatant (quantity of antibodies cited in Table 8, p. 32). IP samples were centrifuged at 6000 rpm and 4°C for 3 min and the supernatant was transferred into a fresh pre-cooled reaction tube, while the antibody–coupled sepharose A beads were washed three times with 1 ml of freshly supplemented lysis buffer (6000 rpm, 4°C, 2 min). Afterwards, the sepharose A beads were resuspended in an adequate amount of lysis buffer and the antibody-coupled beads were equally distributed among the pre-cleared IP samples. Immunoprecipitation was carried out on a spinning shaker at 4°C for 1 h, followed by subsequent centrifugation at 6000 rpm and 4°C for 3 min. The protein A immune complexes were washed 1 – 3x with 1 ml of supplemented lysis buffer. After the last centrifugation step, the lysis buffer was completely removed from the immune complexes and the pellet was mixed with an appropriate amount of 2x laemmli buffer [367]. The samples were boiled at 95°C for 5 min to elute the proteins and stored at -20°C until further analysis (3.8.5, p. 69; 3.8.6, p. 71).

Table 34: 2x laemmli buffer.

2x laemmli buffer	100 mM	Tris/HCl pH 6.8
	20% (v/v)	Glycerol
	4% (w/v)	SDS
	0.2% (w/v)	Bromphenol blue
	1.5% (v/v)	β-Mercaptoethanol
	ad	H_2O

Immunoprecipitation using magnetic beads

Immunoprecipitation assays with magnetic beads were performed using *BioRad SureBeads™ Magnetic Beads* and the inherent *BioRad 16-Tube SureBeads™ Magnetic Rack #1614916*. 50 µl of protein A or protein G *SureBeads™,* respectively, were coupled with the required amount of antibody for 30 min at RT. The beads were magnetized and washed to remove unbound antibody. The antibody-coupled beads were resuspended in an adequate amount of lysis buffer and distributed among the pre-cleared cell lysates. The samples were incubated for 1 h at RT. The complexes were washed 1 – 3x by magnetizing the beads and removing the supernatant containing the unbound protein fractions. The proteins were eluted from the beads by adding 20 µl of 2x laemmli buffer (Table 34, p. 67) and boiling at 95°C. The beads were magnetized and the eluted proteins were transferred to a fresh Eppendorf tube and stored at -20°C until further use.

3.8.4. Nickel-Nitrilotriacetic Acid (NiNTA) Precipitation

Mammalian cells either transiently transfected with a 6xHis-tagged construct or stably expressing 6xHis-tagged protein, are prepared according to experimental set-up (3.2.4, p. 55; 3.3, p. 55; 3.4.1, p. 56). To ensure sufficient number of 6xHis-SUMOylated proteins, two 100 mm dishes were prepared per sample. The cells were harvested according to 3.2.5 until the washing step 1x PBS (Table 21, p. 53). After addition of 1x PBS, 20% of the cells was transferred to a fresh reaction tube, centrifuged at 11000 rpm and 4°C for 3 min and subjected to total-cell lysate preparation with the high-stringent RIPA lysis buffer (3.8.1, p. 65). The remaining cells were centrifuged at 2000 rpm and 4°C for 3 min and the supernatant was discarded. The cell pellet was resuspended in 5 ml of Guanidinium-containing lysis buffer (B1) supplemented freshly with β-mercaptoethanol and either stored at -80°C until further use or directly sonicated three times for 30 sec at 4°C (40 pulses output 0.8; 0.8 impulse/s; *Sonifier 450*). Subsequently, with B1 pre-washed NiNTA beads (30 µl/sample; *Thermo Scientific*) were added to the lysates and incubated on a spinning shaker at 4°C overnight. The following day, samples were centrifuged at 4500 rpm and 4°C for 10 min and the supernatant was removed. The pellet was first washed in 1 ml of B1 buffer and afterwards one time with 1 ml of wash buffer pH 8.0 B2 and two times with 1 ml of wash buffer pH 6.3 B3, all freshly supplemented with β-mercaptoethanol (2000 rpm for 3 min) (Table 35, p. 69). For elution of the proteins the samples were mixed with 20 µl of elution buffer (Table 35, p. 69) and denatured at 95°C for 3 min. The samples were stored at -20°C until detailed analysis (0, p. 69; 3.8.6, p. 71).

Table 35: Buffers used for Nickel-nitrilotriacetic acid (NiNTA) precipitation.

B1	6 M	Guanidinium/HCl	**B2**	8 M	Urea
	0.1 M	Na_2HPO_4		0.1 M	Na_2HPO_4
	0.1 M	NaH_2PO_4		0.1 M	NaH_2PO_4
	10 mM	Tris/HCl pH 8.0		10 mM	Tris/HCl pH 8.0
	20 mM	Imidazole		20 mM	Imidazole
	5 mM	β-mercaptoethanol		5 mM	β-mercaptoethanol
B3	8 M	Urea	**Elution buffer**	200 mM	Imidazole
	0.1 M	Na_2HPO_4		0.1% (v/v)	SDS
	0.1 M	NaH_2PO_4		150 mM	Tris/HCl pH 6.3
	10 mM	Tris/HCl pH 6.3		30% (v/v)	Glycerol
	20 mM	Imidazole		720 mM	β-mercaptoethanol
	5 mM	β-mercaptoethanol		0.01% (w/v)	Bromphenol blue

3.8.5. Sodium Dodecyl Sulfate Polyacrylamide Gel Electrophoresis (SDS-PAGE)

Denatured proteins (3.8.1, p. 65; 3.8.3, p. 67; 3.8.4, p. 68) are separated by SDS-PAGE due to their size. The anionic detergent SDS binds the protein with a high affinity leading to the disruption of the native confirmation and a similar charge to mass ratio, whereby their electrophoretic mobility is depending on their molecular weight. Polyacrylamide gels were prepared using 30% acrylamide/bisacrylamide stock solution (*37.5:1 Rotiphorese Gel 30; Carl Roth*). For the initiation of polymerization free radicals and a stabilizer, such as ammonium persulfate (APS) and TEMED were added. Due to the differences of the pH and the percentage between the stacking and the separating gel, the proteins get concentrated between them and better separation can be achieved. First the proteins were concentrated in a 5% stacking gel with a pH of 6.8 before running into the separating gel with pH 8.8 and a gel density ranging from 8 – 15% depending on the size of the protein of interest (Table 36, p. 70). The *Biometra Multigel* chambers were filled with the separating gel and covered with isopropanol until it was hardened. Afterwards, the isopropanol was removed and the stacking gel was poured and the comb inserted. The electrophoresis was run at 15 mA per gel (*Biometra*) in TGS running buffer. To control the progress of the electrophoresis and to determine the molecular mass of the protein of interest, a molecular size marker was used (*PageRuler Prestained Protein Ladder Plus; Fermentas*).

Subsequently, the proteins were transferred to a nitrocellulose membrane by western blotting (*Hartenstein*) as described in 3.8.6 (p. 71).

Table 36: Buffers and solutions used for SDS-PAGE.

TGS	25 mM	Tris
	192 mM	Glycine
	0.1% (w/v)	SDS
5% stacking gel	17% (v/v)	Acrylamide (30%)
	69% (v/v)	H_2O
	13% (v/v)	1 M Tris/HCl pH 6.8
	0.1% (w/v)	SDS
	0.1% (w/v)	APS
	0.1% (v/v)	TEMED
8% separating gel	26% (v/v)	Acrylamide (30%)
	46% (v/v)	H_2O
	26% (v/v)	1.5 M Tris/HCl pH 8.8
	0.1% (w/v)	SDS
	0.1% (w/v)	APS
	0.06% (v/v)	TEMED
10% separating gel	34% (v/v)	Acrylamide (30%)
	38% (v/v)	H_2O
	26% (v/v)	1.5 M Tris/HCl pH 8.8
	0.1% (w/v)	SDS
	0.1% (w/v)	APS
	0.04% (v/v)	TEMED
15% separating gel	50% (v/v)	Acrylamide (30%)
	22% (v/v)	H_2O
	26% (v/v)	1.5 M Tris/HCl pH 8.8
	0.1% (w/v)	SDS
	0.1% (w/v)	APS
	0.04% (v/v)	TEMED

3.8.6. Western Blot Analysis

Proteins were separated exclusively dependent on their molecular weight via SDS-PAGE (0, p. 69) and transferred on a 0.2 µm or 0.45 µm nitrocellulose membrane (*GE Healthcare*) by western blotting to immobilize them for immunoluminescent detection. The transfer of proteins was carried out in Towbin buffer (Table 37, p. 71) in the *Trans-Blot Electrophoretic Transfer Cell System* from BioRad. The polyacrylamide gels, nitrocellulose membranes, blotting papers (*Hartenstein*) and the blotting pads were soaked in Towbin buffer and layered into a blotting cassette as follows: blotting pad, 2 blotting papers, polyacrylamide gel, nitrocellulose membrane, 2 blotting papers and a blotting pad. The cassettes were placed in the right orientation into the blotting chamber and the transfer was performed in "full wet" at 400 mA for 90 min. Afterwards, the nitrocellulose membranes were placed in 5% (w/v) skim-milk powder (*Sigma-Aldrich*) in 1x PBS (Table 21, p. 53) to saturate unspecific protein binding sites. The membranes were incubated at RT for at least 1 h at 4°C overnight on an orbital shaker (*GFL 3016*). Subsequently, the membranes were washed three times for 5 min in PBS-T (Table 24, p. 57) and incubated in primary antibodies at 4°C overnight. The following day, primary antibodies were removed from the membranes, followed by three washing steps for 5 min with PBS-T. Secondary antibodies conjugated with horseradish peroxidase were diluted 1:10000 (if not stated differently) in 3% (w/v) skim-milk powder in PBS-T and added to the membranes. The membranes were incubated on a reciprocating shaker at RT for at least 3 h or at 4°C overnight. After removal of the secondary antibody solution, nitrocellulose membranes were washed three time for 5 min with PBS-T before visualization by enhanced chemiluminescence. Therefore, 10 ml of solution ECL-A were supplemented with 100 µl ECL-B and 10 µl H_2O_2 (Table 37, p. 71). The membranes were incubated shortly in the chemiluminescent substrate before the protein bands were detected by X-ray films (*CEA*) with developing solutions (*Tetenal*) using the *AGFA Curix 60*. The developed X-rays were labelled, scanned and further processed for figures by using *PowerPoint* (*Microsoft*). Quantification of pixel density was performed using the program *ImageJ* (version 1.53c).

Table 37: Buffers and solutions used for western blotting.

Towbin buffer	25 mM	Tris	**ECL-A**	100 mM	Tris/HCl pH 6.8
	200 mM	Glycine		250 µg/ml	Luminol sodium
	0.05% (w/v)	SDS			
	20% (v/v)	Methanol	**ECL-B**	1.25 mg/ml	p-Coumaric acid in DMSO

3.8.7. Indirect Immunofluorescence (IF) Assay

For immunofluorescence analysis, cells were grown on cover slips and depending on the experimental set-up transfected and/or infected as previously described (3.2.4, p. 55; 3.4.1, p. 56). Media was removed at certain time points and the cells were washed once with 1x PBS. The cells were fixed with either ice-cold methanol at -20°C for 15 min or with 4% (w/v) paraformaldehyde (PFA) in PBS (Table 21, p. 53) at RT for 15 min. Methanol was removed before the air-dried cells were stored at -20°C or washed three times with 1x PBS and stored with PBS at 4°C, respectively. Before antibody incubation, the cells were permeabilized with 0.5% (v/v) Triton-X100 in PBS at RT for 5 min and subsequently, unspecific antibody binding sites were saturated by incubation with 1x TBS-BG (Table 23, p. 57) for at least 1 h on an orbital shaker. The antibody dilutions were prepared in 1x PBS according to Table 8 (p. 32) and cover slips were incubated in the solution at RT for 1 h. Afterwards, the cells were washed three times for 5 min in PBS-T, followed by incubation in fluorescence-coupled secondary antibodies (Table **10**, p. 35) and DAPI (1:200) (Table 38, p. 72) diluted in 1x PBS at RT for 1 h and exclusion of light. The cover slips were washed three time for 5 min with PBS-T to remove unbound antibodies. Finally, the cells were mounted in Mowiol (Table 38, p. 72) on glass slides and dried overnight in a dark environment at RT. The prepared glass slides were stored at 4°C until further analysis at a *Zeiss Axio Observer.Z1* with an *AxioCam HRm*. Obtained digital images were processed and quantified using the *Zeiss Zen 3.2 blue* software and *PowerPoint* (*Microsoft*). Analysis of co-localization by Pearson correlation coefficient was performed using the plug-in *JACoP* [365] with the *ImageJ* software (version 1.53c) [362]. Fluorescence signal intensity was analyzed using the *ImageJ* software (version 1.53c) by measuring the area and mean grey value. Corrected total-cell fluorescence (CTFC) was calculated according to the following formula:

CTCF = Integrated Density - (Area of selected cell × Fluorescence of background readings)

Table 38: Immunofluorescence assay buffers and solutions.

DAPI	14.3 mM	Di-hydrochloride	**Mowiol**	100 mM	Tris/HCl pH 8.5
	10.9 mM	Di-lactate		24% (v/v)	Glycerol
	1 mg/ml	DAPI		9.6% (w/v)	Mowiol
		ad H_2O			ad H_2O
		store at -20°C			store at -20°C

3.9. CUT&RUN assay

To analyze protein-DNA interactions, *CUT&RUN assays* (Cell Signaling Technology) were performed. A549 parental, shCTR and shDEK (Table 3, p. 27) cells were seeded in a 6 well plate according to 3.2.3 one day prior to infection with HAdV-wt at a moi of 20 (3.4.1, p. 56). Cells were harvested 24 h p.i. and 200.000 cells per sample were immediately subjected to perform *CUT&RUN* reactions according to the manufacturer's protocol. Concanavalin A magnetic beads are used to precipitate the chromatin of the permeabilized cells. Primary antibodies specific to the protein of interest are added before incubation with the pAG-MNase fusion protein. The pAG domain of the enzyme binds to the heavy chain of the primary antibody initiating the cleavage of the chromatin region of interest. The Concanavalin beads binding the DNA-protein interactions are magnetized and the supernatant containing cell debris and the unbound chromatin are removed. The protein-DNA complexes are eluted from the beads and purified using DNA purification spin columns (*Cell Signaling Technology*). The input samples were prepared according to the manufacturer's protocol. After harvesting, cells were sonified with a Diagenode Bioruptor on low setting for 30 sec on and 30 sec off for five rounds at 4°C. Input sample DNA was purified using DNA purification spin columns (*Cell Signaling Technology*). The quantification of the obtained DNA is analyzed by qPCR (3.7.3, p. 64).

3.10. Reporter Gene Assay

Quantitative promoter activity was measured using the *Dual-Luciferase® Reporter Assay System* by *Promega*. Therefore, expression of the *Firefly* luciferase (*Photinus pyralis*) under the control of promoter of interest was determined and normalized to the expression of the internal control, a *Renilla* luciferase (*Renilla reniformis*) under the control of the herpes simplex virus thymidine kinase (HSV-TK) promoter. Luciferases are enzymes with a catalytic activity emitting visible light upon substrate conversion according to the following reaction:

$$Luciferin + ATP \rightarrow luciferyl\ adenylate + PPI$$

$$Luciferyl\ adenylate + O_2 \rightarrow oxyluciferin + AMP + ☼$$

Dual luciferase assays were performed in biological triplicates with 2.5 x 10^5 cell per well (12-well plate) as described in 3.2.3 (p. 54). Parental or transduced mammalian cells were

transfected and infected according to the experimental set-up (3.2.4, p. 55; 3.4.1, p. 56). At certain time points cells were harvested by directly adding 150 µl of 1x *Lysis buffer* (*Promega*) per well and incubation at RT for 15 min on an orbital shaker. Samples were measured in a *GlowMax Multi Jr* luminometer (*Promega*) by transferring 5 µl of lysate in a 1.5 ml reaction tube containing pre-dispensed 20 µl of LAR II. Samples were mixed by pipetting and chemiluminescence of *Renilla* was measured (10 sec). Afterwards, 20 µl of Stop and Glow were added to the samples and subjected to sequential measuring of *Firefly* (10 sec).

4. Results

4.1. DEK is a Novel Host Factor Promoting HAdV Infection

4.1.1. HAdV Infection Modulates DEK Gene Expression

DEK was identified as novel regulatory interaction partner of the SWI/SNF complex containing Daxx and ATRX [309, 311]. Recent studies of Schreiner et al. postulate a restrictive function of the Daxx/ATRX complex by repressing viral gene expression. To ensure efficient viral replication, the SWI/SNF complex is targeted by the early viral protein E1B-55K mediating the proteasomal degradation of Daxx. Loss of Daxx is not only crucial to start viral transcription, but also supports the oncogenic potential of HAdVs [207, 243-246]. Likewise, the degradation of the tumor suppressor p53 [141, 145, 267, 268] and inhibition of Rb by HAdV promotes viral replication as well as tumorigenesis during infection [234-236, 370]. Suppression of Rb results in the release of E2F, thereby transcription of genes by E2F is activated [234, 237, 238]. Although DEK is a E2F-responsive gene [329], it also interacts and regulates cellular host factors, such as Daxx [309, 311] and p53 [371, 372], which are targeted for proteasomal degradation during HAdV infection [145, 245, 270, 373]. Therefore, the question arose how DEK expression is modulated during productive infection with HAdV.

To investigate DEK gene expression, mRNA production and protein levels were monitored in the three distinct cell lines H1299, A549 and HepaRG, after infection with HAdV-wt. Cells were harvested at the indicated time points and the collected cells were split for mRNA isolation and preparation of total-cell lysates with subsequent analysis by RT-qPCR or immunoblot assay, respectively. H1299 cells are an immortalized cell line derived from the metastatic site at the lymph node with a lack of p53 expression [374], while A549 is a hypotriploid adenocarcinomic human alveolar basal cell line [345]. In contrast to the transformed H1299 and A549 cells, we used the pseudodiploid, ‘pseudo-primary’ cell line HepaRG with only few substantial rearrangements of chromosomes. It derived from a hepatocellular carcinoma possessing epithelial-like properties during proliferation and can differentiate into hepatocyte-like cells [350, 375, 376].

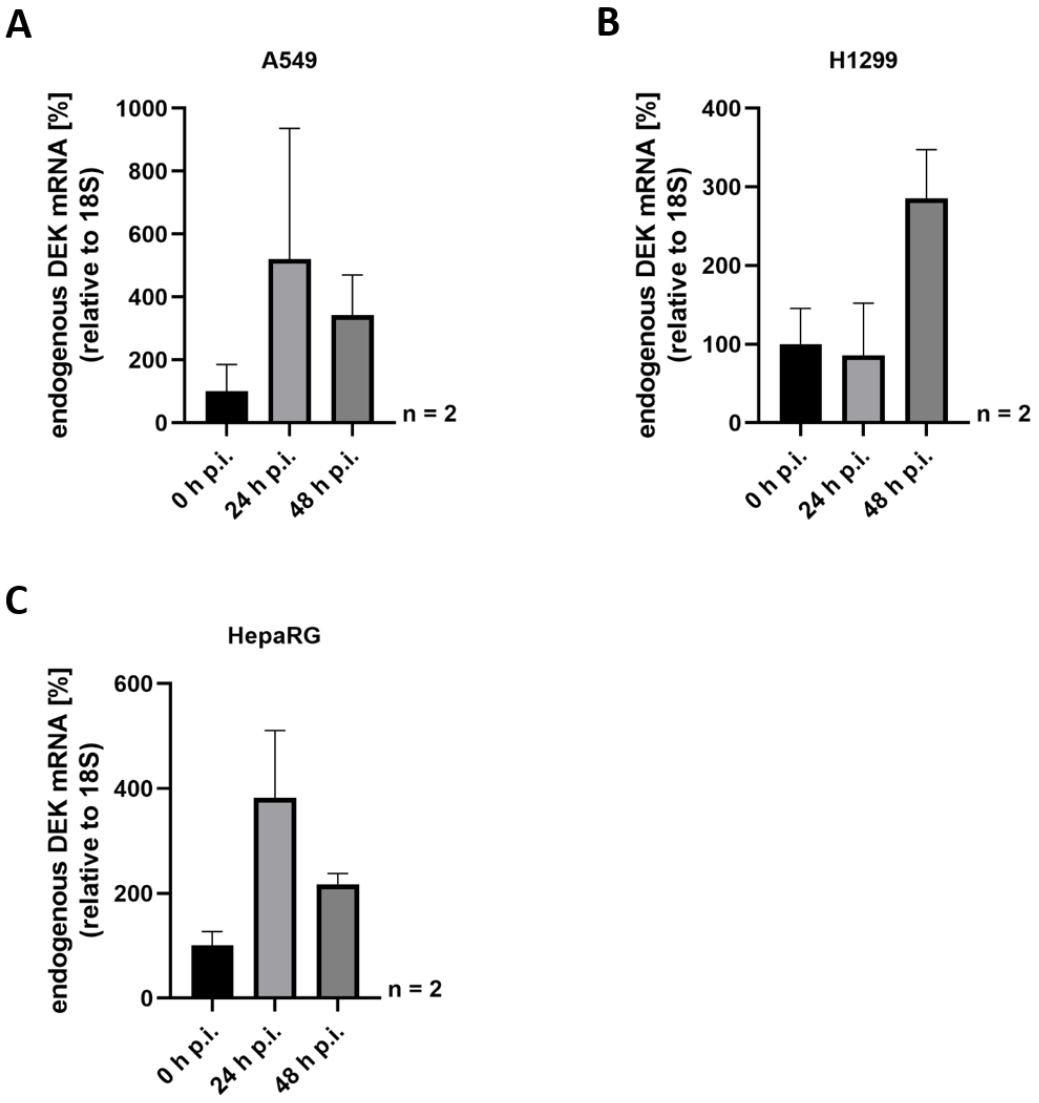

Figure 8: HAdV-wt increases DEK mRNA production. Cells were infected with HAdV-wt at a moi of 20 for **(A)** A549 cells and **(B)** H1299 cells or at a moi of 50 for **(C)** HepaRG cells and harvested 0 h, 24 h and 48 h after infection. Total mRNA was isolated with TRIzol and reversed transcribed into cDNA. Amount of DEK mRNA was quantified by qPCR and specific primers for DEK (#631, #632). The data was normalized to the respective 18S (#187, #188) mRNA levels. Bar charts represent average values and standard deviations based on two independent experiments measured in duplicates.

DEK mRNA levels were shown to be elevated in all three tested cell lines (Figure 8, p. 76). In A549 and HepaRG cells we observed the same time-dependent regulation, since the highest amount of DEK mRNA was detected 24 h p.i with a 5.2-fold increase in A549 (Figure 8 A, p. 76) cells and a 3.8-fold increase in HepaRG cells (Figure 8 C, p. 76). 48 h p.i. DEK mRNA was still increased, however to smaller amount than after 24 h. Here, we observed an upregulation of 3.4-fold and 2.2-fold in A549 or HepaRG cells, respectively (Figure 8 A/C, p. 76). In H1299 cells (Figure 8 C, p. 76) qPCR analysis reflected a different picture than observed in A549 and HepaRG cells. After 24 h we detected 0.25-fold decrease after 24 h, while DEK mRNA production was increased by 2.9-fold 48 h post

infection. Taken together, HAdV-wt induced production of DEK mRNA during the course of infection.

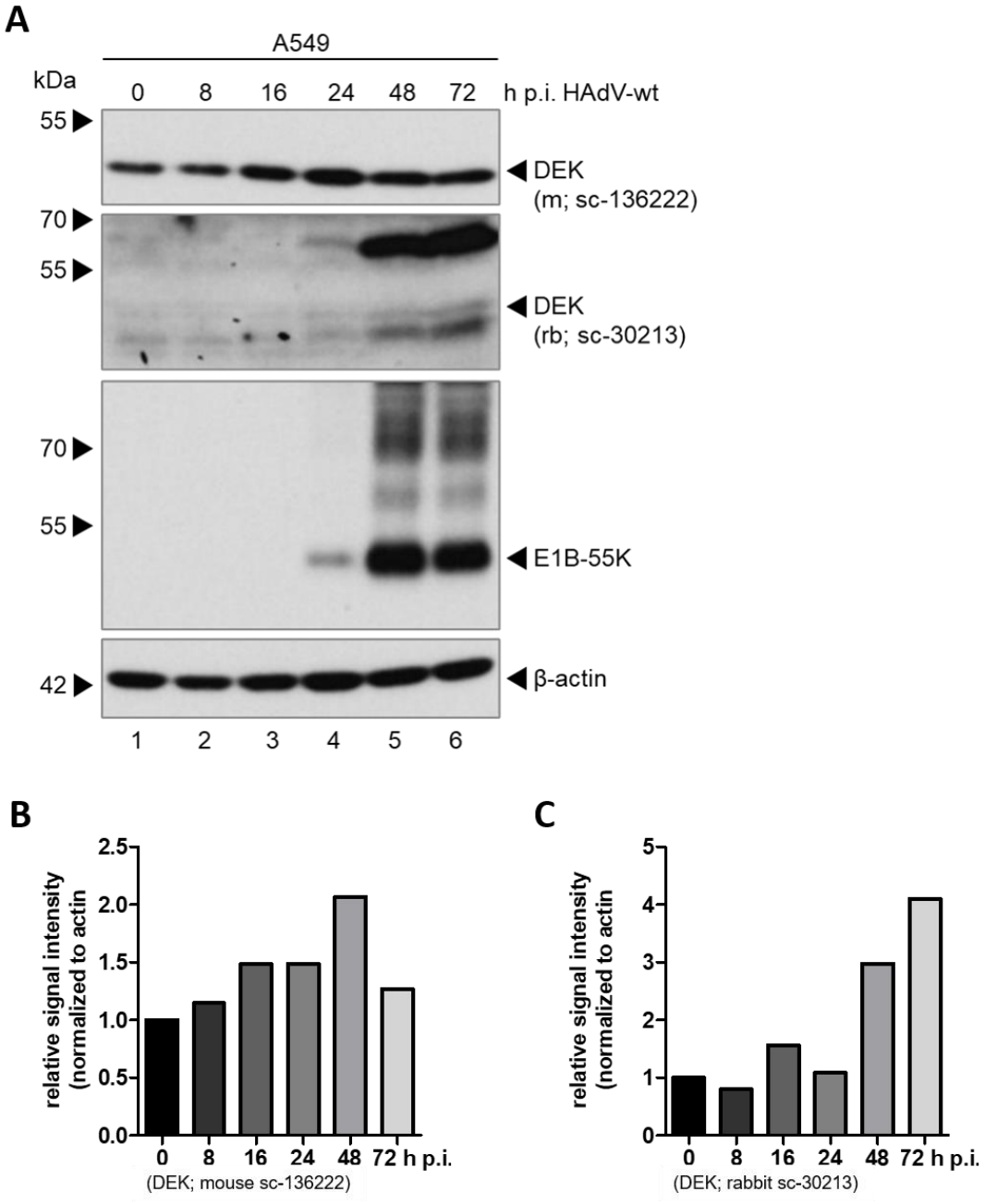

Figure 9: DEK protein levels are upregulated in A549 cells after HAdV-wt infection. A549 cells were infected with HAdV-wt at a moi of 20 and harvested at the indicated time points. Total-protein lysates were prepared using RIPA buffer and subjected to immunoblot analysis. Lysates were resolved by a 10% SDS-PAGE and proteins-of-interest were detected using mouse pAb α-E1B-55K (2A6), mouse mAb α-DEK (sc-136222), rabbit pAb α-DEK (sc-30213) and mouse mAb AC-15 (anti-β-actin). Molecular weights in kDa are indicated on the left, relevant proteins on the right. For quantification of DEK protein levels detected by either **(B)** mouse mAb α-DEK (sc-136222) or **(C)** rabbit pAb α-DEK (sc-30213), densitometric analysis of detected bands was performed using the *ImageJ* software (version 1.53c). Relative protein expression was normalized on the respective α-β-actin steady-state levels.

To further elucidate regulation of DEK expression by HAdVs we prepared total-cell lysates 0 h, 8 h, 16 h, 24 h and 48 h p.i from A549 (Figure 9, p. 77) and H1299 cells (Figure 10, p.

78). Cell lysates were resolved by SDS-PAGE and subjected to immunoblot analysis. We detected an increase in viral E1B-55K levels during the course of infection. In both lung carcinoma cell lines DEK protein levels were shown to be upregulated during adenoviral infection.

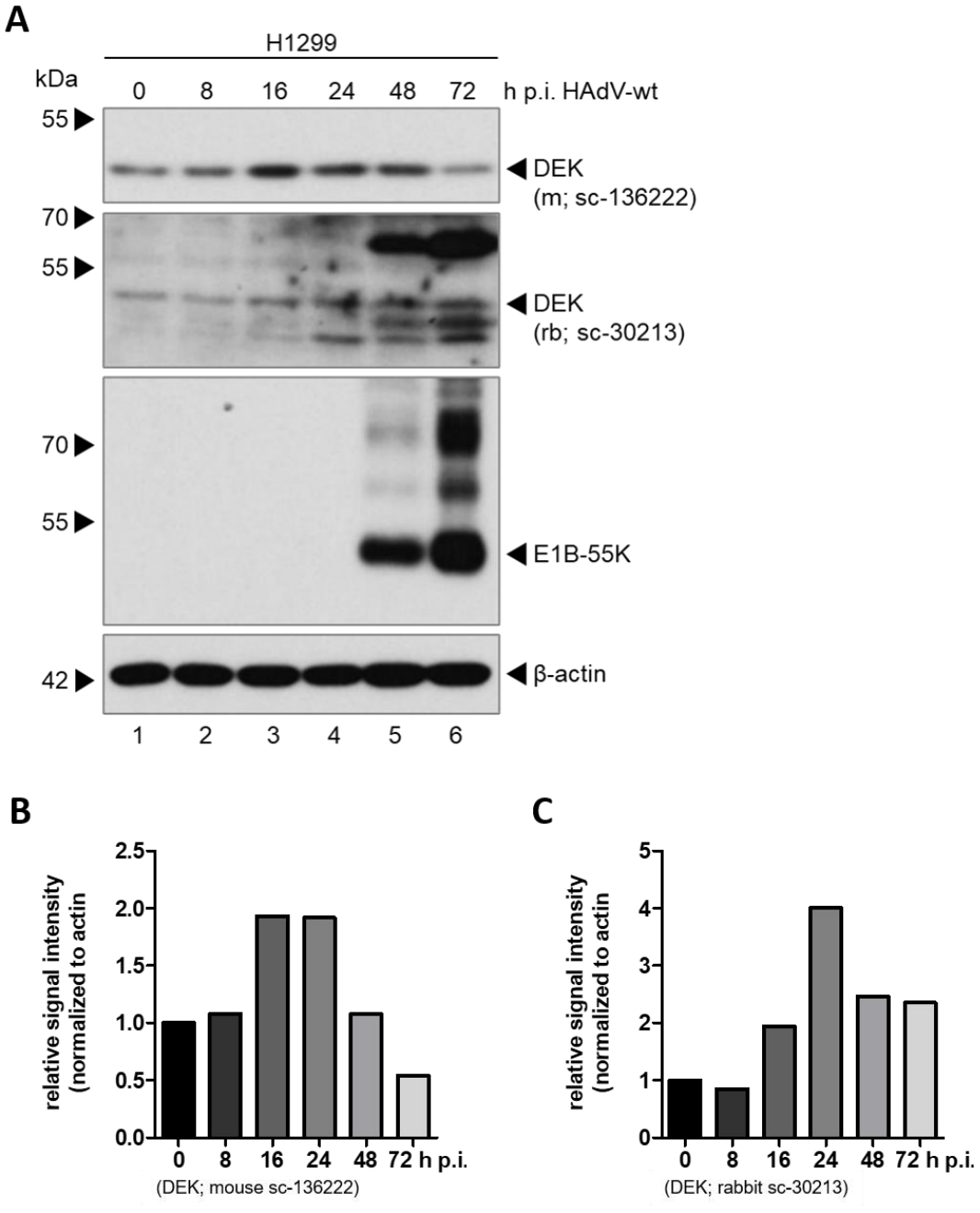

Figure 10: HAdV-wt infection increased DEK protein levels H1299 cells. H1299 cells were infected with HAdV-wt at a moi of 20 and harvested at the indicated time points. Total-protein lysates were prepared using RIPA buffer and subjected to immunoblot analysis. Lysates were resolved by a 10% SDS-PAGE and proteins-of-interest were detected using mouse pAb α-E1B-55K (2A6), mouse mAb α-DEK (sc-136222), rabbit pAb α-DEK (sc-30213) and mouse mAb AC-15 (anti-β-actin). Molecular weights in kDa are indicated on the left, relevant proteins on the right. For quantification of DEK protein levels detected by either **(B)** mouse mAb α-DEK (sc-136222) or **(C)** rabbit pAb α-DEK (sc-30213), densitometric analysis of detected bands was performed using the ImageJ software (version 1.53c). Relative protein expression was normalized on the respective α-β-actin steady-state levels.

In addition, we infected the liver cell line HepaRG with HAdV-wt at a moi of 50. The cells were harvested 0 h, 24 h, 48 h and 72 h p.i. and total-cell lysates were prepared. Cell lysates were resolved by SDS-PAGE and subjected to immunoblot analysis. We detected an accumulation of viral E2A levels. Furthermore, we observed increase of DEK during the course of infection (Figure 11, p. 79) similar to the investigated lung carcinoma cell lines (Figure 9, p. 77; Figure 10, p. 78).

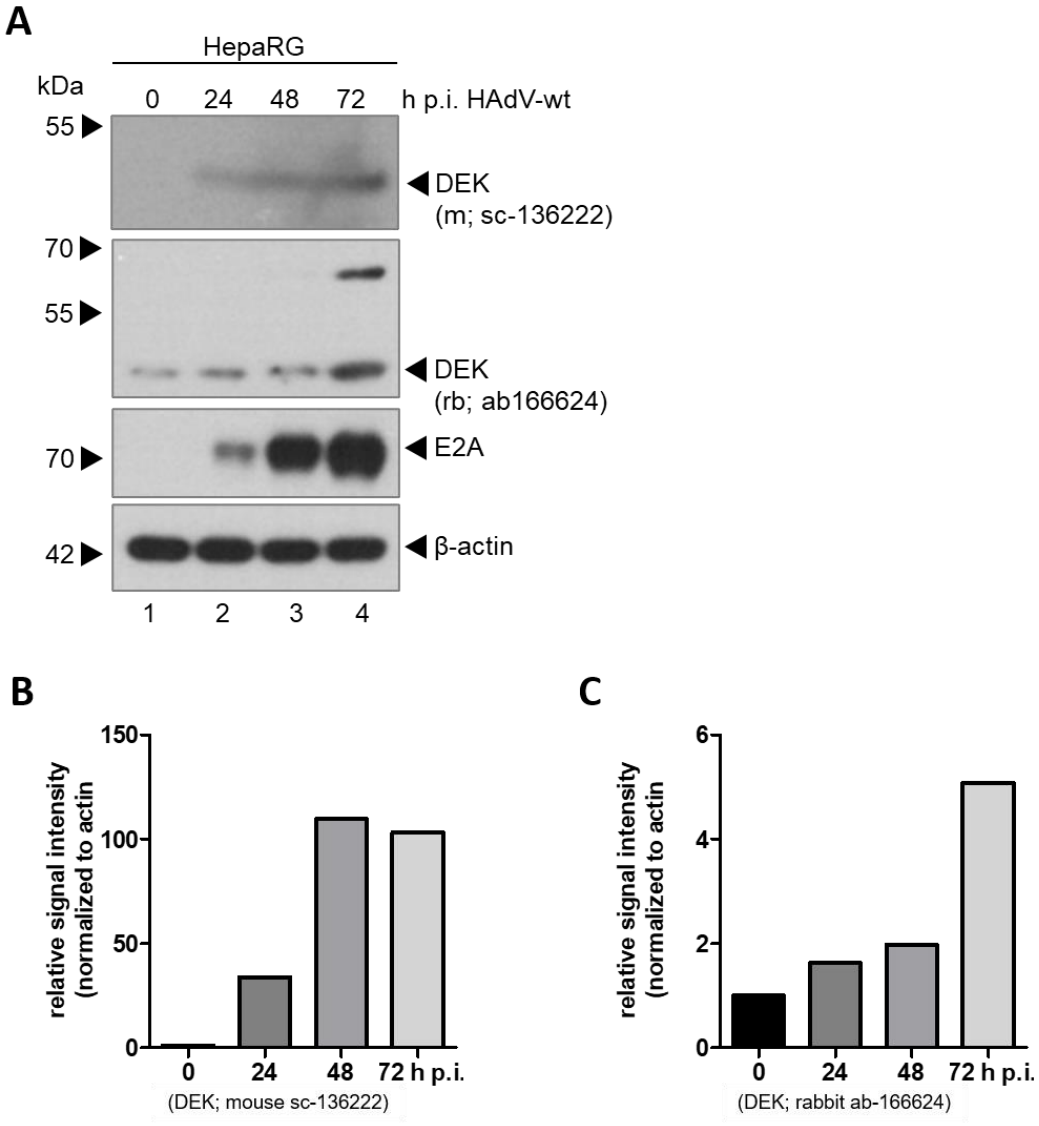

Figure 11: DEK levels increase during the course of adenoviral infection in HepaRG cells. HepaRG cells were infected with HAdV-wt at a moi of 50 and harvested at the indicated time points. Total-protein lysates were prepared using RIPA buffer and subjected to immunoblot analysis. Lysates were resolved by a 10% SDS-PAGE and proteins-of-interest were detected using mouse pAb α-E1B-55K (2A6), mouse mAb α-DEK (sc-136222), rabbit mAb α-DEK (ab166624) and mouse mAb AC-15 (anti-β-actin). Molecular weights in kDa are indicated on the left, relevant proteins on the right. For quantification of DEK protein levels detected by either **(B)** mouse mAb α-DEK (sc-136222) or **(C)** rabbit mAb α-DEK (ab166624), densitometric analysis of detected bands was performed using the ImageJ software (version 1.53c). Relative protein expression was normalized on the respective α-β-actin steady-state levels.

4.1.2. The Chromatin-Associated DEK Protein Modulates HAdV Infection

DEK is a multifunctional protein involved in several processes regarding chromatin remodeling and gene transcription. This protein was described to be highly associated with chromatin by binding transcription start sites or unspecific binding to DNA. Previous studies un-raveled a repressing as well as activating role of DEK in gene transcription, since DEK interacts with and recruits distinct transcription factors, histones and HDAC, whereby it can balance the maintenance of heterochromatin and euchromatin. Additionally, binding of DEK to DNA can also change the topology of DNA, since DEK bears chaperone activity [282, 285, 289, 291, 292, 294, 296, 308, 309, 312, 318, 377]. As DEK is capable of regulating gene transcription and our time course experiments revealed an elevated DEK gene expression upon HAdV-wt infection (4.1.1, p. 75), we next investigated the influence of DEK on viral DNA synthesis, mRNA production, protein levels and progeny production. Therefore, either HeLa cells stably expressing a 6xHis-FLAG-tagged DEK protein with the corresponding control cell lines were used or mammalian cells were transfected with a recombinant FLAG-DEK plasmid. The cells were infected with HAdV-wt and harvested at the indicated time points, before the cells were subdivided and various assays were performed.

4.1.2.1. DEK N-Terminally Fused to FLAG-Tag Can Be Expressed in Human Cell Lines

To investigate the role of the chromatin associated DEK protein on HAdV infection and replication, the generation of a recombinant expression plasmid was mandatory. Therefore, the DEK coding sequence was amplified using specific primers (#420 and #626, 2.3.1, p. 28) on pMIEG His-FLAG-DEK retroviral vector (kindly provided by Prof. Susanne Wells [291]) and the required restriction sites BamHI and XhoI were introduced at 3’ and 5’-end of the sequence. The obtained PCR product was analyzed on an agarose gel and the desired band was removed from the gel. The isolated cDNA and the pCMX3b-FLAG vector were digested with BamHI and XhoI to ligate the DEK sequence in a directed manner. The cloning strategy is shown in Figure 12 (p. 81).

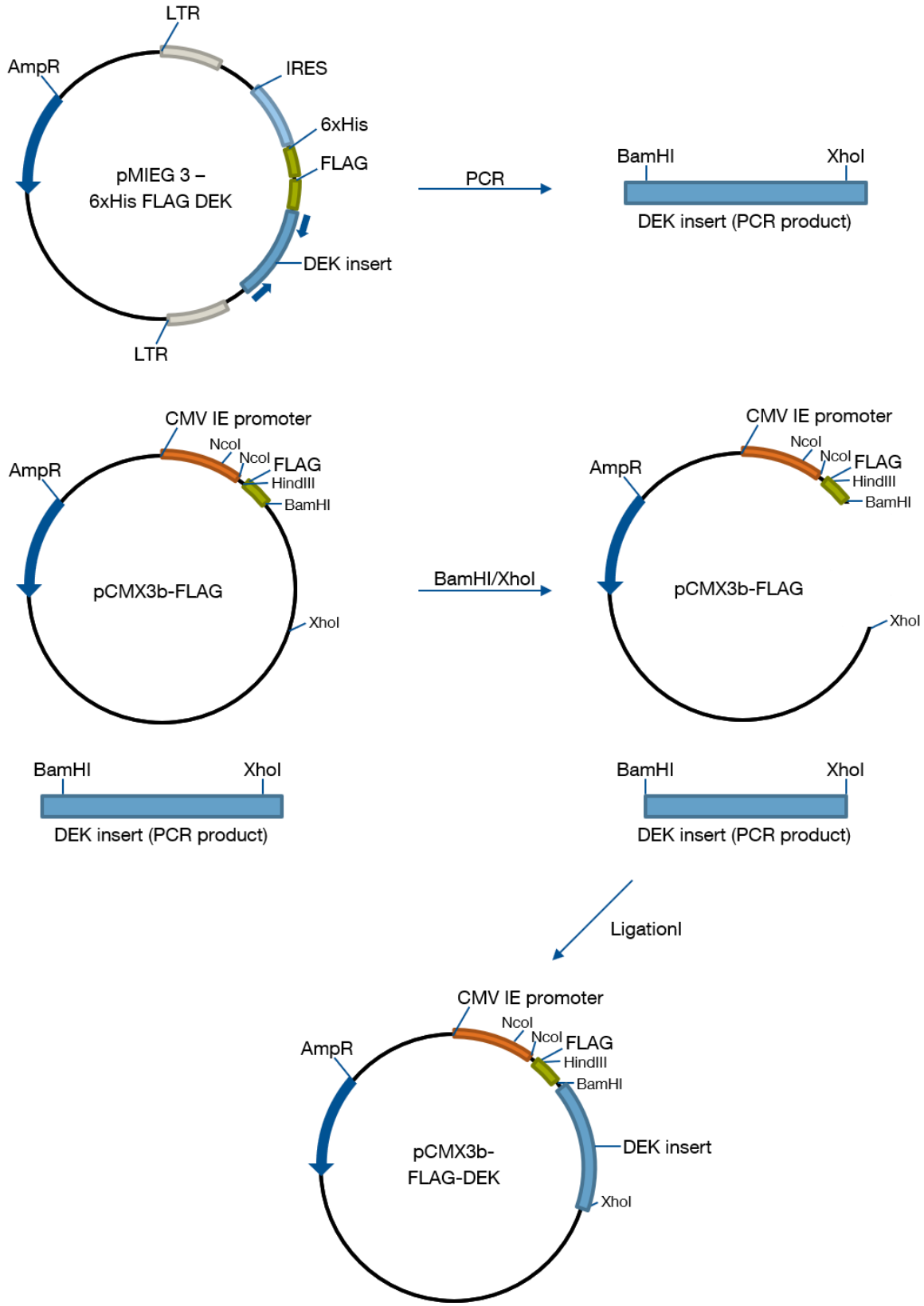

Figure 12: Cloning strategy for N-terminally FLAG-tagged DEK. The open reading frame was amplified by PCR and the pMIEG3-6xHis FLAG DEK retroviral vector served as a template. Restriction sites BamHI and XhoI were introduced by the primers #420 and #626 specific for the coding sequence of DEK. pCMX3b-FLAG vector and the obtained PCR product were digested with BamHI and XhoI prior to ligation.

The obtained expression plasmid encoding for a N-terminally FLAG-tagged DEK protein was verified via Sanger sequencing and synthesis of the recombinant protein in mammalian cells was visualized by qPCR and immunoblotting. We confirmed mRNA overexpression of DEK in H1299 (Figure 13 A, p. 82) and HepaRG cells (Figure 13 B, p. 82) after 24 h and 48 h post transfection.

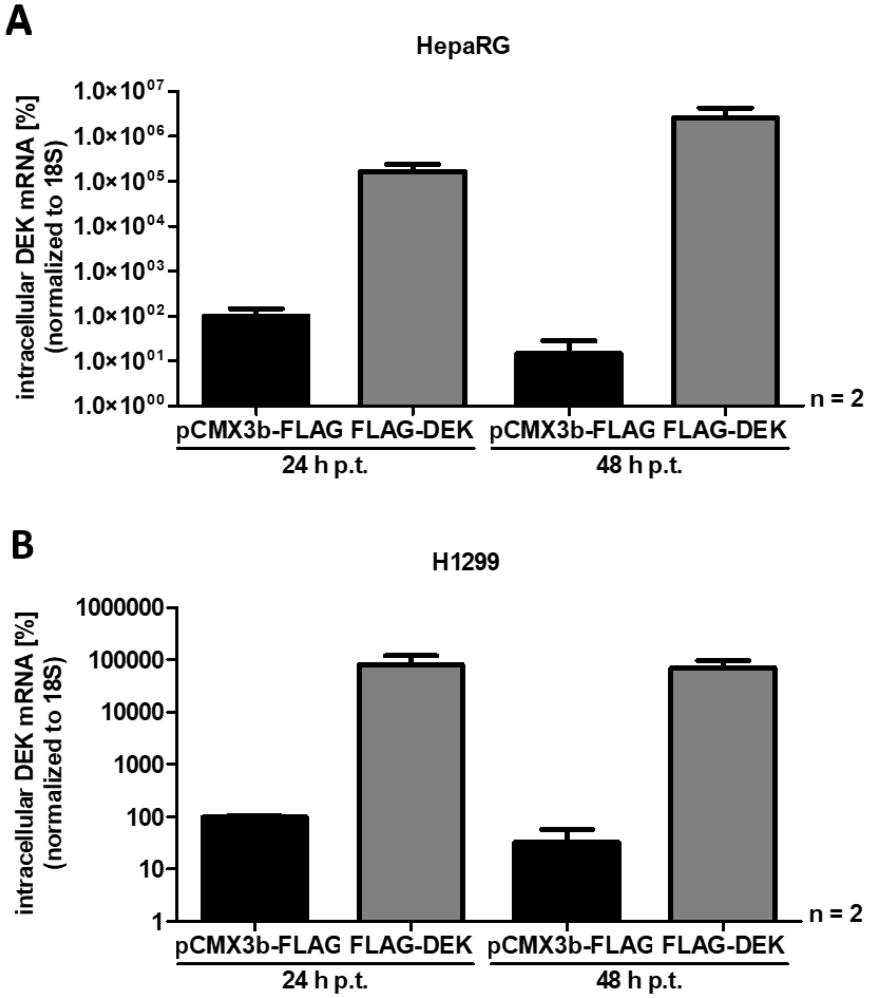

Figure 13: Verification of elevated DEK expression after transfection of FLAG-DEK. (A) HepaRG and **(B)** H1299 cells were transfected with 10 µg of either pCMX3b-FLAG or FLAG-DEK (#V32, #P738) and infected with HAdV-wt at a moi of 50 or 20, respectively. Cells were harvested 24 h and 48 h p.i. and total mRNA was isolated with TRIzol. After reverse transcription, mRNA species were detected using specific primers for DEK (#631, #632). The data was normalized to the respective 18S (#187, #188) mRNA levels. Bar charts represent average values and standard deviations based on two independent experiments measured in triplicates.

Additionally, total-cell lysates were prepared 48 h p.i. and subjected to western blot analysis shown in Figure 14. Expression of FLAG-DEK from the obtained recombinant plasmids was observed in both cell lines in mock (Figure 14 A/B lane 2, p. 83) and HAdV-wt infected cells (Figure 14 A/B lane 4, p. 83). DEK isoform 1 and isoform 2 were detected at their calculated molecular weight of 42.7 kDa and 38.7 kDa.

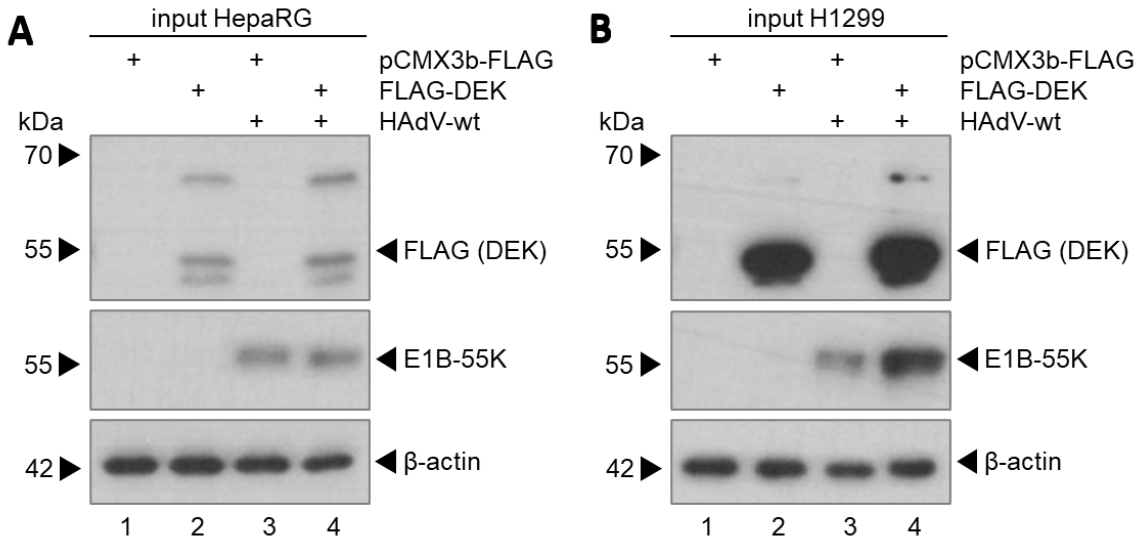

Figure 14: Expression profile of FLAG-DEK in H1299 and HepaRG cells. Cells were transfected with 10 µg of FLAG-DEK (#P738) expression plasmid or the corresponding empty vector control pCMX3b-FLAG (#V32). Cells were infected with HAdV-wt at a moi of 50 for **(A)** HepaRG cells or at a moi of 20 for **(B)** H1299 cells and harvested 48 h after infection. Total-cell lysates were prepared using high-stringent RIPA buffer and subjected to immunoblot analysis. Lysates were resolved by a 10% SDS-PAGE and proteins-of-interest were detected using mouse pAb α-E1B-55K (2A6), mouse mAb α-FLAG-M2 (DEK) and mouse mAb AC-15 (anti-β-actin). Molecular weights in kDa are indicated on the left, relevant proteins on the right.

4.1.2.2. HAdV Replication and Progeny Production Is Promoted by the DEK Protein

To analyze the effect of DEK on viral DNA (vDNA) synthesis and gene expression, mammalian cell lines H1299 and HepaRG cells were transfected with the empty vector control pCMX3b-FLAG or FLAG-DEK before infection with HAdV-wt (H1299: moi 20; HepaRG: moi 50). Cells were harvested 48 h p.i. and the collected cells were split for determination of viral progeny production, vDNA and mRNA isolation and preparation of total-cell lysates with subsequent analysis by quantitative immunofluorescence staining, RT-qPCR or immunoblot assay, respectively.

To elucidate, if DEK is modulating viral DNA synthesis, cells were lysed using high stringent RIPA buffer. After proteinase K digestion, the isolated DNA amount was quantified using qPCR. However, in both investigated cell lines DEK expression had no impact on HAdV DNA synthesis (Figure 15, p. 84).

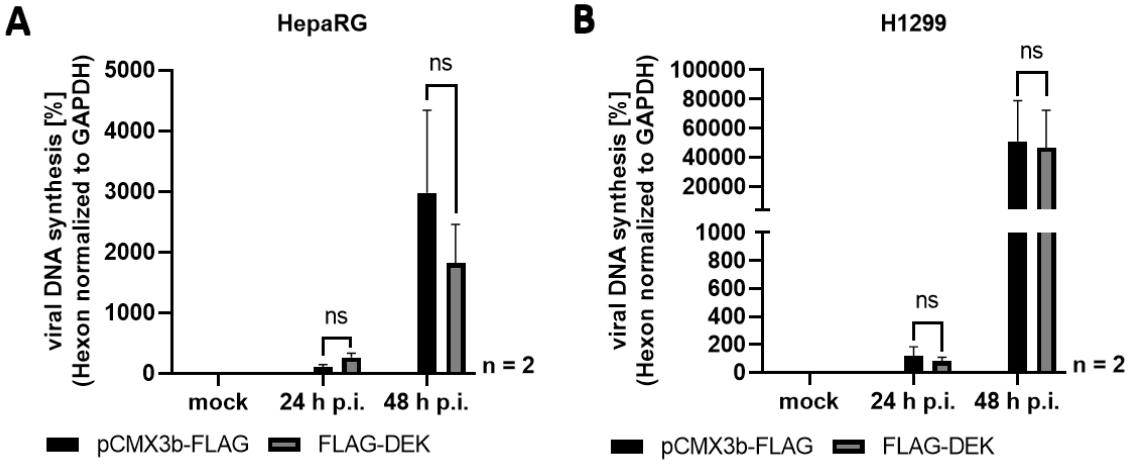

Figure 15: Overexpression of DEK does not change the amount of viral DNA during productive infection. 4 x 10^6 cells were seeded in a 100 mm dish one day in prior. The cells were transfected with 10 µg of either the empty vector control pCMX3b-FLAG (#V32) or the recombinant plasmid encoding for FLAG-DEK (P738) for 3 h and subsequently infected with HAdV-wt **(A)** at a moi of 50 for HepaRG cells and **(B)** at a moi of 20 for H1299 cells. The infected cells were harvested 24 h and 48 h p.i. and total-cell lysates were prepared. 10 µg of RIPA lysate were digested by proteinase K and 5 µl of a 1:200 dilution were amplified by qPCR primers specific against the viral *hexon* (#189, #190) coding region. As an internal control primer against *gapdh* (#197, #198) was used and the respective samples were normalized to the internal control. Bar charts represent average values and standard deviations based on two independent experiments measured in triplicates. Statistically significant differences were assessed using a multiple unpaired t-test with the GraphPad Prism9 software. *ns = not significant*

Subsequently, we determined the amount of viral E1A and hexon mRNA in H1299 and HepaRG cells after transfection of FLAG-DEK (Figure 16, p. 85). In all analyzed samples, we observed elevated viral mRNA production depending on DEK expression. In HepaRG cells, E1A mRNA was 2.8-fold (Figure 16 A, p. 85) and hexon mRNA 2.3-fold increased compared to the control transfected with pCMX3b-FLAG (Figure 16 B, p. 85). We obtained similar observations in H1299 cells, in which DEK expression caused a 1.8-fold elevation of E1A mRNA levels (Figure 16 C, p. 85) and a significant 2-fold induction of hexon mRNA levels (Figure 16 D, p. 85). In sum, DEK expression is not regulating viral DNA synthesis, however DEK is capable of elevating viral mRNA production.

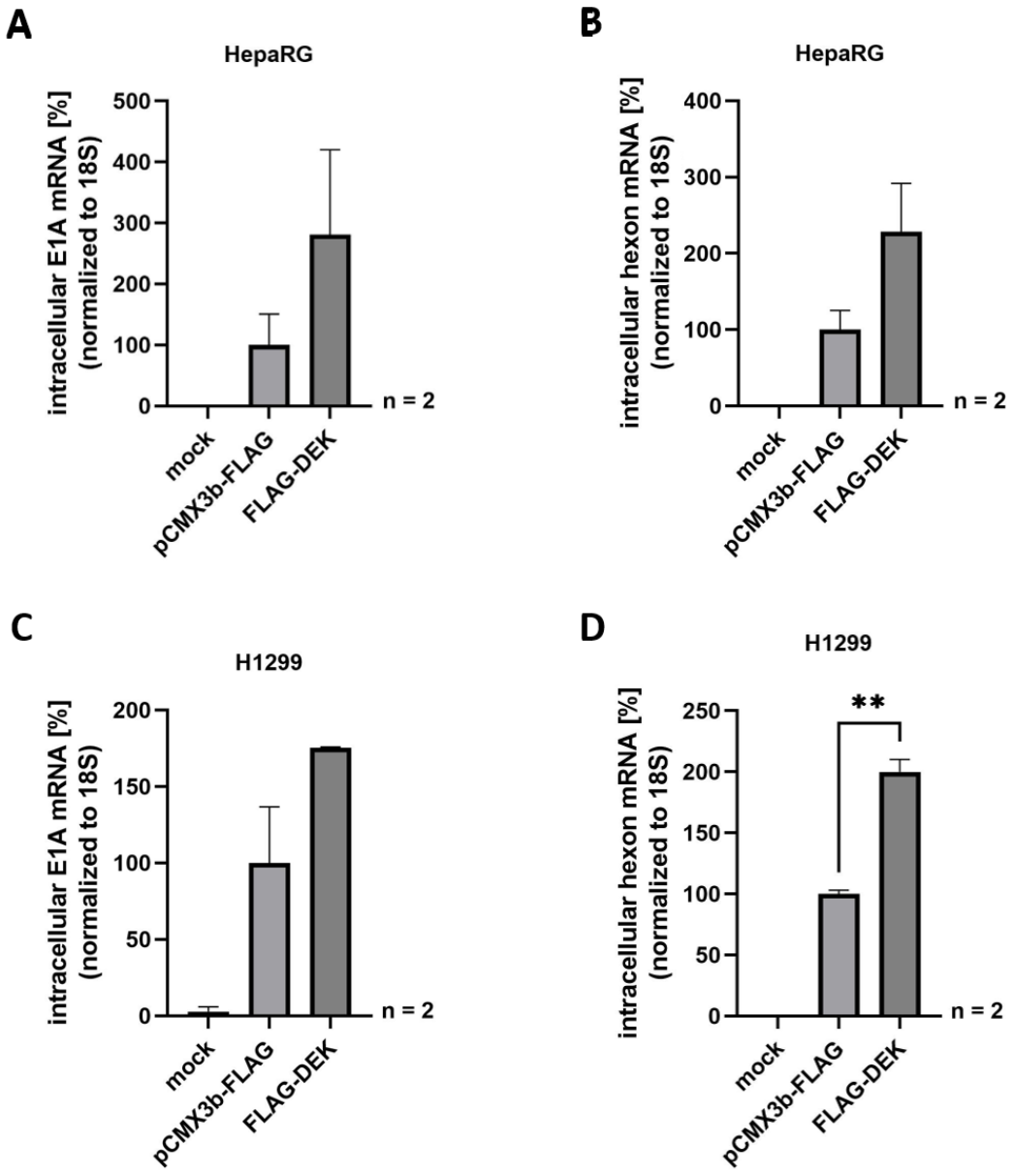

Figure 16: DEK increases viral E1A and hexon mRNA production in HepaRG and H1299 cells. Cells were transfected with 10 µg of FLAG-DEK (P738) expression plasmid or the corresponding empty vector control pCMX3b-FLAG (#V32). Cells were infected with HAdV-wt at a moi of 20 for **(A)** H1299 cells or at a moi of 50 for **(B)** HepaRG cells and harvested 48 h post infection. Total mRNA was isolated with TRIzol and reversed transcribed into cDNA. Amount of mRNA species were quantified by qPCR and specific primers for **(A/C)** E1A (#181, #182) and **(B/D)** hexon (#189, #190). The data was normalized to the respective 18S (#187, #188) mRNA levels. Bar charts represent average values and standard deviations based on two independent experiments measured in duplicates. Statistically significant differences were assessed using a student's unpaired t-test with the GraphPad Prism9 software. ** $p \leq 0.01$

Next, we subjected the prepared total-cell lysates to SDS-PAGE and immunoblot analysis to elucidate the effect of DEK on viral protein levels. In both cell lines we could observe enhanced viral protein levels upon DEK expression (Figure 17, p. 86; Figure 18, p. 87; Figure 19, p. 88). In HepaRG cells, E1A levels were 1.6-fold, E1B-55K levels 1.9-fold, E2A levels 1.5-fold, E4orf3 levels 2.7-fold, pVI levels 1.8-fold (Figure 17 A compare lane 4 to 3, p. 86; Figure 19 A, p. 88) and Capsid levels 1.5-fold increased (Figure 17 B compare lane 4 to 3, p. 86; Figure 19 A, p. 88), while in H1299 we observed an upregulation of 1.5-fold

for E1A, of 2-fold for E1B-55K, of 1.6-fold for E4orf3, of 1.4-fold for pVI (Figure 18 A compare lane 4 to 3, p. 87; Figure 19 B, p. 88) and of 1.4-fold for Capsid (Figure 18 B compare lane 4 to 3, p. 87; Figure 19 B, p. 88). However, E2A levels were not changed in H1299 cells after transfection of FLAG-DEK (Figure 18 A, p. 87 compare lane 4 to 3; Figure 19 B, p. 88). In conclusion, we verified the elevation of viral gene expression by DEK additionally on protein level. Furthermore, we could show that viral proteins expressed at all stages of viral infection were regulated by DEK.

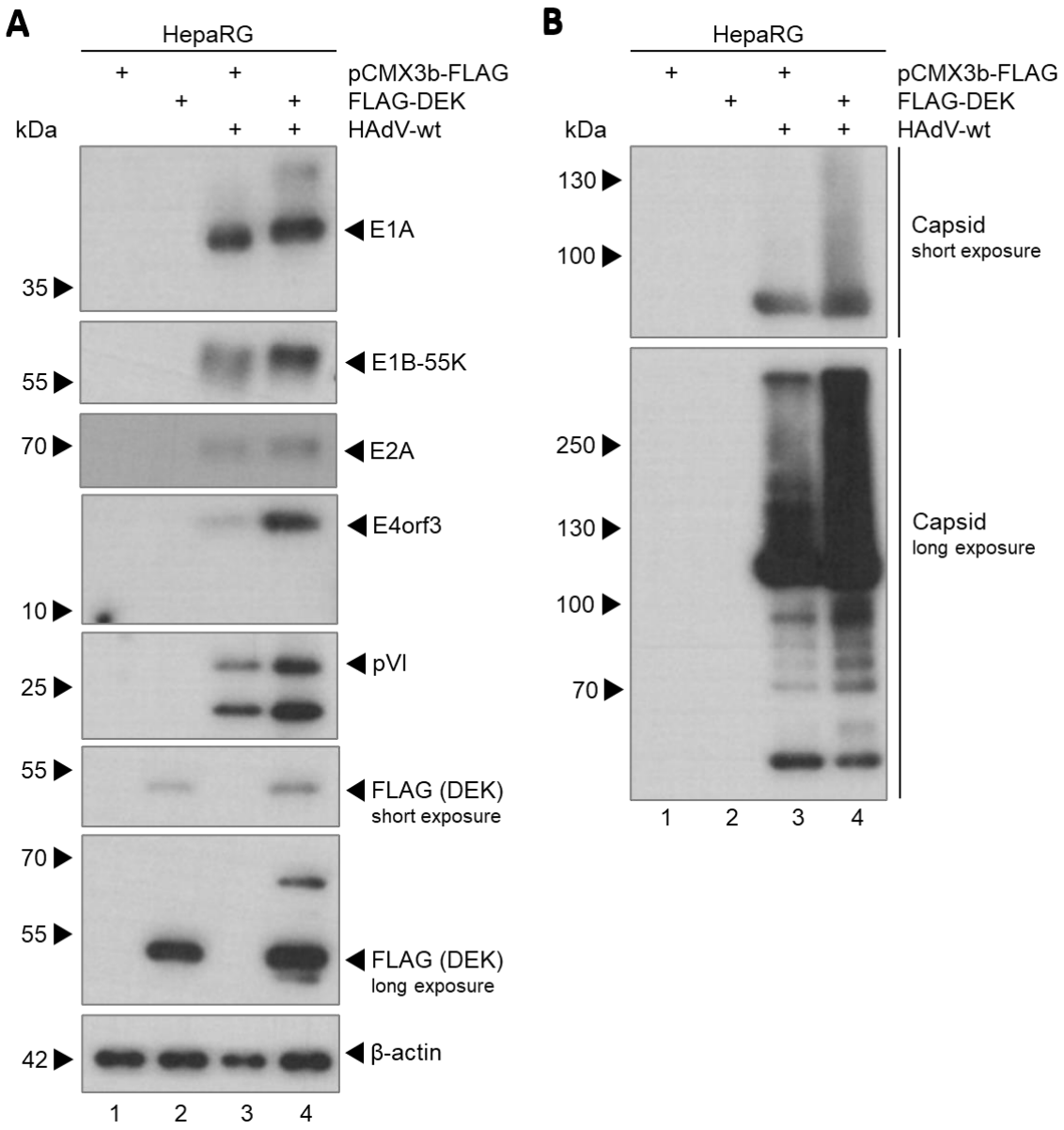

Figure 17: DEK expression increases viral protein levels in HepaRG cells. Cells were transfected with 10 µg of FLAG-DEK (#P738) expression plasmid or the corresponding empty vector control pCMX3b-FLAG (#V32) and infected with HAdV-wt at a moi of 50. Total-cell lysates were prepared using high-stringent RIPA buffer 48 h p.i. and subjected to immunoblot analysis. **(A)** Lysates were resolved by a 15% SDS-PAGE for E4orf3 and pVI and by a 10% SDS-PAGE for E1A, E1B-55K, E2A, FLAG-DEK and actin. **(B)** Capsid proteins were resolved on an 8% SDS-PAGE. Proteins-of-interest were detected using **(A)** mouse mAb α- E1A (M73, sc-25), mouse pAb α-E1B-55K (2A6), mouse mAb α-E2A (B6-8), rat pAb α-E4orf3 (6A11), rabbit pAb α-pVI, mouse mAb α-FLAG-M2 (DEK), mouse

mAb AC-15 (anti-β-actin) and **(B)** rabbit pAb α-Capsid (L133). Molecular weights in kDa are indicated on the left, relevant proteins on the right.

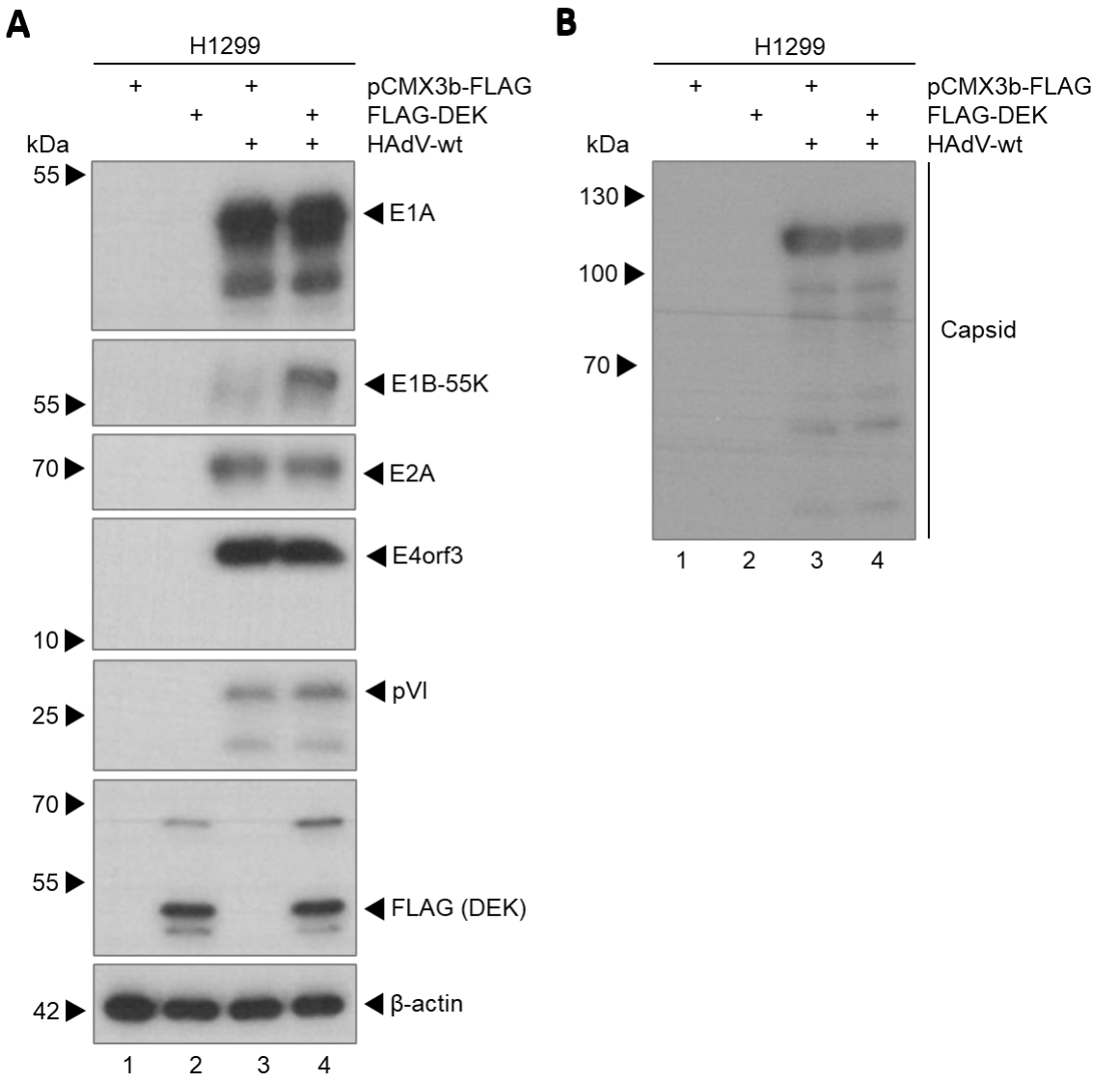

Figure 18: Viral protein levels are elevated by DEK in H1299 cells. Cells were transfected with 10 µg of FLAG-DEK (#P738) expression plasmid or the corresponding empty vector control pCMX3b-FLAG (#V32) and infected with HAdV-wt at a moi of 20. Total-cell lysates were prepared using high-stringent RIPA buffer 48 h p.i. and subjected to immunoblot analysis. **(A)** Lysates were resolved by a 15% SDS-PAGE for E4orf3 and pVI and by a 10% SDS-PAGE for E1A, E1B-55K, E2A, FLAG-DEK and actin. **(B)** Capsid proteins were resolved on an 8% SDS-PAGE. Proteins-of-interest were detected using **(A)** mouse mAb α- E1A (M73, sc-25), mouse pAb α-E1B-55K (2A6), mouse mAb α-E2A (B6-8), rat pAb α-E4orf3 (6A11), rabbit pAb α-pVI, mouse mAb α-FLAG-M2 (DEK), mouse mAb AC-15 (anti-β-actin) and **(B)** rabbit pAb α-Capsid (L133). Molecular weights in kDa are indicated on the left, relevant proteins on the right.

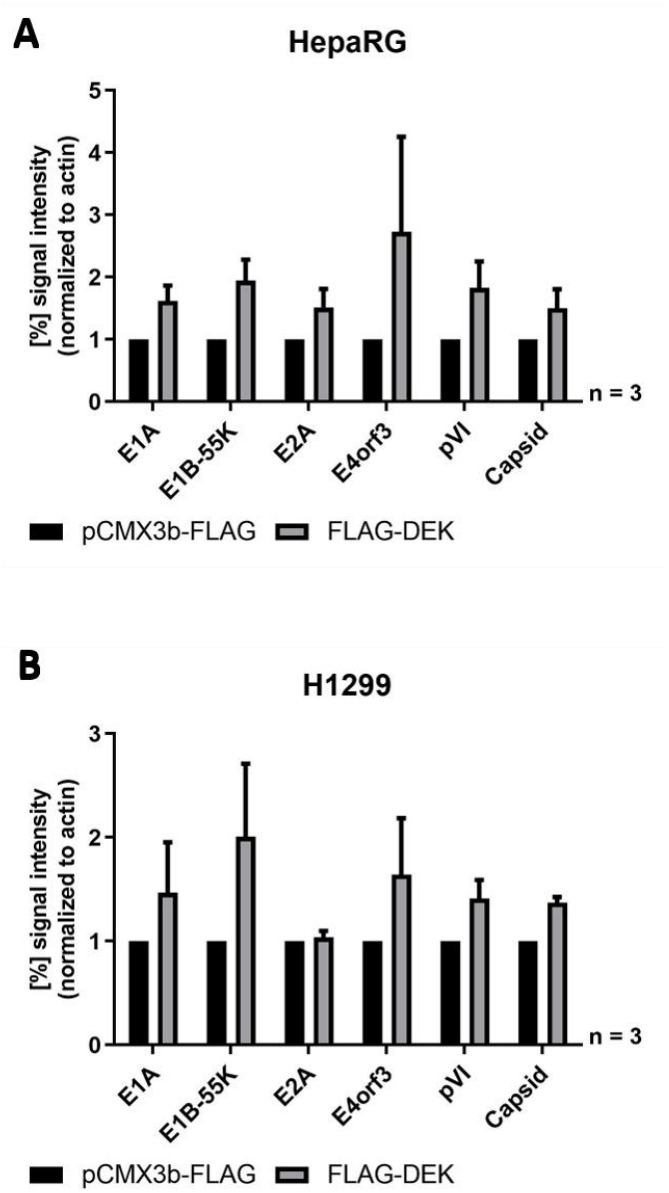

Figure 19: Relative quantification of viral protein levels upon DEK expression in HepaRG and H1299 cells. For quantification of viral protein levels in **(A)** HepaRG cells and **(B)** H1299 cells, densitometric analysis of detected bands (Figure 17, p. 86; Figure 18, p. 87) was performed using the *ImageJ* software (version 1.53c). Relative protein expression was normalized on the respective α-β-actin steady-state levels. Bar charts represent average values and standard deviations based on three biologically independent experiments.

Since we observed a supporting role of DEK on viral mRNA production and protein synthesis, we tested how DEK might regulate viral progeny production. Therefore, we performed virus yield experiments by isolating the newly synthesized virions from DEK-overexpressing and respective parental cells, both infected with HAdV-wt. A serial dilution of the isolated virus was prepared and HEK-293 cells were reinfected. The cells were fixed 24 h p.i. with ice-cold methanol and the viral progeny production was analyzed using quantitative immunofluorescence staining of the viral early replication center marker protein E2A (Figure 20, p. 89).

Compared to the control cell lines, viral progeny production was significantly 681-fold at 24 h, 153-fold at 48 h and 5.9-fold at 72 h p.i. upregulated in HeLa cells stably overexpressing DEK (Figure 20 A, p. 89). Viral particle synthesis was in HepaRG (Figure 20 B, p. 89) and H1299 (Figure 20 C, p. 89) cells significantly 2-fold upregulated after expression of DEK in comparison to the empty vector control. Taken together, we observed induction of adenoviral infection and replication by DEK in all tested cell lines.

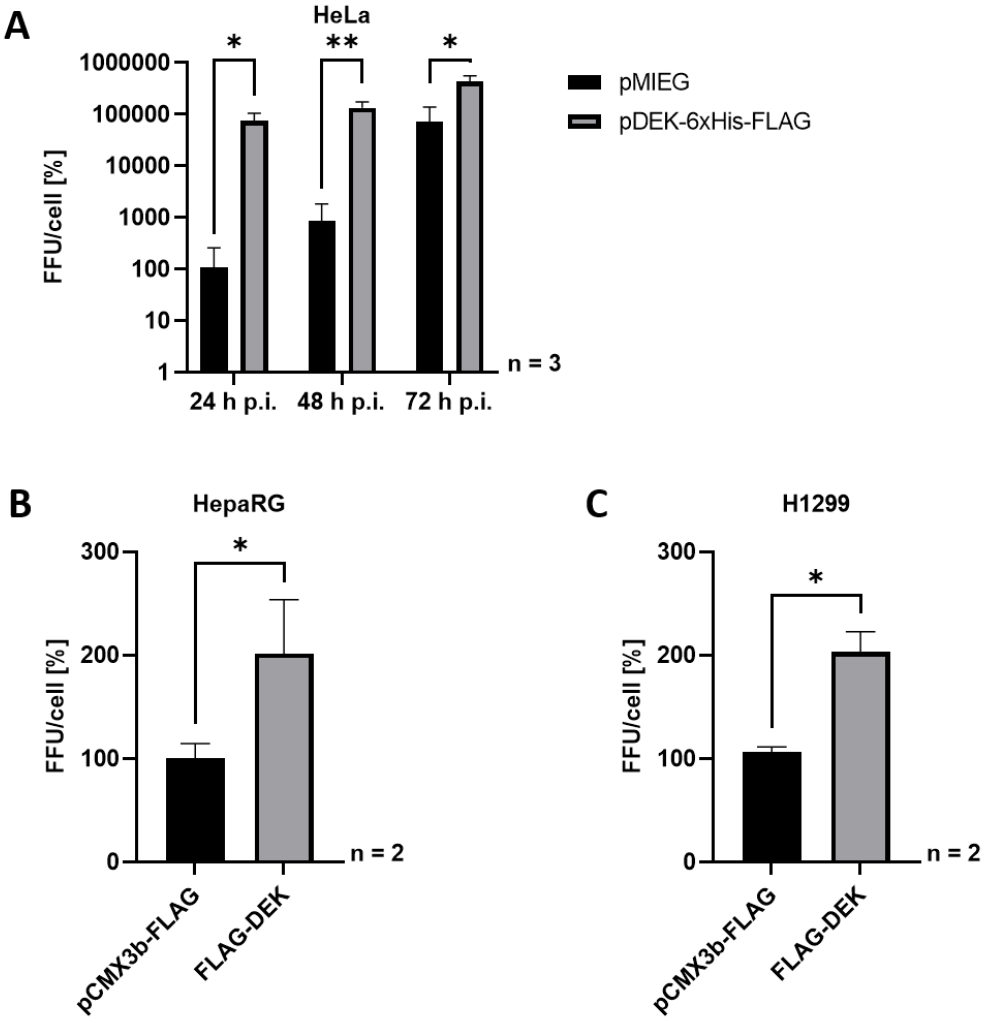

Figure 20: DEK is a positive factor promoting viral progeny production. (A) HeLa pMIEG and pDEK-6xHis-FLAG cell lines were infected at a moi of 20 with HAdV-wt. **(B)** HepaRG cell were infected at a moi of 50 and (**C**) H1299 cells at a moi of 20 after transfection with 10 µg of either empty vector control pCMX3b-FLAG or FLAG-DEK. Viral particles were harvested **(A, B, C)** 24 h p.i. as well as 48 h and 72 h p.i. for **(A)**. Virus yield was determined by quantitative staining of early viral E2A after reinfection of HEK-293 cells with a serial dilution of the newly synthesized virions. FFU/cell was calculated taking the cell number, dilution factor and objective magnification into account. Bar charts represent average values and standard deviations based on **(A)** three or **(B, C)** two independent experiments. Statistically significant differences were assessed using a **(A)** multiple unpaired t-test or a **(B, C)** student's unpaired t-test with the *GraphPad Prism9* software. *$p \leq 0.05$, **$p \leq 0.01$

4.1.3. DEK Localizes with Early Viral Protein E1B-55K

DEK is a nuclear protein known to associate with members of the family of serine/arginine (SR)-rich proteins in splicing complexes and chromatin as well as other chromatin-associated proteins [311, 317, 318]. Furthermore, DEK is co-localizing with PML-NBs components p53, Daxx and ATRX and with PML [311]. To elucidate the subcellular localization of DEK during HAdV-wt infection, we performed immunofluorescence studies for endogenous DEK, PML and early E1B-55K, since this early viral protein was already identified as an interaction partner of PML-IV and -V, p53 and Daxx [139, 213, 243-245]. E1B-55K localization is quite dynamic during adenoviral infection depending on PTM and interaction with distinct proteins [215, 225, 378-380]. At earlier stages of infection E1B-55K localizes in perinuclear bodies [381], while it gets more associated with E4orf3 in PML tracks [382] and viral replication centers at late phases of viral infection [383-386].

Confirming published data, DEK was localizing in a speckled distribution to the host cell nucleus [291, 311, 317, 318] in uninfected cells (Figure 21, panels b and g, p. 91). As expected, PML is reorganized from its dot-like structure (Figure 21, panels d and l, p. 91) into tracks during HAdV-wt infection (Figure 21, panels n and s, p. 91) [363, 387, 388]. We detected E1B-55K in perinuclear bodies (Figure 21, panels m and r, p. 91) as well as localizing to PML tracks during infection. Intriguingly, DEK localization was significantly changed during HAdV-wt infection. We observed, co-localization of DEK with E1B-55K in perinuclear bodies (Figure 21, panels l, q, m, r, o and t, p. 91) and additionally recruitment of DEK to virus-induced PML tracks (Figure 21, panels l, q, n, s, o and t, p. 91).

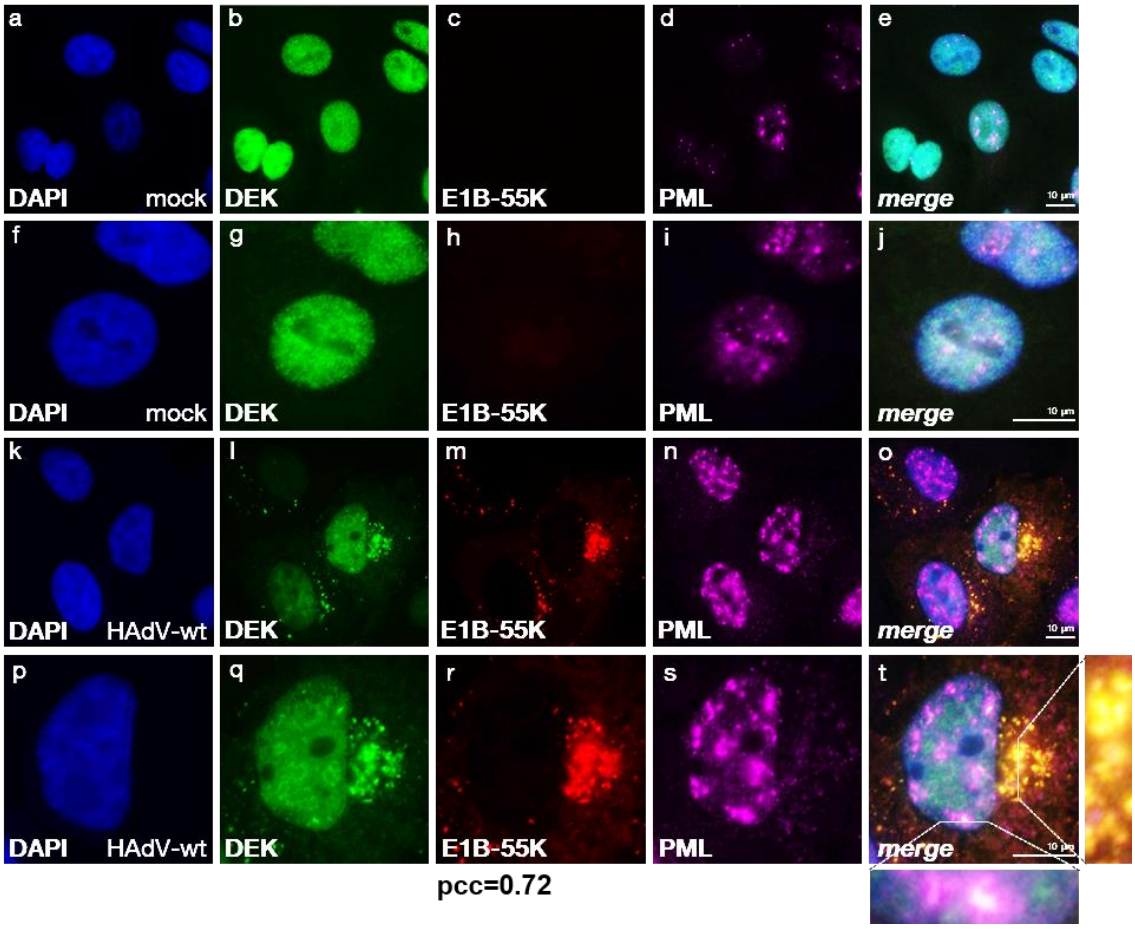

Figure 21: DEK partially co-localizes with early viral E1B-55K and PML tracks. A549 cells were infected with HAdV-wt at a moi of 20 and fixed with 4% PFA 24 h p.i. prior to permeabilization with 0.5% triton. The cells were triple-stained using mouse mAb α-DEK (sc-136222) rat pAb α-E1B-55K (4E8) and rabbit pAb α-PML (ab72137). Primary antibodies were detected with Alexa488- (green; α-DEK), Alexa647- (red; α-E1B-55K) and Alexa568- (magenta; α-PML) conjugated secondary antibodies. DAPI was used for nuclear staining. Representative DEK (b, g, l, q), E1B-55K (c, h, m, r) and PML (d, i, n, s) staining patterns of at least 30 analyzed cells are shown. Overlays of single images (*merge*) are shown in e, j, o and t. White scale bar represents 10 µm. Images were taken using a *Zeiss Axio Observer.Z1*. Cells were analyzed for co-localization of DEK with E1B-55K in mock and HAdV-wt infected samples using Pearson correlation coefficient (pcc) and the *ImageJ* software (version 1.53c) (n = 30).

4.1.4. DEK Interacts with Early E1B-55K in HAdV-Infected Cells

Since earlier experiments identified co-localization of DEK with E1B-55K in HAdV-wt infected cells, we investigated a potential interaction by immunoprecipitation assays. Therefore, HepaRG cells were infected with HAdV-wt and harvested after 24 h p.i. The cells were lysed in NP-40 buffer and 1000 µg of protein were used per sample. Immunoprecipitation assays were performed using *SureBeads*™ Protein A Magnetic Beads and DEK antibody raised in rabbit. The input samples and co-immunoprecipitated proteins were subjected to immunoblot analysis. We detected E1B-55K and DEK to be expressed in our input samples with the expected molecular weight (Figure 22 A, p. 92) and additionally visualized a decent band for the co-immunoprecipitated viral protein E1B-55K at around 55 kDa (Figure 22 B, p. 92), indicating binding between DEK and the viral factor.

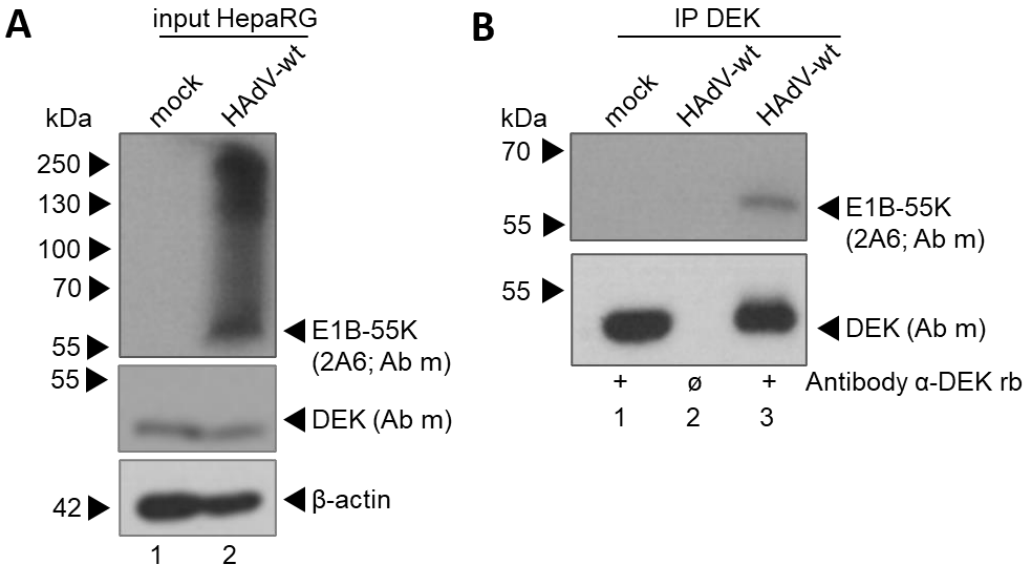

Figure 22: E1B-55K was co-immunoprecipitated with DEK in HAdV-wt infected HepaRG cells. HepaRG cells were infected with HAdV-wt at a moi of 50 and harvested 24 h p.i. NP-40 total-cell lysates were prepared and 1000 µg of protein per sample was used. Protein complexes composed of DEK and its interaction partners were co-immunoprecipitated using SureBeads™ Protein A Magnetic Beads and 0.5 µl of rabbit mAb α-DEK (ab166624) per sample. Proteins were separated on a 10% SDS-PAGE and detected via immunoblotting using mouse pAb α-E1B-55K (2A6), mouse mAb α-DEK (sc-136222) and mouse mAb AC-15 (anti-β-actin). Steady state expression input levels are shown in **(A)** and co-immunoprecipitated proteins in **(B)**. Molecular weights in kDa are indicated on the left, relevant proteins on the right. Data is representative for two biologically independent experiments.

4.1.5. DEK Is a Novel Target for SUMO-2 Modification

Posttranslational modification with SUMO occurs in a three-step enzymatic pathway similar to ubiquitinylation. SUMOylation of proteins play a crucial role in the regulation of various cellular processes, such as cell cycle regulation, senescence, differentiation, transcriptional regulation, protein activity, cell division, protein-protein interaction, DDR as well as antiviral defense mechanisms [160, 162-164, 166, 178, 212, 232, 389-399]. Therefore, early viral proteins exploit the host SUMO machinery to modulate their own as well as host factor's PTM to modulate the host environment for their own benefits [210, 212].

4.1.5.1. DEK Protein Possesses Several Putative SUMOylation Consensus Motifs

In silico analysis of DEK was performed to identify possible putative SUMO conjugation motifs. The *GPS-SUMO* software predicted a SUMOylation consensus motif at position 261 of the DEK protein with a score of 17.711, at position 318 with a score of 25.92 and at position 348 with a score of 35.691 (Figure 23 A/B, p. 93) [364, 400]. According to the *UniProt database* no PTM is known for DEK at those positions until now [283]. The canonical consensus motif for SUMOylation consists of ψKxD/E (ψ: large hydrophobic aa residue; K: lysine where SUMO proteins will be conjugated; x: any aa; D/E: acidic aa

residue) [401, 402]. The SUMO conjugation motif (SCM) at position 261 is located between the NLS and the C-terminal DNA binding and multimerization site with the lysine of the consensus motif 9 aa upstream of the C-terminal domain (Figure 23 C, p. 93) and was the only predicted SUMO site with a canonical consensus motif (Figure 23 A, p. 93). However, according to 'The CUCKOO Workgroup' around 40% of the experimental confirmed SUMOylation sites do not correspond to the consensus motif [364]. The predicted SUMOylation sites at position 318 and 348 of DEK are located in the C-terminal part necessary for multimerization of the protein (Figure 23 C, p. 93) [285]. Potential attachment of SUMO moieties is possible at all three SUMOylation sites for both known DEK isoforms, since isoform 2 differs from the isoform 1 sequence by missing aa 49-82 [403].

A

ProteinID	Position	Peptide	Score	Type
P35659	261	EPPKKTAKREKPKQK	17.711	SUMOylation
P35659	318	PLIKKLKKPPTDEEL	25.92	SUMOylation
P35659	348	VTMKQICKKVYENYP	35.691	SUMOylation

B

```
        10         20         30         40         50
MSASAPAAEG EGTPTQPASE KEPEMPGPRE ESEEEEDEDD EEEEEEEKEK
        60         70         80         90        100
SLIVEGKREK KKVERLTMQV SSLQREPFTI AQGKGQKLCE IERIHFFLSK
       110        120        130        140        150
KKTDELRNLH KLLYNRPGTV SSLKKNVGQF SGFPFEKGSV QYKKKEEMLK
       160        170        180        190        200
KFRNAMLKSI CEVLDLERSG VNSELVKRIL NFLMHPKPSG KPLPKSKKTC
       210        220        230        240        250
SKGSKKERNS SGMARKAKRT KCPEILSDES SSDEDEKKNK EESSDDEDKE
       260        270        280        290        300
SEEEPPKKTA KREKPKQKAT SKSKKSVKSA NVKKADSSTT KKNQNSSKKE
       310        320        330        340        350
SESEDSSDDE PLIKKLKKPP TDEELKETIK KLLASANLEE VTMKQICKKV
       360        370
YENYPTYDLT ERKDFIKTTV KELIS
```

C

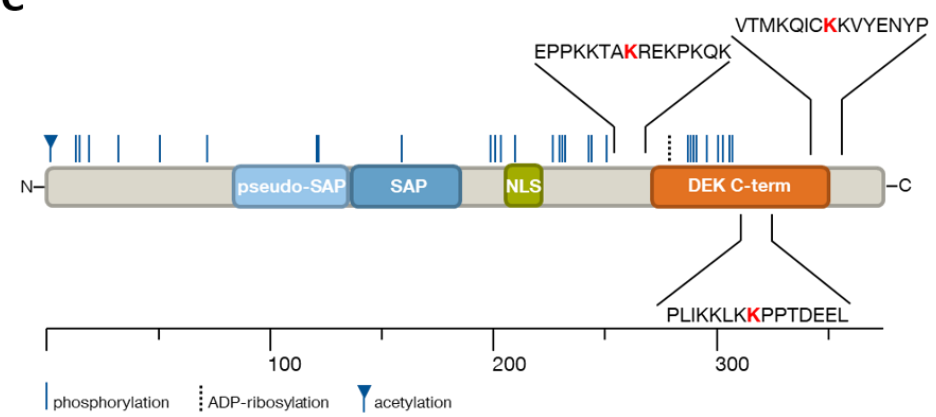

Figure 23: Prediction of DEK SUMOylation sites. *In silico* prediction with *GPS-SUMO* (1.0; The CUCKOO Workgroup; [364, 400]). **(A)** Position, peptide, score and type of the predicted sites of DEK (ProteinID P35659) are listed in the table. Lysine residues for

SUMO attachment are highlighted in red. **(B)** Amino acid sequence of DEK with lysine residues for SUMO attachment are highlighted in red. Missing amino acids 49-82 in isoform 2 are underlined. **(C)** Graphic representation of the locations of DEK SCMs.

4.1.5.2. Early Viral E1B-55K Facilitates SUMOylation of DEK

The early viral protein E1B-55K is crucial during HAdV-wt infection mediating the modulation and degradation of restrictive host factors. E1B-55K has SUMO ligase capacity, whereas it attaches SUMO moieties on Daxx and p53 to inhibit their function during HAdV infection [216, 220]. Since we observed co-localization and interaction of DEK with E1B-55K, the question arose, if E1B-55K is able to SUMOylate DEK during infection. Therefore, we infected HeLa cells overexpressing a 6xHis-tagged SUMO-2 protein and enriched SUMOylated proteins with NiNTA affinity purification after infection with HAdV-wt and with a mutant virus lacking E1B-55K expression (HAdV ΔE1B-55K). The samples were subjected to SDS-PAGE analysis and the protein-of-interests were detected by immunoblotting. Infection with both viruses was shown by expression of the early viral E2A protein (Figure 24 A lane 2 and 3, p. 95) and mutant virus infection was verified, since HAdV ΔE1B-55K was lacking E1B-55K protein levels in comparison to HAdV-wt infected cells (Figure 24 A compare lane 3 to 2, p. 95). Expression of 6x-His-tagged SUMO-2 (Figure 24 A lane 1 - 3, p. 95) and functionality of the NiNTA (Figure 24 B lane 1 - 3, p. 95) was confirmed by His staining indicating SUMO-2 expression. DEK expression was detected in all three samples (Figure 24 A lane 1 - 3, p. 95) and we identified DEK as a novel target for SUMOylation in the NiNTA purifications (Figure 24 B, p. 95). HAdV-wt infection increased 2.2-fold the attachment of SUMO moieties to the DEK protein (Figure 24 B compare lane 2 to 1, p. 95), while infection with a mutant virus lacking E1B-55K expression resulted in less high molecular weight SUMO-2 modified forms of DEK similar to mock uninfected samples (Figure 24 B compare lane 3 to 2, p. 95). Taken together, we identified SUMO conjugation of the chromatin-associated protein DEK, which was increased during HAdV-wt infection specifically by the early viral E1B-55K protein.

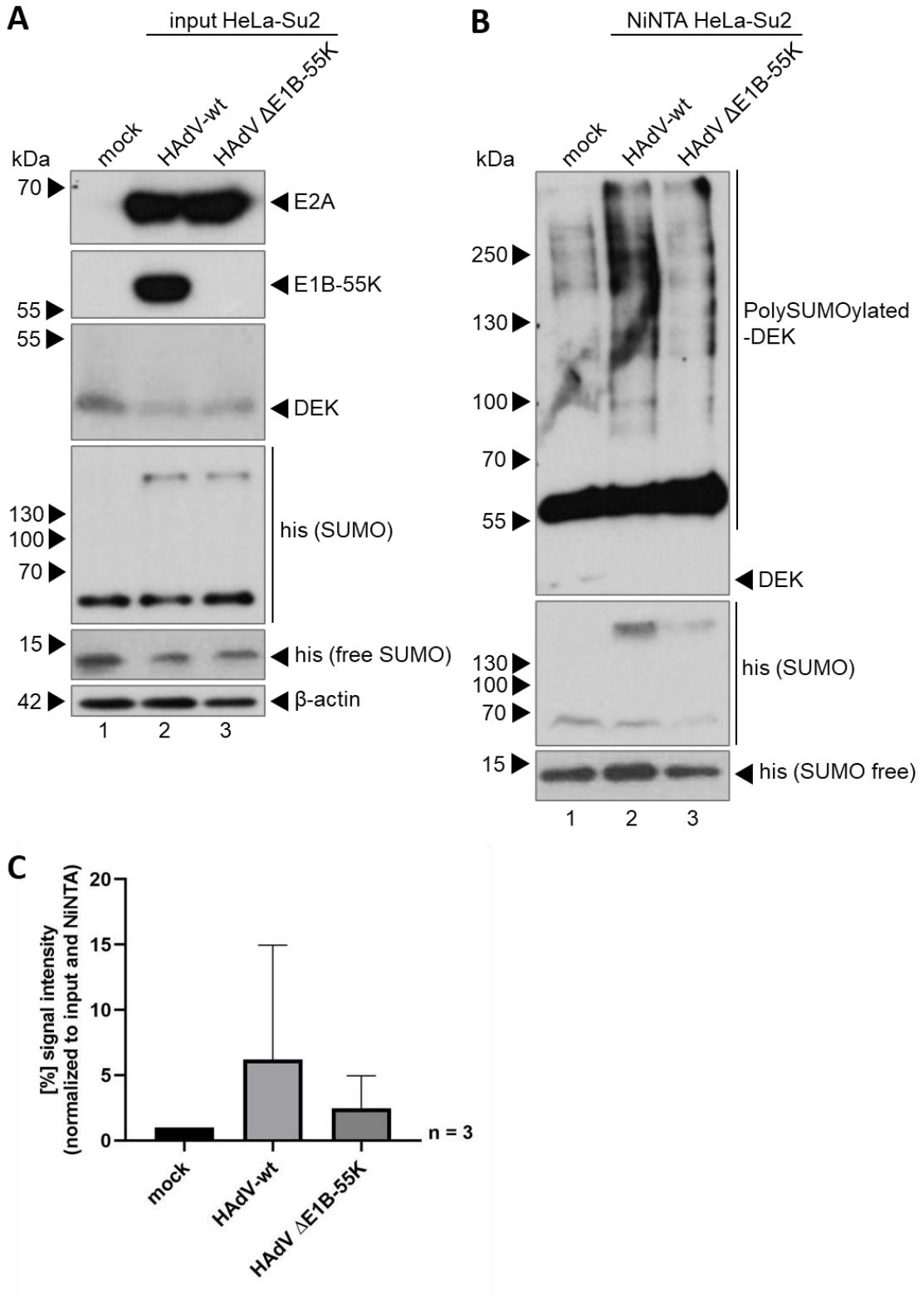

Figure 24: DEK is SUMOylated by E1B-55K during HAdV infection. (A, B) HeLa-Su2 cells were infected with HAdV-wt and HAdV ΔE1B-55K at a moi of 20. Cells were harvested 48 h p.i. and input samples were prepared from one fifth of the collected cells using high-stringent RIPA buffer. The remaining cells were resuspended in B1 buffer and SUMOylated proteins were precipitated by NiNTA beads. Proteins were separated on a 10% SDS-PAGE and detected with mouse pAb α-E2A (B6-8), mouse pAb α-E1B-55K (2A6) mouse mAb α-DEK (sc-136222) and mouse mAb AC-15 (anti-β-actin). 6x-His-tagged SUMO-2 was resolved on a 15% SDS-PAGE and detected with a mouse mAb α-his (Clontech). Steady state expression input levels are shown in **(A)** and SUMOylated proteins from NiNTA precipitation in **(B)**. Molecular weights in kDa are indicated on the left, relevant proteins on the right. Data is representative of two biologically independent experiments. **(C)** For quantification of protein levels, densitometric analysis of detected bands was

performed using the *ImageJ* software (version 1.53c). Relative protein expression was normalized on the respective α-β-actin steady-state levels. Levels of SUMOylated DEK from the NiNTA assay were normalized to precipitated 6xHis-tagged SUMO-2 protein levels and the respective input levels. Bar charts represent average values and standard deviations based on three biologically independent experiments.

4.1.6. DEK Is Partially Recruited to PML Tracks and to the Sites of Viral Replication

SUMOylation plays a crucial role in assembly of PML-NBs and the recruitment of proteins to those multiprotein complexes. Most proteins localizing to PML-NBs are either targeted for SUMOylation or contain a SUMO interacting motif (SIM), which regulates its function and interaction with other host cell factors [189, 190, 194].

4.1.6.1. DEK Associates with E4orf3-Containing PML Tracks during Infection

Since DEK was identified as a target for the SUMOylation machinery, the question arose, if DEK is relocalized to virus-induced E4orf3-containing PML tracks during HAdV-wt infection. To investigate whether DEK is interacting with E4orf3 we performed co-immunoprecipitation assays. Therefore, we infected A549 parental cells with HAdV-wt and harvested the cells 24 h p.i. prior to cells lysis. We detected DEK and E4orf3 to be expressed in the input samples used for immunoblot analysis. Precipitating the endogenous DEK protein and subsequent staining of E4orf3 revealed interaction of both proteins.

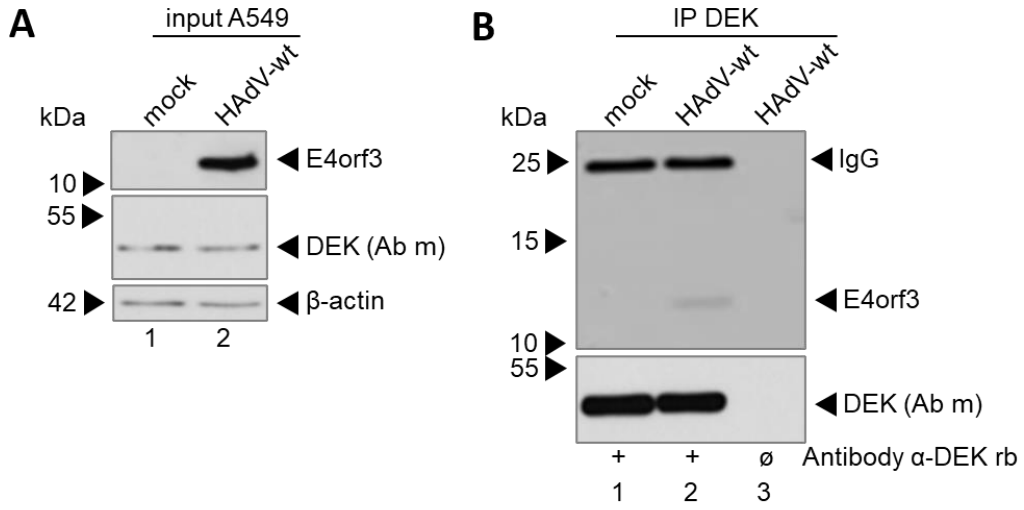

Figure 25: DEK is interacting with the PML-NB-disrupting early viral protein E4orf43 in HAdV-wt infected cells. A549 cells were infected with HAdV-wt at a moi of 20 and harvested 48 h p.i. prior to cell lysis with high stringent RIPA buffer. 1000 µg of total-cell lysate per sample was used. Protein complexes composed of DEK and its interaction partners were co-immunoprecipitated using sepharose A beads coupled with 0.5 µl of rabbit mAb α-DEK (ab166624) per sample. Proteins were separated on a 10% SDS-PAGE and detected via immunoblotting using mouse mAb α-DEK (sc-136222) and mouse mAb AC-15 (anti-β-actin). For early viral E4orf3 detection samples were subjected to a 15% SDS-PAGE, blotted and detected with rat mAb α-E4orf3 (6A11). Steady state expression input levels are shown in **(A)** and co-immunoprecipitated proteins in **(B)**. Molecular weights in kDa are indicated on the left, relevant proteins on the right. Data is representative for two biologically independent experiments.

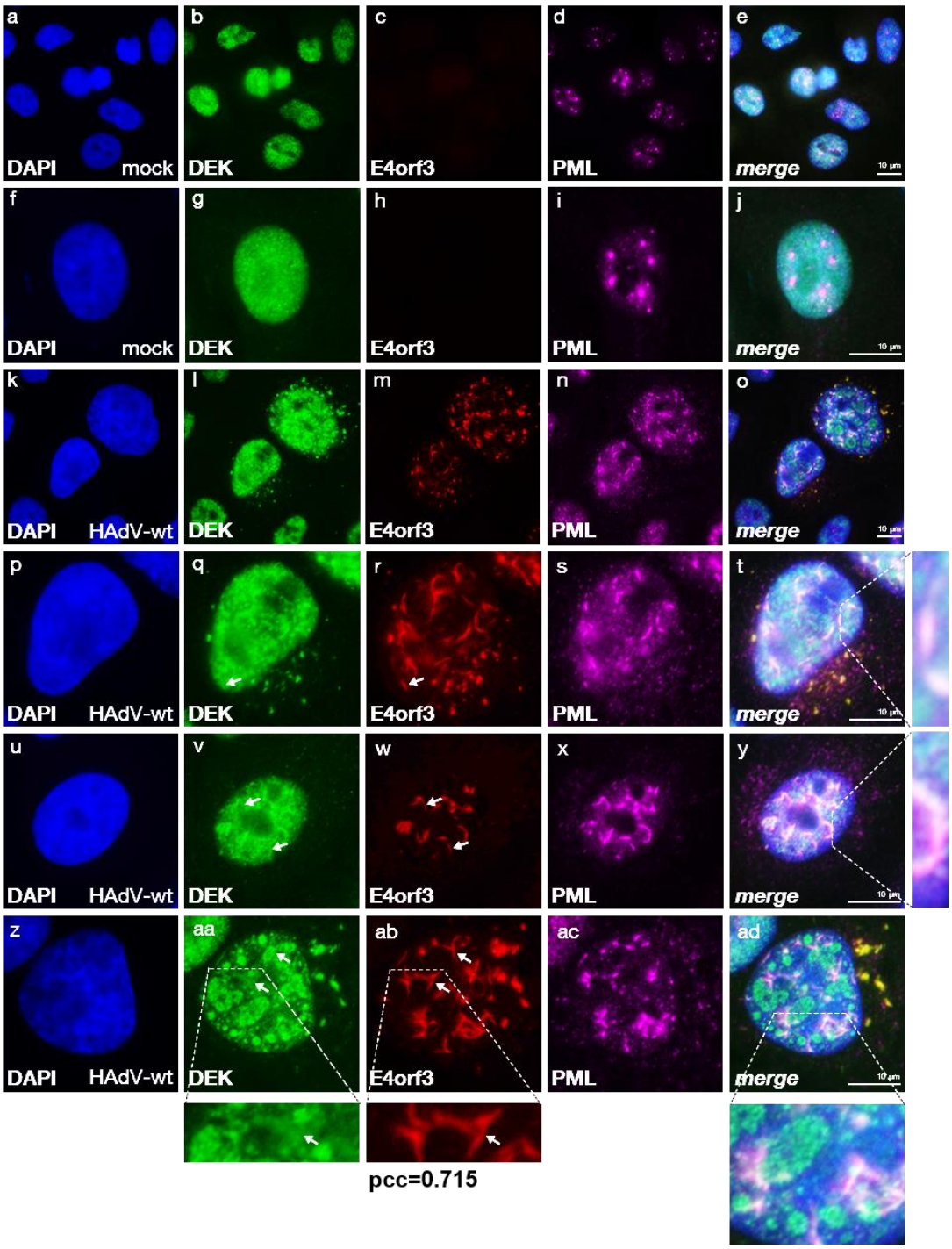

Figure 26: DEK localizes in ring-like structures and is recruited to E4orf-3-containing tracks during HAdV-wt infection. A549 cells were infected with HAdV-wt at a moi of 20 and fixed with 4% PFA 24 h p.i. prior to permeabilization with 0.5% triton. The cells were triple-stained using mouse mAb α-DEK (sc-136222), rat pAb α-E4orf3 (6A11) and rabbit pAb α-PML (ab72137). Primary antibodies were detected with Alexa488- (green; α-DEK), Alexa647- (red; α-E4orf3) and Alexa568- (magenta; α-PML) conjugated secondary antibodies. DAPI was used for nuclear staining. Representative DEK (b, g, l, q, v, aa), E4orf3 (c, h, m, r, w, ab) and PML (d, i, n, s, x, ac) staining patterns of at least 100 analyzed cells are shown. Different phenotypes of DEK subcellular localization during HAdV-wt infection are shown in panels q, u and z. Overlays of single images (*merge*) are shown in e, j, o, t, y and ad. White scale bar represents 10 µm. Images were taken using a *Zeiss Axio Observer.Z1*. White arrows indicate E4orf3-containing PML tracks without DEK co-localization. Cells were analyzed for co-localization of DEK with E4orf3 and HAdV-wt infected samples using Pearson correlation coefficient (pcc) and the *ImageJ* software (version 1.53c) (n = 30).

Next, we verified the data obtained from the co-immunoprecipitations assays by immunofluorescence studies. HAdV-wt infected A549 cells were fixed 24 h p.i. and

immunostained for DEK, viral E4orf3 and PML (Figure 26, p. 97). E4orf3 is interacting with PML-II mediating the relocalization of the dot-like PML-NBs into tracks [248]. In accordance with this, here we observed reorganization of the PML protein and co-localization of the PML tracks with E4orf3 (Figure 26 panels o, t, y, ad; p. 97). As previously described and observed in our foregoing experiment, we detected DEK diffusely with a speckled distribution in the host cell nucleus in uninfected samples (Figure 26 panels p and g, p. 97). During HAdV-wt infection, DEK was relocalized and we observed different phenotypes of DEK localization during infection at a 24 h time point. First, we detected DEK together with E4orf3 outside of the nucleus, probably co-localizing and interacting with E1B-55K as observed in Figure 21 (p. 91) and Figure 22 (p. 92). Furthermore, immunofluorescence stainings revealed recruitment of DEK to E4orf3-containg PML tracks verified by determination of the Pearson correlation coefficient (pcc) (DEK/E4orf3 p=0.715). Additionally, our data indicated enhanced localization of DEK to PML during HAdV-wt infection, since pcc was shown to be significantly enhanced compared to the uninfected samples (Figure 26 panels t and y, p. 97; Figure 27, p. 98), however DEK was not localizing to all E4orf3-containing PML tracks (Figure 26 panels v, w, aa, and ab, indicated by white arrows, p. 97). Remarkably, DEK also changed its localization drastically during viral infection into ring-like structures localizing in close proximity to the PML tracks (Figure 26 panels aa and ad, p. 97). In conclusion, we observed three different phenotypes of co-localization of DEK with E1B-55K and E4orf3-containing PML tracks as well as ring-shaped organization of DEK in the nucleus localizing to PML tracks.

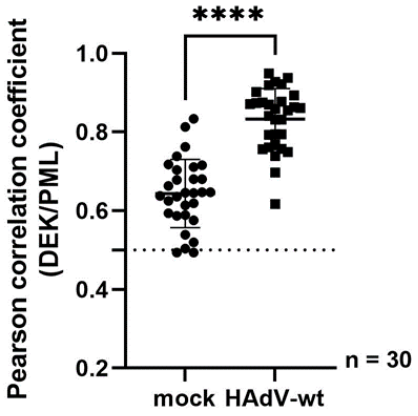

Figure 27: DEK is recruited to PML tracks during HAdV-wt infection. Cells from Figure 21 (p. 91) and Figure 26 (p. 97) were analyzed for co-localization of DEK with PML in mock and HAdV-wt infected samples using Pearson correlation coefficient (pcc) and the *ImageJ* software (version 1.53c). Data of 30 cells was visualized and statistically significant differences were assessed using a student's unpaired t-test with the GraphPad Prism9 software. *****p ≤ 0.0001*

4.1.6.2. DEK Subcellular Localization Is Dependent on Viral Infection Stage

Our immunofluorescent studies showed a drastic change in DEK localization during HAdV-wt infection (Figure 21, p. 91; Figure 26, p. 97). We observed different phenotypes 24 h p.i. with recruitment of DEK to E1B-55K and E4orf3-containing PML tracks. To further elucidate the dynamics in DEK subcellular localization, we infected A549 cells with HAdV-wt at a moi of 20 and fixed the cells with 4% PFA at different stages during the course of infection. We assessed DEK localization with immunostaining of DEK together either with E1B-55K and PML (Figure 28, p. 100), E4orf3 and PML (Figure 30, p. 102) or E2A and E4orf3 (Figure 32, p. 104). DEK was shown to change localization 16 h p.i. with co-localization to E1B-55K in perinuclear bodies at the outer rim of the host cell nucleus (Figure 28 panels l, q, m, r, o and t, p. 100), which was further assessed using pcc calculation (Figure 29, p. 101). Association of DEK with E1B-55K increased during the course of infection with a peak at 24 h p.i., which declined after 36 h (Figure 28 panels o, t, y, ad and an, p. 100; Figure 29, p. 101). Co-localization of DEK with E1B-55K was shown to be significantly decreased after 48 h p.i., where we detected DEK exclusively in a ring-shaped localization close to PML tracks in the host cell nucleus as indicated by our immunostaining and pcc calculations (Figure 28 panels as and ax, p. 100; Figure 29, p. 101). We obtained similar results as we stained for the early viral protein E4orf3, since DEK association with E4orf3-containing tracks was detected 16 h and 24 h p.i. with a pcc of over 0.5 (Figure 30 panels t and ad, p. 102; Figure 31, p. 103). However, apart from DEK localization with E1B-55K, we already observed a significant decrease in DEK association with E4orf3 36 h p.i., where we detected DEK adjacent to E4orf3 tracks (Figure 30 panels an and ax, p. 102; Figure 31, p. 103).

Many DNA viruses, such as HAdV, place their viral replication centers juxtaposed to PML-NBs. HAdV modulate those bodies to either target restrictive host factors for proteasomal degradation or exploit the promoting dependency factors to ensure viral replication [212, 246, 404]. Since we observed a ring-shaped localization of DEK in close proximity to PML tracks starting 24 h p.i., the question arose, if DEK is localizing to viral replication centers during HAdV-wt infection. Therefore, we performed immunofluorescence staining for DEK with the replication center marker E2A and E4orf3 (Figure 32, p. 104). First, E2A was shown to be localized diffusely 16 h p.i., whereby pcc for DEK with E2A was not calculable (Figure 32 panels n, o, s and t, p. 104). However, we observed establishment of RCs 24 h p.i. with

co-localization and strong association of DEK with E2A during the whole course of infection (Figure 32, p. 104), confirming our hypothesis of DEK recruitment to viral RCs.

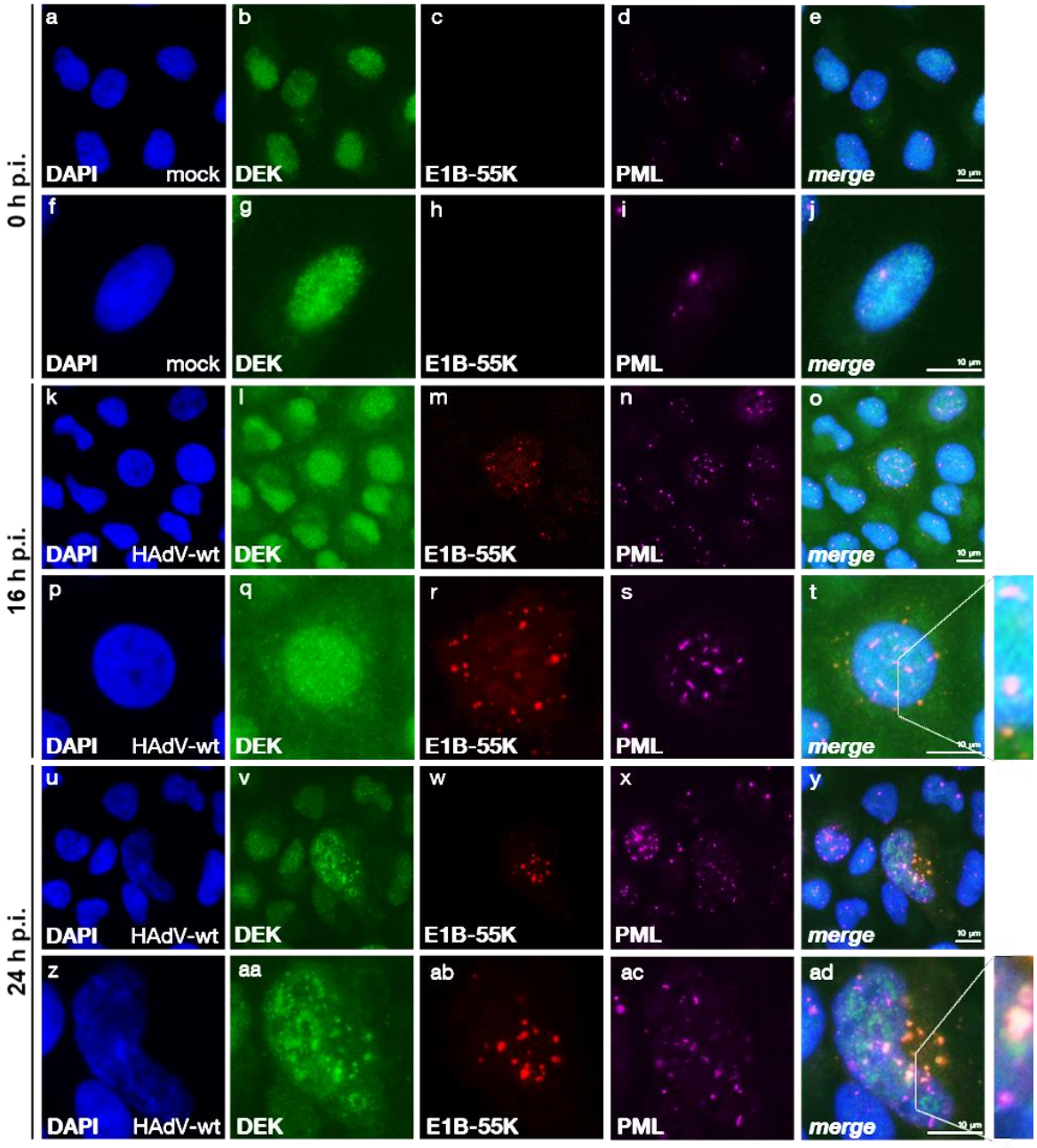

Figure 28: DEK localization with E1B-55K is changed during the course of infection. A549 cells were infected with HAdV-wt at a moi of 20 and fixed with 4% PFA 0 h, 16 h, 24 h, 36 h and 48 h p.i. prior to permeabilization with 0.5% triton. The cells were triple-stained using mouse mAb α-DEK (sc-136222), rat pAb α-E1B-55K (4E8) and rabbit pAb α-PML (ab72137). Primary antibodies were detected with Alexa488- (green; α-DEK), Alexa647- (red; α-E1B-55K) and Alexa568- (magenta; α-PML) conjugated secondary antibodies. DAPI was used for nuclear staining. Representative DEK (b, g, l, q, v, aa, af, ak, ap and au), E1B-55K (c, h, m, r, w, ab, ai, aq and av) and PML (d, i, n, s, x, ac, ah, am, ar and aw) staining patterns of at least 30 analyzed cells are shown. Overlays of single images (*merge*) are shown in e, j, o, t, y, ad, ai, an, as, and ax. White scale bar represents 10 µm. Images were taken using a *Zeiss Axio Observer.Z1*.

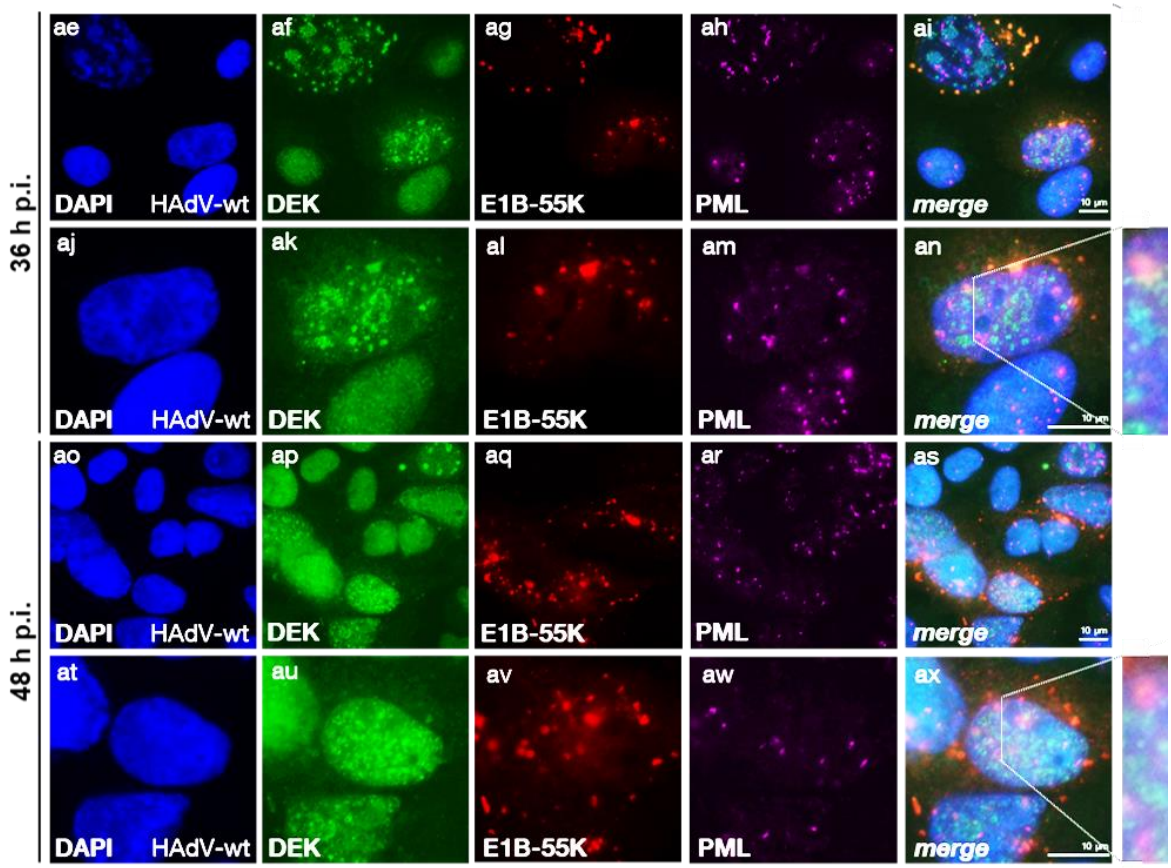

Figure 28: DEK localization with E1B-55K is changed during the course of infection. (continued)

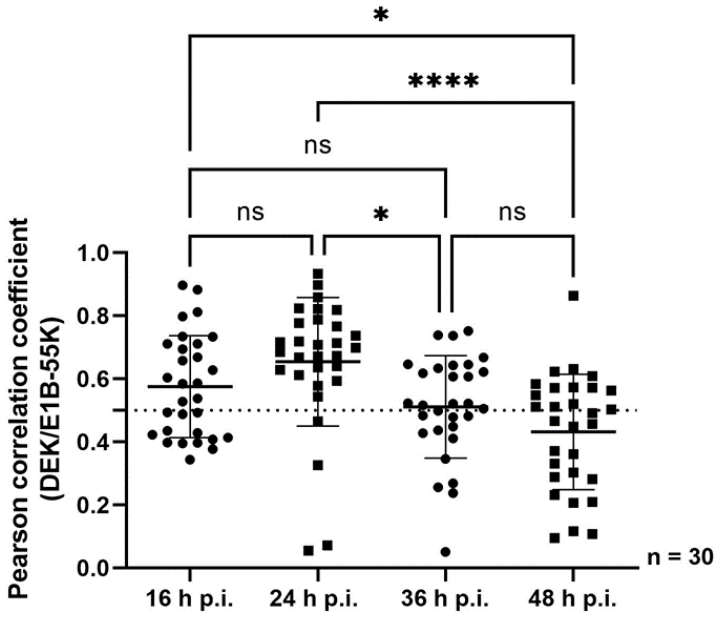

Figure 29: Calculation of DEK co-localization with E1B-55K during HAdV-wt infection. Cells from Figure 28 (p. 100) were analyzed for co-localization of DEK with E1B-55K HAdV-wt infected samples using Pearson correlation coefficient (pcc) and the ImageJ software (version 1.53c). Co-localization was measured 16 h, 24 h, 36 h and 48 h p.i. Data of 30 cells was visualized and statistically significant differences were assessed using an one-way ANOVA and Turkey's post hoc test with the *GraphPad Prism9* software. **p ≤ 0.5, ****p ≤ 0.0001*

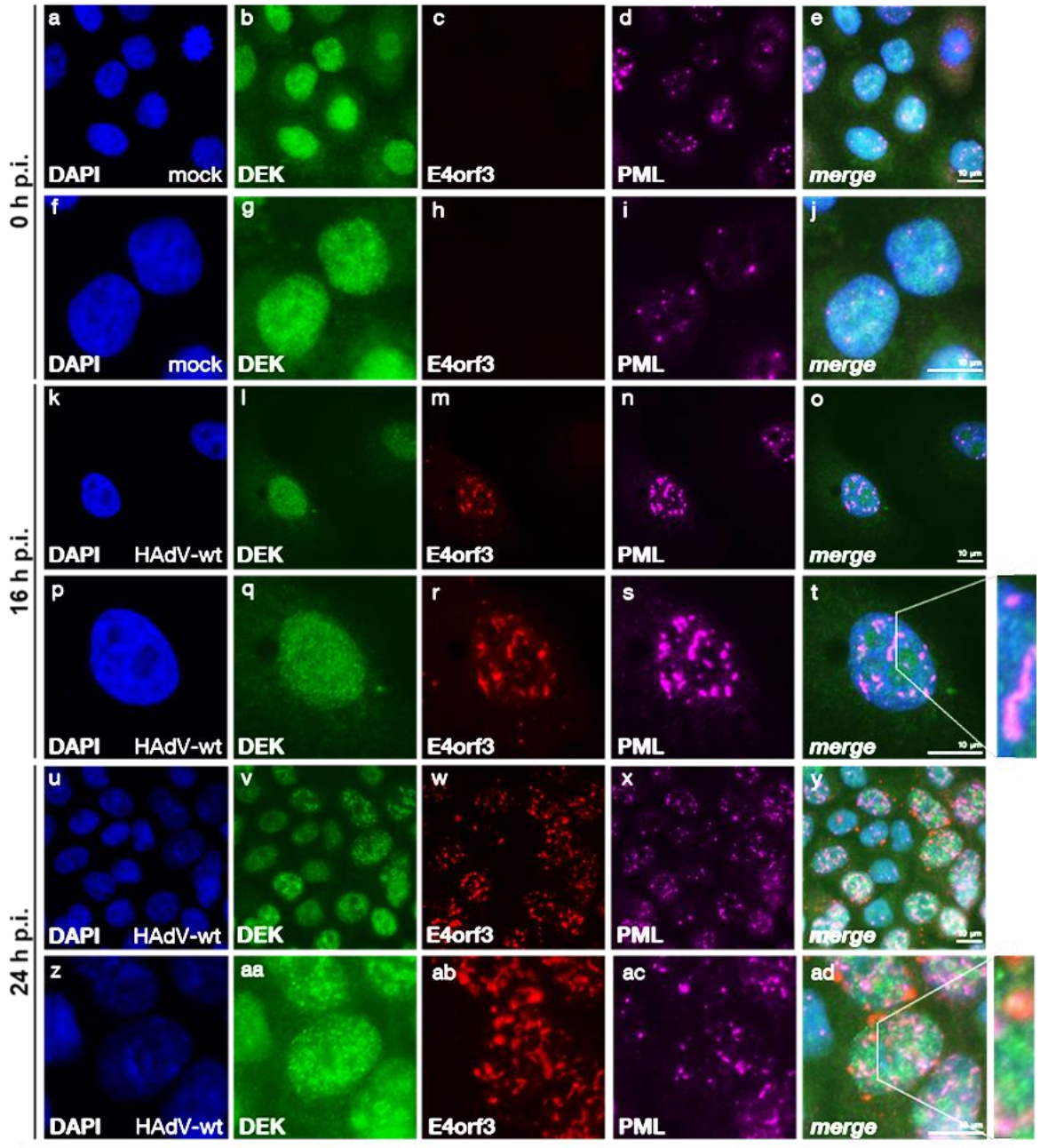

Figure 30: DEK co-localizes with E4orf3 until 36 h p.i. A549 cells were infected with HAdV-wt at a moi of 20 and fixed with 4% PFA 0 h, 16 h, 24 h, 36 h and 48 h p.i. prior to permeabilization with 0.5% triton. The cells were triple-stained using mouse mAb α-DEK (sc-136222), rat pAb α-E4orf3 (6A11) and rabbit pAb α-PML (ab72137). Primary antibodies were detected with Alexa488- (green; α-DEK), Alexa647- (red; α-E4orf3) and Alexa568- (magenta; α-PML) conjugated secondary antibodies. DAPI was used for nuclear staining. Representative DEK (b, g, l, q, v, aa, af, ak, ap, and au), E4orf3 (c, h, m, r, w, ab, ai, aq, and av) and PML (d, i, n, s, x, ac, ah, am, ar and aw) staining patterns of at least 30 analyzed cells are shown. Overlays of single images (*merge*) are shown in e, j, o, t, y, ad, ai, an, as, and ax. White scale bar represents 10 µm. Images were taken using a *Zeiss Axio Observer.Z1*.

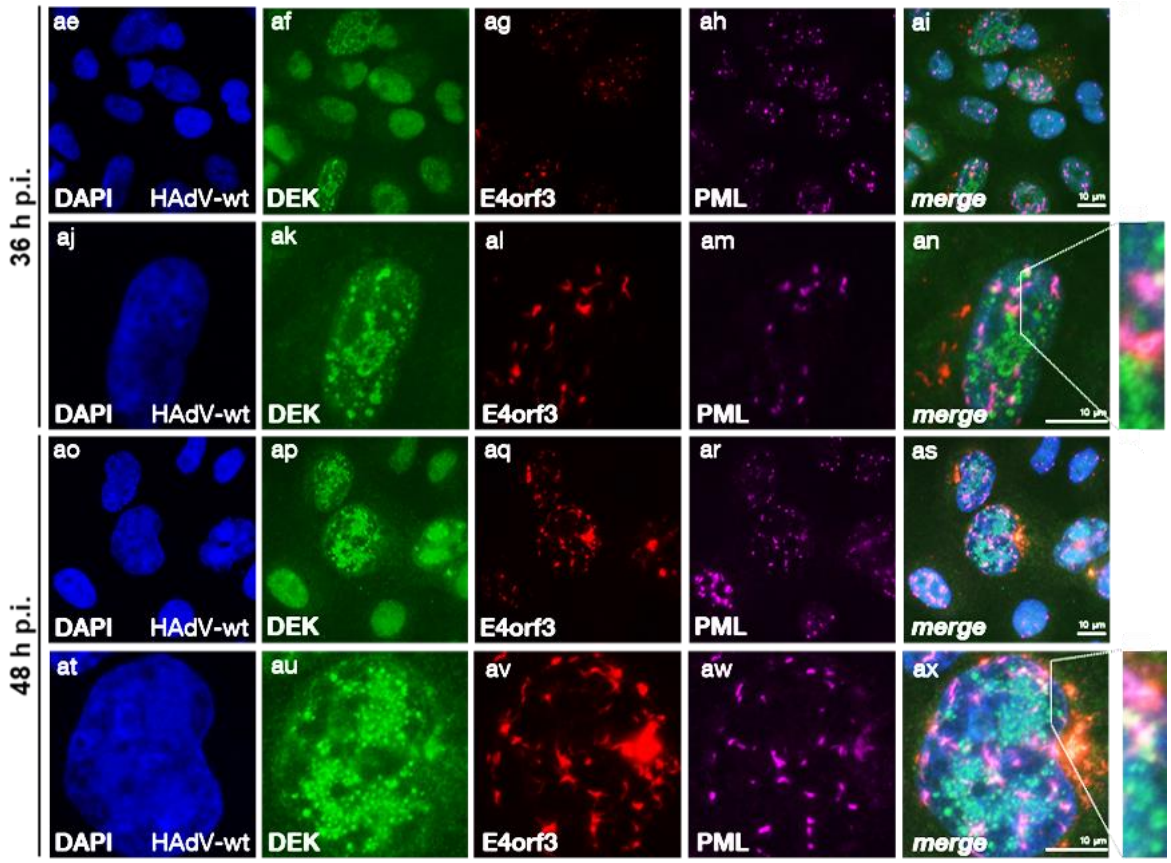

Figure 30: DEK co-localizes with E4orf3 until 36 h p.i. (continued)

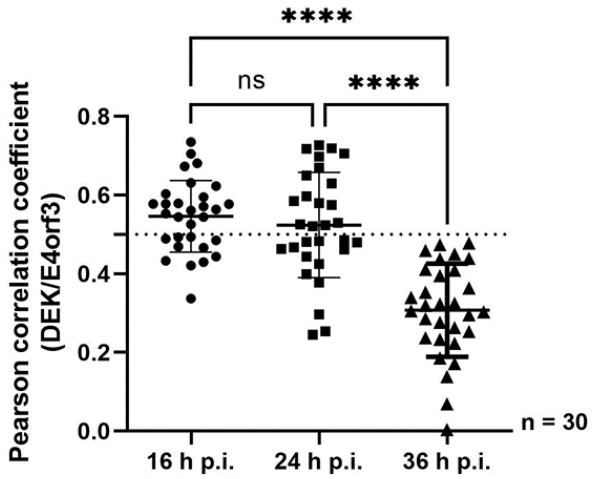

Figure 31: Calculation of DEK co-localization with E4orf3 during HAdV-wt infection. Cells from Figure 30 (p. 102) were analyzed for co-localization of DEK with E4orf3 HAdV-wt infected samples using Pearson correlation coefficient (pcc) and the ImageJ software (version 1.53c). Co-localization was measured 16 h, 24 h and 36 h post infection. Data of 30 cells was visualized and statistically significant differences were assessed using an one-way ANOVA and Turkey's post hoc test with the *GraphPad Prism9* software. *$^{****}p \leq 0.0001$*

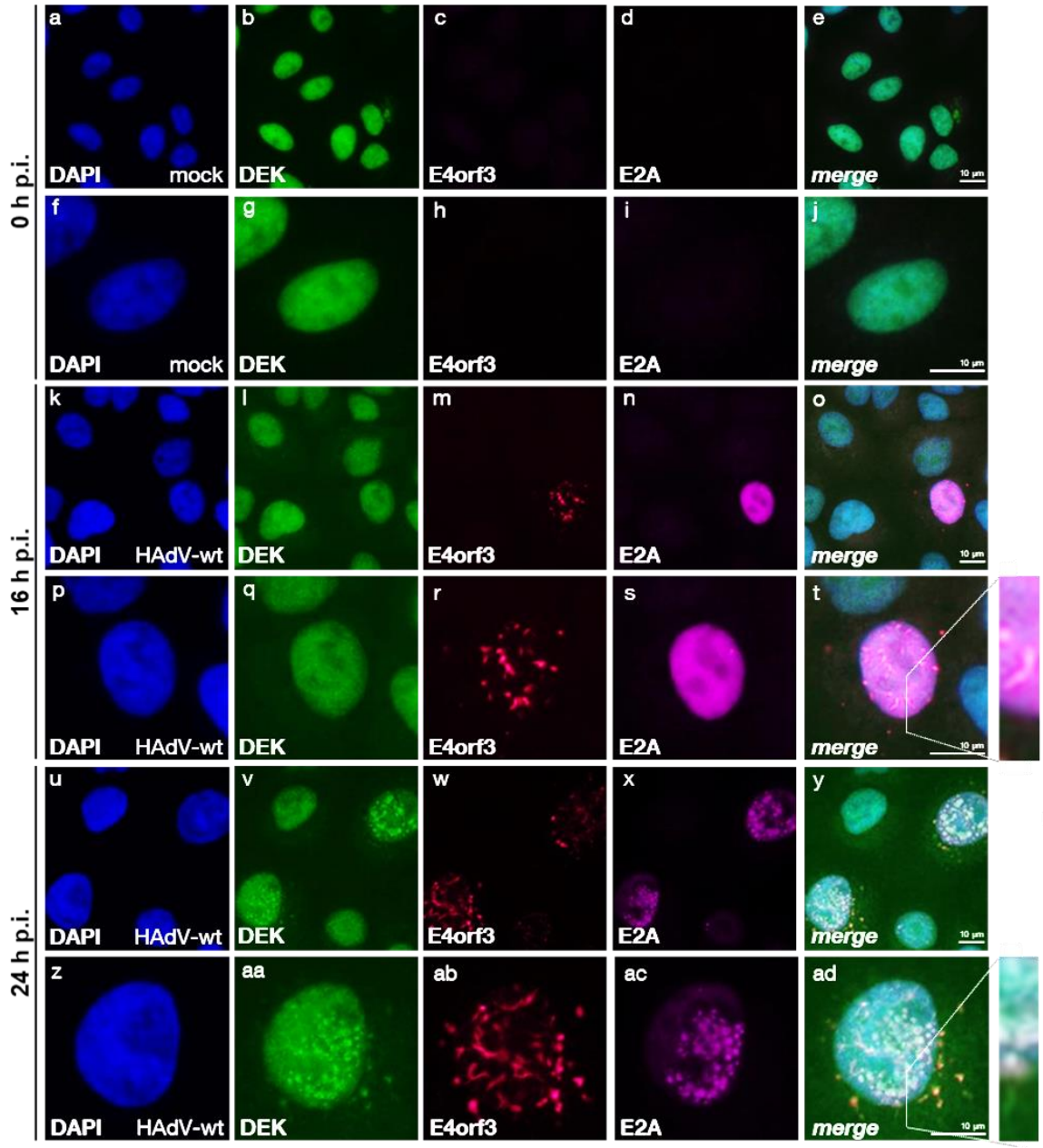

Figure 32: DEK is recruited to replication center marker E2A during HAdV-wt infection. A549 cells were infected with HAdV-wt at a moi of 20 and fixed with 4% PFA 0 h, 16 h, 24 h, 36 h and 48 h p.i. prior to permeabilization with 0.5% triton. The cells were triple-stained using mouse mAb α-DEK (sc-136222), rat pAb α-E4orf3 (6A11) and rabbit pAb α-E2A. Primary antibodies were detected with Alexa488- (green; α-DEK), Alexa647- (red; α-E4orf3) and Alexa568- (magenta; α-E2A) conjugated secondary antibodies. DAPI was used for nuclear staining. Representative DEK (b, g, l, q, v, aa, af, ak, ap, and au), E4orf3 (c, h, m, r, w, ab, ai, aq and av) and E2A (d, i, n, s, x, ac, ah, am, ar and aw) staining patterns of at least 30 analyzed cells are shown. Overlays of single images (*merge*) are shown in e, j, o, t, y, ad, ai, an, as, and ax. White scale bar represents 10 µm. Images were taken using a *Zeiss Axio Observer.Z1*.

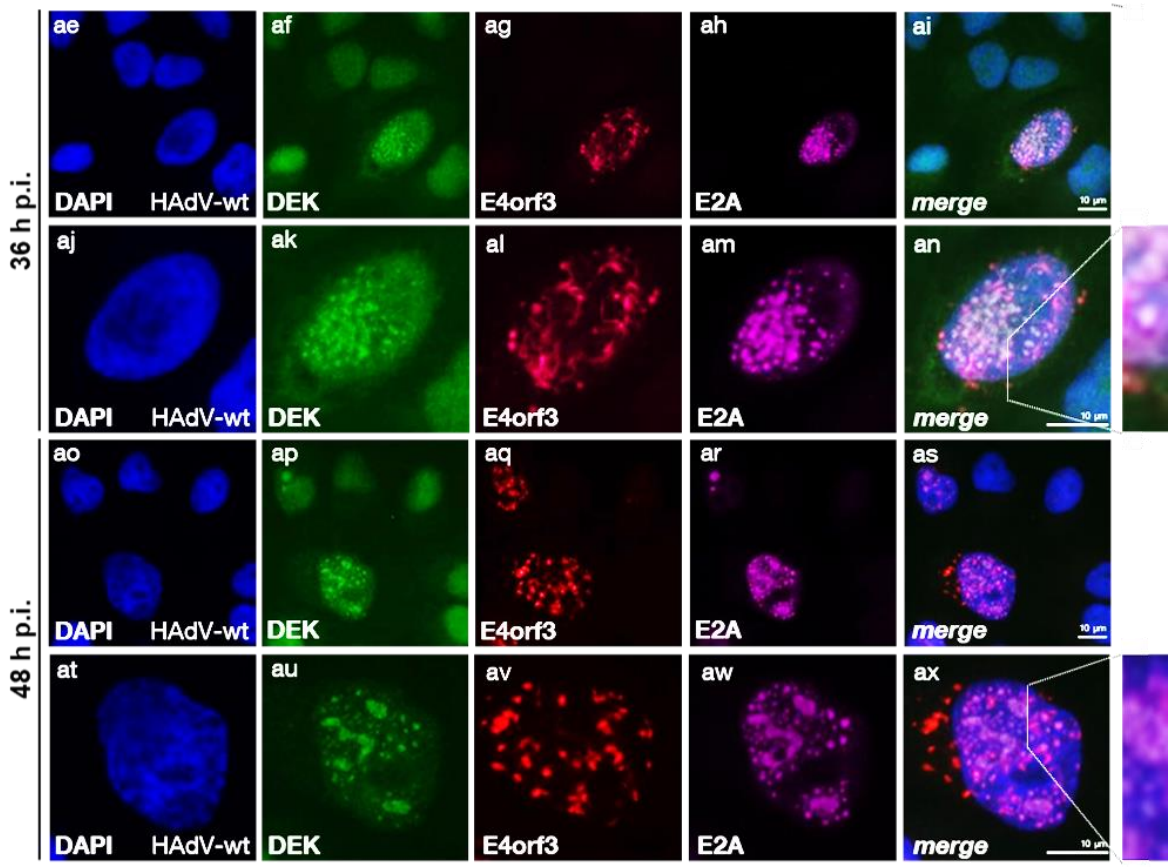

Figure 32: DEK is recruited to replication center marker during HAdV-wt infection. (continued)

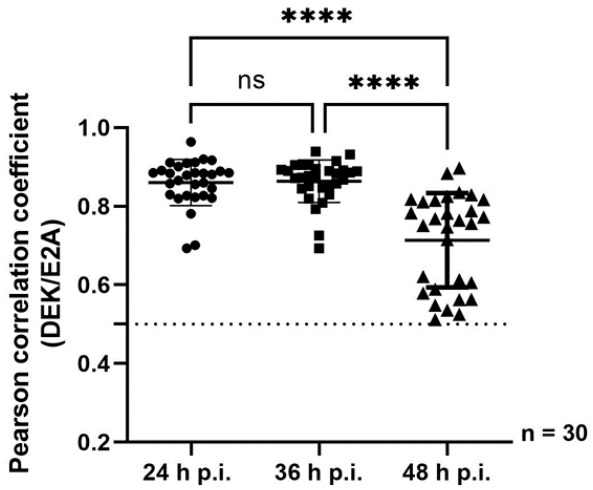

Figure 33: Calculation of DEK co-localization with viral replication center marker E2A. Cells from Figure 32 (p. 104) were analyzed for co-localization of DEK with E1B-55K HAdV-wt infected samples using Pearson correlation coefficient (pcc) and the ImageJ software (version 1.53c). Co-localization was measured 24 h, 36 h and 48 h p.i. Data of 30 cells was visualized and statistically significant differences were assessed using an one-way ANOVA and Turkey's post hoc test with the *GraphPad Prism9* software. *****p ≤ 0.0001*

Taken together, localization of DEK is very dynamic and depends on the stage of viral infection. First, we observed relocalization of DEK to perinuclear bodies with E1B-55K and to PML tracks up to 36 h after infection. However, DEK is sequestered to viral RCs after 24 h p.i. and strongly associated with E2A and RCs during the course of infection (Table 39, p. 106).

Table 39: Time-dependent DEK localization during HAdV-wt infection on the basis of pcc calculations. Association of DEK with E1B-55K, E2A and E4orf3 during the course of infection is listed in the following table. Classification is based on the pcc calculations shown in Figure 29 (p. 101), Figure 31 (p. 103) and Figure 33 (p. 105). / no data, - no co-localization, + co-localization, ++ high co-localization, +++ very high co-localization.

DEK co-localization	16 h p.i.	24 h p.i.	36 h p.i.	48 h p.i.
E1B-55K	+	++	+	-
E4orf3	+	+	-	-
E2A	/	+++	+++	++

4.1.6.3. Viral Replication Center Marker E2A Binds to DEK Protein

E2A is a HAdV DNA binding protein regulating gene expression, mRNA stability, virion assembly and is crucial for efficient viral DNA replication, whereas it is considered to be a marker for viral replications centers (RC) [214, 359, 405-408]. Our previous experiment revealed localization of DEK to adenoviral replication centers during the course of infection (Figure 32, p. 104). To further elucidate whether DEK is merely localizing to E2A or it is in addition interacting with the early viral protein, we performed co-immunoprecipitation assays in HAdV-wt infected H1299 (Figure 34 A; p. 107) and HepaRG cells (Figure 34 C; p. 107). Precipitation of endogenous DEK and subsequent staining of the E2A revealed an interaction of DEK with the early viral replication center marker in both cell lines (Figure 34 B, D; p. 107).

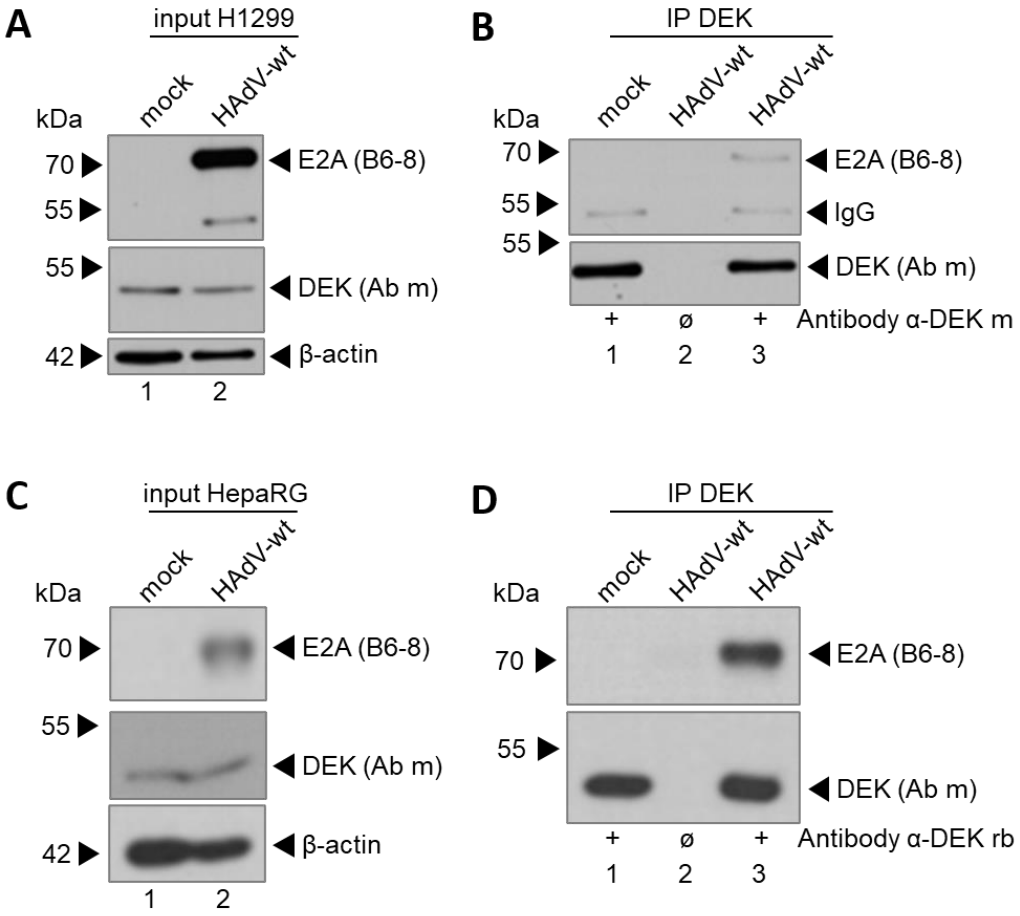

Figure 34: Replication center marker E2A is a novel interaction partner of DEK. (A, B) H1299 and were infected with HAdV-wt at a moi 20 and harvested 48 h p.i. before lysis with high stringent RIPA buffer. 1000 µg of total-cell lysate were used for co-immunoprecipitation assays with sepharose A beads coupled with 0.5 µl of rabbit mAb α-DEK (ab166624) per sample **(C, D)** HepaRG cells were infected with HAdV-wt at a moi 50 and harvested 48 h p.i. before cell lysis with NP-40 buffer. 1000 µg of protein lysate was used per sample. Protein complexes composed of DEK and its interaction partners were co-immunoprecipitated using SureBeads™ Protein A Magnetic Beads and 0.5 µl of rabbit mAb α-DEK (ab166624) per sample. Proteins were separated on a 10% SDS-PAGE and detected via immunoblotting using mouse pAb α-E2A (B6-8), mouse mAb α-DEK (sc-136222) and mouse mAb AC-15 (anti-β-actin). Steady state expression input levels are shown in **(A, C)** and co-immunoprecipitated proteins in **(B, D)**. Molecular weights in kDa are indicated on the left, relevant proteins on the right. Data is representative of two biologically independent experiments.

4.1.7. DEK Binds to Viral Promoter Regions and Modifies Their Activity

4.1.7.1. Adenoviral Gene Expression Is Elevated by DEK Protein Expression

DEK can act as chromatin remodeler by facilitating the distribution of histones and their PTM mediating the balance between euchromatin and repressive heterochromatin [292, 297, 309, 313, 314]. Additionally, it interacts with various transcriptional regulators, such as AP-2α, HP1α, as well as histone methyltransferases and acetylases, whereby it can regulate gene transcription [281, 289, 292, 297, 316]. In this study, we observed promoting activity of DEK on viral mRNA and protein production. Additionally, DEK was shown to co-

localize and to interact with the viral RC marker E2A. Thus, we hypothesized that DEK is a host factor, which is capable of activating viral gene expression from viral promoters.

Therefore, we examined the ability of DEK to modulate gene transcription from viral promoters by performing a transient reporter gene assay. H1299 cells were transfected with reporter gene constructs encoding a luciferase gene under control of various viral promoters. The transfection efficiency was normalized to a *Renilla*-luciferase under the control of the HSV-TK (herpes simplex virus thymidine kinase) promoter. DEK was shown to affect transcription from HAdV-wt E1A promoter (E1Ap) and E4 promoter (E4p) (Figure 35, p. 108). Expression from E1Ap was stimulated 2.5-fold more in DEK expressing cells when compared to the empty vector control transfected with pCMX3b-FLAG. In case of the E4p, we observed an activation of gene expression significantly increased by 2-fold, when DEK is overexpressed in H1299 cells. Thus, DEK is an activator of HAdV E1 and E4 gene transcription.

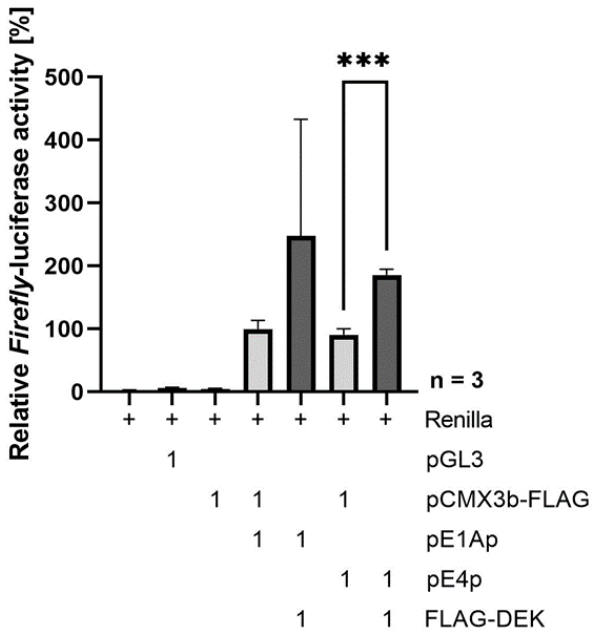

Figure 35: DEK activates gene transcription from viral promoters. H1299 cells were transfected with 1 µg of pRL-TK (*Renilla*-luc; #82), pGL3 empty vector (#P100), pGL3-E1Ap (E1A promoter; #91), pGL3-E4p (E4 promoter; #P97), pCMX3b-FLAG (#V32) or FLAG-DEK (#738) in the combinations indicated in the figure. Luciferase activity was determined 24 h p.t. and absolute *Firefly*-luciferase activity is shown as bar charts. Bar charts represent average values and standard deviations based on three biologically independent experiments. Statistically significant differences were assessed using a student's unpaired t-test with the *GraphPad Prism9* software. ****p ≤ 0.001*

4.1.7.2. DEK Interacts with Adenoviral Early and Late Promoters Sequences

Previous studies reported DEK localizing to chromatin in a non-sequence specific, but rather structural manner. Therefore, DEK is considered to be an architectural protein binding to enhancer and promoter regions thereby changing the topology of DNA and making it more accessible for transcription factors [281, 298, 308, 311, 318, 409]. Additionally, DEK shares structural identity with the transcriptional activator E2F [289]. Our studies revealed DEK as a positive host factor mediating viral mRNA and protein synthesis by activating viral gene transcription from early viral promoters, such as E1 and E4.

To further demonstrate direct binding of DEK to viral promoter regions, we performed a CUT&RUN assay from HAdV-wt infected A549. As a positive control we used monoclonal Tri-Methyl-Histone H3 antibody and performed quantitative real-time PCR with additional control primers included in the kit specific for the human RPL 30 gene (Figure 36 A, p. 110). Enrichment of the immunoprecipitated gene regions bound to DEK were normalized to the negative control rabbit IgG samples. Quantitative real-time PCR was performed using primers specific for the viral promoter regions of E1Ap, E1Bp (E1B promoter), E2Ep (E2 early promoter), E2Lp (E2 late promoter), E4p and MLP. The results show that DEK is associated with viral promoters with enrichment of 2.6-fold at the E1Ap, of 2.4-fold at the E1Bp, of 2.6-fold at the E2Ep, of 1.8-fold at the E2Lp, of 3.1-fold at the E4p and of 1.4-fold at the MLP (Figure 36 B, p. 110).

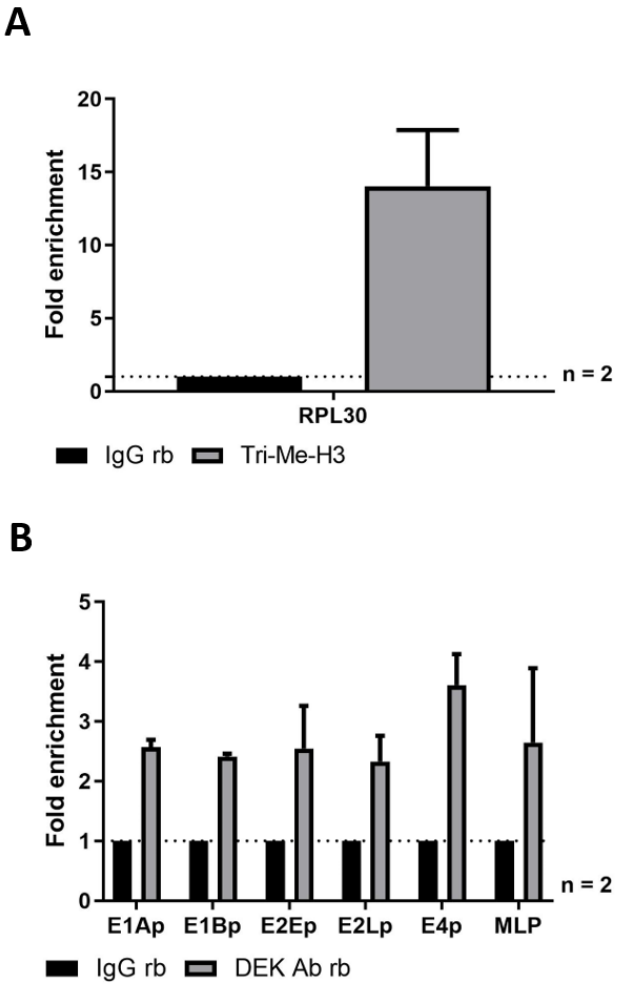

Figure 36: DEK is associated to viral promoters during HAdV-wt infection in A549 cells. A549 cells were seeded and infected with HAdV-wt at a moi 20. 24 h p.i. cells were harvested and 250.000 cells per sample were subjected to CUT&RUN assays (Cell Signaling) according to the manufacturer's protocol. **(A)** The positive control Tri-Methyl-Histone H3 (Lys4) (C42D8) Rabbit mAb (#9751; Cell Signaling) was included and assay functionality was verified by performing qPCR with the included primer set for the human RPL30 gene locus. **(B)** DEK was immunoprecipitated with 1 µl of rabbit mAb α-DEK (ab166624) antibody. Potential viral promoter regions were detected by qPCR using primer sets for E1Ap (#918, #919), E1Bp (#920, #921), E2Ep (#922, #923), E2Lp (#925, #926), E4p (#927, #928) and MLP (#931, #932). **(A, B)** Enrichment of the immunoprecipitated protein at the gene loci were normalized to the corresponding negative IgG antibody control and values are depicted as the fold increase in signal relative to the background signal. Bar charts represent average values and standard deviations based on two biologically independent experiments measured in duplicates.

4.1.8. DEK Binding to Host Transcriptional Regulators Is Changed during HAdV Infection

Transcriptional regulation of DEK is mediated by its interaction with distinct transcriptional regulators as well as the status of its posttranslational modifications [281, 290, 294, 298, 308, 311, 318, 409]. DEK modulates histone acetyltransferase activity of the E1A-interacting protein p300. On the other hand, acetylation of DEK itself is induced by p300-associated PCAF, whereas affinity and binding of DEK to DNA is impaired [296]. Therefore, we hypothesize a change in DEK association with p300 during HAdV-wt infection, to regulate DEK transcription activating capacities and its association with viral DNA.

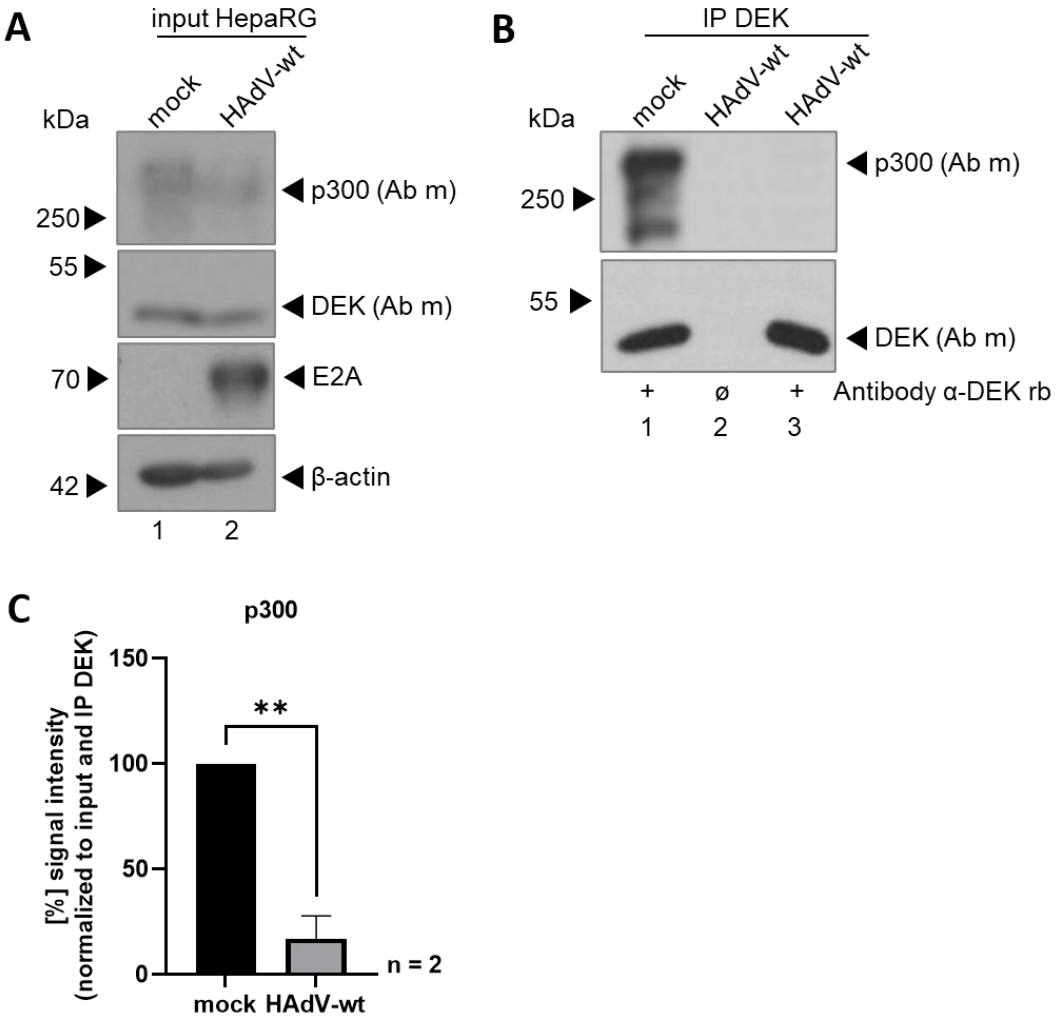

Figure 37: Interaction of DEK with p300 is abolished during HAdV-wt infection. (A, B) HepaRG cells were infected with HAdV-wt at a moi 50 and harvested 48 h p.i. before lysis with NP-40 lysis buffer. Protein complexes composed of DEK and its interaction partners were co-immunoprecipitated using SureBeads™ Protein A Magnetic Beads and 0.5 µl of rabbit mAb α-DEK (ab166624) and 200 µg of whole-cell lysate per sample. Proteins were separated on a 10% SDS-PAGE and detected via immunoblotting using mouse mAb α-DEK (sc-136222) and mouse mAb AC-15 (anti-β-actin) or on an 8% SDS-PAGE and detected via immunoblotting using mouse mAb α-p300 (sc-48343). Steady state expression input levels are shown in **(A)** and co-immunoprecipitated proteins in **(B)**. Molecular weights in kDa are indicated on the left, relevant proteins on the right. Data is representative of two biologically independent experiments. **(C)** For quantification of protein levels, densitometric analysis of detected bands was performed using the *ImageJ* software (version 1.53c). Relative protein expression was normalized on the respective α-β-actin steady-state levels. Levels of co-immunoprecipitated p300 were normalized to precipitated DEK protein levels and the respective input levels. Bar charts represent average values and standard deviations based on two biologically independent experiments. Statistically significant differences were assessed using a student's unpaired t-test with the *GraphPad Prism9* software. ***p ≤ 0.01*

In accordance with published data, we identified DEK as an interaction partner of the acetyltransferase p300 after precipitation of protein complexes with a monoclonal DEK antibody (Figure 37 B, lane 1; p. 111). However, interaction of p300 with DEK was significantly 5.8-fold diminished in HAdV-wt infected HepaRG cells (Figure 37 B, compare lane 3 to 1, C; p. 111) after normalization to actin, input levels and the amount of immunoprecipitated DEK.

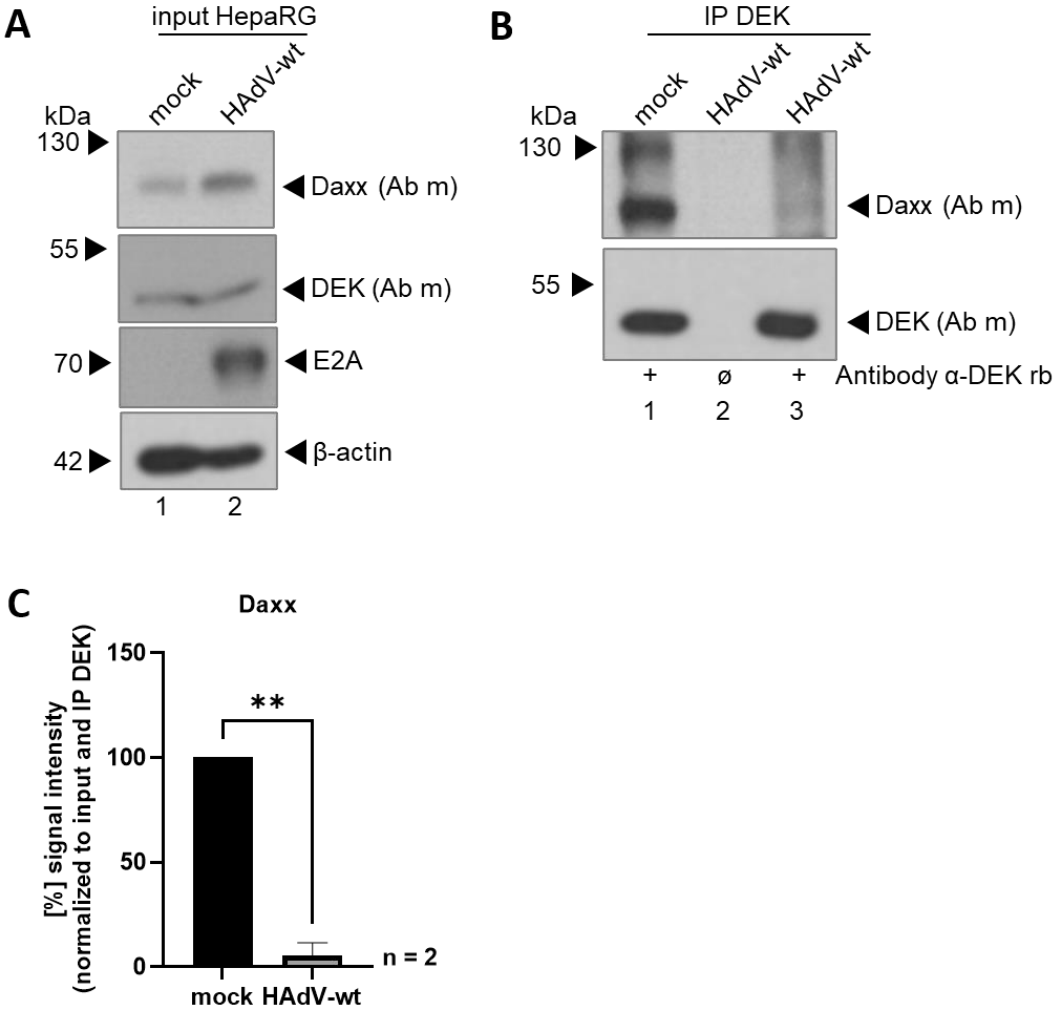

Figure 38: HAdV-wt infection decreases DEK association with Daxx. (A, B) HepaRG cells were infected with HAdV-wt at a moi 50 and harvested 48 h p.i. before lysis with NP-40 lysis buffer. Protein complexes composed of DEK and its interaction partners were co-immunoprecipitated using SureBeads™ Protein A Magnetic Beads and 0.5 µl of rabbit mAb α-DEK (ab166624) and 2000 µg of whole-cell lysate per sample. Proteins were separated on a 10% SDS-PAGE and detected via immunoblotting using mouse mAb α-DEK (sc-136222) and mouse mAb AC-15 (anti-β-actin) or on a 8% SDS-PAGE and detected via immunoblotting using mouse mAb α-Daxx (sc-8043). Steady state expression input levels are shown in **(A)** and co-immunoprecipitated proteins in **(B)**. Molecular weights in kDa are indicated on the left, relevant proteins on the right. Data is representative of two biologically independent experiments. **(C)** For quantification of protein levels, densitometric analysis of detected bands was performed using the *ImageJ* software (version 1.53c). Relative protein expression was normalized on the respective α-β-actin steady-state levels. Levels of co-immunoprecipitated Daxx were normalized to precipitated DEK protein levels and the respective input levels. Bar charts represent average values and standard deviations based on two biologically independent experiments. Statistically significant differences were assessed using a student's unpaired t-test with the *GraphPad Prism9* software. ***p ≤ 0.01*

Recent publications identified DEK as a regulatory interaction partner of Daxx. Depletion of DEK influences the H3.3 distribution and induces its localization to PML-NBs by Daxx. Additionally, Daxx is restrictive host factor repressing HAdV infection. The early viral proteins target Daxx for relocalization and proteasomal degradation to ensure efficient adenoviral replication. To elucidate the interaction of DEK with Daxx during HAdV infection, we infected HepaRG cells at a moi of 50 and performed co-immunoprecipitation assays. In compliance with previous published data, we identified Daxx as an interaction partner of DEK in uninfected cells (Figure 38 B, lane 1; p. 112). This interaction was shown to be

significantly 18.6-fold abolished after infection with HAdV-wt compared to the mock control (Figure 38 B, compare lane 3 to 1, C; p. 112). Taken together, association of DEK with transcriptional modulators p300 and Daxx is counteracted during HAdV-wt infection.

4.1.9. Loss of DEK Protein Expression Negatively Influences Adenoviral Progeny Production

Our preceding experiments in this work identified DEK as novel host regulator of HAdV productive infection. DEK was shown to promote HAdV-wt infection (Figure 20, p. 89), binding to viral promoters (Figure 36, p. 110) and inducing activation of gene expression from viral promoters (Figure 35, p. 108). To further elucidate the role of DEK during HAdV infection, the generation of a DEK depleted cell line was of highest importance to establish a model system to monitor the role of DEK in adenoviral replication.

4.1.9.1. Establishment of a DEK-Negative Mammalian Cell Line

To generate a stable knockdown of DEK in the tumor cell line A549, we produced lentiviruses containing a lentiviral vector, which is expresses a shRNA specific for DEK. A549 cells were infected with the produced lentiviruses and subsequently selected for antibiotic resistance encoded by the lentiviral construct. Hereafter, the established model system (A549 shDEK) was characterized by comparison with the corresponding control cell line (A549 shCTR) transduced with a scrambled shRNA.

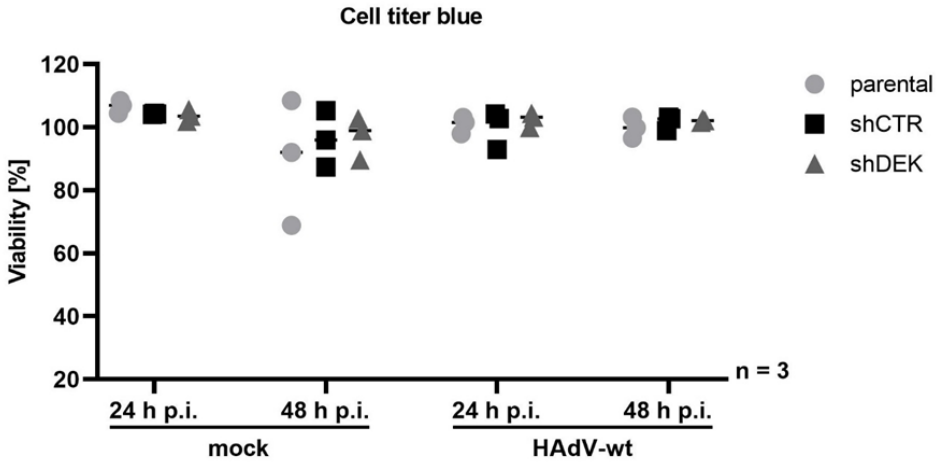

Figure 39: DEK depletion does not affect cell viability of A549 cells. A549 shCTR and shDEK cells were infected with a HAdV-wt at a moi of 20. Cell viability was assessed using the Promega CellTiter-Blue Cell Viability Assay system 24 h and 48 h p.i. and measured using a Tecan Infinite 200M plate reader. *xy* charts represent average values and standard deviations based on three biologically independent experiments measured in triplicates.

First, we monitored the effect of DEK depletion in A549 cells on cellular cytotoxicity by performing CTB assays. We measured cell viability in mock and HAdV-wt infected A549

shCTR and shDEK cells 24 h and 48 h after infection. Gene knockdown of DEK by transduced shRNA does not show an effect on the cell viability of A549 cells compared to the A549 shCTR control cells and the non-transduced A549 parental cell line (Figure 39, p. 113).

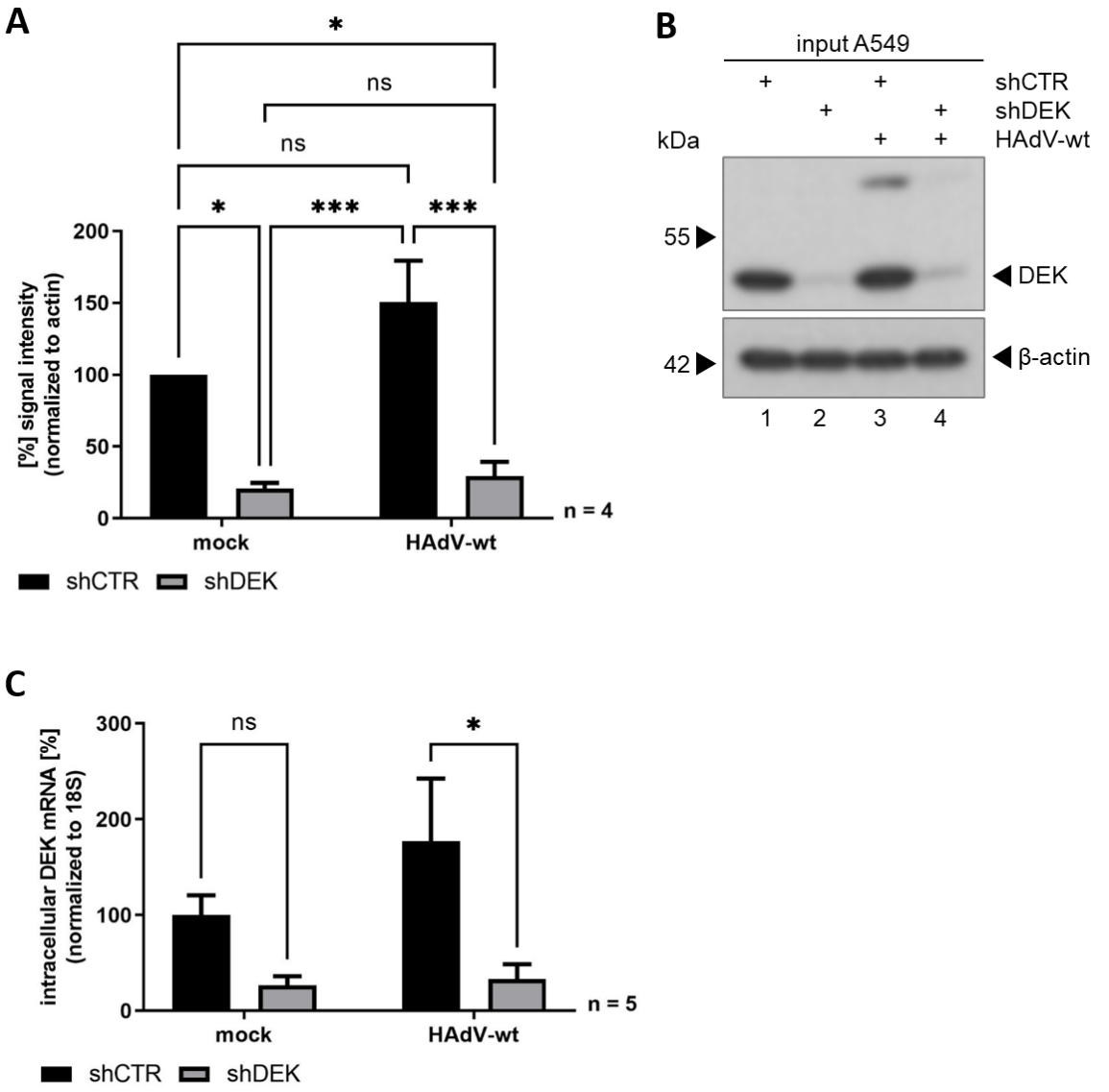

Figure 40: The chromatin-associated DEK protein is efficiently depleted in A549 cells after transduction with shRNA. A549 shCTR and shDEK cells were infected with HAdV-wt at a moi of 20 and harvested 24 h p.i. **(A/B)** Total-cell lysates were prepared with high-stringent RIPA buffer and subjected to immunoblot analysis. Proteins were separated on a 10% SDS-PAGE and detected using rabbit mAb α-DEK (ab166624) and mouse mAb AC-15 (anti-β-actin). **(B)** Molecular weights in kDa are indicated on the left, relevant proteins on the right. Data is representative of two biologically independent experiments. **(A)** For quantification of protein levels, densitometric analysis of detected bands was performed using the *ImageJ* software (version 1.53c). Relative protein expression was normalized on the respective α-β-actin steady-state levels. Bar charts represent average values and standard deviations based on four biologically independent experiments. Statistically significant differences were assessed using a two-way ANOVA and Tukey multiple pairwise-comparison with the *GraphPad Prism9* software. *$p \leq 0.05$, ***$p \leq 0.001$ **(C)** Total mRNA was isolated using TRIzol, reverse transcribed and quantified by RT-qPCR using primers specific for DEK (#631, #632). The data was normalized to the respective 18S (#187, #188) mRNA levels. Bar charts represent average values and standard deviations based on two independent experiments measured in triplicates. Statistically significant differences were assessed using a two-way ANOVA and Šidák correction with the *GraphPad Prism9* software. *$p \leq 0.05$

Next, expression of DEK was examined by RT-qPCR (Figure 40 A, p. 114) and immunoblot analysis (Figure 40 B/C, p. 114). We infected A549 shCTR and shDEK cells at a moi of 20 24 h prior to harvesting. The collected cells were subdivided and either mRNA was prepared via TRIzol isolation or total-cell lysates were prepared with high-stringent RIPA buffer. Immunoblot analysis revealed a strong decrease of DEK signal in A549 shDEK cells compared to the corresponding shCTR control cell line (Figure 40 A and B compare lane2 and 4 to lane 1 and 3, p. 114). DEK expression was significantly decreased in A549 shDEK cells in mock uninfected as well as HAdV-wt infected cells (Figure 40 A, p. 114). Additionally, we verified the depletion of DEK in A549 cells by determining DEK mRNA levels, and could show that DEK mRNA was significantly decreased by 3.8-fold in mock uninfected A549 shDEK cells compared to shCTR cells, while we observed a 5.3-fold decrease of DEK mRNA in HAdV-wt infected DEK-negative cells (Figure 40 C, p. 114).

This data was further confirmed using immunofluorescence analysis of the DEK-negative A549 cells and the respective control cell line. Co-staining of DEK, E4orf3 and PML revealed a reduced DEK expression (Figure 41 A, panels l and q; p. 116) with a significant decrease of signal intensity by 3.7-fold (Figure 41 B; p. 116). Nevertheless, PML-NBs were shown to be reorganized in HAdV-wt infected A549 shDEK cells (Figure 41 A, panel s; p. 116) with discrete localization of viral E4orf3 to the newly formed tracks (Figure 41 A, panel t; p. 116). However, number of PML-NBs was significantly reduced in DEK-depleted A549 cells by 1.94-fold (Figure 41 C, p. 116).

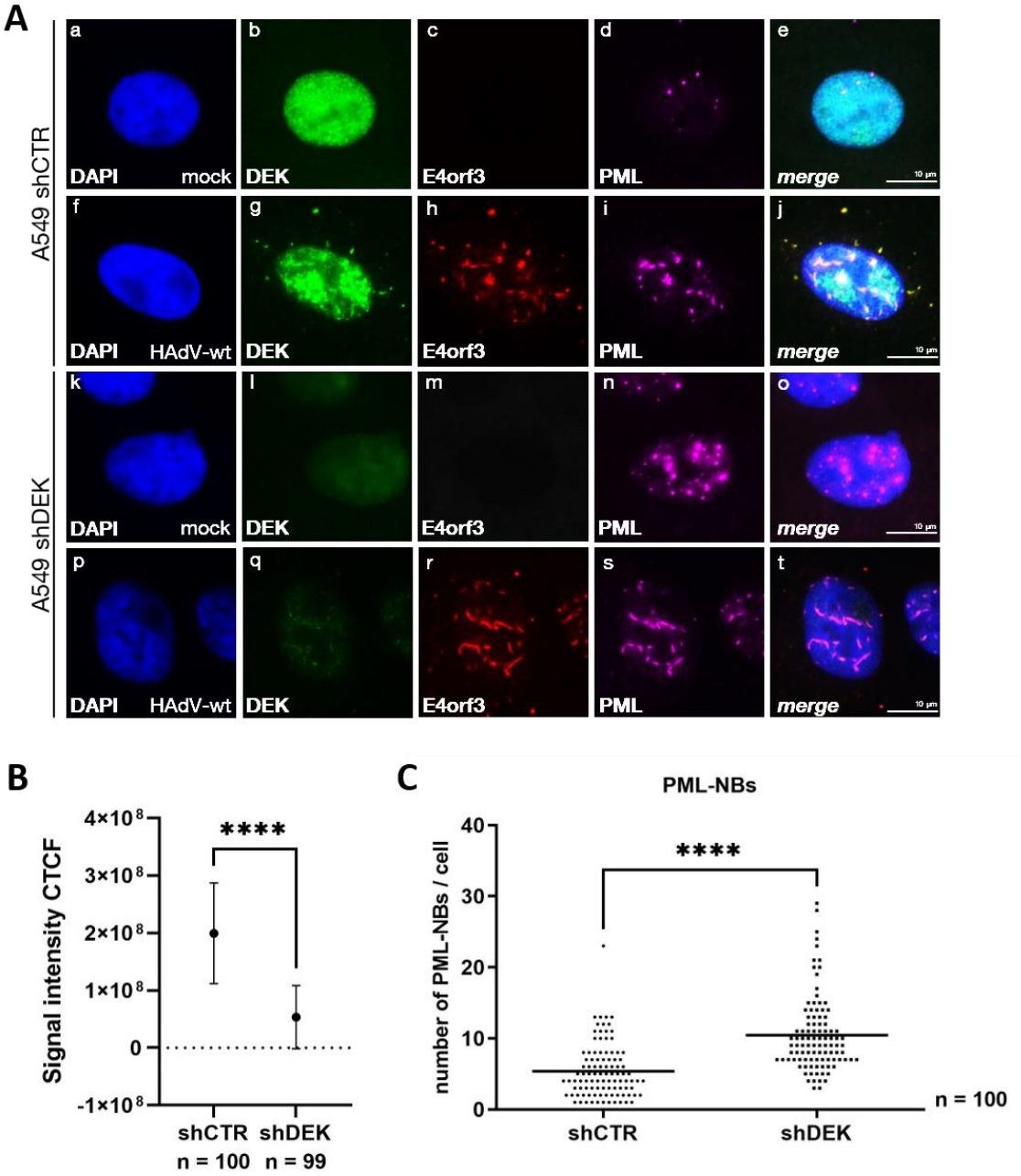

Figure 41: Efficient DEK depletion increases number of PML-NBs in A549 cells. (A) A549 shCTR and shDEK cells were infected with HAdV-wt at a moi of 20. Cells were fixed with 4% PFA 24 h p.i. and labelled with primary antibodies rabbit mAb α-DEK (ab166624), rat pAb α-E4orf3 (6A11) and rabbit pAb α-PML (ab72137). Primary antibodies were detected with Alexa488- (green; α-DEK), Alexa647- (red; α-E4orf3) and Alexa568- (magenta; α-PML) conjugated secondary antibodies. DAPI was used for nuclear staining. Representative DEK (b, g, l, q), E4orf3 (c, h, m, r) and PML (d, i, n, s) staining patterns of at least 100 analyzed cells are shown. Overlays of single images (*merge*) are shown in e, j, o, t. White scale bar represents 10 µm. Images were taken using a *Zeiss Axio Observer.Z1*. **(B)** For 100 cells in shCTR and for 99 cells in shDEK, cell fluorescence signal intensity was measured using the *ImageJ* software (version 1.53c). CTCF was calculated based on the integrated density, cell area and background fluorescence. Pictures were taken with the same laser intensity and exposure time of 84.73 ms for all samples. Statistically significant differences were assessed using a student's unpaired t-test with the GraphPad Prism9 software. ****p ≤ 0.001* **(C)** For 100 cells per cell line, number of PML-NBs per cell was counted. Statistically significant differences were assessed using a student's unpaired t-test with the *GraphPad Prism9* software. *****p ≤ 0.0001*

4.1.9.2. Depletion of DEK Expression Represses HAdV Infection

To verify the observed influence of DEK on HAdV infection, we investigated viral mRNA levels and performed virus yield analysis in the generated DEK-negative cells and the

corresponding control cells. The cells were infected with HAdV-wt at a moi of 20 for 24 h prior to isolation and quantification of total mRNA and newly synthesized virions.

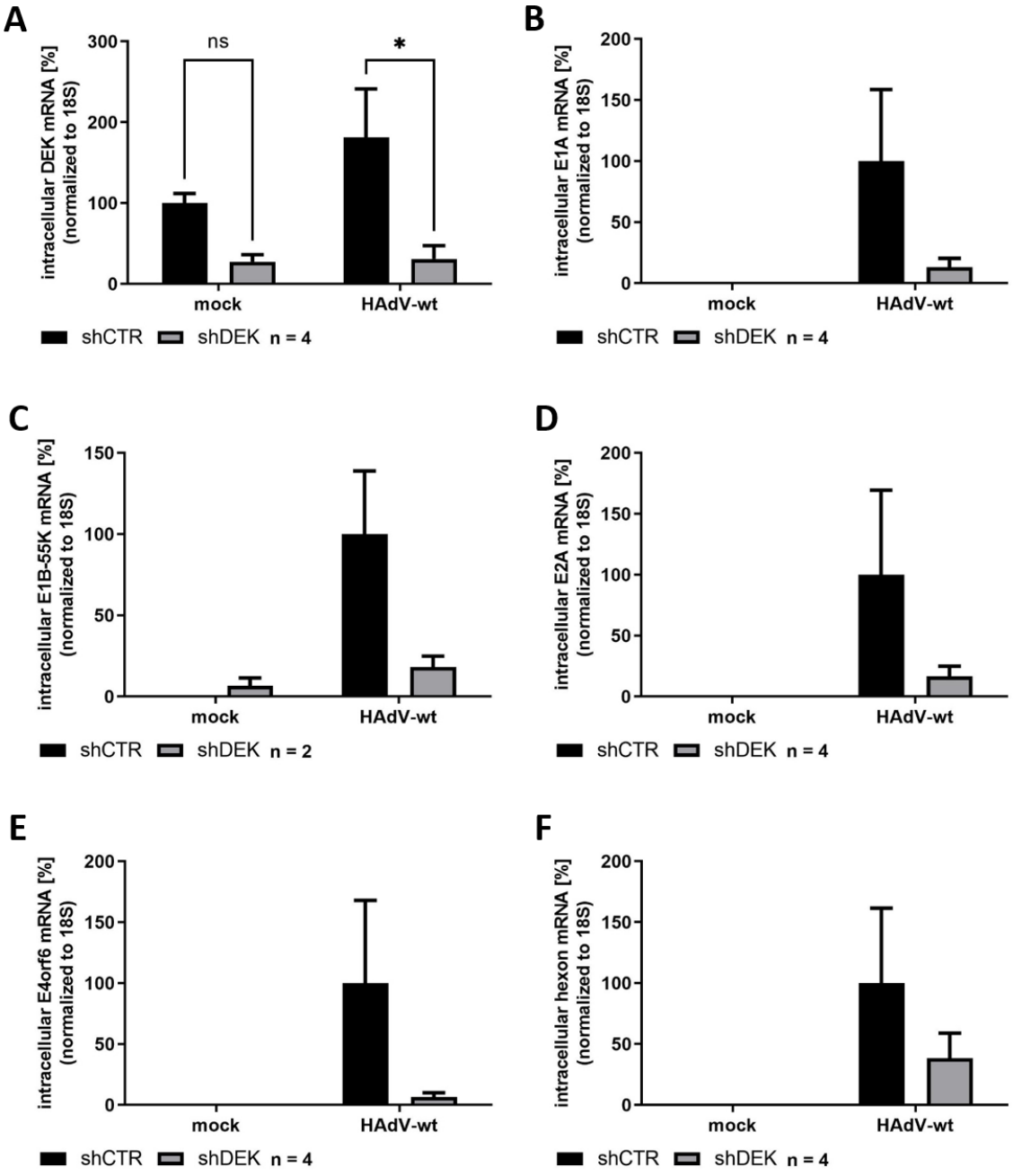

Figure 42: Viral mRNA production is decreased in DEK negative cells. A549 shCTR and shDEK cells were infected with HAdV-wt at a moi of 20. The cells were harvested 24 h p.i. and total mRNA was isolated with TRIzol. Amount of mRNA species were quantified by RT-qPCR and specific primers for **(A)** DEK (#631, #632), **(B)** E1A (#181, #182), **(C)** E1B-55K (#323, #324), **(D)** E2A (#183, #184), **(E)** E4orf6 (#134, #135) and **(F)** hexon (#189, #190). The data was normalized to the respective 18S (#187, #188) mRNA levels. Bar charts represent average values and standard deviations based on two independent experiments measured in duplicates. Statistically significant differences were assessed using a two-way ANOVA and Šidák correction for DEK mRNA or a student's unpaired t-test for viral mRNA with the *GraphPad Prism9* software. *$p \leq 0.05$*

Viral mRNA production was shown to be decreased after depletion of DEK in A549 cells (Figure 42, p. 117). Our qPCR analysis revealed a 7.5-fold for E1A (Figure 42 B, p. 117), a

5.5-fold for E1B-55K (Figure 42 C, p. 117), a 6-fold for E2A (Figure 42 D, p. 117), a 15.4-fold for E4orf6 (Figure 42 E, p. 117) and a 2.6-fold for hexon (Figure 42 F, p. 117) decrease in mRNA.

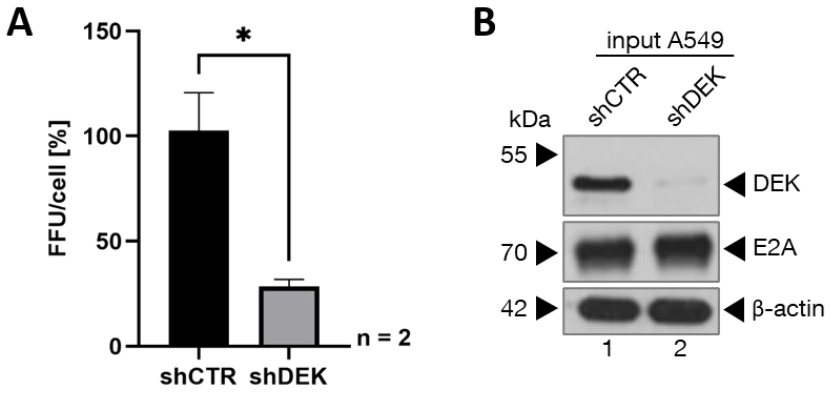

Figure 43: HAdV progeny production is diminished in DEK-negative A549 cells. (A) A549 shCTR and shDEK cells were infected with HAdV-wt at a moi of 20. Viral particles were harvested 24 h p.i. and virus yield was determined by quantitative staining of early viral E2A after reinfection of HEK-293 cells with a serial dilution of the newly synthesized virions. FFU/cell was calculated taking the cell umber, dilution actor and objective magnification into account. Bar charts represent average values and standard deviations based on two biologically independent experiments. Statistically significant differences were assessed using a student's unpaired t-test with the *GraphPad Prism9* software. *$p \leq 0.05$ **(B)** Part of the cells used for virus yield determination were used for immunoblot analysis to verify DEK depletion in A549 cells. Total-cell lysates were prepared with high-stringent RIPA buffer and subjected to a 10% SDS-PAGE. Proteins were detected by using rabbit mAb α-DEK (ab166624), mouse pAb α-E2A (B6-8) and mouse mAb AC-15 (anti-β-actin). Molecular weights in kDa are indicated on the left, relevant proteins on the right.

The newly synthesized virions were isolated by subsequent freeze and thaw-cycles. A virus dilution was prepared and viral progeny production was visualized in HEK-293 cells by quantitative staining of the early viral RC marker E2A. Calculation of the fluorescence forming units per cell showed a significant decrease in viral progeny production by 3.6-fold in A549 shDEK (Figure 43 A, p. 118). Reduced expression of the DEK protein was verified by immunoblot analysis (Figure 43 B, compare lane 2 to lane 1; p. 118).

4.2. DEK Affects Virus-Mediated Oncogenic Transformation Processes

4.2.1. E1A Interaction with p300 Is Dependent on DEK Expression

E1A association with p300 is considered to be important for virus-induced cell transformation by repressing cellular gene transcription and acetylation of H3K18 [235, 241, 263]. To elucidate the role of DEK in E1A and p300 interaction, we infected A549 shCTR and shDEK cells with HAdV-wt at a moi of 20. We harvested the cells 24 h p.i. and performed co-immunoprecipitation assays by precipitating the protein complexes either by using an antibody specific for p300 or for the viral protein E1A.

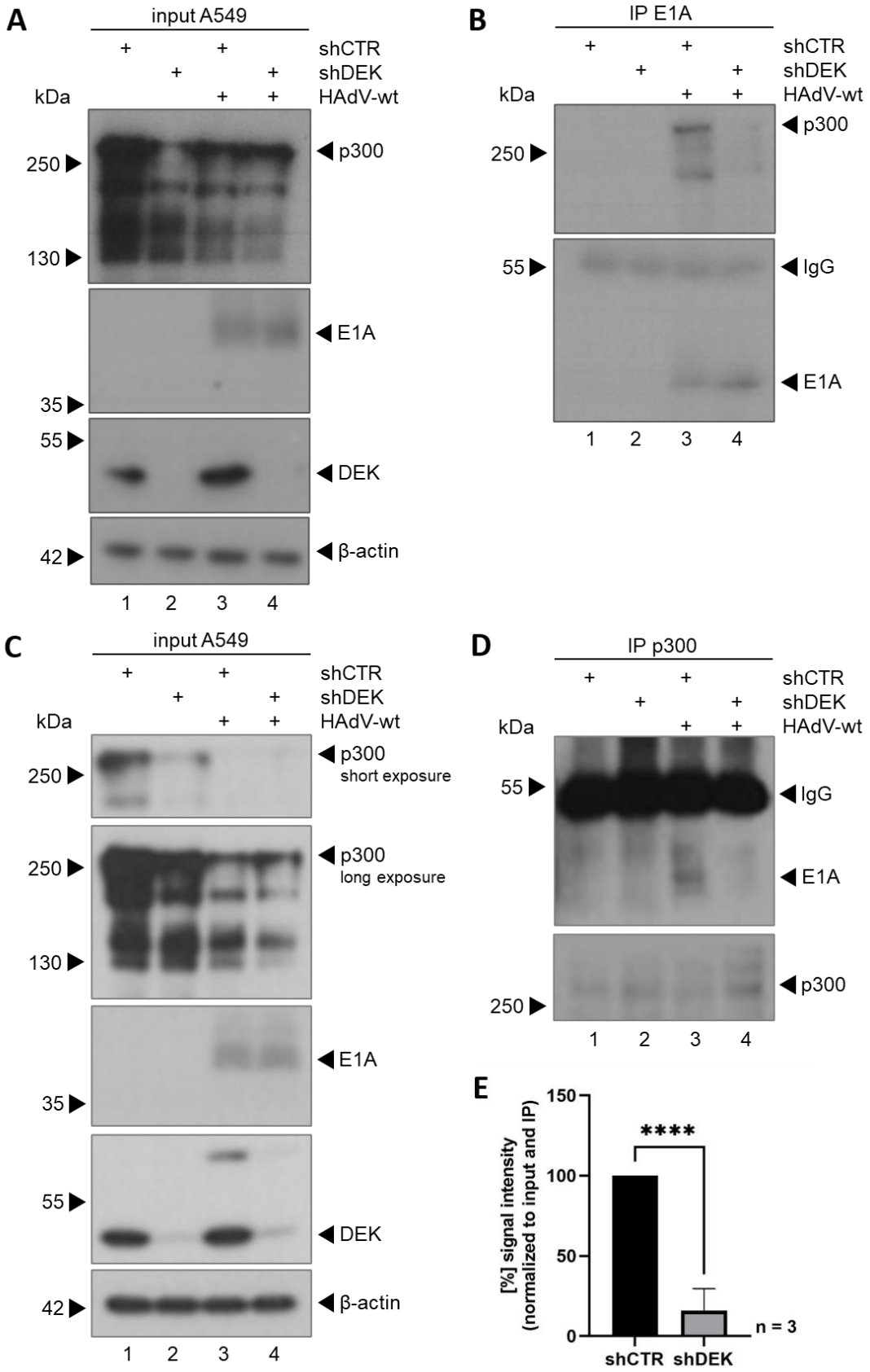

Figure 44: DEK mediates interaction of early viral E1A with p300. (A, B, C, D) A549 shCTR and shDEK cells were infected with HAdV-wt at a moi 20 and harvested 24 h p.i. before lysis with NP-40 lysis buffer. Protein complexes were co-immunoprecipitated using SureBeads™ Protein A Magnetic Beads coupled with **(B)** either 2 µl of mouse mAb α-E1A (M73; sc-25) or **(D)** either 2 µl mouse

mAb α-p300 (sc-48343) and 1000 µg of whole-cell lysate per sample. Proteins were separated on a 10% SDS-PAGE and detected via immunoblotting using mouse mAb α-DEK (sc-136222), mouse mAb α-E1A (M73; sc-25) and mouse mAb AC-15 (anti-β-actin) or on a 8% SDS-PAGE and detected via immunoblotting using mouse mAb α-p300 (sc-48343). Steady state expression input levels are shown in **(A, C)** and co-immunoprecipitated proteins in **(B, D)**. Molecular weights in kDa are indicated on the left, relevant proteins on the right. Data is representative of two biologically independent experiments. **(C)** For quantification of protein levels, densitometric analysis of detected bands was performed using the *ImageJ* software (version 1.53c). Relative protein expression was normalized on the respective α-β-actin steady-state levels. Levels of co-immunoprecipitated were normalized to precipitated protein levels and the respective input levels. Bar charts represent average values and standard deviations based on two biologically independent experiments. Statistically significant differences were assessed using a student's unpaired t-test with the *GraphPad Prism9* software. $^{****}p \leq 0.0001$

We verified depletion of DEK as well as the expression of our protein-of-interests in our input samples (Figure 44 A and C, p. 119). Indeed, precipitation of the proteins and subsequent staining of E1A and p300 revealed the necessity of DEK expression for efficient interaction of E1A with the host deacetylase p300 (Figure 44 B and D, p. 119). We could show that interaction of E1A with p300 is significantly decreased by 6.3-fold in DEK negative cells (Figure 44 E, p. 119).

4.2.2. DEK Depletion Interferes with Interaction of E1B-55K with Host Restrictive Factors

After p53 stabilization and induction of apoptosis by E1A, E1B-55K counteracts p53 functions. To repress p53, E1B-55K binds to p53 [139] and mediates SUMOylation [215, 216] and proteasomal degradation [145, 215, 270] of the tumor suppressor. To investigate DEK-mediated interaction of E1B-55K with p53, we performed co-immunoprecipitation with an antibody specific for p53 in HAdV-wt infected A549 shCTR and shDEK cells (Figure 45, p. 121). All proteins were shown to be expressed, while DEK was not detected in shDEK cells, as expected (Figure 45 A, p. 121). A higher migrating band of p53 at around 60 kDa was observed in HAdV-wt infected shCTR cells, though being significantly 1.9-fold decreased in DEK negative cells (Figure 45 A compare lane 43 to 3, D, p. 121). The data confirmed previous publications as E1B-55K was shown to be co-immunoprecipitated with p53. However, this ability was significantly lost by 2.2-fold in A549 cells lacking expression of the DEK protein (Figure 45 B compare lane 3 and 4, p. 121). These findings indicate DEK acts as a key mediator for the interaction of E1B-55K and p53, and thus being important for E1B-55K mediated inhibition of p53 apoptotic functions and E1B-55K dependent SUMOylation of p53.

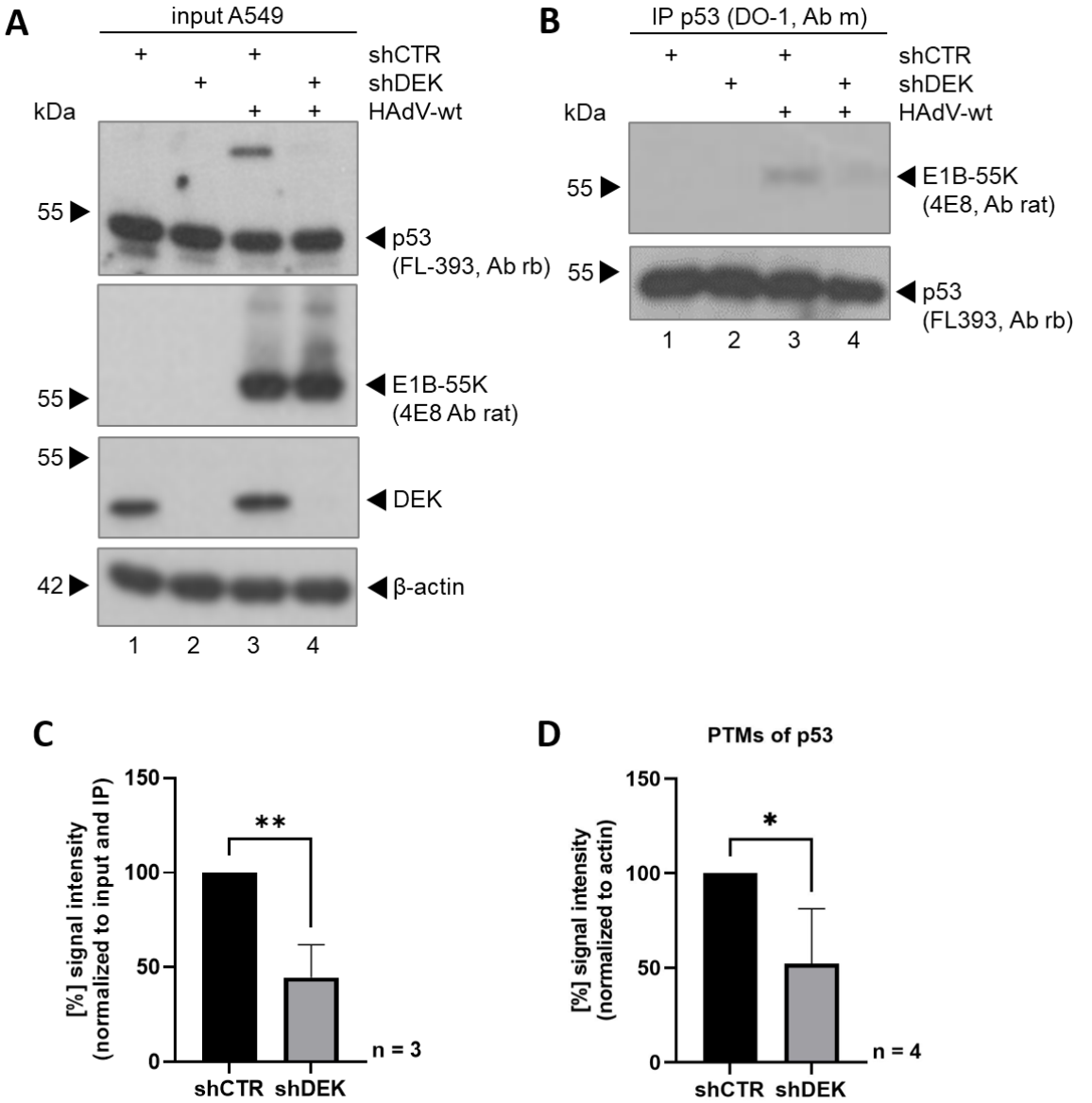

Figure 45: DEK is essential for early viral E1B-55K interaction with tumor suppressor p53. (A, B) A549 shCTR and shDEK cells were infected with HAdV-wt at a moi 20 and harvested 24 h p.i. before lysis with NP-40 lysis buffer. Protein complexes were co-immunoprecipitated using SureBeads™ Protein A Magnetic Beads coupled with 0.25 µl of mouse mAb α-p53 (DO-1; sc-126) and 1000 µg of whole-cell lysate per sample. Proteins were separated on a 10% SDS-PAGE and detected via immunoblotting using mouse mAb α-DEK (sc-136222), mouse mAb α-E1B-55K (4E8), mouse mAb α-p53 (DO-1; sc-126) and mouse mAb AC-15 (anti-β-actin). Steady state expression input levels are shown in **(A)** and co-immunoprecipitated proteins in **(B)**. Molecular weights in kDa are indicated on the left, relevant proteins on the right. Data is representative of two biologically independent experiments. **(C, D)** For quantification of protein levels, densitometric analysis of detected bands was performed using the *ImageJ* software (version 1.53c). Relative protein expression was normalized on the respective α-β-actin steady-state levels. Levels of co-immunoprecipitated E1B-55K were normalized to precipitated p53 protein levels and the respective input levels. Protein levels for p53 are shown in **(C)** and for higher migrating PTMs of p53 are shown in **(D)**. Bar charts represent average values and standard deviations based on four biologically independent experiments. Statistically significant differences were assessed using a student's unpaired t-test with the *GraphPad Prism9* software. ***p ≤ 0.01*

4.2.3. E1B-55K Is Not Able to Inhibit p53 Function in DEK-Negative Cells

E1B-55K binds together with PML-IV and PML-V to p53 to block the association of p53 to p53-responsive promoter regions [139]. Additionally, p53 is SUMOylated by E1B-55K to suppress p53-mediated transcription [215, 216, 246]. The importance of DEK expression on E1B-55K-mediated p53 regulation was further determined by detection of mRNA of

p53-responsive genes MDM2, p21 and PCNA, since we observed reduced E1B-55K association with p53 (4.2.2, p. 120).

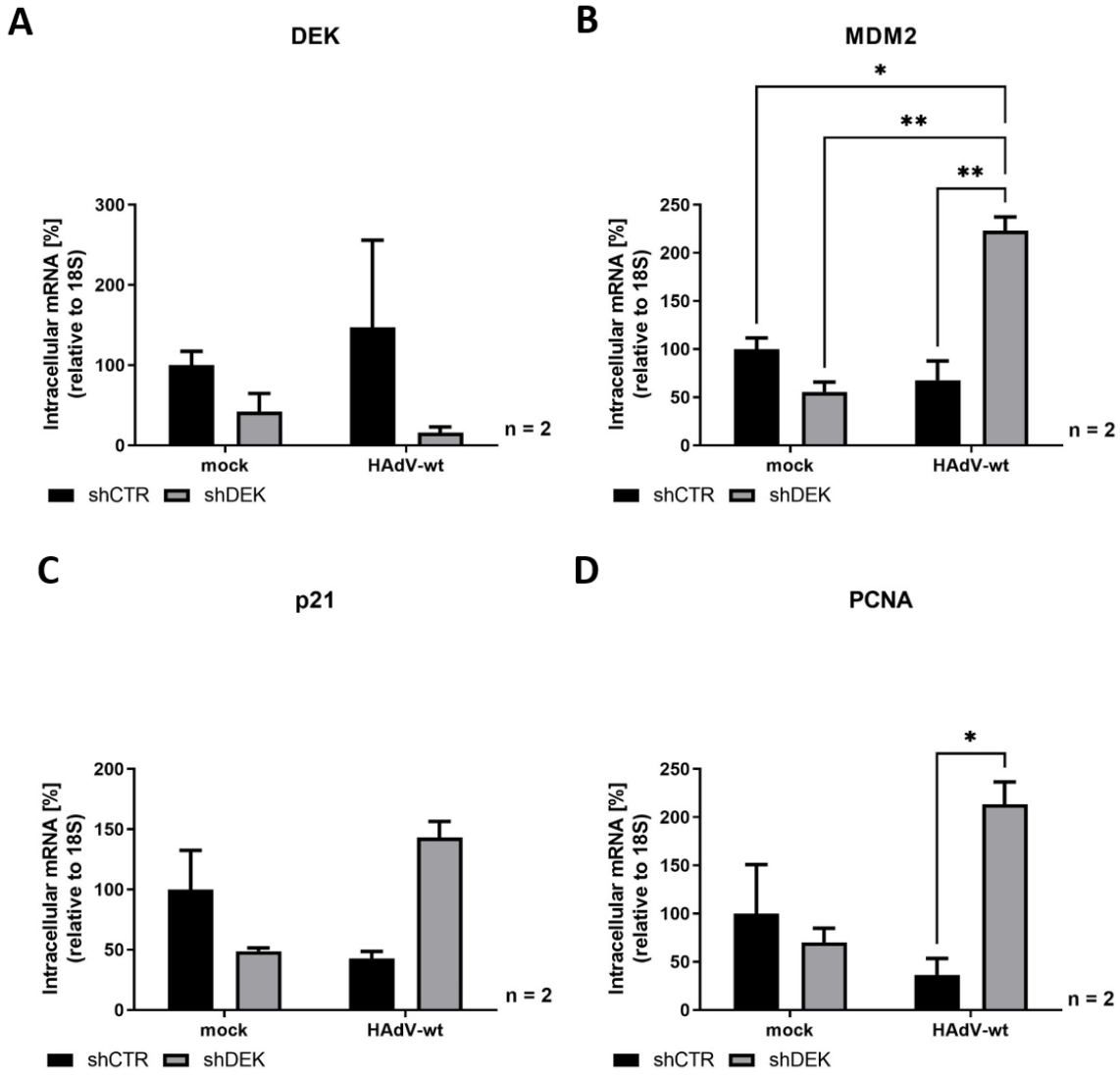

Figure 46: E1B-55K-mediated inhibition of p53 transactivating functions are diminished after DEK depletion. A549 shCTR and shDEK cells were infected with HAdV-wt at a moi of 20. The cells were harvested 24 h p.i. and total mRNA was isolated with TRIzol. Amount of mRNA species were quantified by RT-qPCR and specific primers for **(A)** DEK (#631, #632), **(B)** MDM2 (#929, #930), **(C)** p21 (#933, #934) and **(D)** PCNA (#935, #936). The data was normalized to the respective 18S (#187, #188) mRNA levels. Bar charts represent average values and standard deviations based on two independent experiments measured in duplicates. Statistically significant differences were assessed using a two-way ANOVA and Tukey multiple pairwise-comparison with the *GraphPad Prism9* software. *$p \leq 0.05$, **$p \leq 0.01$*

Therefore, A549 shCTR and shDEK cells were infected with HAdV-wt and 24 h p.i. total RNA was isolated by TRIzol. After reverse transcription, mRNA species were quantified by qPCR with specific primer for DEK, MDM2, p21 and PCNA. Depletion of DEK in A549 shDEK cells was verified by using specific primers for DEK (Figure 46 a, p. 122). Our experiments indicated a diverse regulation of p53-responsive mRNA production in DEK negative and the corresponding control cell line (Table 40, p. 123). All three p53-responsive

genes were decreased during HAdV-wt infection by 1.5-fold for MDM2 (Figure 46 B, p. 122), 2.3-fold for p21 (Figure 46 C, p. 122) and 2.7-fold for PCNA (Figure 46 D, p. 122). Likewise, DEK depletion displayed a similar phenotype, since we observed downregulation of MDM2 mRNA by 1.8-fold (Figure 46 B, p. 122), of p21 mRNA by 2-fold (Figure 46 C, p. 122) and PCNA mRNA by 1.4-fold (Figure 46 D, p. 122). Intriguingly, production of mRNA from p53-responsive genes was quite differentially regulated in A549 shDEK cells. After depletion of DEK, mRNA of MDM2, p21 and PCNA was increased during HAdV-wt infection compared to the respective mock samples (Figure 46, p. 122). Here, we detected a significant increase of 4-fold in MDM2 mRNA level (Figure 46 B, p. 122), of 2.9-fold in p21 mRNA levels (Figure 46 C, p. 122) and of 5.9-fold in PCNA mRNA (Figure 46 D, p. 122). Comparison of mRNA levels in the two cell lines infected with HAdV-wt emphasized E1B-55K inability to inhibit p53 function in DEK-negative cells. In all three cases mRNA production was increased in A549 shDEK cells compared to the shCTR cells in HAdV-wt infected cells, with a significant elevation of 3.3-fold and 5.9-fold in mRNA of MDM2 (Figure 46 B, p. 122) and PCNA (Figure 46 D, p. 122), respectively. PCNA mRNA was shown to be 3.3-fold increased during HAdV-wt infection in cells depleted for DEK (Figure 46 C, p. 122). In conclusion, DEK is crucial for inhibition of the transactivating function of p53 by E1B-55K during HAdV-wt infection.

Table 40: Regulation of mRNA production of p53-responsive genes in DEK-negative cells. Data obtained from experiment illustrated in Figure 46 (p. 122) was calculated relative to the respective 18S Ct values. mRNA levels from A549 shCTR mock uninfected samples were set on 100%.

	A549 shCTR		A549 shDEK	
mRNA levels	**mock**	**HAdV-wt**	**mock**	**HAdV-wt**
DEK	100%	147.1%	41.87%	15.91%
MDM2	100%	67.59%	55.46%	223.1%
p21	100%	42.8%	48.78%	143.0%
PCNA	100%	36.37%	69.81%	213.4%

5. Discussion

HAdVs are the cause of sporadic and epidemic infection events, inducing a variety of clinical syndromes, like respiratory diseases, pneumonia, hepatitis, myocarditis, keratoconjunctivitis, or gastroenteritis, depending on the serotype and tissue that they infect [25, 26, 28, 31, 34, 37, 41, 43, 44, 47-49, 410-412]. In immunocompetent patients they mostly cause a mild non-febrile self-limiting infection. However, in immunosuppressed patients, HAdV infections have a lethal outcome in up to 82% of the infected individuals [19, 38, 46, 51]. Furthermore, newly evolving serotypes, such as HAdV 14p1, were shown to cause severe pulmonary diseases with increased intensity of inflammation even in non-immunocompromised patients [50, 413]. Until today adenoviral infections are only treated symptomatically with antiviral drugs, like ribavirin and cidofovir, since there is no specific treatment nor vaccination available [73-75, 78, 79, 414, 415]. Therefore, identifying novel targets for antiviral therapy strategies is of high importance.

PML-NBs are dynamic ring-like structures with over 160 proteins known to localize in these domains. The formation, integrity, and function of PML-NBs, as well as the recruitment of protein partners, is dependent on SUMOylation [189, 190, 194]. Most of SUMOylation pathway enzymes localize at PML-NBs and 56% of PML-NB-associated proteins are modified by SUMO. PML-NBs and their components play a crucial role in transcription, apoptosis, senescence, response to DNA-damage and antiviral defense [183, 190, 193, 240, 416-421]. Recent studies implicate a bivalent role of PML-NBs during HAdV infection. On the one hand certain factors like PML-II are utilized for efficient replication [214, 247, 248, 279, 422], while on the other hand proteins, like e.g. the SWI/SNF complex, are repressing HAdV infection by repressing viral gene transcription [145, 244, 245, 270, 373, 423]. Additionally, HAdV place their genomes and sites of viral transcription in close proximity to PML tracks.

An additional PML-NB associated regulatory interaction partner of Daxx is the so-called DEK protein [309, 311]. This multifunctional protein is involved in epigenetic regulation, transcription, splicing, oncogenic pathways and modulation of viral infections [285, 289-292, 294, 296, 317, 336, 341, 342, 371, 409]. Since little is known about the early stages of HAdV infection, viral gene transcription and virus-mediated oncogenesis, this study aims to investigate the functional role of DEK during HAdV infection to identify novel therapeutic approaches against HAdVs.

5.1. DEK Is a Novel Host Factor Promoting HAdV Infection

After viral entry, the viral genome is tightly associated with the core and core-associated proteins pV, pVII and Mu. However, following the uncoating of the virus, Mu and pV were shown to disassociate from the viral DNA [109, 408, 424-426]. The viral genome is imported into the nucleus packed with the histone-like viral protein pVII, which condenses the viral DNA into so-called 'adenosomes', thus protecting the DNA from recognition by the host cell's DDR [424, 425, 427-431]. However, removal of pVII from the viral DNA is essential for active viral gene transcription. Within the first 6 h of infection, host H3.3 and acetylated histones are loaded on the viral DNA, mediating the organization of the viral genome in nucleosomes and inducing the active viral transcription [241, 428-435]. Our data indicates a role of the DNA-binding protein DEK during adenoviral transcription and replication.

Here, we identified DEK as positive regulator of HAdV infection supporting viral gene expression and progeny production (Figure 20, p. 89). While DEK expression does not change viral DNA synthesis (Figure 15, p. 84), we observed enhanced viral mRNA production (Figure 16, p. 85) and protein synthesis (Figure 17, p. 86; Figure 18, p. 87) of early as well as late genes by DEK independently of the investigated tissues. Hence, it modulates viral transcription throughout the complete HAdV replication cycle. Our gene knockdown experiments further suggest DEK to be indispensable for efficient viral productive infection (Figure 43, p. 118; Figure 42, p. 117). Furthermore, we observed increase in PML-NB formation after loss of DEK (Figure 41, p. 116). Although, certain PML isoforms were identified as positive regulators promoting p53 inhibition by E1B-55K and viral gene transcription by E1A [139, 240], PML-NBs are considered to be antiviral structures and depletion of PML increases adenoviral progeny production [139, 240, 247, 422].

HAdV E1A protein activates the cell cycle control and drives the host cell into S phase to provide the transcription machinery for viral replication. Therefore, E1A diminishes Rb SUMOylation with the subsequent release of the transcription factor E2F and the transcription of its responsive genes [436-438]. DEK was identified as an E2F-responsive gene, since mutations of the E2F binding sites in the DEK promoter abolish active gene transcription. This goes along with diseases associated with Rb deficiencies, such as retinoblastomas and small cell lung cancers, demonstrating induced DEK mRNA production. Similar outcomes were observed during infection with other DNA viruses, such

as HPV and EBV. The early viral E7 protein of HPV, which has homologous functions like the adenoviral E1A protein [439], mediates DEK mRNA overexpression during infection. Therefore, DEK upregulation is considered to be a feature of DNA tumor viruses and diseases associated with Rb loss [325-331]. Consistent with Rb inhibition, HAdV infection induces DEK mRNA and protein levels (Figure 8, p. 76; Figure 9, p. 77; Figure 10, p. 78; Figure 11, p. 79). Conversely, DEK expression elevates E1A levels, not just post-transcriptional, but already on a mRNA level (Figure 16, p. 85; Figure 17, p. 86; Figure 18, p. 87). The upregulation of E1A on mRNA and protein level by DEK could positively affect E1A transactivation capacity and gene expression of viral genes. The E1A-13S protein is associated und regulates various cellular chromatin remodeling factors such as HAT proteins, p300, PCAF, and members of the SWI/SNF family [260, 440-442], which is indispensable for the early stages of infection [240, 443].

Additionally, our data indicates a positive effect of DEK on further early viral protein levels, such as E1B-55K, E2A and E4orf3 (Figure 17, p. 86; Figure 18, p. 87). E1B-55K is a multifunctional protein regulating viral replication and modulating the host cell to induce a favorable environment for infection. Besides regulation of protein synthesis, vDNA replication, viral RNA (vRNA) biogenesis, cell cycle control and assembly of an E3 ubiquitin ligase together with E4orf6 to target host proteins for proteasomal degradation, E1B-55K can function as E3 SUMO ligase modulating the function of other proteins [215].

E2A is a nuclear viral protein being essential at multiple steps during HAdV infection, such as regulation of viral gene expression, mRNA stability or virion assembly, as well as the recruitment of several host cell factors and viral proteins to viral RCs [406, 444-448]. Those replication compartments are localizing in close proximity to the nuclear PML tracks [214, 405]. Track formation occurs due to interaction of E4orf3 with PML-II mediating the disruption of the dot-like structure [248]. Hence, negative factors can be repressed, while positive factors are utilized for HAdV replication. Additionally, recent publication reported a role of E4orf3 in the regulation of the host's DDR independently from E1B-55K and E4orf6. Here, E4orf3 relocalizes Mre11 to insoluble aggresomes to inactivate its restrictive function. In addition, E4orf3 mediates the degradation of the negative host factor TIF1γ [249, 252].

Furthermore, DEK expression promoted late viral protein synthesis of pVI and Capsid proteins (Figure 17, p. 86; Figure 18, p. 87). Before virus release, maturation and assembly of the progeny virions is taking place. Therefore, the adenovirus protease (AVP) processes

the newly synthesized precursor proteins IIIa, VI and VIII, as well as core proteins VII, μ and TP. For efficient cleavage of the structural proteins by AVP, pVI functions as a co-activator of the viral protease. The expression of the Capsid proteins, as well as the maturation of the proteins, is crucial for production of infectious virion particles [449].

Taken together, induced expression of DEK in distinct cell lines from different tissue origins favors protein synthesis of early, as well as late genes. The viral proteins, which were more expressed after DEK transfection, are known to be crucial for efficient HAdV replication and virion assembly. Therefore, we can assume that the increased quantity of viral proteins favors efficient infection and progeny production. However, it is clearly preliminary to speculate about the impact of the upregulated expression of the distinct proteins. Nevertheless, sufficient production of those viral factors is of high importance and the increased release of infectious particles in the DEK-overexpressing cells highlight the promoting quality of DEK (Figure 20, p. 89).

5.2. DEK Function Is Dependent on Its PTM

DEK is a highly posttranslational modified protein targeted for phosphorylation, acetylation, ubiquitinylation and PARylation [285, 290, 294-296, 298, 450-452]. Until now, the exact regulation of DEK modification remains unclear, however it is suggested, that PTMs of DEK could explain the conflicting and controversial data about the functions of the chromatin-associated protein. Phosphorylation of DEK differs during the different stages of cell cycle with a peak during G_1 phase [294]. Protein kinase CK2 mediates phosphorylation of DEK and thereby its association to DNA [285, 294]. The C-terminal region of DEK serves as a DNA-binding as well as a multimerization site. Phosphorylation of this site decreases the affinity of DEK to DNA, but increases DEK-DEK interactions. However, DEK-DEK interaction is dependent on the association of DEK with DNA, since unphosphorylated DEK binds to the chromatin with subsequent multimerization of phosphorylated DEK to the chromatin-bound protein. As a consequence, multimerization of DEK induces DNA twists, which represses gene transcription [285]. We observe extensive attachment of SUMO moieties to DEK during HAdV-wt infection by early viral E1B-55K (Figure 24, p. 95), which serves as a viral E3 SUMO ligase [216]. Since the predicted SCM are located in the C-terminal part of DEK (Figure 23, p. 93), we assume that DEK SUMOylation interferes with phosphorylation and multimerization of the protein, whereas DEK is bound to viral DNA

with reduced DEK-DEK interaction. Indeed, we detect DEK associated to the promoters at the viral DNA (Figure 36, p. 110) inducing active viral gene transcription (Figure 35, p. 108).

Moreover, SUMOylation of DEK may interfere with ubiquitinylation. Equal to SUMO, ubiquitin is covalently linked to lysine residues of the target protein [453]. Frequently, SUMO and ubiquitin compete for the same lysine residues [169, 391, 454]. In the case of DEK, ubiquitinylation is crucial to maintain homeostasis of the protein. Loss of the ubiquitin ligases Fbxw7 and SPOP, which target DEK for proteasomal degradation, and the subsequent upregulation of DEK is associated with deregulated cell proliferation and host cell pathways [451, 452]. Likewise, in our studies we detected an increase in DEK protein levels during HAdV-wt infection (Figure 9, p. 77; Figure 10, p. 78; Figure 11, p. 79) indicating inhibition of DEK ubiquitinylation most likely due to its increased SUMOylation (Figure 24, p. 95).

Additionally, DEK is PAR-mediated covalently modified at its C-terminus [290, 298, 450]. PARylation is involved in DEK multimerization as well as localization. It interferes with the DNA-dependent multimerization activities of DEK, but lowers DEK's affinity to chromatin [298]. Upon cell stress, DEK is extensively phosphorylated and PARylated mediating its disassociation from DNA and release into the extracellular matrix, which is essential for apoptosis [290, 298]. PARylation is induced during HAdV infection, however E1B-55K and E4orf3 prevent nuclear fragmentation by redistributing PARylated proteins [280]. Both viral proteins interact with DEK during productive HAdV infection (Figure 22, p. 92; Figure 25, p. 96). We observed relocalization of DEK to E4orf3-containg PML tracks and viral RCs (Figure 27, p. 98; Figure 30, p. 103; Figure 32, p. 104; Figure 33, p. 105), where DEK binds to the viral DNA (Figure 36, p. 110). This suggests, regulation of DEK by E1B-55K and E4orf3 to mediate DEK localization to viral sites of transcription and replication. Hence, it needs to be further investigated, if DEK regulation is only dependent on relocalization, but also on dePARylation. However, PARylation of DEK is taking place in close proximity to its SCMs (Figure 23, p. 93). During adenoviral infection, PTM of DEK is influenced by E1B-55K (Figure 24, p. 95), suggesting dePARylation with subsequent SUMOylation.

DEK is also a target for acetylation by PCAF/p300, which together with phosphorylation modifies DEK functions and immunogenicity [295, 296]. Acetylated DEK has a low affinity to DNA, but is recruited to interchromatin granule clusters (IGCs). Those are sub-nuclear structures accumulating RNA processing factors. Therefore, acetylation could be considered to be the molecular switch necessary to convert DEK from a DNA-binding

protein to a component of splicing complexes [296]. In line with this, during HAdV infection DEK was no longer associated with p300 (Figure 37, p. 111), presumably with decreased acetylation of DEK, whereas it is recruited to viral RCs and binds the vDNA (Figure 36, p. 110).

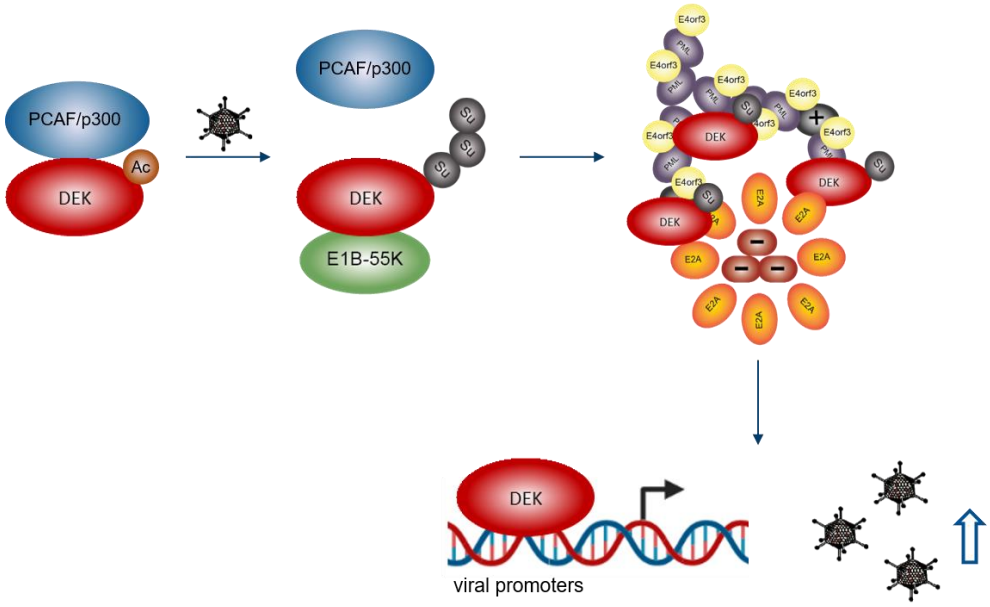

Figure 47: DEK PTM is changed during infection promoting its DNA-binding capacity and viral progeny production. DEK association with p300, which acetylates DEK [296], is abolished during infection. Deacetylated DEK has a higher affinity to bind DNA. Early viral protein facilitates DEK SUMOylation and DEK is binding to viral DNA to induce viral gene transcription and viral replication.

In sum, DEK is a highly posttranslational modified protein involved in many distinct pathways depending on its phosphorylation, acetylation, ubiquitinylation and PARylation status. In our studies, we observed extensive SUMOylation of DEK by adenoviral E1B-55K. Hence, we assume that PTMs of DEK with other molecules is highly modulated, whereas DEK's affinity for DNA is increased with simultaneously impeded multimerization (Figure 47, p. 129).

5.3. Dynamic Localization of DEK during Infection

Published data suggest that localization of DEK is dependent on its PTM status [285, 290, 294-296, 298, 450-452]. In most cases DEK has a nuclear distribution due to its localization to chromatin, PML-NBs or to RNA processing complexes [285, 290, 294-296, 298, 318, 450-452]. However, under stress extensive phosphorylation and PARylation of DEK mediates its translocation out of the cell nucleus, thus inhibiting the anti-apoptotic function of DEK [290]. During HAdV infection, DEK is still localizing to the host nucleus, however a part of the expressed proteins accumulates in aggresomes in the cytoplasm, as well as in

perinuclear bodies together with viral E1B-55K (Figure 28, p. 100). During the early stages of infection, E1A modulates the cell cycle, thereby inducing p53 expression and subsequent cell apoptosis [137, 455, 456], which is counteracted by E1B-55K [266]. Therefore, in response to viral infection and the induction of apoptosis, the host's viral defense mechanism could lead to increase of DEK PARylation to initiate cell death and to counteract HAdV infection.

Additionally, pVI could be the viral factor mediating DEK localization to the cytoplasm at early stages of infection. Schreiner and co-workers could elucidate the role of pVI in viral transcription initiation of the viral E1A promoter. It translocates the restrictive host factor Daxx to the cytoplasm [129]. DEK is a regulatory interaction partner of Daxx [309, 311], whereas DEK could shuttle in a complex together with Daxx and pVI to the host cell's cytoplasm were it is recruited to E1B-55K aggresomes ([380]; Figure 28, p. 100). E1B-55K localization is highly diverse and dynamic during the course of infection. Transformation status of the cell [215, 269, 378, 379, 457], PTMs, and protein-protein interactions [271, 273, 380, 458] are responsible for the varying sub-populations of E1B-55K. The shuttling of the viral E1B-55K is dependent on the export receptor CRM1 [224, 459, 460] and the viral proteins E4orf3 and E4orf6. However, recent publications also identified a mechanism of E1B-55K relocalization to the host cell nucleus without expression of another viral protein, thus suggesting the involvement of a cellular protein [381]. E1B-55K functions as E3 SUMO ligase enhancing the attachment of SUMO moieties to DEK during infection, what is known to mediate nuclear localization of proteins [390, 461, 462]. Therefore, we assume DEK as a cellular protein mediating the E1B-55K localization to the nucleus in the context of a non-viral background. SUMOylation of DEK could initiate the translocation back into the nucleus, shuttling the associated E1B-55K to the PML tracks and the periphery of viral RC, since DEK is not degraded by E1B-55K and stays with it associated even at the later stages of infection, where we detect DEK exclusively at the viral RCs (Figure 29, p. 101; Figure 32, p. 104; Table 39,p. 106). Hence, DEK could function as novel host factor mediating the subcellular localization of E1B-55K. However, it remains a subject of further investigations to elucidate if DEK mediates the localization of E1B-55K or vice versa.

Additionally, E4orf3 and E4orf6 could indirectly promote the effect of E1B-55K translocation by DEK, since E4orf3 interacts with DEK in PML tracks and in the cytoplasm at early stages of infection (Figure 30, p. 102; Figure 31, p. 103; Figure 26, p. 97; Figure 25, p. 96; Table 39, p. 106). These two genes of the early viral E4 region modulate the

localization of E1B-55K by reorganizing viral as well as host factors, thereby recruiting E1B-55K to viral RCs [363, 382, 384, 387, 458, 463].

Taken together, DEK is localizing to perinuclear bodies in the cytoplasm together with E1B-55K during infection. We suggest, that after SUMOylation of DEK, the chromatin-associated protein could mediate the translocation of E1B-55K to the nucleus in collaboration with E4orf3, whereas they are recruited to PML tracks (Figure 27, p. 98) and sites of viral DNA (Table 39, p. 106).

E2A, the DNA-binding protein, interacts with ssDNA and dsDNA during viral replication, thus considered to be a marker of viral RCs [444, 464-466]. We observed association of E2A and DEK, once the first RCs were established (Figure 32, p. 104; Figure 33, p. 105; Figure 34, p. 107). Presumably, a subpopulation of DEK, which is not translocated to the cytoplasm, is immediately binding to the DNA to initiate the viral transcription (Figure 16, p. 85; Figure 35, p. 108; Figure 36, p. 110; Figure 42, p. 117). Afterwards, DEK stays associated with the vDNA and the translocated subpopulation is recruited to the RCs to regulate viral replication and epigenetics (Table 39, p. 106).

5.4. DEK – a Novel Host Factor for Viral Epigenetic Regulation

DEK favors to bind euchromatin *in vivo*, where it is associated with acetylated histones at sites of active transcription [292, 309, 318]. Hollenbach and co-workers suggest a role of DEK-Daxx interaction in repression of gene expression. Therefore, Daxx binds to DEK, which is associated to DNA and the acetylated histones, and recruits the HDAC II via its Ser/Pro/Thr- (SPT-) domain. Hence, histone tails are deacetylated leading to formation of heterochromatin and consequently to transcriptional repression [309]. In line with this, we could confirm diminished Daxx binding to DEK during HAdV infection (Figure 38, p. 112) to ensure efficient viral gene expression (Figure 16, p. 85; Figure 17, p. 86; Figure 18, p. 87; Figure 19, p. 88). However, there have to be additional pathways how HAdVs utilize DEK for efficient replication aside from disruption of DEK-Daxx binding, since viral mRNA (Figure 42, p. 117) and progeny production (Figure 43, p. 118) was effectively impaired after depletion of DEK (Figure 48, p. 132).

DEK is a DNA-binding protein considered to be an architectural protein for chromatin structure by binding to enhancer and promoter elements [285, 287, 318]. It possesses folding properties, chaperone activity and induces supercoils into naked DNA by changing

the DNA topology [281, 292, 298, 311]. Therefore, gene transcription can be modulated either through direct binding of DEK itself or due to a more accessible DNA for transcription factors, such as AP-2α [281, 312, 315, 316]. Early viral protein E1A interacts with a co-repressor of the AP-2α promoter, thereby impedes its function and consequently mediates the active expression of the transcription factor AP-2α. Additionally, E1A interacts with AP-2α and mediates the repression of host genes and simultaneously activates viral gene transcription, since various host and viral promoter/enhancer contain a AP-2α element [467, 468]. Previous studies identified the transcription factor AP-2α to interact motif specific with DEK, which stimulates the transactivation activity of AP-2α. During adenoviral infection, DEK might mediate active viral gene transcription (Figure 35, p. 108) by activating transcription factor AP-2α, which is highly synthesized in E1A-expressing cells (Figure 16, p. 85; Figure 17, p. 86; Figure 18, p. 87, Figure 19, p. 88).

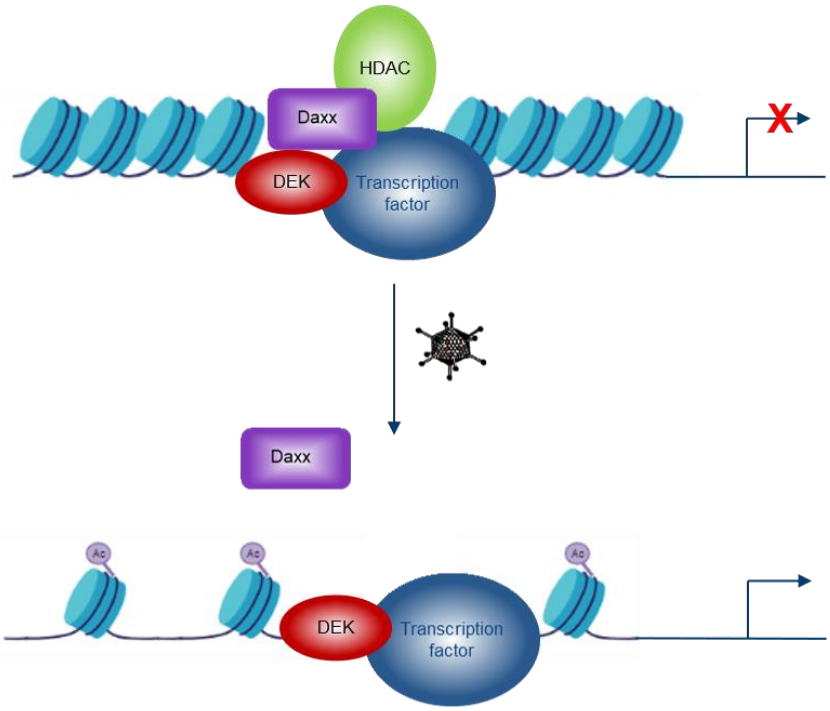

Figure 48: Graphic representation of epigenetic regulation by DEK during HAdV infection. Daxx associates with DEK at active sites of transcription and recruits HDAC II [309]. During HAdV infection, DEK interaction with Daxx is diminished blocking the deacetylation of histones.

The transactivating properties of E1A are additionally dependent on its interaction with the HAT p300 [241, 242]. The conserved region 3 (CR3) of E1A binds to p300 and recruits it to viral E2E and E4 promoters during infection, consequently initiating the active transcription of viral genes [133, 242, 469]. HAdV E1A mutants defective in p300 binding are associated with decreased E2 and E4 mRNAs, decreased binding of H3K18/27ac to viral E2E, E2L and E4 promoter, and impeded assembly of the pre-initiation complex consisting of the

TATA-binding protein (TBP) and Pol II at the E2Ep [241]. Here, we identified DEK as the crucial factor mediating the interaction of E1A with p300 during HAdV-wt infection (Figure 44, p. 119). E1A failed to transactivate viral gene expression after loss of DEK (Figure 42, p. 117). Moreover, E1A interacts in a complex together with p300 and Rb. Thus, E1A and Rb are acetylated by the HAT p300 and the complex is enriched at sites of p300-target genes. Binding of the E1A-p300-Rb complex to restrictive host genes modulates the acetylation of histones located at the host's chromatin with subsequent chromatin condensation and transcriptional repression [133, 234, 235, 253]. Taken together, E1A interaction with p300 is essential to repress host gene transcription, which interfere with viral replication, and to transactivate viral promoters. We could show the assembly of this multiprotein complex consisting of E1A and p300 is dependent on DEK expression (Figure 49, p. 137; Figure 44, p. 119). Subsequently, the crucial functions of E1A are limited after loss of DEK (Figure 42, p. 117), what we observed in strikingly diminished production of viral progeny (Figure 43, p. 118). However, it remains a subject of further investigations to unravel the exact mechanism underlying.

In addition, the C-terminal part of DEK seems to be homolog to the structure of the E2F/DP (dimerization partner) transcription factor family [289, 329]. Proteins of the E2F family are necessary for the transactivation of gene expression to induce the G_1/S transition [470]. To suppress E2F function, Rb is bound to the transcription factor. However, to start cell cycle progression, phosphorylated Rb disassociates from E2F and mediates the transactivation of the target genes [471-474]. E2F complexes with DP in a heterodimer to bind dsDNA via its winged helix motif, consisting of three α helices, located in the DNA-binding domain of DP. This domain possesses a RRVYD motif, which forms with every arginine residue a hydrogen bond to the guanine bases mediating its DNA-binding properties [475-477]. NMR structural analysis of DEK revealed structural similarities of its C-terminal part (aa 309-375) with the DNA-binding domain of DP. It also consists of three tightly packed α helices, where in addition α2 contains a similar aa sequence: KKVYE. DEK was found to be bound to E2F/DP consensus DNA sequence. However, association was shown to be weak, suggesting the necessity of another protein to increase efficient DEK binding to consensus sequences [289]. During HAdV infection, early viral E1A abolishes E2F association with Rb by preventing Rb SUMOylation, whereas transactivation of S phase genes is induced [436-438]. Previously published data identified E2F binding sites in the HAdV genome. E2F binding sites are located in the E1A sequence and promoter region of E2-early (E2E) of the adenoviral DNA [478]. Transactivation of those promoters is induced by the viral protein

pVI in the case of the E1Ap, and by E1A. E4orf6/7 and proteins of the E2F family mediate transcription from the E2Ep. However, the complete mechanism of viral genome decondensation and induction of viral gene transcription remains elusive [129, 237, 239, 479]. Schreiner and colleagues identified the HAdV Capsid protein pVI as a transactivator of E1A gene transcription. Therefore, pVI targets - via its PPxY-motif - the restrictive host factor Daxx. Hence, the repression of the E1Ap by Daxx is circumvented by relocalization of Daxx from PML-NBs and viral DNA to the host cell cytoplasm. The Capsid protein pVI itself was also found to be associated with E1 and E2 promoter regions. This mechanism was proved to be highly conserved and not only restricted to HAdV, since E1Ap can also be activated by tegument proteins of distinct DNA viruses (e.g. pp71 of human cytomegalovirus (HCMV) or L2 of HPV) and pVI was shown to induce CMV promoter activity. However, the mechanism how pVI and the different tegument are recruited to the sites of viral promoters and can transactivate gene expression has not been investigated yet [129]. Comparably, stimulation of the E2Ep is mediated by E2F during infection. Therefore, E1A-13S and E4orf6/7 interact with E2F promoting the transcription of E2 genes. However, literature suggests the requisiteness of an additional host factor for stable and functional transcription, since infection with mutant viruses deficient in binding E2 still induce transcription [237, 239, 478-480]. Our experiments identified DEK as a novel host interaction partner of the RC marker E2A (Figure 34, p. 107), capable of localizing to viral RCs (Figure 32, p. 104; Figure 33, p. 105), and activating gene transcription from viral promoters, such as E1Ap (Figure 35, p. 108). As a DNA-binding protein with a C-terminal structure homolog to the transcription factor E2F/DP, which is essential for the association to E2F-binding sites, DEK is a potential candidate to be the cellular host factor necessary to mediate the transactivation of viral E1Ap and E2Ep as suggested by various publications [239, 289, 479]. Indeed, this is supported by our data, since we detected DEK to be bound to the viral E1Ap and E2Ep (Figure 36, p. 110) and after DEK depletion transcription of genes regulated by E1Ap and E2E was impeded (Figure 42, p. 117).

Furthermore, DEK regulates the distribution of histone variant H3.3 [311]. During the first 6 h of HAdV infection, viral pVII disassociates from the viral DNA, while host H3.3 and acetylated histones are loaded on the viral genome to induce decondensation and active gene transcription [241, 428-435]. We observed the requirement of DEK expression for sufficient viral gene expression and progeny production (Figure 8, p. 76; Figure 9, p. 77; Figure 10, p. 78; Figure 11, p. 79; Figure 42, p. 117; Figure 43, p. 118). Furthermore, DEK is recruited to viral RCs where it binds viral DNA (Figure 32, p. 104; Figure 33, p. 105; Figure

34, p. 107; Figure 36, p. 110). Therefore, we assume a role of DEK in the regulation of viral chromatin architecture through changing PTMs of histones and loading histone variants on the viral DNA. Non-nucleosomal H3.3 are localized to PML-NBs in the presence of DEK, whereas chromatin loading of H3.3 is prevented. However, loss of DEK mediates redistribution of H3.3 on the host chromatin in a HIRA-dependent way [311]. We suggest, that on the one hand, induction of DEK expression during HAdV-wt leads to removal of H3.3 from the host chromatin resulting in host chromatin condensation and inactive gene transcription, but on the other hand, H3.3 is subsequently recruited to PML-NBs where they localize in close proximity to viral RCs and can be loaded on the vDNA for efficient gene expression. Additionally, DEK was shown to preferentially interact with active histone marks, so it presumably could recruit acetylated histones or HAT to the sites of viral transcription and replication [292].

In summary, we provide first evidence for the role of DEK in regulating epigenetic remodeling of HAdV DNA during infection to provide decondensation of the viral genome and the induction of active viral gene transcription. We assume modulation of the viral genome by DEK through direct binding, whereas it changes the topology of DNA, recruitment of distinct transcription factors and histones and mediating the binding of the viral proteins with transactivating properties to the vDNA. However, the exact mechanism underlying remains elusive. Nevertheless, we provide strong evidence, that E1A association with p300 is extensively dependent on DEK, which highlights the importance of DEK function during HAdV-wt infection.

5.5. DEK Might Represent a Potential Regulator of the HAdV Oncogenic Potential in Non-Permissive Cells

Previously published data link the pro-tumorigenic functions of DEK to inhibiting apoptosis, cell differentiation and senescence [341, 371, 481]. During cell death DEK is highly phosphorylated and PARylated, whereas the localization of DEK is changed to the extracellular matrix, thus the anti-apoptotic function of DEK is inhibited [290]. As we already discussed above (5.2, p. 127; 5.3, p. 129), HAdV seem to counteract consequences, which are connected to PARylation of DEK. First, DEK is relocalized to viral replication centers and the associated PML tracks during infection (Figure 26, p. 97; Figure 32, p. 104), which would argue that HAdV interfere with DEK PARylation to inhibit apoptosis. Second, modulation of PARylated proteins is mediated by adenoviral

interaction partners (Figure 22, p. 92; Figure 25, p. 96) E4orf3 and E1B-55K of DEK [280]. Additionally, DEK contains three SCMs in close proximity to its PARylation site (Figure 23, p. 93), hence extensive SUMOylation of DEK by E1B-55K (Figure 24, p. 95) could interfere with PARylation, which could illustrate a novel mechanism how HAdVs inhibit cell apoptosis and senescence to induce cellular transformation.

Ubiquitinylation is a further PTM of DEK, which is presumably highly affected by increased SUMOylation during infection (Figure 23, p. 93; Figure 24, p. 95). DEK ubiquitinylation is crucial for the homeostasis due to the subsequent proteasomal degradation of DEK [451, 452]. During our studies DEK was upregulated and highly expressed during HAdV infection (Figure 9, p. 77; Figure 10, p. 78; Figure 11, p. 79). Mutant versions of the tumor suppressors SPOP and Fbxw7, defective in ubiquitinylating DEK, are connected to accumulation of DEK and thus to increased cell division in human colorectal tumor tissues and carcinogenesis [451, 452]. Fbxw7 is a component of the SCF (SKP1-CUL1-F-box protein) E3 ubiquitin ligase, which recognizes the target proteins by recognizing phosphorylation sites. Moreover, adenoviral E1A binds directly to the RING finger protein and CUL1 of the SCF/Fbxw7 ubiquitin ligase complex, thus inhibiting the ubiquitinylation of SCF/Fbxw7 target proteins. Interference with the ubiquitinylation of the SCF/Fbxw7 target substrates, including DEK, mediates uncontrolled cell growth and proliferation [256], as described for several cancer types [451, 452]. Thus, inhibition of SCF/Fbxw7 by E1A and subsequent upregulation of DEK protein levels may represent a novel pathway for HAdV-mediated carcinogenesis. Overexpression of DEK is linked to various cancer types, such as breast cancer [409], ovarian cancer [482, 483], retinoblastomas [484], translational cell carcinoma (TCC) bladder tumors [485], malignant melanomas [372, 486, 487] and lung cancerous tissues [488]. In many cases DEK functions as a biomarker [485] for distinct cancer types and is associated with poor prognosis. Here, DEK promotes tumor cell growth [409] by repressing apoptosis, DDR [483], cell proliferation, invasion [488] and tumor progression [486].

Moreover, DEK serves as oncogenic mediator during EBV and HPV infection. Overexpression of DEK in latent EBV-infected nasopharyngal carcinoma (NPC) and HPV18-positive cancer cells as well as cervical cancer is associated with repression of Rb family proteins to induce cellular proliferation and viral replication, as we also observe during HAdV infection [234, 237, 326, 331, 481, 489-491]. Oncogenic potential of HPV is linked to inhibition of apoptosis due to destabilization and inactivation of p53 by DEK,

whose expression is extensively induced by high-risk HPV E7, but not by low-risk HPV E7 [371, 481].

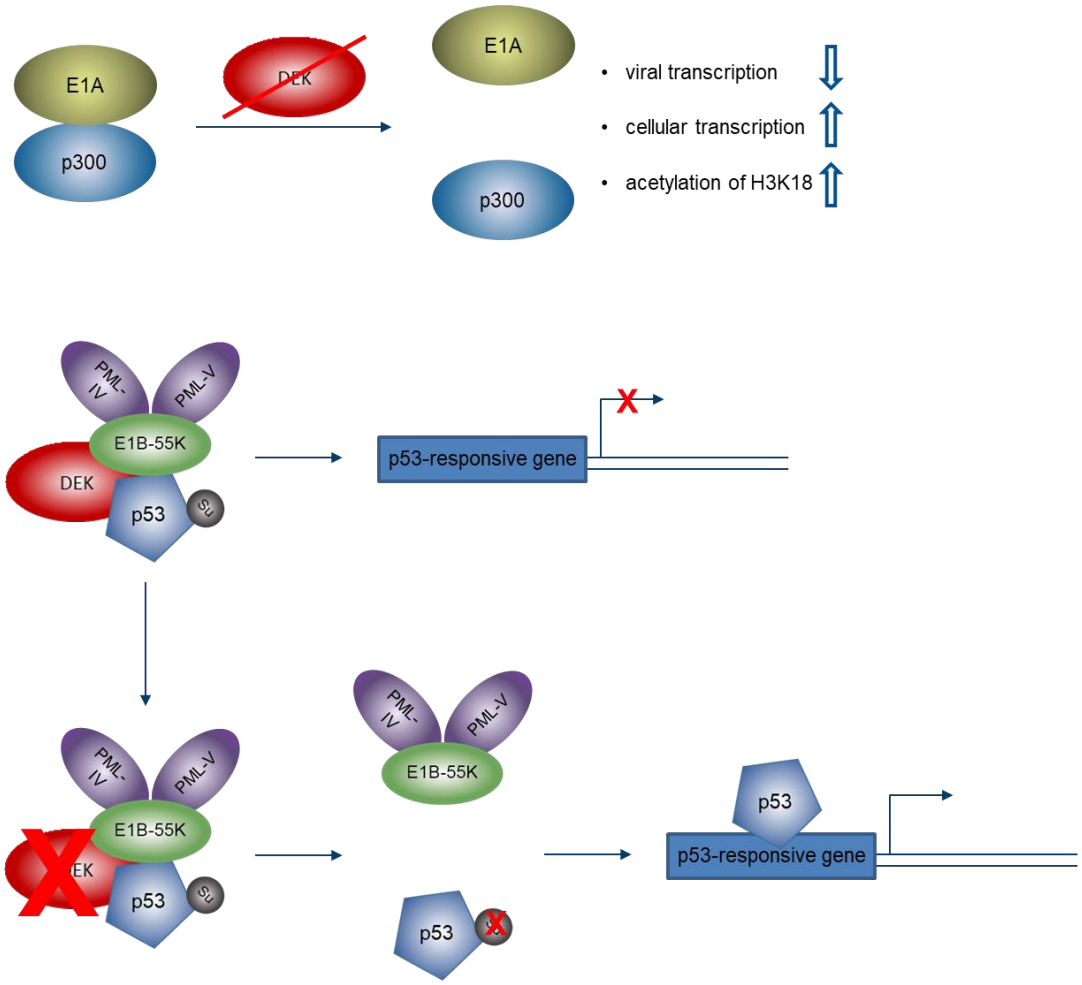

Figure 49: Schematic representation of repressed DEK expression during HAdV infection. Depletion of DEK reduces association of E1A with p300 and of E1B-55K with p53, which are involved in virus-induced cell transformation.

Based on published data, it is assumed, that transformation of cells by HAdVs occurs via a hit-and-run mechanism. It is suggested, that HAdVs do not integrate their genome into the host cell, but induce tumor growth by expression of the viral E1 and E4 oncogenes, which are not detectable at later stages of tumor development [150]. Virus-mediated oncogenesis is initiated by E1A due to uncontrolled DNA synthesis and cell proliferation [492] by inhibition of Rb and modulation of p300 [234-237, 258, 259, 370, 489]. In this study, we identified DEK as a crucial factor mediating the association of E1A with p300 (Figure 44, p. 119). Inhibition of E1A-p300 complex formation represses E1A functions in viral transcriptional activation and E1A-induced transforming potential [259, 261]. E1A modulates p300 functions, thereby counteracting the G_0/G_1 transition, and redirects p300 from active cellular sites of transcription to viral promoters [133, 257, 469, 493].

Additionally, acetylation of H3K18ac is extensively decreased due to E1A binding to p300, which is linked to prostate carcinomas with poor prognosis [263]. Transformation of E1A-immortalized cells is promoted by E1B-55K and the genes of the E4 region [137, 266, 494]. While E4orf3 and E4orf6 inhibit the host's DDR for efficient transformation [152, 249, 250, 267, 278, 495], E1B-55K represses Daxx and p53 functions [142, 144, 213, 224, 244, 245, 496, 497], mainly by assembling a viral E3 ubiquitin ligase to target those substrates for proteasomal degradation [145, 245]. Induction of apoptosis [142, 498, 499] and cell cycle arrest by p53 is repressed due to direct binding, subsequent SUMOylation of p53 along with nuclear targeting to PML-NBs and perinuclear bodies by E1B-55K together with PML-IV and PML-V [139, 141, 143, 184, 213, 216, 246, 500-503]. Depletion of DEK diminishes E1B-55K binding to p53 (Figure 45, p. 121), which is indispensable for E1B-55K-mediated repression of p53 [504]. Additionally, we observed decreased PTM of p53 in HAdV-infected cells after loss of DEK expression, presumably due to defective E1B-55K association (Figure 45, p. 121). Consequently, HAdVs were incapable in transcriptional repression of p53-responsive genes during infection (Figure 46, p. 122).

In sum, our studies revealed a possible role of DEK in mediating the oncogenic potential of HAdVs. This seems contradictory to the promoting effect of DEK during lytic infection with HAdVs (5.1, p. 125), since cell transformation is linked to an incomplete infection cycle (see chapter 1.3, p. 20). However, as shown in Table 1 (p. 6), until today over 80 types of HAdV are described, which infect all kinds of different tissues causing a variety of diseases, and differ in their oncogenic potential. Tropism and the infection course of the distinct HAdV types are connected to differences in their structural proteins, mediating the attachment of the virus to the host cell as well as to different modulations of host factors by viral regulatory proteins. Subsequently, degradation and interaction with host factors, inhibition of DDR, and PTM of host proteins differ among the adenoviral types [218, 250-252, 273, 373, 505-507]. Gene transcription, senescence, apoptosis, PTM to name a few, are known to be differentially regulated in distinct cell types mediating a diverse regulation of key processes and pathways in the host cells [508-511]. Moreover, DEK PTM by acetylation was already shown to be differentially regulated in distinct tissues [295, 296]. Hence, DEK expression and its PTM status in the different tissues could lead to a different outcome of HAdV infection. Additionally, different regulation of DEK expression and PTM by the distinct HAdV types could determine the switch from lytic infection to cell transformation. Therefore, it would be of high importance to further investigate the role and modulation of DEK after HAdV infection with different types in distinct tissues to elucidate

the impact of DEK on viral gene transcription and virus-mediated carcinogenesis (Figure 49, p. 137).

5.6. Clinical Relevance and Future Therapeutic Options

In this study, we provided novel insights on virus-host interactions during early stages of HAdV infection regarding epigenetic regulation of vDNA, viral gene transcription and virus-mediated oncogenesis. We identified DEK as a novel host factor regulating carcinogenesis by viral oncoproteins and promoting HAdV infection by inducing viral gene expression. HAdVs induce severe infections in immunocompromised patients and hospitalized children with a high mortality rate [19, 38, 46, 51]. Furthermore, newly evolving pneumotropic HAdV types linked to intense inflammation of the infected tissue cause severe diseases with lethal outcome even in immunocompetent patients [50, 413]. However, therapeutical treatment of patients occurs merely symptomatically with antiviral drugs, such as ribavirin and cidofovir, due to the lack in specific treatment or vaccination for the broad population against HAdV [73-75, 78, 79, 414, 415]. Thus, development of novel antiviral therapeutic strategies against HAdV is consequential for efficient treatment of adenoviral infections.

Previous studies suggest therapeutical treatment by inhibition of the target molecules using so-called aptamers [512-516]. Aptamers are short DNA or RNA oligonucleotides specifically binding and inactivating target proteins and their application was already approved for other target molecules, such as the pro-angiogenic molecule vascular endothelial growth factor in macular degeneration [295, 517]. Recently, aptamers specifically inactivating DEK were generated as therapeutic treatment in chronic inflammatory diseases. Those aptamers were shown to not change DEK expression, however articular injection of the aptamers specifically modulated inflammatory processes in juvenile idiopathic arthritis regulated by DEK [295, 514, 515, 517]. Additionally, DEK was already suggested as a target protein for cancer therapy [315, 335, 483]. Recent publications suggest a chemical or RNAi-based therapeutic approach to repress DEK anti-apoptotic and inflammatory functions, especially since there was hardly any effect on normal and differentiated cells after DEK repression [340, 371]. Thus, DEK could serve as a novel target substrate to repress adenoviral gene transcription, replication, and progeny production. This might be highly relevant especially for immunosuppressed patients that undergo for instance HSCT settings and suffer from life-threatening HAdV infections.

References

1. Rowe, W.P., et al., *Isolation of a Cytopathogenic Agent from Human Adenoids Undergoing Spontaneous Degeneration in Tissue Culture.* Proceedings of the Society for Experimental Biology and Medicine, 1953. **84**(3): p. 570-573.
2. Hilleman, M.R. and J.H. Werner, *Recovery of new agent from patients with acute respiratory illness.* Proc Soc Exp Biol Med, 1954. **85**(1): p. 183-8.
3. Enders, J.F., et al., *Adenoviruses: group name proposed for new respiratory-tract viruses.* Science, 1956. **124**(3212): p. 119-20.
4. Benkö, M. and B. Harrach, *A proposal for a new (third) genus within the family Adenoviridae.* Arch Virol, 1998. **143**(4): p. 829-37.
5. Davison, A.J., M. Benko, and B. Harrach, *Genetic content and evolution of adenoviruses.* J Gen Virol, 2003. **84**(Pt 11): p. 2895-2908.
6. Harrach, B., Z.L. Tarján, and M. Benkő, *Adenoviruses across the animal kingdom: a walk in the zoo.* FEBS Letters, 2019. **593**(24): p. 3660-3673.
7. Benkó, M., et al., *First molecular evidence for the existence of distinct fish and snake adenoviruses.* Journal of virology, 2002. **76**(19): p. 10056-10059.
8. Doszpoly, A., et al., *Partial characterization of a new adenovirus lineage discovered in testudinoid turtles.* Infect Genet Evol, 2013. **17**: p. 106-12.
9. Hage, E., et al., *Human mastadenovirus type 70: a novel, multiple recombinant species D mastadenovirus isolated from diarrhoeal faeces of a haematopoietic stem cell transplantation recipient.* J Gen Virol, 2015. **96**(9): p. 2734-2742.
10. *Family - Adenoviridae*, in *Virus Taxonomy*, A.M.Q. King, et al., Editors. 2012, Elsevier: San Diego. p. 125-141.
11. Davison, A.J., M. Benko, and B. Harrach, *Genetic content and evolution of adenoviruses.* J Gen Virol, 2003. **84**(Pt 11): p. 2895-908.
12. Bailey, A. and V. Mautner, *Phylogenetic relationships among adenovirus serotypes.* Virology, 1994. **205**(2): p. 438-52.
13. Leen, A.M. and C.M. Rooney, *Adenovirus as an emerging pathogen in immunocompromised patients.* Br J Haematol, 2005. **128**(2): p. 135-44.
14. Chen, S. and X. Tian, *Vaccine development for human mastadenovirus.* J Thorac Dis, 2018. **10**(Suppl 19): p. S2280-s2294.
15. Shenk, T., *Adenoviridae: the viruses and their replication.* Virology. 2001. 2265-2300.
16. Dhingra, A., et al., *Molecular Evolution of Human Adenovirus (HAdV) Species C.* Scientific Reports, 2019. **9**(1): p. 1039.
17. Wadell, G., *Adenoviridae: The Adenoviruses*, in *Laboratory Diagnosis of Infectious Diseases Principles and Practice: VOLUME II Viral, Rickettsial, and Chlamydial Diseases*, E.H. Lennette, et al., Editors. 1988, Springer New York: New York, NY. p. 284-300.
18. Hashimoto, S., et al., *Recombinant type Human mastadenovirus D85 associated with epidemic keratoconjunctivitis since 2015 in Japan.* J Med Virol, 2018. **90**(5): p. 881-889.
19. Lion, T., *Adenovirus infections in immunocompetent and immunocompromised patients.* Clin Microbiol Rev, 2014. **27**(3): p. 441-62.
20. Robinson, C.M., et al., *Molecular evolution of human species D adenoviruses.* Infection, genetics and evolution : journal of molecular epidemiology and evolutionary genetics in infectious diseases, 2011. **11**(6): p. 1208-1217.

21. Walsh, M.P., et al., *Computational analysis identifies human adenovirus type 55 as a re-emergent acute respiratory disease pathogen.* J Clin Microbiol, 2010. **48**(3): p. 991-3.
22. Robinson, C.M., et al., *Molecular evolution of human adenoviruses.* Sci Rep, 2013. **3**: p. 1812.
23. Lukashev, A.N., et al., *Evidence of frequent recombination among human adenoviruses.* J Gen Virol, 2008. **89**(Pt 2): p. 380-388.
24. Liu, H., L. Wu, and Z.H. Zhou, *Model of the trimeric fiber and its interactions with the pentameric penton base of human adenovirus by cryo-electron microscopy.* J Mol Biol, 2011. **406**(5): p. 764-74.
25. Jones, M.S., 2nd, et al., *New adenovirus species found in a patient presenting with gastroenteritis.* J Virol, 2007. **81**(11): p. 5978-84.
26. Ginsberg, H.S., et al., *Relation of the new respiratory agents to acute respiratory diseases.* Am J Public Health Nations Health, 1955. **45**(7): p. 915-22.
27. Harrach, B. and M. Benko, *Phylogenetic analysis of adenovirus sequences.* Methods Mol Med, 2007. **131**: p. 299-334.
28. Gray, G.C., et al., *Adult adenovirus infections: loss of orphaned vaccines precipitates military respiratory disease epidemics. For the Adenovirus Surveillance Group.* Clin Infect Dis, 2000. **31**(3): p. 663-70.
29. Garnett, C.T., et al., *Prevalence and quantitation of species C adenovirus DNA in human mucosal lymphocytes.* J Virol, 2002. **76**(21): p. 10608-16.
30. Garnett, C.T., et al., *Latent species C adenoviruses in human tonsil tissues.* J Virol, 2009. **83**(6): p. 2417-28.
31. Lin, K.-H., et al., *A two decade survey of respiratory adenovirus in Taiwan: The reemergence of adenovirus types 7 and 4.* Journal of Medical Virology, 2004. **73**(2): p. 274-279.
32. Jawetz, E., et al., *A laboratory infection with adenovirus type 8; laboratory and epidemiologic observations.* Am J Hyg, 1959. **69**(1): p. 13-20.
33. Dingle, J.H. and A.D. Langmuir, *Epidemiology of acute, respiratory disease in military recruits.* Am Rev Respir Dis, 1968. **97**(6): p. Suppl:1-65.
34. Barnadas, C., et al., *Molecular epidemiology of human adenovirus infections in Denmark, 2011–2016.* Journal of Clinical Virology, 2018. **104**: p. 16-22.
35. Lewis, P., et al., *A Community-Based Outbreak of Severe Respiratory Illness Caused by Human Adenovirus Serotype 14.* The Journal of infectious diseases, 2009. **199**: p. 1427-34.
36. Ampuero, J.S., et al., *Adenovirus Respiratory Tract Infections in Peru.* PLOS ONE, 2012. **7**(10): p. e46898.
37. Siminovich, M. and P. Murtagh, *Acute lower respiratory tract infections by adenovirus in children: histopathologic findings in 18 fatal cases.* Pediatr Dev Pathol, 2011. **14**(3): p. 214-7.
38. Savón, C., et al., *A myocarditis outbreak with fatal cases associated with adenovirus subgenera C among children from Havana City in 2005.* J Clin Virol, 2008. **43**(2): p. 152-7.
39. Treacy, A., et al., *First Report of Sudden Death Due to Myocarditis Caused by Adenovirus Serotype 3.* Journal of Clinical Microbiology, 2010. **48**(2): p. 642-645.
40. Shauer, A., et al., *Acute viral myocarditis: current concepts in diagnosis and treatment.* Isr Med Assoc J, 2013. **15**(3): p. 180-5.
41. de Ory, F., et al., *Viral infections of the central nervous system in Spain: a prospective study.* J Med Virol, 2013. **85**(3): p. 554-62.
42. Ishiko, H., et al., *Novel human adenovirus causing nosocomial epidemic keratoconjunctivitis.* J Clin Microbiol, 2008. **46**(6): p. 2002-8.

43. Chhabra, P., et al., *Etiology of viral gastroenteritis in children <5 years of age in the United States, 2008-2009.* J Infect Dis, 2013. **208**(5): p. 790-800.
44. Celik, C., et al., *Rotavirus and adenovirus gastroenteritis: time series analysis.* Pediatrics International, 2015. **57**(4): p. 590-596.
45. Uhnoo, I., L. Svensson, and G. Wadell, *Enteric adenoviruses.* Baillieres Clin Gastroenterol, 1990. **4**(3): p. 627-42.
46. Yolken, R.H., et al., *Gastroenteritis associated with enteric type adenovirus in hospitalized infants.* J Pediatr, 1982. **101**(1): p. 21-6.
47. Kumthip, K., et al., *Enteric and non-enteric adenoviruses associated with acute gastroenteritis in pediatric patients in Thailand, 2011 to 2017.* PloS one, 2019. **14**(8): p. e0220263-e0220263.
48. Esposito, S., et al., *Adenovirus 36 infection and obesity.* J Clin Virol, 2012. **55**(2): p. 95-100.
49. Shang, Q., et al., *Serological data analyses show that adenovirus 36 infection is associated with obesity: a meta-analysis involving 5739 subjects.* Obesity (Silver Spring), 2014. **22**(3): p. 895-900.
50. Carr, M.J., et al., *Deaths associated with human adenovirus-14p1 infections, Europe, 2009-2010.* Emerging infectious diseases, 2011. **17**(8): p. 1402-1408.
51. Buckwalter, S.P., et al., *Real-time qualitative PCR for 57 human adenovirus types from multiple specimen sources.* J Clin Microbiol, 2012. **50**(3): p. 766-71.
52. Carrigan, P.D.R., *Adenovirus Infections in Immunocompromised Patients.* The American Journal of Medicine, 1997. **102**(3, Supplement 1): p. 71-74.
53. Hierholzer, J.C., *Adenoviruses in the immunocompromised host.* Clin Microbiol Rev, 1992. **5**(3): p. 262-74.
54. Berciaud, S., et al., *Adenovirus infections in Bordeaux University Hospital 2008-2010: clinical and virological features.* J Clin Virol, 2012. **54**(4): p. 302-7.
55. Detrait, M., et al., *Fulminant isolated adenovirus hepatitis 5 months after haplo-identical HSCT for AML.* Clinical case reports, 2015. **3**(10): p. 802-805.
56. Echavarría, M., *Adenoviruses in immunocompromised hosts.* Clin Microbiol Rev, 2008. **21**(4): p. 704-15.
57. Lion, T., et al., *Molecular monitoring of adenovirus in peripheral blood after allogeneic bone marrow transplantation permits early diagnosis of disseminated disease.* Blood, 2003. **102**(3): p. 1114-20.
58. Lion, T., et al., *Monitoring of adenovirus load in stool by real-time PCR permits early detection of impending invasive infection in patients after allogeneic stem cell transplantation.* Leukemia, 2010. **24**(4): p. 706-714.
59. Ison, M.G., *Adenovirus infections in transplant recipients.* Clin Infect Dis, 2006. **43**(3): p. 331-9.
60. Trentin, J.J., Y. Yabe, and G. Taylor, *The quest for human cancer viruses: a new approach to an old problem reveals cancer induction in hamster hy human adenoviruses.* Science, 1962. **137**: p. 835-849.
61. Kosulin, K., et al., *Investigation of adenovirus occurrence in pediatric tumor entities.* J Virol, 2007. **81**(14): p. 7629-35.
62. Kosulin, K., et al., *Presence of adenovirus species C in infiltrating lymphocytes of human sarcoma.* PloS one, 2013. **8**(5): p. e63646-e63646.
63. Crystal, R.G., *Adenovirus: the first effective in vivo gene delivery vector.* Human gene therapy, 2014. **25**(1): p. 3-11.
64. Wu, T.C., et al., *Virus-associated RNAs (VA-I and VA-II). An efficient target for the detection of adenovirus infections by in situ hybridization.* Am J Pathol, 1992. **140**(4): p. 991-8.
65. Terletskaia-Ladwig, E., et al., *Laboratory approaches to the diagnosis of adenovirus infection depending on clinical manifestations.* Infection, 2007. **35**(6): p. 438-43.

66. Neofytos, D., et al., *Treatment of adenovirus disease in stem cell transplant recipients with cidofovir.* Biol Blood Marrow Transplant, 2007. **13**(1): p. 74-81.
67. Levent, F., et al., *Performance of a new immunochromatographic assay for detection of adenoviruses in children.* J Clin Virol, 2009. **44**(2): p. 173-5.
68. Lee, W.M., et al., *High-throughput, sensitive, and accurate multiplex PCR-microsphere flow cytometry system for large-scale comprehensive detection of respiratory viruses.* J Clin Microbiol, 2007. **45**(8): p. 2626-34.
69. Lankester, A.C., et al., *Effect of ribavirin on the plasma viral DNA load in patients with disseminating adenovirus infection.* Clin Infect Dis, 2004. **38**(11): p. 1521-5.
70. Lankester, A.C., et al., *Quantification of adenovirus DNA in plasma for management of infection in stem cell graft recipients.* Clin Infect Dis, 2002. **34**(6): p. 864-7.
71. Herrmann, J.E., D.M. Perron-Henry, and N.R. Blacklow, *Antigen detection with monoclonal antibodies for the diagnosis of adenovirus gastroenteritis.* J Infect Dis, 1987. **155**(6): p. 1167-71.
72. Becroft, D.M., *Histopathology of fatal adenovirus infection of the respiratory tract in young children.* J Clin Pathol, 1967. **20**(4): p. 561-9.
73. Gavin, P. and B. Katz, *Intravenous Ribavirin Treatment for Severe Adenovirus Disease in Immunocompromised Children.* Pediatrics, 2002. **110**: p. e9.
74. Fowler, C.J., et al., *Life-threatening adenovirus infections in the setting of the immunocompromised allogeneic stem cell transplant patients.* Advances in hematology, 2010. **2010**: p. 601548-601548.
75. Ljungman, P., et al., *Cidofovir for adenovirus infections after allogeneic hematopoietic stem cell transplantation: a survey by the Infectious Diseases Working Party of the European Group for Blood and Marrow Transplantation.* Bone Marrow Transplant, 2003. **31**(6): p. 481-6.
76. Ljungman, P., *Treatment of adenovirus infections in the immunocompromised host.* Eur J Clin Microbiol Infect Dis, 2004. **23**(8): p. 583-8.
77. Alcamo, A.M., et al., *Successful Use of Cidofovir in an Immunocompetent Child With Severe Adenoviral Sepsis.* Pediatrics, 2020. **145**(1).
78. Safrin, S., J. Cherrington, and H.S. Jaffe, *Clinical uses of cidofovir.* Reviews in Medical Virology, 1997. **7**(3): p. 145-156.
79. Cundy, K.C., *Clinical Pharmacokinetics of the Antiviral Nucleotide Analogues Cidofovir and Adefovir.* Clinical Pharmacokinetics, 1999. **36**(2): p. 127-143.
80. Berk, A.J., *Adenoviridae: The Viruses and Their Replication* in *Fields Virology*, D.M.H. Knipe, P. M., Editor. 2007, Lippincott Williams & Wilkins. p. 2356-2394.
81. van Oostrum, J. and R.M. Burnett, *Molecular composition of the adenovirus type 2 virion.* J Virol, 1985. **56**(2): p. 439-48.
82. Burnett, R.M., M.G. Grutter, and J.L. White, *The structure of the adenovirus capsid. I. An envelope model of hexon at 6 A resolution.* J Mol Biol, 1985. **185**(1): p. 105-23.
83. Russell, W.C., *Adenoviruses: update on structure and function.* J Gen Virol, 2009. **90**(Pt 1): p. 1-20.
84. San Martín, C., *Latest insights on adenovirus structure and assembly.* Viruses, 2012. **4**(5): p. 847-77.
85. Bergelson, J.M., et al., *Isolation of a common receptor for Coxsackie B viruses and adenoviruses 2 and 5.* Science, 1997. **275**(5304): p. 1320-3.
86. Wu, Q., et al., *Adenovirus-mediated type I interferon expression delays and reduces disease signs in cattle challenged with foot-and-mouth disease virus.* J Interferon Cytokine Res, 2003. **23**(7): p. 359-68.
87. Wang, H., et al., *Desmoglein 2 is a receptor for adenovirus serotypes 3, 7, 11 and 14.* Nat Med, 2011. **17**(1): p. 96-104.

88. Wang, A.Y., et al., *Adenovirus transduction is required for the correction of diabetes using Pdx-1 or Neurogenin-3 in the liver.* Mol Ther, 2007. **15**(2): p. 255-63.
89. Gaggar, A., D.M. Shayakhmetov, and A. Lieber, *CD46 is a cellular receptor for group B adenoviruses.* Nat Med, 2003. **9**(11): p. 1408-12.
90. Wolfrum, N. and U.F. Greber, *Adenovirus signalling in entry.* Cellular Microbiology, 2013. **15**(1): p. 53-62.
91. Huang, S., et al., *Adenovirus interaction with distinct integrins mediates separate events in cell entry and gene delivery to hematopoietic cells.* J Virol, 1996. **70**(7): p. 4502-8.
92. Chiu, C.Y., et al., *Structure of adenovirus complexed with its internalization receptor, alphavbeta5 integrin.* J Virol, 1999. **73**(8): p. 6759-68.
93. Albinsson, B. and A.H. Kidd, *Adenovirus type 41 lacks an RGD alpha(v)-integrin binding motif on the penton base and undergoes delayed uptake in A549 cells.* Virus Res, 1999. **64**(2): p. 125-36.
94. Mathias, P., et al., *Multiple adenovirus serotypes use alpha v integrins for infection.* J Virol, 1994. **68**(10): p. 6811-4.
95. Stewart, P.L., et al., *Cryo-EM visualization of an exposed RGD epitope on adenovirus that escapes antibody neutralization.* The EMBO Journal, 1997. **16**(6): p. 1189-1198.
96. Wickham, T.J., et al., *Integrins αv6̂3 and αv6̂5 promote adenovirus internalization but not virus attachment.* Cell, 1993. **73**(2): p. 309-319.
97. Wickham, T.J., et al., *Integrin alpha v beta 5 selectively promotes adenovirus mediated cell membrane permeabilization.* J Cell Biol, 1994. **127**(1): p. 257-64.
98. Nemerow, G.R., et al., *Insights into adenovirus host cell interactions from structural studies.* Virology, 2009. **384**(2): p. 380-388.
99. Reddy, V.S. and G.R. Nemerow, *Structures and organization of adenovirus cement proteins provide insights into the role of capsid maturation in virus entry and infection.* Proceedings of the National Academy of Sciences, 2014. **111**(32): p. 11715-11720.
100. Tang, Y., et al., *Derivation of a Triple Mosaic Adenovirus for Cancer Gene Therapy.* PLOS ONE, 2010. **4**(12): p. e8526.
101. Goosney, D.L. and G.R. Nemerow, *Adenovirus Infection: Taking the Back Roads to Viral Entry.* Current Biology, 2003. **13**(3): p. R99-R100.
102. Chatterjee, P.K., M.E. Vayda, and S.J. Flint, *Interactions among the three adenovirus core proteins.* J Virol, 1985. **55**(2): p. 379-86.
103. Liu, H., et al., *Atomic structure of human adenovirus by cryo-EM reveals interactions among protein networks.* Science, 2010. **329**(5995): p. 1038-43.
104. Christensen, J.B., et al., *Presence of the adenovirus IVa2 protein at a single vertex of the mature virion.* J Virol, 2008. **82**(18): p. 9086-93.
105. Weber, J.M., *Synthesis and Assay of Recombinant Adenovirus Protease*, in *Adenovirus Methods and Protocols: Volume 2: Ad Proteins, RNA Lifecycle, Host Interactions, and Phylogenetics*, W.S.M. Wold and A.E. Tollefson, Editors. 2007, Humana Press: Totowa, NJ. p. 251-255.
106. Ahi, Y.S. and S.K. Mittal, *Components of Adenovirus Genome Packaging.* Frontiers in microbiology, 2016. **7**: p. 1503-1503.
107. Benevento, M., et al., *Adenovirus composition, proteolysis, and disassembly studied by in-depth qualitative and quantitative proteomics.* J Biol Chem, 2014. **289**(16): p. 11421-30.
108. Gyurcsik, B., et al., *Binding Modes of the Precursor of Adenovirus Major Core Protein VII to DNA and Template Activating Factor I: Implication for the Mechanism of Remodeling of the Adenovirus Chromatin.* Biochemistry, 2006. **45**(1): p. 303-313.

109. Russell, W.C. and B. Precious, *Nucleic acid-binding properties of adenovirus structural polypeptides.* J Gen Virol, 1982. **63 (Pt 1)**: p. 69-79.
110. Sung, M.T., et al., *Gene and protein sequences of adenovirus protein VII, a hybrid basic chromosomal protein.* Proc Natl Acad Sci U S A, 1983. **80**(10): p. 2902-6.
111. Lee, T.W., G.E. Blair, and D.A. Matthews, *Adenovirus core protein VII contains distinct sequences that mediate targeting to the nucleus and nucleolus, and colocalization with human chromosomes.* J Gen Virol, 2003. **84**(Pt 12): p. 3423-8.
112. Vayda, M.E., A.E. Rogers, and S.J. Flint, *The structure of nucleoprotein cores released from adenovirions.* Nucleic Acids Research, 1983. **11**(2): p. 441-460.
113. Burg, J.L., J. Schweitzer, and E. Daniell, *Introduction of superhelical turns into DNA by adenoviral core proteins and chromatin assembly factors.* J Virol, 1983. **46**(3): p. 749-55.
114. Wodrich, H., et al., *Adenovirus Core Protein pVII Is Translocated into the Nucleus by Multiple Import Receptor Pathways.* Journal of Virology, 2006. **80**(19): p. 9608-9618.
115. Karen, K.A. and P. Hearing, *Adenovirus Core Protein VII Protects the Viral Genome from a DNA Damage Response at Early Times after Infection.* Journal of Virology, 2011. **85**(9): p. 4135-4142.
116. Chen, J., N. Morral, and D.A. Engel, *Transcription releases protein VII from adenovirus chromatin.* Virology, 2007. **369**(2): p. 411-422.
117. Turinsky, A.L., et al., *DAnCER: Disease-Annotated Chromatin Epigenetics Resource.* Nucleic Acids Research, 2010. **39**(suppl_1): p. D889-D894.
118. Hoeben, R.C. and T.G. Uil, *Adenovirus DNA replication.* Cold Spring Harbor perspectives in biology, 2013. **5**(3): p. a013003-a013003.
119. Smart, J.E. and B.W. Stillman, *Adenovirus terminal protein precursor. Partial amino acid sequence and the site of covalent linkage to virus DNA.* J Biol Chem, 1982. **257**(22): p. 13499-506.
120. Gräble, M. and P. Hearing, *cis and trans requirements for the selective packaging of adenovirus type 5 DNA.* Journal of virology, 1992. **66**(2): p. 723-731.
121. Weinmann, R., H.J. Raskas, and R.G. Roeder, *Role of DNA-dependent RNA polymerases II and III in transcription of the adenovirus genome late in productive infection.* Proc Natl Acad Sci U S A, 1974. **71**(9): p. 3426-39.
122. Ying, B., A.E. Tollefson, and W.S. Wold, *Identification of a previously unrecognized promoter that drives expression of the UXP transcription unit in the human adenovirus type 5 genome.* J Virol, 2010. **84**(21): p. 11470-8.
123. Tollefson, A., et al., *Identification of a New Human Adenovirus Protein Encoded by a Novel Late l-Strand Transcription Unit.* Journal of virology, 2008. **81**: p. 12918-26.
124. Zhao, H., M. Chen, and U. Pettersson, *A new look at adenovirus splicing.* Virology, 2014. **456-457**: p. 329-41.
125. Greber, U.F., et al., *Stepwise dismantling of adenovirus 2 during entry into cells.* Cell, 1993. **75**(3): p. 477-86.
126. Varga, M.J., C. Weibull, and E. Everitt, *Infectious entry pathway of adenovirus type 2.* J Virol, 1991. **65**(11): p. 6061-70.
127. Smith, J.G., et al., *Adenovirus.* Curr Top Microbiol Immunol, 2010. **343**: p. 195-224.
128. Wiethoff, C.M., et al., *Adenovirus protein VI mediates membrane disruption following capsid disassembly.* J Virol, 2005. **79**(4): p. 1992-2000.
129. Schreiner, S., et al., *Transcriptional activation of the adenoviral genome is mediated by capsid protein VI.* PLoS Pathog, 2012. **8**(2): p. e1002549.
130. Nevins, J.R., *Adenovirus E1A-dependent trans-activation of transcription.* Semin Cancer Biol, 1990. **1**(1): p. 59-68.
131. Berk, A.J., *Recent lessons in gene expression, cell cycle control and cell biology from adenovirus.* Oncogene, 2005. **24**(52): p. 7673--7685.

132. Flint, J. and T. Shenk, *Adenovirus E1A protein paradigm viral transactivator.* Annu Rev Genet, 1989. **23**: p. 141-61.
133. Gallimore, P.H. and A.S. Turnell, *Adenovirus E1A: remodelling the host cell, a life or death experience.* Oncogene, 2001. **20**(54): p. 7824-7835.
134. Frisch, S.M. and J.S. Mymryk, *Adenovirus-5 E1A: paradox and paradigm.* Nature Reviews Molecular Cell Biology, 2002. **3**(6): p. 441--452.
135. Soriano, A.M., et al., *Adenovirus 5 E1A Interacts with E4orf3 To Regulate Viral Chromatin Organization.* J Virol, 2019. **93**(10).
136. Pelka, P., et al., *Intrinsic structural disorder in adenovirus E1A: a viral molecular hub linking multiple diverse processes.* Journal of virology, 2008. **82**(15): p. 7252--7263.
137. Ben-Israel, H. and T. Kleinberger, *Adenovirus and cell cycle control.* Front Biosci, 2002. **7**: p. d1369-95.
138. Rao, L., et al., *The adenovirus E1A proteins induce apoptosis, which is inhibited by the E1B 19-kDa and Bcl-2 proteins.* Proceedings of the National Academy of Sciences of the United States of America, 1992. **89**(16): p. 7742--7746.
139. Wimmer, P., et al., *PML isoforms IV and V contribute to adenovirus-mediated oncogenic transformation by functionally inhibiting the tumor-suppressor p53.* Oncogene, 2016. **35**(1): p. 69-82.
140. Kao, C.C., P.R. Yew, and A.J. Berk, *Domains required for in vitro association between the cellular p53 and the adenovirus 2 E1B 55K proteins.* Virology, 1990. **179**(2): p. 806-14.
141. Martin, M.E. and A.J. Berk, *Adenovirus E1B 55K represses p53 activation in vitro.* J Virol, 1998. **72**(4): p. 3146-54.
142. Teodoro, J.G. and P.E. Branton, *Regulation of p53-dependent apoptosis, transcriptional repression, and cell transformation by phosphorylation of the 55-kilodalton E1B protein of human adenovirus type 5.* Journal of virology, 1997. **71**(5): p. 3620--3627.
143. Yew, P.R., X. Liu, and A.J. Berk, *Adenovirus E1B oncoprotein tethers a transcriptional repression domain to p53.* Genes Dev, 1994. **8**(2): p. 190-202.
144. Yew, P.R. and A.J. Berk, *Inhibition of p53 transactivation required for transformation by adenovirus early 1B protein.* Nature, 1992. **357**(6373): p. 82--85.
145. Querido, E., et al., *Degradation of p53 by adenovirus E4orf6 and E1B55K proteins occurs via a novel mechanism involving a Cullin-containing complex.* Genes Dev., 2001. **15**(23): p. 3104-3117.
146. Querido, E., et al., *Regulation of p53 levels by the E1B 55-kilodalton protein and E4orf6 in adenovirus-infected cells.* Journal of virology, 1997. **71**(5): p. 3788--3798.
147. Dekker, J., et al., *Multimerization of the adenovirus DNA-binding protein is the driving force for ATP-independent DNA unwinding during strand displacement synthesis.* Embo j, 1997. **16**(6): p. 1455-63.
148. Bennett, E.M., et al., *Cutting edge: adenovirus E19 has two mechanisms for affecting class I MHC expression.* J Immunol, 1999. **162**(9): p. 5049-52.
149. Täuber, B. and T. Dobner, *Adenovirus early E4 genes in viral oncogenesis.* Oncogene, 2001. **20**: p. 7847-7854.
150. Nevels, M., et al., "*Hit-and-run*" *transformation by adenovirus oncogenes.* J. Virol., 2001. **75**: p. 3089-3094.
151. Tauber, B. and T. Dobner, *Molecular regulation and biological function of adenovirus early genes: the E4 ORFs.* Gene, 2001. **278**(1-2): p. 1-23.
152. Nevels, M., et al., *Transforming potential of the adenovirus type 5 E4orf3 protein.* J Virol, 1999. **73**(2): p. 1591-600.
153. Berget, S.M., C. Moore, and P.A. Sharp, *Spliced segments at the 5' terminus of adenovirus 2 late mRNA.* Proc Natl Acad Sci U S A, 1977. **74**(8): p. 3171-5.

154. Lutz, P., M. Rosa-Calatrava, and C. Kedinger, *The product of the adenovirus intermediate gene IX is a transcriptional activator.* J Virol, 1997. **71**(7): p. 5102-9.
155. Lutz, P. and C. Kedinger, *Properties of the adenovirus IVa2 gene product, an effector of late-phase-dependent activation of the major late promoter.* J Virol, 1996. **70**(3): p. 1396-405.
156. Babiss, L.E., H.S. Ginsberg, and J.E. Darnell, Jr., *Adenovirus E1B proteins are required for accumulation of late viral mRNA and for effects on cellular mRNA translation and transport.* Mol Cell Biol, 1985. **5**(10): p. 2552-8.
157. Beltz, G.A. and S.J. Flint, *Inhibition of HeLa cell protein synthesis during adenovirus infection. Restriction of cellular messenger RNA sequences to the nucleus.* J Mol Biol, 1979. **131**(2): p. 353-73.
158. SHENK, T.E., *Adenoviridae : The Viruses and Their Replication.* FUNDAMENTAL VIROLOGY, 2001: p. 1053--1088.
159. Waye, M.M.Y. and C.W. Sing, *Anti-Viral Drugs for Human Adenoviruses.* Pharmaceuticals, 2010. **3**(10): p. 3343-3354.
160. Wang, Y. and M. Dasso, *SUMOylation and deSUMOylation at a glance.* J Cell Sci, 2009. **122**(Pt 23): p. 4249-52.
161. Liang, Y.C., et al., *SUMO5, a Novel Poly-SUMO Isoform, Regulates PML Nuclear Bodies.* Sci Rep, 2016. **6**: p. 26509.
162. Seeler, J.-S. and A. Dejean, *Nuclear and unclear functions of SUMO.* Nature reviews. Molecular cell biology, 2003. **4**(9): p. 690--699.
163. Song, J., et al., *Identification of a SUMO-binding motif that recognizes SUMO-modified proteins.* Proceedings of the National Academy of Sciences of the United States of America, 2004. **101**(40): p. 14373--14378.
164. Wilkinson, K.A. and J.M. Henley, *Mechanisms, regulation and consequences of protein SUMOylation.* Biochem J, 2010. **428**(2): p. 133-45.
165. Van Damme, E., et al., *A manually curated network of the PML nuclear body interactome reveals an important role for PML-NBs in SUMOylation dynamics.* Int J Biol Sci, 2010. **6**(1): p. 51-67.
166. Gong, L. and E.T.H. Yeh, *Characterization of a family of nucleolar SUMO-specific proteases with preference for SUMO-2 or SUMO-3.* The Journal of biological chemistry, 2006. **281**(23): p. 15869--15877.
167. Gong, L., et al., *Molecular cloning and characterization of human AOS1 and UBA2, components of the sentrin-activating enzyme complex.* FEBS Lett, 1999. **448**(1): p. 185-9.
168. Desterro, J.M., et al., *Identification of the enzyme required for activation of the small ubiquitin-like protein SUMO-1.* The Journal of biological chemistry, 1999. **274**(15): p. 10618--10624.
169. Desterro, J.M., J. Thomson, and R.T. Hay, *Ubch9 conjugates SUMO but not ubiquitin.* FEBS Lett, 1997. **417**(3): p. 297-300.
170. Johnson, E.S., et al., *The ubiquitin-like protein Smt3p is activated for conjugation to other proteins by an Aos1p/Uba2p heterodimer.* The EMBO journal, 1997. **16**(18): p. 5509--5519.
171. Saitoh, H. and J. Hinchey, *Functional heterogeneity of small ubiquitin-related protein modifiers SUMO-1 versus SUMO-2/3.* Journal of Biological Chemistry, 2000. **275**(9): p. 6252--6258.
172. Hay, R.T., *SUMO: a history of modification.* Mol Cell, 2005. **18**(1): p. 1-12.
173. Cubenas-Potts, C. and M.J. Matunis, *SUMO: a multifaceted modifier of chromatin structure and function.* Dev Cell, 2013. **24**(1): p. 1-12.
174. Gill, G., *SUMO and ubiquitin in the nucleus: different functions, similar mechanisms?* Genes Dev, 2004. **18**(17): p. 2046-59.

175. Hilgarth, R.S., et al., *Regulation and function of SUMO modification.* J Biol Chem, 2004. **279**(52): p. 53899-902.
176. Kerscher, O., *SUMO junction-what's your function? New insights through SUMO-interacting motifs.* EMBO Rep, 2007. **8**(6): p. 550-5.
177. Kadoya, T., et al., *Desumoylation activity of Axam, a novel Axin-binding protein, is involved in downregulation of beta-catenin.* Mol Cell Biol, 2002. **22**(11): p. 3803-19.
178. He, X., et al., *Characterization of the loss of SUMO pathway function on cancer cells and tumor proliferation.* PLoS One, 2015. **10**(4): p. e0123882.
179. Dellaire, G., et al., *Mitotic accumulations of PML protein contribute to the re-establishment of PML nuclear bodies in G1.* Journal of cell science, 2006. **119**(Pt 6): p. 1034--1042.
180. Di Bacco, A., et al., *The SUMO-specific protease SENP5 is required for cell division.* Molecular and cellular biology, 2006. **26**(12): p. 4489--4498.
181. Du, L., et al., *Role of SUMO activating enzyme in cancer stem cell maintenance and self-renewal.* Nature Communications, 2016. **7**(1): p. 12326.
182. Bischof, O., et al., *Deconstructing PML-induced premature senescence.* Embo j, 2002. **21**(13): p. 3358-69.
183. Shen, T.H., et al., *The mechanisms of PML-nuclear body formation.* Mol Cell, 2006. **24**(3): p. 331-9.
184. Zhong, S., et al., *Role of SUMO-1-modified PML in nuclear body formation.* Blood, 2000. **95**(9): p. 2748--2752.
185. Zhong, S., P. Salomoni, and P.P. Pandolfi, *The transcriptional role of PML and the nuclear body.* Nat Cell Biol, 2000. **2**(5): p. E85-90.
186. Ishov, A.M., et al., *PML is critical for ND10 formation and recruits the PML-interacting protein daxx to this nuclear structure when modified by SUMO-1.* The Journal of cell biology, 1999. **147**(2): p. 221--234.
187. Stuurman, N., et al., *The nuclear matrix from cells of different origin. Evidence for a common set of matrix proteins.* J Biol Chem, 1990. **265**(10): p. 5460-5.
188. Ascoli, C.A. and G.G. Maul, *Identification of a novel nuclear domain.* J Cell Biol, 1991. **112**(5): p. 785-95.
189. Bernardi, R. and P.P. Pandolfi, *Role of PML and the PML-nuclear body in the control of programmed cell death.* Oncogene, 2003. **22**(56): p. 9048--9057.
190. Bernardi, R. and P.P. Pandolfi, *Structure, dynamics and functions of promyelocytic leukaemia nuclear bodies.* Nat Rev Mol Cell Biol, 2007. **8**(12): p. 1006-16.
191. Melnick, A. and J.D. Licht, *Deconstructing a disease: RARalpha, its fusion partners, and their roles in the pathogenesis of acute promyelocytic leukemia.* Blood, 1999. **93**(10): p. 3167-215.
192. Lallemand-Breitenbach, V., et al., *Arsenic degrades PML or PML-RARalpha through a SUMO-triggered RNF4/ubiquitin-mediated pathway.* Nat Cell Biol, 2008. **10**(5): p. 547-55.
193. Lallemand-Breitenbach, V. and H. de The, *PML nuclear bodies.* Cold Spring Harb Perspect Biol, 2010. **2**(5): p. a000661.
194. Bernardi, R. and P.P. Pandolfi, *A Dialog on the First 20 Years of PML Research and the Next 20 Ahead.* Frontiers in oncology, 2014. **4**: p. 23.
195. Sahin, U., et al., *Oxidative stress-induced assembly of PML nuclear bodies controls sumoylation of partner proteins.* J Cell Biol, 2014. **204**(6): p. 931-45.
196. Weidtkamp-Peters, S., et al., *Dynamics of component exchange at PML nuclear bodies.* J. Cell Sci., 2008. **121**: p. 2731-43.
197. Regad, T., et al., *PML mediates the interferon-induced antiviral state against a complex retrovirus via its association with the viral transactivator.* EMBO J, 2001. **20**(13): p. 3495-505.

198. Carbone, R., et al., *PML NBs associate with the hMre11 complex and p53 at sites of irradiation induced DNA damage.* Oncogene, 2002. **21**(11): p. 1633-40.
199. Pearson, M., et al., *PML regulates p53 acetylation and premature senescence induced by oncogenic Ras.* Nature, 2000. **406**(6792): p. 207-10.
200. Bischof, O., et al., *Regulation and localization of the Bloom syndrome protein in response to DNA damage.* J Cell Biol, 2001. **153**(2): p. 367-80.
201. Dellaire, G. and D.P. Bazett-Jones, *PML nuclear bodies: dynamic sensors of DNA damage and cellular stress.* Bioessays, 2004. **26**(9): p. 963-977.
202. Everett, R.D., *DNA viruses and viral proteins that interact with PML nuclear bodies.* Oncogene, 2001. **20**(49): p. 7266-73.
203. Scherer, M. and T. Stamminger, *Emerging Role of PML Nuclear Bodies in Innate Immune Signaling.* Journal of virology, 2016. **90**(13): p. 5850--5854.
204. Kim, Y.E., et al., *Human cytomegalovirus infection causes degradation of Sp100 proteins that suppress viral gene expression.* J Virol, 2011. **85**(22): p. 11928-37.
205. Merkl, P.E., M.H. Orzalli, and D.M. Knipe, *Mechanisms of Host IFI16, PML, and Daxx Protein Restriction of Herpes Simplex Virus 1 Replication.* J Virol, 2018. **92**(10).
206. Sahin, U., V. Lallemand-Breitenbach, and H. de Thé, *PML nuclear bodies: regulation, function and therapeutic perspectives.* The Journal of pathology, 2014. **234**(3): p. 289--291.
207. Schreiner, S. and H. Wodrich, *Virion factors that target Daxx to overcome intrinsic immunity.* J Virol, 2013. **87**(19): p. 10412-22.
208. Ullman, A.J. and P. Hearing, *Cellular proteins PML and Daxx mediate an innate antiviral defense antagonized by the adenovirus E4 ORF3 protein.* J Virol, 2008. **82**(15): p. 7325-35.
209. Borden, K.L., *Pondering the promyelocytic leukemia protein (PML) puzzle: possible functions for PML nuclear bodies.* Mol Cell Biol, 2002. **22**(15): p. 5259-69.
210. Sohn, S.Y. and P. Hearing, *Adenovirus Early Proteins and Host Sumoylation.* MBio, 2016. **7**(5).
211. Freudenberger, N., et al., *Human Adenovirus Core Protein V Is Targeted by the Host SUMOylation Machinery To Limit Essential Viral Functions.* J Virol, 2018. **92**(4).
212. Wimmer, P., S. Schreiner, and T. Dobner, *Human pathogens and the host cell SUMOylation system.* Journal of virology, 2012. **86**(2): p. 642--654.
213. Wimmer, P., et al., *SUMO modification of E1B-55K oncoprotein regulates isoform-specific binding to the tumour suppressor protein PML.* Oncogene, 2010. **29**(40): p. 5511-5522.
214. Stubbe, M., et al., *Viral DNA Binding Protein SUMOylation Promotes PML Nuclear Body Localization Next to Viral Replication Centers.* mBio, 2020. **11**(2): p. e00049-20.
215. Pennella, M.A., et al., *Adenovirus E1B 55-kilodalton protein is a p53-SUMO1 E3 ligase that represses p53 and stimulates its nuclear export through interactions with promyelocytic leukemia nuclear bodies.* J Virol, 2010. **84**(23): p. 12210-25.
216. Muller, S. and T. Dobner, *The adenovirus E1B-55K oncoprotein induces SUMO modification of p53.* Cell Cycle, 2008. **7**(6): p. 754-8.
217. Sohn, S.-Y. and P. Hearing, *The adenovirus E4-ORF3 protein functions as a SUMO E3 ligase for TIF-1γ sumoylation and poly-SUMO chain elongation.* Proceedings of the National Academy of Sciences of the United States of America, 2016. **113**(24): p. 6725--6730.
218. Bridges, R.G., et al., *The Adenovirus E4-ORF3 Protein Stimulates SUMOylation of General Transcription Factor TFII-I to Direct Proteasomal Degradation.* MBio, 2016. **7**(1): p. e02184-15.

219. Sohn, S.Y. and P. Hearing, *Adenovirus regulates sumoylation of Mre11-Rad50-Nbs1 components through a paralog-specific mechanism.* J Virol, 2012. **86**(18): p. 9656-65.
220. Muncheberg, S., et al., *E1B-55K-Mediated Regulation of RNF4 SUMO-Targeted Ubiquitin Ligase Promotes Human Adenovirus Gene Expression.* J Virol, 2018. **92**(13).
221. Yousef, A.F., et al., *Identification of a molecular recognition feature in the E1A oncoprotein that binds the SUMO conjugase UBC9 and likely interferes with polySUMOylation.* Oncogene, 2010. **29**(33): p. 4693-704.
222. Bürck, C., et al., *KAP1 Is a Host Restriction Factor That Promotes Human Adenovirus E1B-55K SUMO Modification.* Journal of virology, 2015. **90**(2): p. 930-946.
223. Sohn, S.Y. and P. Hearing, *Mechanism of Adenovirus E4-ORF3-Mediated SUMO Modifications.* mBio, 2019. **10**(1).
224. Kindsmuller, K., et al., *Intranuclear targeting and nuclear export of the adenovirus E1B-55K protein are regulated by SUMO1 conjugation.* Proc Natl Acad Sci U S A, 2007. **104**(16): p. 6684-9.
225. Lethbridge, K.J., *Nuclear matrix localization and SUMO-1 modification of adenovirus type 5 E1b 55K protein are controlled by E4 Orf6 protein.* Journal of General Virology, 2003. **84**(2): p. 259--268.
226. Lin, D., et al., *Identification of a Substrate Recognition Site on Ubc9.* Journal of Biological Chemistry, 2002. **277**(24): p. 21740--21748.
227. Tatham, M.H., Y. Chen, and R.T. Hay, *Role of two residues proximal to the active site of Ubc9 in substrate recognition by the Ubc9.SUMO-1 thiolester complex.* Biochemistry, 2003. **42**(11): p. 3168--3179.
228. Duprez, E., et al., *SUMO-1 modification of the acute promyelocytic leukaemia protein PML: implications for nuclear localisation.* Journal of cell science, 1999. **112 (Pt 3)**: p. 381--393.
229. Kurtzman, A.L. and N. Schechter, *Ubc9 interacts with a nuclear localization signal and mediates nuclear localization of the paired-like homeobox protein Vsx-1 independent of SUMO-1 modification.* Proceedings of the National Academy of Sciences, 2001. **98**(10): p. 5602--5607.
230. Knipscheer, P., et al., *Ubc9 sumoylation regulates SUMO target discrimination.* Molecular cell, 2008. **31**(3): p. 371--382.
231. Sun, H., J.D. Leverson, and T. Hunter, *Conserved function of RNF4 family proteins in eukaryotes: targeting a ubiquitin ligase to SUMOylated proteins.* EMBO J, 2007. **26**(18): p. 4102-12.
232. Tatham, M.H., et al., *RNF4 is a poly-SUMO-specific E3 ubiquitin ligase required for arsenic-induced PML degradation.* Nat Cell Biol, 2008. **10**(5): p. 538-46.
233. Yageta, M., et al., *The adenovirus E1A domains required for induction of DNA rereplication in G2/M arrested cells coincide with those required for apoptosis.* Oncogene, 1999. **18**(34): p. 4767--4776.
234. Ferrari, R., et al., *Adenovirus Small E1A Employs the Lysine Acetylases p300/CBP and Tumor Suppressor Rb to Repress Select Host Genes and Promote Productive Virus Infection.* Cell Host & Microbe, 2014. **16**(5): p. 663-676.
235. Ferrari, R., et al., *Epigenetic reprogramming by adenovirus e1a.* Science, 2008. **321**(5892): p. 1086-8.
236. Ledl, A., D. Schmidt, and S. Muller, *Viral oncoproteins E1A and E7 and cellular LxCxE proteins repress SUMO modification of the retinoblastoma tumor suppressor.* Oncogene, 2005. **24**(23): p. 3810-8.
237. Pelka, P., et al., *Adenovirus E1A Directly Targets the E2F/DP-1 Complex.* Journal of Virology, 2011. **85**(17): p. 8841-8851.

238. Hiebert, S.W., et al., *Role of E2F transcription factor in E1A-mediated trans activation of cellular genes.* J Virol, 1991. **65**(7): p. 3547-52.
239. Swaminathan, S. and B. Thimmapaya, *Transactivation of Adenovirus E2-early Promoter by E1A and E4 6/7 in the Context of Viral Chromosome.* Journal of Molecular Biology, 1996. **258**(5): p. 736-746.
240. Berscheminski, J., et al., *The adenoviral oncogene E1A-13S interacts with a specific isoform of the tumor suppressor PML to enhance viral transcription.* J Virol, 2013. **87**(2): p. 965-77.
241. Hsu, E., et al., *Adenovirus E1A Activation Domain Regulates H3 Acetylation Affecting Varied Steps in Transcription at Different Viral Promoters.* Journal of Virology, 2018. **92**(18): p. e00805-18.
242. Pelka, P., et al., *Transcriptional control by adenovirus E1A conserved region 3 via p300/CBP.* Nucleic Acids Research, 2009. **37**(4): p. 1095-1106.
243. Schreiner, S., et al., *Adenovirus Type 5 Early Region 1B 55K Oncoprotein-Dependent Degradation of Cellular Factor Daxx Is Required for Efficient Transformation of Primary Rodent Cells.* J. Virol., 2011. **85**(17): p. 8752-65.
244. Schreiner, S., et al., *Control of human adenovirus type 5 gene expression by cellular Daxx/ATRX chromatin-associated complexes.* Nucleic Acids Res, 2013. **41**(6): p. 3532-50.
245. Schreiner, S., et al., *Proteasome-dependent degradation of Daxx by the viral E1B-55K protein in human adenovirus-infected cells.* J Virol, 2010. **84**(14): p. 7029-38.
246. Wimmer, P., et al., *Cross-talk between phosphorylation and SUMOylation regulates transforming activities of an adenoviral oncoprotein.* Oncogene, 2013. **32**(13): p. 1626--1637.
247. Berscheminski, J., et al., *Sp100A is a tumor suppressor that activates p53-dependent transcription and counteracts E1A/E1B-55K-mediated transformation.* Oncogene, 2015.
248. Hoppe, A., et al., *Interaction of the adenovirus type 5 E4 Orf3 protein with promyelocytic leukemia protein isoform II is required for ND10 disruption.* J Virol, 2006. **80**(6): p. 3042-9.
249. Araujo, F.D., et al., *Adenovirus type 5 E4orf3 protein targets the Mre11 complex to cytoplasmic aggresomes.* J Virol, 2005. **79**(17): p. 11382-91.
250. Stracker, T.H., et al., *Serotype-specific reorganization of the Mre11 complex by adenoviral E4orf3 proteins.* J Virol, 2005. **79**(11): p. 6664-73.
251. Pancholi, N.J. and M.D. Weitzman, *Serotype-specific restriction of wild-type adenoviruses by the cellular Mre11-Rad50-Nbs1 complex.* Virology, 2018. **518**: p. 221-231.
252. Forrester, N.A., et al., *Adenovirus E4orf3 Targets Transcriptional Intermediary Factor 1γ for Proteasome-Dependent Degradation during Infection.* Journal of Virology, 2012. **86**(6): p. 3167-3179.
253. Chan, H.M., et al., *Acetylation control of the retinoblastoma tumour-suppressor protein.* Nat Cell Biol, 2001. **3**(7): p. 667-74.
254. Buchkovich, K., et al., *Cellular proteins that are targets for transformation by DNA tumour viruses.* Ciba Foundation symposium, 1990. **150**: p. 262--71-- discussion 271--8.
255. Liu, X. and R. Marmorstein, *Structure of the retinoblastoma protein bound to adenovirus E1A reveals the molecular basis for viral oncoprotein inactivation of a tumor suppressor.* Genes Dev, 2007. **21**(21): p. 2711-6.
256. Isobe, T., et al., *Adenovirus E1A inhibits SCF(Fbw7) ubiquitin ligase.* J Biol Chem, 2009. **284**(41): p. 27766-79.
257. Arany, Z., et al., *A family of transcriptional adaptor proteins targeted by the E1A oncoprotein.* Nature, 1995. **374**(6517): p. 81-4.

258. Somasundaram, K. and W.S. El-Deiry, *Inhibition of p53-mediated transactivation and cell cycle arrest by E1A through its p300/CBP-interacting region.* Oncogene, 1997. **14**(9): p. 1047--1057.
259. Eckner, R., et al., *Molecular cloning and functional analysis of the adenovirus E1A-associated 300-kD protein (p300) reveals a protein with properties of a transcriptional adaptor.* Genes Dev, 1994. **8**(8): p. 869-84.
260. Yang, X.J., et al., *A p300/CBP-associated factor that competes with the adenoviral oncoprotein E1A.* Nature, 1996. **382**(6589): p. 319--324.
261. Howe, J.A., et al., *Retinoblastoma growth suppressor and a 300-kDa protein appear to regulate cellular DNA synthesis.* Proc Natl Acad Sci U S A, 1990. **87**(15): p. 5883-7.
262. Datto, M.B., et al., *The viral oncoprotein E1A blocks transforming growth factor beta-mediated induction of p21/WAF1/Cip1 and p15/INK4B.* Mol Cell Biol, 1997. **17**(4): p. 2030-7.
263. Horwitz, G.A., et al., *Adenovirus small e1a alters global patterns of histone modification.* Science, 2008. **321**(5892): p. 1084-5.
264. Liu, Y., et al., *Adenovirus E1B 55-kilodalton oncoprotein inhibits p53 acetylation by PCAF.* Mol. Cell. Biol., 2000. **20**(15): p. 5540-5553.
265. Lethbridge, K.J., G.E. Scott, and K.N. Leppard, *Nuclear matrix localization and SUMO-1 modification of adenovirus type 5 E1b 55K protein are controlled by E4 Orf6 protein.* Journal of General Virology, 2003. **84**(2): p. 259-268.
266. Debbas, M. and E. White, *Wild-type p53 mediates apoptosis by E1A, which is inhibited by E1B.* Genes & development, 1993. **7**(4): p. 546-54.
267. Nevels, M., et al., *The adenovirus E4orf6 protein can promote E1A/E1B-induced focus formation by interfering with p53 tumor suppressor function.* Proc. Natl. Acad. Sci. USA, 1997. **94**: p. 1206-1211.
268. Blanchette, P., et al., *Both BC-box motifs of adenovirus protein E4orf6 are required to efficiently assemble an E3 ligase complex that degrades p53.* Mol Cell Biol, 2004. **24**(21): p. 9619-29.
269. Schwartz, R.A., et al., *Distinct requirements of adenovirus E1b55K protein for degradation of cellular substrates.* J Virol, 2008. **82**(18): p. 9043-55.
270. Querido, E., et al., *Identification of three functions of the adenovirus E4orf6 protein that mediate p53 degradation by the E4orf6-E1B55K complex.* J. Virol., 2001. **75**(2): p. 699-709.
271. Rubenwolf, S., et al., *Structural analysis of the adenovirus type 5 E1B 55-kilodalton-E4orf6 protein complex.* J Virol, 1997. **71**(2): p. 1115-23.
272. Schreiner, S., P. Wimmer, and T. Dobner, *Adenovirus degradation of cellular proteins.* Future Microbiol, 2012. **7**(2): p. 211-25.
273. Blackford, A.N., et al., *Adenovirus 12 E4orf6 inhibits ATR activation by promoting TOPBP1 degradation.* Proc Natl Acad Sci U S A, 2010. **107**(27): p. 12251-6.
274. Higashino, F., J.M. Pipas, and T. Shenk, *Adenovirus E4orf6 oncoprotein modulates the function of the p53-related protein, p73.* Proceedings of the National Academy of Sciences, 1998. **95**(26): p. 15683--15687.
275. Nevels, M., et al., *The adenovirus E4orf6 protein contributes to malignant transformation by antagonizing E1A-induced accumulation of the tumor suppressor protein p53.* Oncogene, 1999. **18**(1): p. 9--17.
276. Hart, L.S., et al., *The Adenovirus E4orf6 Protein Inhibits DNA Double Strand Break Repair and Radiosensitizes Human Tumor Cells in an E1B-55K-independent Manner.* Journal of Biological Chemistry, 2005. **280**(2): p. 1474--1481.
277. Vink, E.I., et al., *Adenovirus E4-ORF3-dependent relocalization of TIF1alpha and TIF1gamma relies on access to the Coiled-Coil motif.* Virology, 2012. **422**(2): p. 317-25.

278. Stracker, T.H., C.T. Carson, and M.D. Weitzman, *Adenovirus oncoproteins inactivate the Mre11-Rad50-NBS1 DNA repair complex.* Nature, 2002. **418**(6895): p. 348-52.
279. Leppard, K.N., et al., *Adenovirus type 5 E4 Orf3 protein targets promyelocytic leukaemia (PML) protein nuclear domains for disruption via a sequence in PML isoform II that is predicted as a protein interaction site by bioinformatic analysis.* J Gen Virol, 2009. **90**(Pt 1): p. 95-104.
280. Turner, R.L., J.C. Wilkinson, and D.A. Ornelles, *E1B and E4 oncoproteins of adenovirus antagonize the effect of apoptosis inducing factor.* Virology, 2014. **456-457**: p. 205-219.
281. Alexiadis, V., et al., *The protein encoded by the proto-oncogene DEK changes the topology of chromatin and reduces the efficiency of DNA replication in a chromatin-specific manner.* Genes & development, 2000. **14**(11): p. 1308-1312.
282. Waldmann, T., et al., *The DEK protein—an abundant and ubiquitous constituent of mammalian chromatin.* Gene, 2004. **343**(1): p. 1-9.
283. Consortium, U. *UniProtKB - P35659 (DEK_HUMAN)*. 22nd March 2021; Available from: https://www.uniprot.org/uniprot/P35659.
284. Devany, M., et al., *Solution NMR structure of the N-terminal domain of the human DEK protein.* Protein Sci, 2008. **17**(2): p. 205-15.
285. Kappes, F., et al., *Functional domains of the ubiquitous chromatin protein DEK.* Mol Cell Biol, 2004. **24**(13): p. 6000-10.
286. Bohm, F., et al., *The SAF-box domain of chromatin protein DEK.* Nucleic Acids Res, 2005. **33**(3): p. 1101-10.
287. Waldmann, T., et al., *Structure-specific binding of the proto-oncogene protein DEK to DNA.* Nucleic Acids Res, 2003. **31**(23): p. 7003-10.
288. Devany, M., N.P. Kotharu, and H. Matsuo, *Expression and isotopic labeling of structural domains of the human protein DEK.* Protein Expr Purif, 2005. **40**(2): p. 244-7.
289. Devany, M., N.P. Kotharu, and H. Matsuo, *Solution NMR structure of the C-terminal domain of the human protein DEK.* Protein Sci, 2004. **13**(8): p. 2252-9.
290. Kappes, F., et al., *DEK is a poly(ADP-ribose) acceptor in apoptosis and mediates resistance to genotoxic stress.* Mol Cell Biol, 2008. **28**(10): p. 3245-57.
291. Smith, E.A., et al., *DEK is required for homologous recombination repair of DNA breaks.* Scientific Reports, 2017. **7**(1): p. 44662.
292. Sawatsubashi, S., et al., *A histone chaperone, DEK, transcriptionally coactivates a nuclear receptor.* Genes & development, 2010. **24**(2): p. 159-170.
293. Ageberg, M., et al., *Identification of a novel and myeloid specific role of the leukemia-associated fusion protein DEK-NUP214 leading to increased protein synthesis.* Genes Chromosomes Cancer, 2008. **47**(4): p. 276-87.
294. Kappes, F., et al., *Phosphorylation by Protein Kinase CK2 Changes the DNA Binding Properties of the Human Chromatin Protein DEK.* Molecular and Cellular Biology, 2004. **24**(13): p. 6011-6020.
295. Mor-Vaknin, N., et al., *DEK in the synovium of patients with juvenile idiopathic arthritis: Characterization of DEK antibodies and posttranslational modification of the DEK autoantigen.* Arthritis & Rheumatism, 2011. **63**(2): p. 556-567.
296. Cleary, J., et al., *p300/CBP-associated Factor Drives DEK into Interchromatin Granule Clusters.* The Journal of biological chemistry, 2005. **280**: p. 31760-7.
297. Ko, S.I., et al., *Regulation of histone acetyltransferase activity of p300 and PCAF by proto-oncogene protein DEK.* FEBS Lett, 2006. **580**(13): p. 3217-22.
298. Fahrer, J., et al., *High-Affinity Interaction of Poly(ADP-ribose) and the Human DEK Oncoprotein Depends upon Chain Length.* Biochemistry, 2010. **49**(33): p. 7119-7130.

299. Kappes, F., et al., *Phosphorylation by protein kinase CK2 changes the DNA binding properties of the human chromatin protein DEK.* Mol Cell Biol, 2004. **24**(13): p. 6011-20.
300. von Lindern, M., et al., *Translocation t(6;9) in acute non-lymphocytic leukaemia results in the formation of a DEK-CAN fusion gene.* Baillieres Clin Haematol, 1992. **5**(4): p. 857-79.
301. von Lindern, M., et al., *The translocation (6;9), associated with a specific subtype of acute myeloid leukemia, results in the fusion of two genes, dek and can, and the expression of a chimeric, leukemia-specific dek-can mRNA.* Mol Cell Biol, 1992. **12**(4): p. 1687-97.
302. Soekarman, D., et al., *The translocation (6;9) (p23;q34) shows consistent rearrangement of two genes and defines a myeloproliferative disorder with specific clinical features.* Blood, 1992. **79**(11): p. 2990-7.
303. Soekarman, D., et al., *Dek-can rearrangement in translocation (6;9)(p23;q34).* Leukemia, 1992. **6**(6): p. 489-94.
304. Broxmeyer, H.E., et al., *DEK regulates hematopoietic stem engraftment and progenitor cell proliferation.* Stem cells and development, 2012. **21**(9): p. 1449-1454.
305. Larramendy, M.L., et al., *Overexpression of translocation-associated fusion genes of FGFRI, MYC, NPMI, and DEK, but absence of the translocations in acute myeloid leukemia. A microarray analysis.* Haematologica, 2002. **87**(6): p. 569-77.
306. Oancea, C., et al., *The t(6;9) associated DEK/CAN fusion protein targets a population of long-term repopulating hematopoietic stem cells for leukemogenic transformation.* Leukemia, 2010. **24**(11): p. 1910-9.
307. Ageberg, M., U. Gullberg, and A. Lindmark, *The involvement of cellular proliferation status in the expression of the human proto-oncogene DEK.* Haematologica, 2006. **91**(2): p. 268-9.
308. Hu, H.G., et al., *The distribution of the DEK protein in mammalian chromatin.* Biochem Biophys Res Commun, 2007. **358**(4): p. 1008-14.
309. Hollenbach, A.D., et al., *Daxx and histone deacetylase II associate with chromatin through an interaction with core histones and the chromatin-associated protein Dek.* J Cell Sci, 2002. **115**(Pt 16): p. 3319-30.
310. Cleary, J., et al., *p300/CBP-associated factor drives DEK into interchromatin granule clusters.* J Biol Chem, 2005. **280**(36): p. 31760-7.
311. Ivanauskiene, K., et al., *The PML-associated protein DEK regulates the balance of H3.3 loading on chromatin and is important for telomere integrity.* Genome research, 2014. **24**.
312. Waldmann, T., et al., *The ubiquitous chromatin protein DEK alters the structure of DNA by introducing positive supercoils.* J Biol Chem, 2002. **277**(28): p. 24988-94.
313. Kappes, F., et al., *The DEK oncoprotein is a Su(var) that is essential to heterochromatin integrity.* Genes Dev, 2011. **25**(7): p. 673-8.
314. Ivanauskiene, K., et al., *The PML-associated protein DEK regulates the balance of H3.3 loading on chromatin and is important for telomere integrity.* Genome Res, 2014. **24**(10): p. 1584-94.
315. Sandén, C. and U. Gullberg, *The DEK oncoprotein and its emerging roles in gene regulation.* Leukemia, 2015. **29**(8): p. 1632-1636.
316. Campillos, M., et al., *Transcriptional activation by AP-2alpha is modulated by the oncogene DEK.* Nucleic Acids Res, 2003. **31**(5): p. 1571-5.
317. McGarvey, T., et al., *The acute myeloid leukemia-associated protein, DEK, forms a splicing-dependent interaction with exon-product complexes.* J Cell Biol, 2000. **150**(2): p. 309-20.

318. Kappes, F., et al., *Subcellular localization of the human proto-oncogene protein DEK.* J Biol Chem, 2001. **276**(28): p. 26317-23.
319. Le Hir, H., et al., *The spliceosome deposits multiple proteins 20-24 nucleotides upstream of mRNA exon-exon junctions.* Embo j, 2000. **19**(24): p. 6860-9.
320. Soares, L.M.M., et al., *Intron Removal Requires Proofreading of U2AF/3' Splice Site Recognition by DEK.* Science, 2006. **312**(5782): p. 1961-1965.
321. Voith von Voithenberg, L., et al., *Recognition of the 3' splice site RNA by the U2AF heterodimer involves a dynamic population shift.* Proceedings of the National Academy of Sciences, 2016. **113**(46): p. E7169-E7175.
322. Fu, G.K., G. Grosveld, and D.M. Markovitz, *DEK, an autoantigen involved in a chromosomal translocation in acute myelogenous leukemia, binds to the HIV-2 enhancer.* Proc Natl Acad Sci U S A, 1997. **94**(5): p. 1811-5.
323. Faulkner, N.E., J.M. Hilfinger, and D.M. Markovitz, *Protein phosphatase 2A activates the HIV-2 promoter through enhancer elements that include the pets site.* J Biol Chem, 2001. **276**(28): p. 25804-12.
324. Krithivas, A., et al., *Protein interactions targeting the latency-associated nuclear antigen of Kaposi's sarcoma-associated herpesvirus to cell chromosomes.* J Virol, 2002. **76**(22): p. 11596-604.
325. Pease, N.A., T. Wise-Draper, and L. Privette Vinnedge, *Dissecting the Potential Interplay of DEK Functions in Inflammation and Cancer.* J Oncol, 2015. **2015**: p. 106517.
326. Chen, X., et al., *Meta-analysis of nasopharyngeal carcinoma microarray data explores mechanism of EBV-regulated neoplastic transformation.* BMC Genomics, 2008. **9**: p. 322.
327. Wise-Draper, T.M., et al., *The human DEK proto-oncogene is a senescence inhibitor and an upregulated target of high-risk human papillomavirus E7.* J Virol, 2005. **79**(22): p. 14309-17.
328. Wise-Draper, T.M., et al., *Apoptosis inhibition by the human DEK oncoprotein involves interference with p53 functions.* Mol Cell Biol, 2006. **26**(20): p. 7506-19.
329. Carro, M.S., et al., *DEK Expression is controlled by E2F and deregulated in diverse tumor types.* Cell Cycle, 2006. **5**(11): p. 1202-7.
330. Grasemann, C., et al., *Gains and overexpression identify DEK and E2F3 as targets of chromosome 6p gains in retinoblastoma.* Oncogene, 2005. **24**(42): p. 6441-9.
331. Adams, A.K., et al., *DEK promotes HPV-positive and -negative head and neck cancer cell proliferation.* Oncogene, 2015. **34**(7): p. 868-77.
332. Mor-Vaknin, N., et al., *DEK in the synovium of patients with juvenile idiopathic arthritis: characterization of DEK antibodies and posttranslational modification of the DEK autoantigen.* Arthritis Rheum, 2011. **63**(2): p. 556-67.
333. Khodadoust, M.S., et al., *Melanoma proliferation and chemoresistance controlled by the DEK oncogene.* Cancer Res, 2009. **69**(16): p. 6405-13.
334. Kappes, F., et al., *DEK expression in melanocytic lesions.* Hum Pathol, 2011. **42**(7): p. 932-8.
335. Privette Vinnedge, L.M., et al., *The DEK oncogene is a target of steroid hormone receptor signaling in breast cancer.* PLoS One, 2012. **7**(10): p. e46985.
336. Liu, S., et al., *DEK overexpression is correlated with the clinical features of breast cancer.* Pathol Int, 2012. **62**(3): p. 176-81.
337. Han, S., et al., *Clinicopathological significance of DEK overexpression in serous ovarian tumors.* Pathol Int, 2009. **59**(7): p. 443-7.
338. Wang, J., et al., *DEK depletion negatively regulates Rho/ROCK/MLC pathway in non-small cell lung cancer.* J Histochem Cytochem, 2013. **61**(7): p. 510-21.
339. Zhao, T., et al., *Expression of DEK in pancreatic cancer and its correlation with clinicopathological features and prognosis.* J Cancer, 2019. **10**(4): p. 911-917.

340. Wise-Draper, T.M., et al., *Overexpression of the cellular DEK protein promotes epithelial transformation in vitro and in vivo.* Cancer research, 2009. **69**(5): p. 1792-1799.
341. Wise-Draper, T.M., et al., *DEK proto-oncogene expression interferes with the normal epithelial differentiation program.* Am J Pathol, 2009. **174**(1): p. 71-81.
342. Zhang, Y., et al., *The DEK oncogene activates VEGF expression and promotes tumor angiogenesis and growth in HIF-1α-dependent and -independent manners.* Oncotarget, 2016. **7**(17): p. 23740-23756.
343. Privette Vinnedge, L.M., et al., *The human DEK oncogene stimulates β-catenin signaling, invasion and mammosphere formation in breast cancer.* Oncogene, 2011. **30**(24): p. 2741-52.
344. Hanahan, D., *Studies on transformation of Escherichia coli with plasmids.* Journal of Molecular Biology, 1983. **166**(4): p. 557-580.
345. Giard, D.J., et al., *In vitro cultivation of human tumors: establishment of cell lines derived from a series of solid tumors.* J Natl Cancer Inst, 1973. **51**(5): p. 1417-23.
346. Mitsudomi, T., et al., *Mutations of ras genes distinguish a subset of non-small-cell lung cancer cell lines from small-cell lung cancer cell lines.* Oncogene, 1991. **6**(8): p. 1353-62.
347. Vertegaal, A.C., et al., *A proteomic study of SUMO-2 target proteins.* J Biol Chem, 2004. **279**(32): p. 33791-8.
348. Tatham, M.H., et al., *Detection of protein SUMOylation in vivo.* Nat Protoc, 2009. **4**(9): p. 1363-71.
349. Matrka, M.C., et al., *DEK over-expression promotes mitotic defects and micronucleus formation.* Cell Cycle, 2015. **14**(24): p. 3939-3953.
350. Gripon, P., et al., *Infection of a human hepatoma cell line by hepatitis B virus.* Proc Natl Acad Sci U S A, 2002. **99**(24): p. 15655-60.
351. Graham, F.L., et al., *Characteristics of a human cell line transformed by DNA from human adenovirus type 5.* J. Gen. Virol., 1977. **36**: p. 59-72.
352. DuBridge, R.B., et al., *Analysis of mutation in human cells by using an Epstein-Barr virus shuttle system.* Mol Cell Biol, 1987. **7**(1): p. 379-87.
353. Kindsmüller, K., et al., *Intranuclear targeting and nuclear export of the adenovirus E1B-55K protein are regulated by SUMO1 conjugation.* Proc. Natl. Acad. Sci. USA, 2007. **104**: p. 6684-6689.
354. Frost, J.R., et al., *The interaction of adenovirus E1A with the mammalian protein Ku70/XRCC6.* Virology, 2017. **500**: p. 11-21.
355. O'Shea, C.C., et al., *Late viral RNA export, rather than p53 inactivation, determines ONYX-015 tumor selectivity.* Cancer Cell, 2004. **6**(6): p. 611--623.
356. Beyer, W.R., et al., *Oncoretrovirus and lentivirus vectors pseudotyped with lymphocytic choriomeningitis virus glycoprotein: generation, concentration, and broad host range.* J Virol, 2002. **76**(3): p. 1488-95.
357. Dull, T., et al., *A third-generation lentivirus vector with a conditional packaging system.* J Virol, 1998. **72**(11): p. 8463-71.
358. Sarnow, P., C.A. Sullivan, and A.J. Levine, *A monoclonal antibody detecting the adenovirus type 5-E1b-58Kd tumor antigen: characterization of the E1b-58Kd tumor antigen in adenovirus-infected and -transformed cells.* Virology, 1982. **120**(2): p. 510-7.
359. Reich, N.C., et al., *Monoclonal antibodies which recognize native and denatured forms of the adenovirus DNA-binding protein.* Virology, 1983. **128**(2): p. 480-4.
360. Wodrich, H., et al., *A capsid-encoded PPxY-motif facilitates adenovirus entry.* PLoS Pathog, 2010. **6**(3): p. e1000808.

361. Marton, M.J., et al., *The adenovirus E4 17-kilodalton protein complexes with the cellular transcription factor E2F, altering its DNA-binding properties and stimulating E1A-independent accumulation of E2 mRNA.* J Virol, 1990. **64**(5): p. 2345-59.
362. Schindelin, J., et al., *Fiji: an open-source platform for biological-image analysis.* Nature Methods, 2012. **9**(7): p. 676-682.
363. Doucas, V., et al., *Adenovirus replication is coupled with the dynamic properties of the PML nuclear structure.* Genes Dev, 1996. **10**(2): p. 196-207.
364. Zhao, Q., et al., *GPS-SUMO: a tool for the prediction of sumoylation sites and SUMO-interaction motifs.* Nucleic Acids Research, 2014. **42**(W1): p. W325-W330.
365. Bolte, S. and F.P. Cordelières, *A guided tour into subcellular colocalization analysis in light microscopy.* J Microsc, 2006. **224**(Pt 3): p. 213-32.
366. Grundemann, D. and E. Schomig, *Protection of DNA during preparative agarose gel electrophoresis against damage induced by ultraviolet light.* Biotechniques, 1996. **21**(5): p. 898-903.
367. Laemmli, U.K., *Cleavage of Structural Proteins during the Assembly of the Head of Bacteriophage T4.* Nature, 1970. **227**(5259): p. 680-685.
368. Bradford, M.M., *A rapid and sensitive method for the quantitation of microgram quantities of protein utilizing the principle of protein-dye binding.* Anal Biochem, 1976. **72**: p. 248-54.
369. Beer, *Bestimmung der Absorption des rothen Lichts in farbigen Flüssigkeiten.* Annalen der Physik, 1852. **162**(5): p. 78-88.
370. Helt, A.-M. and D.A. Galloway, *Mechanisms by which DNA tumor virus oncoproteins target the Rb family of pocket proteins.* Carcinogenesis, 2003. **24**(2): p. 159-169.
371. Wise-Draper, T.M., et al., *Apoptosis Inhibition by the Human DEK Oncoprotein Involves Interference with p53 Functions.* Molecular and Cellular Biology, 2006. **26**(20): p. 7506-7519.
372. Khodadoust, M.S., et al., *Melanoma Proliferation and Chemoresistance Controlled by the DEK Oncogene.* Cancer Research, 2009. **69**(16): p. 6405-6413.
373. Cheng, C.Y., et al., *The E4orf6/E1B55K E3 ubiquitin ligase complexes of human adenoviruses exhibit heterogeneity in composition and substrate specificity.* J Virol, 2011. **85**(2): p. 765-75.
374. Mitsudomi, T., et al., *p53 gene mutations in non-small-cell lung cancer cell lines and their correlation with the presence of ras mutations and clinical features.* Oncogene, 1992. **7**(1): p. 171--180.
375. Guillouzo, A., et al., *The human hepatoma HepaRG cells: a highly differentiated model for studies of liver metabolism and toxicity of xenobiotics.* Chem Biol Interact, 2007. **168**(1): p. 66-73.
376. Aninat, C., et al., *Expression of cytochromes P450, conjugating enzymes and nuclear receptors in human hepatoma HepaRG cells.* Drug Metab Dispos, 2006. **34**(1): p. 75-83.
377. Smith, E.A., et al., *The nuclear DEK interactome supports multi-functionality.* Proteins: Structure, Function, and Bioinformatics, 2018. **86**(1): p. 88-97.
378. Tejera, B., et al., *The human adenovirus type 5 E1B 55kDa protein interacts with RNA promoting timely DNA replication and viral late mRNA metabolism.* PLOS ONE, 2019. **14**(4): p. e0214882.
379. Zantema, A., et al., *Adenovirus serotype determines association and localization of the large E1B tumor antigen with cellular tumor antigen p53 in transformed cells.* Molecular and cellular biology, 1985. **5**(11): p. 3084--3091.
380. Zantema, A., et al., *Localization of the E1 B proteins of adenovirus 5 in transformed cells, as revealed by interaction with monoclonal antibodies.* Virology, 1985. **142**(1): p. 44-58.

381. Liu, Y., et al., *Adenovirus exploits the cellular aggresome response to accelerate inactivation of the MRN complex.* J Virol, 2005. **79**(22): p. 14004-16.
382. Leppard, K.N. and R.D. Everett, *The adenovirus type 5 E1b 55K and E4 Orf3 proteins associate in infected cells and affect ND10 components.* J. Gen. Virol., 1999. **80**(Pt 4): p. 997-1008.
383. Ornelles, D.A. and T. Shenk, *Localization of the adenovirus early region 1B 55-kilodalton protein during lytic infection: association with nuclear viral inclusions requires the early region 4 34-kilodalton protein.* J. Virol., 1991. **65**(1): p. 424-429.
384. Dobbelstein, M., et al., *Nuclear export of the E1B 55-kDa and E4 34-kDa adenoviral oncoproteins mediated by a rev-like signal sequence.* Embo J, 1997. **16**(14): p. 4276-84.
385. Marshall, L.J., et al., *RUNX1 permits E4orf6-directed nuclear localization of the adenovirus E1B-55K protein and associates with centers of viral DNA and RNA synthesis.* J Virol, 2008. **82**(13): p. 6395-408.
386. Goodrum, F.D., T. Shenk, and D.A. Ornelles, *Adenovirus early region 4 34-kilodalton protein directs the nuclear localization of the early region 1B 55-kilodalton protein in primate cells.* J. Virol., 1996. **70**: p. 6323-6335.
387. Carvalho, T., et al., *Targeting of adenovirus E1A and E4-ORF3 proteins to nuclear matrix-associated PML bodies.* J Cell Biol, 1995. **131**(1): p. 45-56.
388. Puvion-Dutilleul, F., et al., *Adenovirus infection induces rearrangements in the intranuclear distribution of the nuclear body-associated PML protein.* Exp. Cell Res., 1995. **218**(1): p. 9-16.
389. Yang, Y., et al., *Acetylated hsp70 and KAP1-mediated Vps34 SUMOylation is required for autophagosome creation in autophagy.* Proceedings of the National Academy of Sciences of the United States of America, 2013. **110**(17): p. 6841--6846.
390. Sun, X., et al., *Characterization of nuclear localization and SUMOylation of the ATBF1 transcription factor in epithelial cells.* PloS one, 2014. **9**(3): p. e92746-e92746.
391. Hendriks, I.A. and A.C.O. Vertegaal, *A comprehensive compilation of SUMO proteomics.* Nature reviews. Molecular cell biology, 2016. **17**(9): p. 581--595.
392. Shiio, Y. and R.N. Eisenman, *Histone sumoylation is associated with transcriptional repression.* Proceedings of the National Academy of Sciences of the United States of America, 2003. **100**(23): p. 13225--13230.
393. Galisson, F., et al., *A novel proteomics approach to identify SUMOylated proteins and their modification sites in human cells.* Molecular \& cellular proteomics : MCP, 2011. **10**(2): p. M110.004796.
394. Hannoun, Z., et al., *Post-translational modification by SUMO.* Toxicology, 2010. **278**(3): p. 288-93.
395. Gareau, J.R. and C.D. Lima, *The SUMO pathway: emerging mechanisms that shape specificity, conjugation and recognition.* Nat Rev Mol Cell Biol, 2010. **11**(12): p. 861-71.
396. Andreou, A.M. and N. Tavernarakis, *SUMOylation and cell signalling.* Biotechnology journal, 2009. **4**(12): p. 1740--1752.
397. Texari, L. and F. Stutz, *Sumoylation and transcription regulation at nuclear pores.* Chromosoma, 2015. **124**(1): p. 45--56.
398. Miteva, M., et al., *Sumoylation as a Signal for Polyubiquitylation and Proteasomal Degradation*, in *Conjugation and Deconjugation of Ubiquitin Family Modifiers*. 2010, Springer, New York, NY: New York, NY. p. 195--214.
399. Bae, S.-H., et al., *Sumoylation increases HIF-1alpha stability and its transcriptional activity.* Biochemical and biophysical research communications, 2004. **324**(1): p. 394--400.

400. Ren, J., et al., *Systematic study of protein sumoylation: Development of a site-specific predictor of SUMOsp 2.0.* PROTEOMICS, 2009. **9**(12): p. 3409-3412.
401. Sampson, D.A., M. Wang, and M.J. Matunis, *The small ubiquitin-like modifier-1 (SUMO-1) consensus sequence mediates Ubc9 binding and is essential for SUMO-1 modification.* The Journal of biological chemistry, 2001. **276**(24): p. 21664--21669.
402. Rodriguez, M.S., C. Dargemont, and R.T. Hay, *SUMO-1 conjugation in vivo requires both a consensus modification motif and nuclear targeting.* J Biol Chem, 2001. **276**(16): p. 12654-9.
403. Ota, T., et al., *Complete sequencing and characterization of 21,243 full-length human cDNAs.* Nat Genet, 2004. **36**(1): p. 40-5.
404. Hofmann, S., et al., *Double-edged role of PML nuclear bodies during human adenovirus infection.* Virus Res, 2021. **295**: p. 198280.
405. de Jong, R.N., P.C. van der Vliet, and A.B. Brenkman, *Adenovirus DNA replication: protein priming, jumping back and the role of the DNA binding protein DBP.* Curr Top Microbiol Immunol, 2003. **272**: p. 187-211.
406. Chang, L.S. and T. Shenk, *The adenovirus DNA-binding protein stimulates the rate of transcription directed by adenovirus and adeno-associated virus promoters.* Journal of virology, 1990. **64**(5): p. 2103-2109.
407. van Breukelen, B., et al., *Adenovirus Type 5 DNA Binding Protein Stimulates Binding of DNA Polymerase to the Replication Origin.* Journal of Virology, 2003. **77**(2): p. 915-922.
408. Hidalgo, P., et al., *Morphological, Biochemical, and Functional Study of Viral Replication Compartments Isolated from Adenovirus-Infected Cells.* Journal of Virology, 2016. **90**(7): p. 3411-3427.
409. Privette Vinnedge, L.M., et al., *The human DEK oncogene stimulates β-catenin signaling, invasion and mammosphere formation in breast cancer.* Oncogene, 2011. **30**(24): p. 2741-2752.
410. Gray, G.C., et al., *Genotype Prevalence and Risk Factors for Severe Clinical Adenovirus Infection, United States 2004-2006.* Clinical Infectious Diseases, 2007. **45**(9): p. 1120-1131.
411. Esposito, S., et al., *Impact of viral infections in children with community-acquired pneumonia: results of a study of 17 respiratory viruses.* Influenza Other Respir Viruses, 2013. **7**(1): p. 18-26.
412. Esposito, S., et al., *Is there a link between infection due to adenovirus 36 and childhood obesity?* The Pediatric infectious disease journal, 2012. **31**(11): p. 1184--1186.
413. Lamson, D.M., et al., *Detection and Genetic Characterization of Adenovirus Type 14 Strain in Students with Influenza-Like Illness, New York, USA, 2014-2015.* Emerging infectious diseases, 2017. **23**(7): p. 1194-1197.
414. Lenaerts, L., E. De Clercq, and L. Naesens, *Clinical features and treatment of adenovirus infections.* Rev Med Virol, 2008. **18**(6): p. 357-74.
415. Ganapathi, L., et al., *Use of cidofovir in pediatric patients with adenovirus infection.* F1000Research, 2016. **5**: p. 758-758.
416. Brand, P., T. Lenser, and P. Hemmerich, *Assembly dynamics of PML nuclear bodies in living cells.* PMC Biophys., 2010. **3**.
417. Condemine, W., et al., *Characterization of endogenous human promyelocytic leukemia isoforms.* Cancer research, 2006. **66**(12): p. 6192--6198.
418. Nisole, S., et al., *Differential Roles of PML Isoforms.* Front Oncol, 2013. **3**: p. 125.
419. Everett, R.D. and M.K. Chelbi-Alix, *PML and PML nuclear bodies: implications in antiviral defence.* Biochimie, 2007. **89**(6-7): p. 819-30.

420. Wang, Z.G., et al., *PML is essential for multiple apoptotic pathways.* Nat Genet, 1998. **20**(3): p. 266-72.
421. Sahin, U., H. de The, and V. Lallemand-Breitenbach, *PML nuclear bodies: assembly and oxidative stress-sensitive sumoylation.* Nucleus, 2014. **5**(6): p. 499-507.
422. Berscheminski, J., et al., *Sp100 isoform-specific regulation of human adenovirus 5 gene expression.* Journal of virology, 2014. **88**(11): p. 6076--6092.
423. Forrester, N.A., et al., *Adenovirus E4orf3 targets transcriptional intermediary factor 1gamma for proteasome-dependent degradation during infection.* J Virol, 2012. **86**(6): p. 3167-79.
424. Kremer, E.J. and G.R. Nemerow, *Adenovirus tales: from the cell surface to the nuclear pore complex.* PLoS Pathog, 2015. **11**(6): p. e1004821.
425. Chatterjee, P.K., M.E. Vayda, and S.J. Flint, *Identification of proteins and protein domains that contact DNA within adenovirus nucleoprotein cores by ultraviolet light crosslinking of oligonucleotides 32P-labelled in vivo.* J Mol Biol, 1986. **188**(1): p. 23-37.
426. Russell, W.C., W.G. Laver, and P.J. Sanderson, *Internal Components of Adenovirus.* Nature, 1968. **219**(5159): p. 1127-1130.
427. Avgousti, D.C., et al., *A core viral protein binds host nucleosomes to sequester immune danger signals.* Nature, 2016. **535**(7610): p. 173-177.
428. Giberson, A.N., A.R. Davidson, and R.J. Parks, *Chromatin structure of adenovirus DNA throughout infection.* Nucleic Acids Res, 2012. **40**(6): p. 2369-76.
429. Komatsu, T., H. Haruki, and K. Nagata, *Cellular and viral chromatin proteins are positive factors in the regulation of adenovirus gene expression.* Nucleic Acids Res, 2011. **39**(3): p. 889-901.
430. Ross, P.J., et al., *Assembly of helper-dependent adenovirus DNA into chromatin promotes efficient gene expression.* J Virol, 2011. **85**(8): p. 3950-8.
431. Ross, P.J., M.A. Kennedy, and R.J. Parks, *Host cell detection of noncoding stuffer DNA contained in helper-dependent adenovirus vectors leads to epigenetic repression of transgene expression.* J Virol, 2009. **83**(17): p. 8409-17.
432. Knipe, D.M., et al., *Snapshots: Chromatin control of viral infection.* Virology, 2013. **435**(1): p. 141-156.
433. Giberson, A.N., et al., *Human adenoviral DNA association with nucleosomes containing histone variant H3.3 during the early phase of infection is not dependent on viral transcription or replication.* Biochemistry and Cell Biology, 2018. **96**(6): p. 797-807.
434. Jenuwein, T. and C.D. Allis, *Translating the Histone Code.* Science, 2001. **293**(5532): p. 1074-1080.
435. Bode, A.M. and Z. Dong, *Inducible Covalent Posttranslational Modification of Histone H3.* Science's STKE, 2005. **2005**(281): p. re4-re4.
436. White, E., *Regulation of the cell cycle and apoptosis by the oncogenes of adenovirus.* Oncogene, 2001. **20**(54): p. 7836-7846.
437. Berk, A.J., *Adenovirus promoters and E1A transactivation.* Annu Rev Genet, 1986. **20**: p. 45-79.
438. Berk, A.J., *Functions of adenovirus E1A.* Cancer Surv, 1986. **5**(2): p. 367-87.
439. Dyson, N., et al., *Homologous sequences in adenovirus E1A and human papillomavirus E7 proteins mediate interaction with the same set of cellular proteins.* Journal of virology, 1992. **66**(12): p. 6893-6902.
440. Arany, Z., et al., *A family of transcriptional adaptor proteins targeted by the E1A oncoprotein.* Nature, 1995. **374**(6517): p. 81--84.
441. Eckner, R., et al., *Molecular cloning and functional analysis of the adenovirus E1A-associated 300-kD protein (p300) reveals a protein with properties of a transcriptional adaptor.* Genes \& development, 1994. **8**(8): p. 869--884.

442. Fuchs, M., et al., *The p400 Complex Is an Essential E1A Transformation Target.* Cell, 2001. **106**(3): p. 297-307.
443. Mymryk, J.S. and M.M. Smith, *Influence of the adenovirus 5 E1A oncogene on chromatin remodelling.* Biochem Cell Biol, 1997. **75**(2): p. 95-102.
444. Lazaridis, I., A. Babich, and J.R. Nevins, *Role of the adenovirus 72-kDa DNA binding protein in the rapid decay of early viral mRNA.* Virology, 1988. **165**(2): p. 438-445.
445. Xu, X., et al., *Adenovirus DNA binding protein inhibits SrCap-activated CBP and CREB-mediated transcription.* Virology, 2003. **313**(2): p. 615-621.
446. Babich, A. and J.R. Nevins, *The stability of early adenovirus mRNA is controlled by the viral 72 kd DNA-binding protein.* Cell, 1981. **26**(3, Part 1): p. 371-379.
447. Ahi, Y.S., S.V. Vemula, and S.K. Mittal, *Adenoviral E2 IVa2 protein interacts with L4 33K protein and E2 DNA-binding protein.* J Gen Virol, 2013. **94**(Pt 6): p. 1325-1334.
448. Sheng, Y., et al., *Molecular recognition of p53 and MDM2 by USP7/HAUSP.* Nature Structural & Molecular Biology, 2006. **13**(3): p. 285-291.
449. Kulanayake, S. and S.K. Tikoo, *Adenovirus Core Proteins: Structure and Function.* Viruses, 2021. **13**(3): p. 388.
450. Gamble, M.J. and R.P. Fisher, *SET and PARP1 remove DEK from chromatin to permit access by the transcription machinery.* Nature Structural & Molecular Biology, 2007. **14**(6): p. 548-555.
451. Babaei-Jadidi, R., et al., *FBXW7 influences murine intestinal homeostasis and cancer, targeting Notch, Jun, and DEK for degradation.* Journal of Experimental Medicine, 2011. **208**(2): p. 295-312.
452. Theurillat, J.-P.P., et al., *Ubiquitylome analysis identifies dysregulation of effector substrates in SPOP-mutant prostate cancer.* Science, 2014. **346**(6205): p. 85-89.
453. Mattiroli, F. and T.K. Sixma, *Lysine-targeting specificity in ubiquitin and ubiquitin-like modification pathways.* Nature Structural & Molecular Biology, 2014. **21**(4): p. 308-316.
454. Tammsalu, T., et al., *Proteome-wide identification of SUMO2 modification sites.* Sci Signal, 2014. **7**(323): p. rs2.
455. Zhang, X., et al., *Accumulation of p53 in response to adenovirus early region 1A sensitizes human cells to tumor necrosis factor alpha-induced apoptosis.* Elsevier.
456. Nakajima, T., et al., *Stabilization of p53 by adenovirus E1A occurs through its amino-terminal region by modification of the ubiquitin-proteasome pathway.* J Biol Chem, 1998. **273**(32): p. 20036-45.
457. Ching, W., T. Dobner, and E. Koyuncu, *The human adenovirus type 5 E1B 55-kilodalton protein is phosphorylated by protein kinase CK2.* J Virol, 2012. **86**(5): p. 2400-15.
458. Ornelles, D.A. and T. Shenk, *Localization of the adenovirus early region 1B 55-kilodalton protein during lytic infection: association with nuclear viral inclusions requires the early region 4 34-kilodalton protein.* Journal of Virology, 1991. **65**(1): p. 424-429.
459. Kindsmuller, K., et al., *A 49-kilodalton isoform of the adenovirus type 5 early region 1B 55-kilodalton protein is sufficient to support virus replication.* Journal of virology, 2009. **83**(18): p. 9045-56.
460. Blanchette, P., et al., *Control of mRNA export by adenovirus E4orf6 and E1B55K proteins during productive infection requires E4orf6 ubiquitin ligase activity.* J Virol, 2008. **82**(6): p. 2642-51.
461. Chen, L., et al., *Sumoylation regulates nuclear localization and function of zinc finger transcription factor ZIC3.* Biochim Biophys Acta, 2013. **1833**(12): p. 2725-2733.
462. Wen, D., et al., *SUMOylation Promotes Nuclear Import and Stabilization of Polo-like Kinase 1 to Support Its Mitotic Function.* Cell Rep, 2017. **21**(8): p. 2147-2159.

463. Krätzer, F., et al., *The adenovirus type 5 E1B-55k oncoprotein is a highly active shuttle protein and shuttling is independent of E4orf6, p53 and Mdm2.* Oncogene, 2000. **19**: p. 850-857.
464. Stuiver, M.H. and P.C. van der Vliet, *Adenovirus DNA-binding protein forms a multimeric protein complex with double-stranded DNA and enhances binding of nuclear factor I.* Journal of virology, 1990. **64**(1): p. 379-386.
465. Cleghon, V. and D.F. Klessig, *Characterization of the nucleic acid binding region of adenovirus DNA binding protein by partial proteolysis and photochemical cross-linking.* Journal of Biological Chemistry, 1992. **267**(25): p. 17872-17881.
466. Morin, N., C. Delsert, and D.F. Klessig, *Nuclear localization of the adenovirus DNA-binding protein: requirement for two signals and complementation during viral infection.* Molecular and cellular biology, 1989. **9**(10): p. 4372-4380.
467. Schuierer, M., et al., *Induction of AP-2alpha expression by adenoviral infection involves inactivation of the AP-2rep transcriptional corepressor CtBP1.* J Biol Chem, 2001. **276**(30): p. 27944-9.
468. Somasundaram, K., et al., *Repression of a matrix metalloprotease gene by E1A correlates with its ability to bind to cell type-specific transcription factor AP-2.* Proc Natl Acad Sci U S A, 1996. **93**(7): p. 3088-93.
469. Fax, P., et al., *Binding of PKA-RIIalpha to the Adenovirus E1A12S oncoprotein correlates with its nuclear translocation and an increase in PKA-dependent promoter activity.* Virology, 2001. **285**(1): p. 30-41.
470. Wu, L., et al., *The E2F1–3 transcription factors are essential for cellular proliferation.* Nature, 2001. **414**(6862): p. 457-462.
471. Takahashi, Y., J.B. Rayman, and B.D. Dynlacht, *Analysis of promoter binding by the E2F and pRB families in vivo: distinct E2F proteins mediate activation and repression.* Genes Dev, 2000. **14**(7): p. 804-16.
472. Wells, J., et al., *Target Gene Specificity of E2F and Pocket Protein Family Members in Living Cells.* Molecular and Cellular Biology, 2000. **20**(16): p. 5797-5807.
473. Nielsen, S.J., et al., *Rb targets histone H3 methylation and HP1 to promoters.* Nature, 2001. **412**(6846): p. 561-565.
474. Narita, M., et al., *Rb-Mediated Heterochromatin Formation and Silencing of E2F Target Genes during Cellular Senescence.* Cell, 2003. **113**(6): p. 703-716.
475. Slansky, J.E. and P.J. Farnham, *Introduction to the E2F family: protein structure and gene regulation.* Curr Top Microbiol Immunol, 1996. **208**: p. 1-30.
476. Helin, K., *Regulation of cell proliferation by the E2F transcription factors.* Curr Opin Genet Dev, 1998. **8**(1): p. 28-35.
477. Zheng, N., et al., *Structural basis of DNA recognition by the heterodimeric cell cycle transcription factor E2F-DP.* Genes Dev, 1999. **13**(6): p. 666-74.
478. Kovesdi, I., R. Reichel, and J.R. Nevins, *Role of an adenovirus E2 promoter binding factor in E1A-mediated coordinate gene control.* Proc Natl Acad Sci U S A, 1987. **84**(8): p. 2180-4.
479. Huang, M.M. and P. Hearing, *The adenovirus early region 4 open reading frame 6/7 protein regulates the DNA binding activity of the cellular transcription factor, E2F, through a direct complex.* Genes Dev, 1989. **3**(11): p. 1699-710.
480. Kovesdi, I., R. Reichel, and J.R. Nevins, *Identification of a cellular transcription factor involved in E1A trans-activation.* Cell, 1986. **45**(2): p. 219-28.
481. Wise-Draper, T.M., et al., *The Human DEK Proto-Oncogene Is a Senescence Inhibitor and an Upregulated Target of High-Risk Human Papillomavirus E7.* Journal of Virology, 2005. **79**(22): p. 14309-14317.
482. Han, S., et al., *Clinicopathological significance of DEK overexpression in serous ovarian tumors.* Pathology International, 2009. **59**(7): p. 443-447.

483. Hacker, K.E., et al., *The DEK Oncoprotein Functions in Ovarian Cancer Growth and Survival.* Neoplasia, 2018. **20**(12): p. 1209-1218.
484. Grasemann, C., et al., *Gains and overexpression identify DEK and E2F3 as targets of chromosome 6p gains in retinoblastoma.* Oncogene, 2005. **24**(42): p. 6441-6449.
485. Datta, A., et al., *Oncoprotein DEK as a tissue and urinary biomarker for bladder cancer.* BMC Cancer, 2011. **11**(1): p. 234.
486. Kappes, F., et al., *DEK expression in melanocytic lesions.* Human Pathology, 2011. **42**(7): p. 932-938.
487. Riveiro-Falkenbach, E., et al., *DEK oncogene is overexpressed during melanoma progression.* Pigment Cell & Melanoma Research, 2017. **30**(2): p. 194-202.
488. Zhou, Q.C., et al., *Oncogene DEK is highly expressed in lung cancerous tissues and positively regulates cell proliferation as well as invasion.* Oncol Lett, 2018. **15**(6): p. 8573-8581.
489. Whyte, P., et al., *Association between an oncogene and an anti-oncogene: the adenovirus E1A proteins bind to the retinoblastoma gene product.* Nature, 1988. **334**(6178): p. 124-9.
490. Felsani, A., A.M. Mileo, and M.G. Paggi, *Retinoblastoma family proteins as key targets of the small DNA virus oncoproteins.* Oncogene, 2006. **25**(38): p. 5277-85.
491. Knight, J.S., N. Sharma, and E.S. Robertson, *Epstein–Barr virus latent antigen 3C can mediate the degradation of the retinoblastoma protein through an SCF cellular ubiquitin ligase.* Proceedings of the National Academy of Sciences of the United States of America, 2005. **102**(51): p. 18562-18566.
492. Houweling, A., P.J. van den Elsen, and A.J. van der Eb, *Partial transformation of primary rat cells by the leftmost 4.5% fragment of adenovirus 5 DNA.* Virology, 1980. **105**(2): p. 537-50.
493. Hamamori, Y., et al., *Regulation of histone acetyltransferases p300 and PCAF by the bHLH protein twist and adenoviral oncoprotein E1A.* Cell, 1999. **96**(3): p. 405-13.
494. Boyer, J., K. Rohleder, and G. Ketner, *Adenovirus E4 34k and E4 11k inhibit double strand break repair and are physically associated with the cellular DNA-dependent protein kinase.* Virology, 1999. **263**(2): p. 307-12.
495. Smith, G.C. and S.P. Jackson, *The DNA-dependent protein kinase.* Genes Dev, 1999. **13**(8): p. 916-34.
496. Müller, S. and T. Dobner, *The adenovirus E1B-55K oncoprotein induces SUMO modification of p53.* Cell cycle (Georgetown, Tex.), 2008. **7**(6): p. 754--758.
497. Savelyeva, I. and M. Dobbelstein, *Infection with E1B-mutant adenovirus stabilizes p53 but blocks p53 acetylation and activity through E1A.* Oncogene, 2011. **30**(7): p. 865--875.
498. Chinnadurai, G., *Control of Apoptosis by Human Adenovirus Genes.* Seminars in Virology, 1998. **8**(5): p. 399-408.
499. White, E., *Regulation of the cell cycle and apoptosis by the oncogenes of adenovirus.* Oncogene, 2001. **20**(54): p. 7836-46.
500. Sarnow, P., et al., *Adenovirus E1b-58kd tumor antigen and SV40 large tumor antigen are physically associated with the same 54 kd cellular protein in transformed cells.* Cell, 1982. **28**(2): p. 387-394.
501. Martin, M.E. and A.J. Berk, *Corepressor required for adenovirus E1B 55,000-molecular-weight protein repression of basal transcription.* Mol Cell Biol, 1999. **19**(5): p. 3403-14.
502. Fogal, V., et al., *Regulation of p53 activity in nuclear bodies by a specific PML isoform.* Embo j, 2000. **19**(22): p. 6185-95.

503. Endter, C., et al., *SUMO-1 modification required for transformation by adenovirus type 5 early region 1B 55-kDa oncoprotein.* Proc. Natl. Acad. Sci. USA, 2001. **98**: p. 11312-11317.
504. Hutton, F.G., et al., *Consequences of disruption of the interaction between p53 and the larger adenovirus early region 1B protein in adenovirus E1 transformed human cells.* Oncogene, 2000. **19**(3): p. 452-462.
505. Forrester, N.A., et al., *Serotype-specific inactivation of the cellular DNA damage response during adenovirus infection.* Journal of virology, 2011. **85**(5): p. 2201-2211.
506. Cheng, C.Y., et al., *Role of E1B55K in E4orf6/E1B55K E3 Ligase Complexes Formed by Different Human Adenovirus Serotypes.* Journal of Virology, 2013. **87**(11): p. 6232--6245.
507. Blanchette, P., et al., *Aggresome formation by the adenoviral protein E1B55K is not conserved among adenovirus species and is not required for efficient degradation of nuclear substrates.* J Virol, 2013. **87**(9): p. 4872-81.
508. Garcia, B.A., et al., *Tissue-specific expression and post-translational modification of histone H3 variants.* Journal of proteome research, 2008. **7**(10): p. 4225-4236.
509. Wang, W., et al., *Tissue-specific pathway association analysis using genome-wide association study summaries.* Bioinformatics, 2016. **33**(2): p. 243-247.
510. Puigserver, P., *Tissue-specific regulation of metabolic pathways through the transcriptional coactivator PGC1-alpha.* Int J Obes (Lond), 2005. **29 Suppl 1**: p. S5-9.
511. Sonawane, A.R., et al., *Understanding Tissue-Specific Gene Regulation.* Cell reports, 2017. **21**(4): p. 1077-1088.
512. Ng, E.W. and A.P. Adamis, *Anti-VEGF aptamer (pegaptanib) therapy for ocular vascular diseases.* Ann N Y Acad Sci, 2006. **1082**: p. 151-71.
513. Zhou, J. and J.J. Rossi, *Cell-type-specific, Aptamer-functionalized Agents for Targeted Disease Therapy.* Mol Ther Nucleic Acids, 2014. **3**(6): p. e169.
514. Song, Y., et al., *DEK-targeting aptamer DTA-64 attenuates bronchial EMT-mediated airway remodelling by suppressing TGF-β1/Smad, MAPK and PI3K signalling pathway in asthma.* Journal of Cellular and Molecular Medicine, 2020. **24**(23): p. 13739-13750.
515. Cao, J., et al., *Novel DEK-Targeting Aptamer Delivered by a Hydrogel Microneedle Attenuates Collagen-Induced Arthritis.* Molecular Pharmaceutics, 2021. **18**(1): p. 305-316.
516. Ng, E.W., et al., *Pegaptanib, a targeted anti-VEGF aptamer for ocular vascular disease.* Nat Rev Drug Discov, 2006. **5**(2): p. 123-32.
517. Mor-Vaknin, N., et al., *DEK-targeting DNA aptamers as therapeutics for inflammatory arthritis.* Nat Commun, 2017. **8**: p. 14252.

Appendix II

Publications in Peer-Reviewed Journals

Samuel Hofmann, **Julia Mai**, Sawinee Masser, Peter Groitl, Alexander Herrmann, Thomas Sternsdorf, Ruth Brack-Werner, and Sabrina Schreiner (2020). *ATO (Arsenic Trioxide) Effects on Promyelocytic Leukemia Nuclear Bodies Reveals Antiviral Intervention Capacity.* Adv Sci. 2020 Feb 27;7(8):1902130. doi: 10.1002/advs.201902130.

Miona Stubbe, **Julia Mai**, Christina Paulus, Hans Christian Stubbe, Julia Berscheminski, Maryam Karimi, Samuel Hofmann, Elisabeth Weber, Kamyar Hadian, Ron Hay, Peter Groitl, Michael Nevels, Thomas Dobner, Sabrina Schreiner (2020). *Viral DNA Binding Protein SUMOylation Promotes PML Nuclear Body Localization Next to Viral Replication Centers.* mBio. 2020 Mar 17;11(2):e00049-20. doi: 10.1128/mBio.00049-20.

Samuel Hofmann, Miona Stubbe, **Julia Mai** and Sabrina Schreiner. *Double-edged Role of PML Nuclear Bodies during Human Adenovirus Infection.* Virus Res. 2020 Dec 25;295:198280. doi: 10.1016/j.virusres.2020.198280.

Julia Mai, Miona Stubbe, Samuel Hofmann, Sawinee Masser, Roger Everett, Thomas Dobner, Chris Boutell, Peter Groitl, and Sabrina Schreiner (2021). *PML alternative splice products differentially regulate HAdV productive infection in stably transformed lung/liver cell lines.* under revision

Sawinee Masser, **Julia Mai**, Samuel Hofmann, Peter Groitl, Josephine Maaz, Jane McKeating, Sabrina Schreiner. *Modulation of hypoxia by HAdV*. manuscript in preparation

Julia Mai, Sawinee Masser, Ilka Simons, Samuel Hofmann, Peter Groitl, Susanne I. Wells and Sabrina Schreiner. *The chromatin-associated DEK protein is a novel host factor promoting HAdV infection.* manuscript in preparation

Conferences

Poster Presentations

Lab Retreat Institute of Virology, TUM

Impaired assembly of the immunoproteasome supports efficient HAdV replication. Herrsching/Ammersee, Germany, 2018

29th Annual Meeting of the Society for Virology

Role of the chromatin-associated proto-oncogene DEK during productive infection with HAdV. Düsseldorf, Germany, 2019

Chromatin Dynamics Symposium

The chromatin-associated proto-oncogene DEK is a novel host factor promoting HAdV replication and gene expression. MPI, Biochemie, Martinsried, Germany, 2019

30th Annual Meeting of the Society for Virology

The chromatin-associated DEK is a novel host factor promoting HAdV infection. Hannover, Germany, 2021

Oral Presentations

28th Annual Meeting of the Society for Virology

Bivalent role of PML isoforms during HAdV productive infection. Würzburg, Germany, 2018

DNA Tumor Virus Meeting

Apobec3A is a novel restriction factor antagonizing efficient HAdV replication. Madison, WI, USA, 2018

Lab Retreat Institute of Virology, TUM

Role of the chromatin-associated proto-oncogene DEK during productive infection with HAdV. Herrsching/Ammersee, Germany, 2019

DNA Tumor Virus Meeting

Role of the chromatin-associated proto-oncogene DEK during productive infection with HAdV.

Trieste, Italy, 2019

1st MGC Science Day

The chromatin-associated proto-oncogene DEK is a novel host factor promoting HAdV replication and gene expression.

Klinikum rechts der Isar, Munich, Germany, 2019

Awarded with the 1st prize for "Best Talk of the Session"

Participation in Scientific Meetings / Workshops

Lab Retreat Institute of Virology, TUM

Tutzing, Germany, 2017

Munich Epigenetics Spotlight Meeting

Helmholtz Zentrum München, Großhadern Campus, Munich, Germany, 2017

Symposium: Regulation of Transcription: RNA Pol II and Myc

MPI Biochemie, Martinsried, Germany, 2018

The Proteasome hub: Fine-tuning of proteolysis according to cellular needs

Schloss Hohenkammer, Hohenkammer, Germany, 2018

TUM Kick-Off Seminar

TUM Science and Study Center, Raitenhaslach, Germany, 2019

(I&I) Immunology & Inflammation – A Virtual Symposium on Covid-19

Helmholtz Association, Online-based conference, Germany, 2021

Trainings and Certification Courses

First-Aid-Training

TUM Talent Factory, Helmholtz Zentrum München, Neuherberg, 2018

Biostatistics with GraphPad Prism

Helmholtz Zentrum München, Neuherberg, 2018

Webinar “Zitieren statt Plagiieren”

Universitätsbibliothek, TU Munich, Germany, 2019

Staatlich anerkannte, MPG-interne Fortbildungsveranstaltung nach § 15 Abs. 4 Satz 1 GenTSV

Max-Planck-Gesellschaft zur Förderung der Wissenschaften e.V., Martinsried, 2019

Nachwuchsakademie ACHIEVE: „Stepping stone to an academic career in virology”

interactive seminars on topics related to science communication

- writing manuscripts
- third-party funding application

Society of Virology, web-based workshop

Grants

Jürgen Manchot Stiftung e.V.

PhD scholarship, July 2017 – June 2020

Acknowledgement

First, I want to thank my first supervisor Prof. Dr. Sabrina Schreiner for the opportunity to work on this interesting project in her research group. Her guidance and advice were of great value for me as a scientist and personally. I am grateful for her support in all situations and the time we have spent in and outside of the lab. I will always remember the great and fun time that we had and I am looking forward to our future work in Hannover!

I want to thank my second supervisor Prof. Dr. Thomas Floss and my mentor Dr. Michelle Vincendeau for their great support by providing helpful suggestions and discussions of results and hypotheses.

I am very thankful to my colleagues of the Schreiner lab for their support, discussions and the great time we have spent together. Thanks a lot Sawinee Masser, Samuel Hofmann, Nathalie Skvorc, Miona Stubbe, Christina Weiß, Peter Groitl, Anna Hoffereck, Johanna Markert, Verena Plank, Lilian Göttig, Maryam Karimi and Ute Finkel. Thank you to Ilka Simons for her great support and the fun in the lab, and for proofreading my thesis together with Sawinee and Samuel. I am especially very grateful to Sawinee, Samuel und Nathalie for our close friendship. Thanks for helping me through the good and bad times. Without you, life and work would’nt be the same!

I would like to thank the Jürgen-Manchot-Stiftung for supporting my PhD by providing me a scholarship.

Ein ganz besonderer Dank von ganzem Herzen gilt meinen Eltern, die mich immer in all der Zeit und in meinen Entscheidungen unterstützt haben. Danke für alles, was sie für mich getan haben und dafür, dass sie immer für mich da sind. Vielen lieben Dank an meinen Bruder Marlon dafür, dass immer auf ihn Verlass ist, und für all die schönen gemeinsamen Erinnerungen. Dafür widme ich meiner Familie diese Arbeit. Ich möchte mich auch bei meinen Großeltern für alles, was sie für mich getan haben, bedanken. Ich bedanke mich auch von Herzen bei Holger, dass er immer für mich da ist in allen Höhen und Tiefen. Ohne sein Verständnis, seine Unterstützung und Hilfe wäre Vieles nicht möglich gewesen. Danke, dass du mich immer zum Lachen bringst, und ich freue mich schon auf mehr gemeinsame, freie Wochenenden!